UNDERSTANDING THE CONSERVED AND SPECIES-SPECIFIC FUNCTIONS OF FOXP2, A GENE IMPLICATED IN SPEECH AND LANGUAGE DEVELOPMENT

by

STEPHANIE LEPP HICKEY

DISSERTATION

Presented to the Faculty of the Graduate School of Biomedical Sciences

The University of Texas Southwestern Medical Center at Dallas

In Partial Fulfillment of the Requirements

For the Degree of

DOCTOR OF PHILOSOPHY

The University of Texas Southwestern Medical Center

Dallas, Texas

August, 2018

UNDERSTANDING THE CONSERVED AND SPECIES-SPECIFIC FUNCTIONS OF FOXP2, A GENE IMPLICATED IN SPEECH AND LANGUAGE DEVELOPMENT

Stephanie Lepp Hickey

The University of Texas Southwestern Medical Center at Dallas, 2018

Genevieve Konopka, Ph.D

ABSTRACT

During my dissertation work I sought to better understand the conserved and human-specific functions of FoxP2. Intrigued by the enrichment of *FOXP2* in the human subplate layer, I hypothesized that FOXP2 regulates evolutionarily distinct subplate gene expression patterns and tested this theory by performing RNA-seq in human differentiating neurons and leveraging publically available developmental expression data from human, macaque, and mouse cortex in order to identify human specific,

primate specific, and conserved subplate genes regulated by FOXP2. This study not only identified human specific targets in this expanded, transient region, but it may also inspire research of the conserved, non-cell-autonomous role of FoxP2 in the maturation of thalamocortical circuitry. Additionally, I performed ChIP-seq and RNA-seq in human neural progenitor cells and found evidence that FOXP2 may actively modify the chromatin landscape. This lead me to hypothesize that by modifying the chromatin landscape of neural progenitors FOXP2 turns off cellular programs that maintain an undifferentiated state while turning on programs that drive a cell towards a neuronal fate. To test this hypothesis, I identified areas of nucleosomal depletion using ATAC-seq and correlated epigenetic changes caused by *FOXP2* expression to changes in gene expression in proliferating and differentiating human neurons. This allowed me to define two separate molecular mechanisms by which FOXP2 regulates gene expression in human neurons, even finding a potential FOXP2 co-activator. Together, these studies push forward our understanding of the function of FoxP2, especially in human neurons, and provide a source of data from which the next hypotheses concerning FoxP2 and human language formation may be derived.

TABLE OF CONTENTS

CHAPTER ONE: Background and Introduction

The KE family exhibits a heritable form of verbal dyspraxia

The neural and genetic foundation of language

Communication via speech and language underlies our uniquely human ability to accumulate knowledge through generations and contributes to the success of the human species. While many species use vocalizations to impart information, few species are vocal learners that hone communication skills over time, and only humans imbed vocal utterances into a scaffold of syntactic rules to form language. In the late 1800s, Pierre Paul Broca and Karl Wernicke famously studied brain lesions of patients with aphasia and began to uncover the neural underpinnings of language use (Chang et al., 2015). These studies identified the inferior frontal gyrus (Broca's area) and superior temporal gyrus (Wernicke's area) as the first language associated brain regions. Subsequently, the basal ganglia, cerebellum, and neural circuits connecting these regions to the cortex have been shown to be important for the sensory motor aspects of speech production and higher order cognitive abilities required for language learning (Konopka and Roberts, 2016). Though cortico-cortical, cortico-basal-ganglia-thalamo-cortical, and cortico-cerebellar circuits may facilitate speech perception, motor control for speech production, and language learning (Konopka and Roberts, 2016) the exact mechanisms by which these speech and language networks are constructed are not fully understood.

Patients with speech and language disorders have been invaluable not only in locating language related brain regions, but also in attempting to identify a genetic basis for language ability. For example, in 1995 Bishop *et al.* recruited a large cohort of mono-

and dizygotic twins in which at least one member of each pair was diagnosed with selective language impartment (SLI) (Bishop et al., 1995). SLI is characterized by developmental deficits in articulation, expressive and/or receptive language ability that is not accompanied by other developmental disorders such as autism, intellectual disability or other overt neurological disabilities (Bishop et al., 1995). Moreover, language deficiency in these patients is not a side effect of hearing impairment. Thus, by studying the heritability of SLI, Bishop et al. sought provide evidence for a genetic component of language development separate from the development of general cognitive ability. Using multiple statistical methods, the study showed that impairments in both expressive receptive language are highly heritable (Bishop et al., 1995) supporting the hypothesis that the development of the neural circuits involved in language processing is genetically encoded.

Affected KE family members show deficits in articulation and expressive and receptive language

An important piece of evidence strengthening the hypothesis that specific genes could underlie the formation of human language arose in 1990 when Hurst *et al.* described a three-generation family in which half of the members exhibited the same speech and language disorder (Hurst et al., 1990). The family's pedigree suggested an autosomal dominant inheritance pattern, leading to the intriguing possibility that a mutation in a single genetic locus was responsible for the disorder. Affected members of the KE family, as they came to be known in the literature, exhibit severe problems with articulation of speech that make them nearly incomprehensible to the naïve listener (Hurst et al., 1990, Vargha-Khadem et al., 1995). Moreover, they are significantly

impaired compared to unaffected family members in tasks requiring repetition of words or non-word sounds as well as tasks involving the performance of individual facial movements (e.g. “open your mouth” and “close your left eye”) or series of facial movements (e.g. “stick out your tongue, lick your upper lip, and smack your lips”) (Hurst et al., 1990, Vargha-Khadem et al., 1995). These findings demonstrate that orofacial dyspraxia, the inability to rapidly form the complex facial movements necessary for speech, is a major component of the KE family disorder (Vargha-Khadem et al., 1995).

Along with speech impairments caused by poor facial fine motor skills, affected KE family members have deficiencies in expressive and receptive language (Vargha-Khadem et al., 1995, Gopnik and Crago, 1991). Affected subjects have difficulty supplying the correct verb tense or plural form, highlighting deficiencies in expressive language. For example, when asked to complete sentences such as “Every day I wash my clothes. Yesterday I [blank] my clothes.” they provided the correct tense, “washed”, only half of the time (Vargha-Khadem et al., 1995). Providing the proper pluralized noun for singular nouns ending in consonants or sibilants was also challenging for affected individuals. Subjects were shown a picture of an imaginary animal and told, for example, that this animal is a “zoop” or a “zash”. When asked to provide plural versions of the nonsense animal nouns they were impaired in supplying the expected response, i.e. “zoops” or “zashes” (Gopnik and Crago, 1991). The problems marking plurals are not caused by the inability to pronounce the “s” sound at the end of the word as the affected individuals perform as well as unaffected controls when asked to provide the correct possessive noun (“The [baby’s] mother.”) (Gopnik and Crago, 1991).

Affected family members not only have difficulty with expressive language, but also with perceiving proper use of verb tenses and plural forms. They can recognize incorrect thematic relations within sentences when presented with nonsensical phrase. For example when presented with *"The boy eats the girl a cookie."* affected individuals readily identify this sentence as incorrect (Gopnik and Crago, 1991). However, they were significantly worse than unaffected family members at identifying sentences with incorrect tense ("Yesterday the girl eat a cookie.") or inappropriate plural verb and noun matching ("The boy eats three cookie.") suggesting receptive language difficulties surrounding specific grammatical inflections (Gopnik and Crago, 1991). Affected family members have other grammar related challenges like difficulty providing proper comparative and superlative adjective forms that, along with the inability to recognizing correct tense and plural forms, suggests a failure to internalize inflectional morphosyntactic rules (Vargha-Khadem et al., 1995). This is controversial, however, given that the affected family members are equally impaired in irregular and regular past tense verb production (Watkins et al., 2002a). Because irregular verb forms are essentially memorized and do not follow inflectional morphosyntactic rules like regular verbs, this suggests a broader problem in compiling lexical knowledge (Watkins et al., 2002a).

Other measures of receptive language were less clearly disrupted. For instance, Gopnik and Crago found no difference compared with unaffected family members in the ability for affected individuals to act out a command like "please touch the books" when presented with various groups of items (Gopnik and Crago, 1991). When given more complex instructions like *"Here are three crayons. Drop the yellow one on the floor, give*

me the blue one and pick up the red one," affected individuals still performed similarly to unaffected family members (Gopnik and Crago, 1991). Additionally, when Gopnik and Crago showed sets of pictures depicting various scenarios to subjects, described one scenario for the subject, and asked the subject to choose the picture being described, the affected subjects chose the correct picture as often as unaffected individuals (Gopnik and Crago, 1991). By contrast, Vargha-Khadem and colleagues did find deficits in affected individuals in the Test for Reception of Grammar (TROG) test, which also asks subjects to identify which picture is being described (Vargha-Khadem et al., 1995). Obviously, the reduced receptive language capabilities of the affected KE family members are restricted to specific grammatical forms and do not apply to all spoken language.

In the mid 1990s, these findings suggested that a single genetic locus could underlie motor and cognitive aspects of language production. However, this interpretation was complicated by the fact that average non-verbal IQ of the affected KE family members is lower than unaffected members average non-verbal IQ. Though the ranges of the non-verbal IQs of affected (71-111) and unaffected individuals (84-119) overlap, six of the affected individuals have a non-verbal IQ so low that they would be excluded from a diagnosis of SLI (Vargha-Khadem et al., 1995). Thus, the genetic locus responsible for the KE phenotype is certainly involved in the motor aspects of speech production and may be implicated in cognition generally.

Comparison of affected KE family members to aphasics

In order to understand if the language deficits exhibited by affected KE family members are due to overall developmental cognitive impairment, or if non-verbal IQ is

separate from language impairments, Watkins and colleagues compared the behavioral phenotype of affected KE family members with individuals suffering from aphasia following stroke (Watkins et al., 2002a). This comparison allows for the separation of cognitive phenotypes caused by long-term developmental disruption of circuitry from insults acquired after normal development (Watkins et al., 2002a).

Importantly, Watkins et al. found that the affected group had a significantly lower non-verbal IQ than both the unaffected family members and the aphasic group, and that the non-verbal IQs of the aphasic and unaffected groups did not differ from one another (Watkins et al., 2002a). The only test of receptive language for which the affected KE family members were impaired while the aphasic group was not was the lexical decision test (Watkins et al., 2002a). During the lexical decision test subjects heard both words and non-words sounds and were asked to distinguish between the two. The aphasic patients were unimpaired, as they had learned to distinguish words from non-words during the time before their strokes. However, the affected KE family members did not obtain this lexical knowledge during development (Watkins et al., 2002a).

Interesting results were also obtained from the word and non-word repetition tests for expressive language impairment. Scores for all three groups in both word and non-word repetition test decreased as number of syllables per word/non-word increased, as expected (Watkins et al., 2002a). However, the affected family members exhibited the largest deficit compared to unaffected family members on the word repetition task with the aphasic subjects falling between the two groups (Watkins et al., 2002a). Interestingly, aphasics and affected family members were equally impaired in the non-word repetition compared to unaffected family members suggesting that

because the aphasics were previously able to use proper articulation patterns for forming known words they were better able to repeat these words than novel non-words after stroke (Watkins et al., 2002a). For affected KE family members, on the other hand, novel non-words and true English words presented the same challenge in this task further suggesting that there is a learning disability inherent to the KE speech and language disorder.

However, the impairments in derivational and inflection morphology and verb tense selection, which are potentially due to an inability to learn grammatical rules, were observed in both KE family members, as previously described (Vargha-Khadem et al., 1995, Gopnik and Crago, 1991), and aphasic subjects (Watkins et al., 2002a). Therefore, it is difficult to determine whether the orofacial articulation impairment aspect of the disorder, which is shared by aphasics, is at the root of the language learning disorder or whether the cognitive and motor aspects of the disorder are separate. Watkins suggests that the articulation deficit leads to poor phonology, or the systematic organization of sounds, which then could cause impairments in derivational and inflection morphology (Watkins et al., 2002a). Ultimately, the relationships between the articulation deficits, poor phonology, impairments in derivational and inflection morphology, and difficulties with lexical learning exhibited by affected KE family members still require explanation.

Mutations in FOXP2 cause a developmental speech and language disorder

Localization of the SPCH1, the genetic locus that co-segregates with the KE family speech and language disorder

While the affected members of the KE family were extensively phenotyped, a simultaneous hunt for the genetic mutation causing the disorder was afoot. In 1998, Simon Fisher and colleagues performed a genome-wide search for co-inheritance of polymorphic genetic markers and the gene responsible for the speech and language disorder (Fisher et al., 1998). Genetic markers are regions of the genome with two attributes, 1) a sequence of bases common among the population but unique across the genome that allow the marker to be localized to a discrete position and 2) a variable component that allows the region to be distinguished between different individuals and homologous chromosomes (Burton et al., 2005). Microsatellite repeats meet these criteria and were used to map the location of the mutation responsible for the KE family's disorder (Fisher et al., 1998). These regions consist of multiple repeats of a short sequence, and, importantly, the number of repeats is variable among individuals so the length of the microsatellite region differentiates alleles (Burton et al., 2005). Moreover, most people are heterozygous for microsatellite alleles so homologous chromosomes can be distinguished (Burton et al., 2005). Additionally, microsatellites are uniformly distributed across the genome making them ideal for linkage mapping of disease genes (Weber, 1990).

In order to identify linked markers, or markers that infrequently segregate by recombination, Fisher employed fluorescence-based micro-satellite genotyping on 27 KE family members and strong evidence for linkage was observed for makers on the long arm of chromosome 7 (Fisher et al., 1998). When Fisher analyzed the marker haplotypes, or the groups of alleles that are passed down together, he found six contiguous markers for which all affected family members possessed one specific set of

alleles but no unaffected family members possessed that specific set. This suggested that the mutation responsible for the KE family's disorder resided among these markers. Because this haplotype block spans a large, 27.4-cM, region of the genome, many additional microsatellite markers within the region were used identify a more precise linkage. This finer analysis revealed 6 markers spanning a ~5.6-cM in the chromosomal band 7q31 whose alleles segregated perfectly with the disorder (Fisher et al., 1998). They named this interval SPCH1 (Fisher et al., 1998).

FOXP2 is the critical gene within SPCH1

SPCH1 contains several genes that, when mutated, could possibly cause abnormal neurodevelopment, but before the causative mutation could be localized to a single gene, a detailed sequence map of 7q31 was needed (Lai et al., 2000). In 2000, Lai and Fisher set out to finely map 7q31 and identify a microdeletion present in affected KE family members. By bioinformatically analyzing 152 sequence tagged sites, or short 200 to 500 bp regions of the genome with known locations and sequences, known to reside within 7q31 and previously sequenced YAC, BAC, and PAC contigs, Lai and Fisher assembled a detailed sequence map of SPCH1 (Lai et al., 2000). With this information in hand, chromosomes of the affected individuals were screened for sequence tagged sites within SPCH1, the absence of which would suggest a microdeletion (Lai et al., 2000). No microdeletions were identified, however, so an even finer map of SPCH1 was generated using novel polymorphic markers derived from the SPCH1 sequence. This map refined the SPCH1 interval further and excluded four candidate genes. The gene within SPCH1 that was likely responsible for proper speech and language formation was located after identification of a patient, know as CS, with a

translocation break point within SPCH1 who was diagnosed with verbal dyspraxia similar to that exhibited by the KE family. The translocation disrupted the *CAGH44* locus, a previously localized, brain-expressed gene encoding a long polyglutamine tract (Lai et al., 2000).

Unfortunately, only 869 bases on the 5' side of the open reading frame of *CAGH44* had been determined at the time that *CAGH44* was implicated as a speech and language gene, and no mutation in this piece of known sequence was identified in the affected KE family members (Lai et al., 2000). Thus, Lai and Fisher's next pursuit was to determine the full sequence of *CAGH44* and search for the causative mutation. In October 2001, Lai and Fisher published the full sequence of *CAGH44*, and found that the sequence matched that of a newly identified member of the winged-helix/forkhead box family of transcription factors, *FOXP2*, which had been cloned from mouse cDNA only months earlier (Lai et al., 2001, Shu et al., 2001). Shu *et al.* showed that *FOXP2* was expressed in developing mouse lung, intestines, heart and nervous system, and that it acted as a transcriptional repressor (Shu et al., 2001). Lai and Fisher localized the CS translocation to the intron between exons 3b and 4 of *FOXP2*, and were finally able to detect a G-to-A point mutation which causes an R553H substitution in the forkhead DNA-binding domain of affected KE family members (Lai et al., 2001). Thus, *FOXP2* was the first gene to be implicated in speech production and language learning.

FoxP2 is expressed in brain regions important for speech and language production

Once the sequence of *FoxP2* was known, it became possible to determine FoxP2 transcript and protein localization in the brain. Strengthening the hypothesis that

FoxP2 is important for speech production and language learning, brain regions including the cortex, thalamus, basal ganglia and cerebellum, which form the circuits responsible for proper speech and receptive and expressive language, were found to be FoxP2 positive (Barbas et al., 2013, Konopka and Roberts, 2016). In one model of language processing, for example, speech sounds are received in in the cortex in the auditory regions of superior temporal gyrus (including Wernike's area) and the superior temporal sulcus bilaterally (Hickok et al., 2011). Subsequently, input to those regions is passed through dorsal, left-side biased frontal cortical circuits supporting sensorimotor integration and articulation which involve the parietal-temporal junction, the inferior frontal gyrus (Broca's area) and premotor cortex (Hickok et al., 2011). Simultaneously, the initial input flows through a ventral, temporal stream that supports speech comprehension, and these dorsal and ventral circuits, along with other more widely distributed cortical regions important for semantic processing, feed back on one another to control language comprehension and speech production (Hickok et al., 2011). These cortical streams send input directly to the striatum, and that message is then filtered through the globus pallidus, on either the direct or indirect pathway, to the thalamus which closes the loop by sending excitatory input back to the frontal cortex (Barbas et al., 2013). Disruption of these corticostriatal-thalamocortical loops interferes with motor and cognitive processing essential for language (Barbas et al., 2013). Moreover, the cerebellum has been associated with both motor and cognitive aspects of language, and it, too, forms connections through the thalamus to the frontal cortex (Konopka and Roberts, 2016, Murdoch, 2010). Expression of FoxP2 in the cortex, basal ganglia,

thalamus and cerebellum, detailed below, further suggests a role for Foxp2 in the development or language circuits.

FoxP2 in the cortex

In the developing mouse, Foxp2 mRNA and protein are consistently shown to be expressed in the deep layers of the cortical plate during cortical development as early as E14.5 (Ferland et al., 2003, Takahashi et al., 2003, Lai et al., 2003). Interestingly, Ferland *et al.* specifically mention *Foxp2* expression in the subplate, but they do not distinguish between the subplate and cortical plate in their figures (Ferland et al., 2003). Takahashi *et al*., on the other hand, do demark the subplate zone in their figures, and while the overlaying cortical plate expresses *Foxp2*, expression is not detectable in the subplate zone (Takahashi et al., 2003). *Foxp2* expression is not observed in the intermediate or marginal zones (Ferland et al., 2003, Takahashi et al., 2003, Lai et al., 2003). Unlike expression in post mitotic neurons, *Foxp2* expression in ventricular zone is controversial. *Foxp2* transcript is detected at low levels in mouse embryos between E12 and E17 but no protein is detected in this region (Ferland et al., 2003). However, Tusi *et al*. observed Foxp2 protein in cultured cortical progenitor cells, and Takahashi showed sparse *Foxp2* expression in the cortical subventricular zone (Takahashi et al., 2003, Tsui et al., 2013).

In developing human cortex, like in mouse, *in situ* hybridization showed *FOXP2* expression in the cortical plate, but this method did not detect expression in germinal layers (Lai et al., 2003). Expression microarray data derived from mRNA collected from laser micro-dissected developing cortical layers confirmed that *FOXP2* is highly expressed subplate and inner cortical plate. However, the method also detected

expression in the ventricular zone (Miller et al., 2014). In fact, while *FOXP2* expression across the entire developing cortex is correlated with the subplate, when anterior cortical subregions are isolated it correlates best with the ventricular zone (Miller et al., 2014). This suggests that, in humans, FOXP2 might play a role in the transition between neural progenitor and post mitotic neuron.

In the postnatal and adult mouse cortex, *Foxp2* expression is restricted to a subpopulation of projection neurons in layer VI, though it is expressed in a few layer V neurons in the motor cortex and hindlimb and forelimb regions of the primary somatosensory cortex (Ferland et al., 2003, Hisaoka et al., 2010). In the cortex, Foxp2 is present in GluR1^{-}/GluR2/3^{+} exhibitory projection neurons, but is not detected in interneuron populations (Hisaoka et al., 2010). Additionally, all Foxp2^{+} neurons in layer VI express DARPP-32 (Hisaoka et al., 2010). In layer V, Foxp2 neurons are Ctip2^{+} suggesting that they project to the spinal cord, while, in layer VI, they represent a subpopulation of Tbr1^{+} corticothalamic projection neurons (Hisaoka et al., 2010). These expression patterns suggest that FoxP2 is important for the development, and potentially the maintenance, of a subpopulation of excitatory projection neurons.

FoxP2 in the basal ganglia

In developing mouse brain at embryonic day (E) 13, *Foxp2* transcript is detectable in what is presumably the differentiated zone of the ganglionic eminence, and by E14 strong expression of *Foxp2* in the differentiated mantle zone of the of the lateral ganglionic eminence (LGE) is observed with weak expression in cells of the ganglionic eminence subventricular zone (SVZ) (Ferland et al., 2003, Takahashi et al., 2003). However, no *Foxp2* expression was seen in the medial ganglionic eminence

(MGE). At E16, *Foxp2* expression remains at high in the LGE derived dorsal striatum in mantel zone and is lower in the SVZ (Ferland et al., 2003, Takahashi et al., 2003). The pallidum, which is derived from the MGE, is unsurprisingly devoid of *Foxp2* mRNA (Takahashi et al., 2003). In neonatal mice, *Foxp2* in the striatum is more highly expressed in the striosome compartment of the striatum than the matrix compartment, and this expression pattern remains stable in the adult animal (Takahashi et al., 2003). Moreover, using mice expressing GFP in either D1 receptor expressing or D2 receptor expressing spiny projection neurons it was determined that Foxp2 does not co-localize with striatal interneurons but is expressed in both D1 and D2 spiny projection neurons with comparatively higher expression in D1 expressing neurons (Vernes et al., 2011).

Three studies find Foxp2 mRNA and/or protein in the shell of the nucleus accumbens (Ferland et al., 2003, Takahashi et al., 2003, Lai et al., 2003), while a third study showed that dopaminergic neurons in the nucleus accumbens lack Foxp2 expression (Wijchers et al., 2006b). Moreover, this study did not show co-localization between markers of dopaminergic neurons and Foxp2 in any brain region including the ventral tagmental area (Wijchers et al., 2006b).

FOXP2 expression patterns in developing human basal ganglia are consistent with those in mouse. Diffuse expression was observed in the caudate nucleus starting at Carnegie stage 23 corresponding to the end of post conception week 8 (Lai et al., 2003). Moreover, *FOXP2* transcript was detected in the nucleus accumbens (Lai et al., 2003). These expression patterns imply a conserved role for FoxP2 in the developing basal ganglia.

FoxP2 expression in thalamus and hypothalamus

At E13 in mouse and Carnegie Stage 23 in human *FoxP2* transcript is seen in the medial region of the hypothalamus and the thalamus (Lai et al., 2003). During the early thalamic development in mouse (E12-E14) *Foxp2* expression is graded in the thalamic primordium in the with greater expression posteriorly than anteriorly (Ebisu et al., 2016). Later, in mouse at E16.5 and human fetal stage 1, expression in these regions increases further (Lai et al., 2003), but the graded pattern is lost (Ebisu et al., 2016). In the adult mouse, it is clear that Foxp2 is expressed in a subset of thalamic nuclei, such as in the paraventricular and lateral posterior thalamic nuclei, the habenula, the medial and lateral geniculate, and a variety of dorsal thalamic nuclei. Moreover, Foxp2 transcript is present in neurons in the paraventricular nucleus of the hypothalamus while no $Foxp2^{+}$ neurons are seen in the ventromedial nucleus (Ferland et al., 2003).

FoxP2 in hindbrain

In both mouse and human *FoxP2* is highly expressed in discrete regions of the cerebellum. At E13.5 and Carnegie stage 23 *FoxP2* can already be detected in the alar plate of the cerebellar primordium (Lai et al., 2003). At E16.5 in mouse and fetal stage S1 in human the deep cerebellar nuclei and Purkinje cells in piriform layer were found to be *FoxP2* positive, but no cells in the molecular layer or the granular layer expressed *FoxP2* (Lai et al., 2003). In postnatal and adult mouse cerebellum, high *Foxp2* expression restricted to Purkinje cell is maintained (Ferland et al., 2003); however, in humans this expression decreases dramatically after birth (Kang et al., 2011, Usui et al., 2014).

In mouse and human *FoxP2* expression is first observed in the myelencephalic part of the rhombencephalon, precursor to the medulla oblongata (Lai et al., 2003). Later, expression is observed in the medullary raphe and in restricted areas of the medulla oblongata. By E16 in mouse, it becomes clear that these regions of discrete expression are the developing in inferior olives, and expression here persists throughout adulthood (Lai et al., 2003, Ferland et al., 2003). Neurons in the inferior olives send excitatory projection neurons to Purkinje cells and this circuit is important for coordination and timing of motor control (Lai et al., 2003).

Altered brain morphology and activity in affected KE family members

In the late nineties and early 2000s, both the effected and unaffected members of the KE family generously gave their time to participate in studies that uncovered potential structural and functional brain alterations that contributed to the speech and language disorder caused by a mutation in *FOXP2*. Combine, the studies showed altered morphology and activity in areas where *FOXP2* is expressed during development including the basal ganglia, cerebellum, and several cortical regions including Broca's and Wernike's areas (Belton et al., 2003, Vargha-Khadem et al., 2005, Vargha-Khadem et al., 1998, Watkins et al., 2002b). These findings, summarized here, suggest that altered FOXP2 function during development leads to abnormal morphology and/or function in regions where the gene is usually expressed.

Altered brain morphology in affected KE family members

Three studies undertaken by Vargha-Khadem and colleagues aimed to detect altered brain morphology in the affected KE family members (Vargha-Khadem et al., 1998, Belton et al., 2003, Watkins et al., 2002b) with two *a priori* hypotheses. Firstly,

based on the behavioral phenotype of the affected individuals they hypothesized that the aberrant brain regions would be in motor system. Secondly, they hypothesized that the differences from controls would be bilateral. Speech disorders caused by unilateral lesions during development often resolve themselves overtime as neural circuits in the unaffected lobe reorganize (Vargha-Khadem et al., 1985). However, affected KE family members remain impaired throughout their lives, suggesting the disruption of speech and language circuits bilaterally (Vargha-Khadem et al., 2005). To test these hypotheses, the studies used an MRI data set collected from affected and unaffected KE family members and normal, unrelated controls. They used voxel-based brain morphometry to compare gray matter volumes between affected KE family members and unaffected members and/or controls on a voxel-by-voxel basis. While each study used different statistical techniques, all three studies identified volumetric differences in the basal ganglia and various cortical regions including many regions previously identified to be important for speech and language production such as Broca's and Wernike's areas (Vargha-Khadem et al., 1998, Belton et al., 2003, Watkins et al., 2002b). These volume changes correspond well the FoxP2 expression in the striatum and cortex.

Perhaps the most intriguing result of these studies is the correlation between the volume of the caudate nucleus and behavior (Watkins et al., 2002b). Across all analyses, reduced gray matter volume was observed in this region in the affected KE family members compared to unaffected (Belton et al., 2003, Vargha-Khadem et al., 1998, Watkins et al., 2002b). When the volume of the left caudate nucleus was compared to the right, the asymmetry between the two correlated with the subject's

score in a test for non-verbal facial movements, such that a smaller left caudate nucleus corresponded to a greater impairment (Watkins et al., 2002b). Thus, the reduction in caudate nucleus volume could be responsible for orofacial dyspraxia, the inability to rapidly form the complex facial movements necessary for speech, a major component of the KE family disorder.

Interestingly, though *FoxP2* expression is high in the deep cerebellar nuclei and in Purkinje cells, decreased cerebellar volume compared to unaffected family members was only detected in the ventral cerebellum lobule with a statistical method designed to specifically uncover bilateral volume differences (Belton et al., 2003). The significance of the decrease did not survive correction for multiple comparisons (Belton et al., 2003). Moreover, decreased cerebellar gray matter was observed unilaterally in the left anterior cerebellum in both affected and unaffected KE family members compared to unrelated controls, suggesting that while the ventral cerebellum lobule may be particularly important for speech and language formation, other regions of the cerebellum may be aberrant in the KE family in general (Belton et al., 2003).

Abnormal brain activity exhibited by affected KE family members

In addition to analyzing the brain morphology of the KE family, Vargha-Khadem's group carried out studies of the activity patterns in the KE family during speech related tasks (Liegeois et al., 2003, Liegeois et al., 2011, Vargha-Khadem et al., 1998) and found aberrant activity in areas where FOXP2 is expressed during development. For example, in one test affected and unaffected family members were asked to repeat aloud words being read to them while positron emission tomography (PET) scans were taken. A baseline condition wherein subjects were instructed to repeat one specified

word when they heard reversed words was also recorded, and the subtraction of these two signals allowed activity in the major speech and language areas of the left hemisphere to be visualized (Vargha-Khadem et al., 1998). Because both tasks required acoustic processing and motor output, activity related to these aspects of speech could be filtered out of the analysis (Vargha-Khadem et al., 1998). They found differential activity in several cortical regions including increased activity in Broca's area and premotor cortex, areas typically activated when normal subjects are required to generate words fluently, reflecting possible compensatory mechanisms (Vargha-Khadem et al., 1998). Moreover, the left caudate nucleus was overactive compared to controls and was the only differentially active region found in corresponding MRI data to have structural abnormalities solidifying the importance of FOXP2 in the basal ganglia for speech and language development (Vargha-Khadem et al., 1998).

Liegeois and colleagues also studied the brain activity of affected KE family members during a word repetition task, but used fMRI instead of PET (Liegeois et al., 2003). Moreover, the baseline condition used in this study differed from the PET analysis. While the PET study filtered out activity required for acoustic processing and motor output, the fMRI study used resting while listening to white noise as the baseline condition (Liegeois et al., 2003, Vargha-Khadem et al., 1998). Differences in the results of these studies could be attributed to differences in the data collection techniques as well as the differing baseline conditions. For example, while activity in Broca's areas was increased in affected family members in the PET study, the fMRI study showed a decreased activity in this region (Liegeois et al., 2003, Vargha-Khadem et al., 1998).

Surprisingly, this study did not identify differential activity in the caudate nucleus (Liegeois et al., 2003). Liegeois and colleagues reported that task itself did not reliably activate this region in either group. However, the previous PET study did report decreased caudate nucleus activity during the word repetition task suggesting that filtering out activity associated with acoustic processing and motor output highlights aberrant caudate nucleus function tied to the phonological analysis and reformulation of speech sounds necessary for articulation plans (Vargha-Khadem et al., 1998), while a resting control does not. Still, activity in another basal ganglia component where FOXP2 is expressed, the putamen, was reported to be decreased (Liegeois et al., 2003).

While the previous studies analyzed activity during known word repetition, a deficit in the ability to repeat non-word utterances is a defining characteristic of the KE family disorder (Belton et al., 2003, Vargha-Khadem et al., 1995, Watkins et al., 2002a). Thus, comparisons of fMRI activity between affected KE family members and unrelated controls matched for age, sex and handedness during a non-word repetition task were valuable for understanding the functional underpinnings of this phenotype (Liegeois et al., 2011). As in the word repetition fMRI study, this analysis used resting during white noise as the baseline condition (Liegeois et al., 2011). This time, Liegeois and colleagues showed that, unlike in tasks of known word production (Liegeois et al., 2003, Vargha-Khadem et al., 1998), activity in Broca's area in affected KE family members was consistent with controls (Liegeois et al., 2011). However, regions involved in motor sequence planning (anterior cingulate, and supplementary motor area) and speech production regions including the pre-central gyrus were found to be underactive (Liegeois et al., 2011). Outside of the cortex the putamen was, again, found to have

reduced activation, and, importantly, this is the only functional study to show aberrant activation in the cerebellum where FOXP2 is highly expressed during development. Specifically, during non-word repetition tasks the hem of left lobule IX was under activated (Liegeois et al., 2011).

Using fMRI, the activity patterns underlying overt verb generation (where verbs were spoken aloud in response to nouns), covert verb generation (where subjects thought of verb responses but the responses were not spoken aloud) were analyzed (Liegeois et al., 2003, Liegeois et al., 2011). These tasks differed from previous word and non-word repetition tasks in that subjects were required to independently generate a word rather than repeating a supplied word highlighting activity patterns involved in word retrieval. In the covert task, unaffected family members showed stereotypical, left-sided activity in Broca's area whereas the affected family members showed no activity in this region. Instead, when supplying verbs covertly, more bilateral and posterior and cortical activity was observed in affected family members similar to the activity pattern observed in the word repetition task fMRI (Liegeois et al., 2003). Moreover, Wernike's area was shown to be overactive, further suggesting that aberrant FOXP2 function during cortical development leads to impaired cortical circuitry (Liegeois et al., 2003, Vargha-Khadem et al., 2005). The putamen was also underactive in this task (Liegeois et al., 2003). Because the verbs supplied by the subjects in this task were not spoken, these data suggest that the affected KE family members have language impairments that are separate from their ability to speak.

During the overt verb task, activity patterns in unaffected family members were similar to the covert task. Unlike during the covert task, affected family members did

display activity in Broca's area. This activity, though detectable, was still significantly decreased compare with controls. In addition, there was no over-activation of Wernike's area, or any other region, in the overt task (Liegeois et al., 2003). Thus, Liegeois found Broca's areas to be underactive during tasks of word retrieval regardless of the word being spoken out loud and during word repetition tasks. Posterior regions that are not usually involved in language, including the postcentral, posterior parietal and occipital regions, are more active in affected family members during tasks of word retrieval if the word is not spoken out loud and during word repetition tasks (Liegeois et al., 2003, Vargha-Khadem et al., 2005). Moreover, while controls have left side activation in covert retrieval tasks and bilateral activation in word repetition tasks, affected family members exhibit bilateral activation in both tasks (Liegeois et al., 2003). Notably, while affected KE family members are deficient word and non-word repetition tasks, they have little trouble with single-word finding compared to control (Liegeois et al., 2003).

Overall, various speech and language tasks, when performed by effected members of the KE family, elicit aberrant activity in the cerebellum, basal ganglia, and various cortical subregions including Broca's and Wernike's areas. FOXP2 is expressed in all of these regions during normal development. Thus, aberrant FOXP2 function during development leads to irregular morphology and activity patterns in regions where FOXP2 is expresses, which suggests that FOPX2 lays the groundwork for proper speech and language pathways during brain development. However, questions still exist as to how FOXP2 performs this role.

Foxp2 loss of function animal models

In order to further understand the how FoxP2 exerts control over language circuitry, several groups created Foxp2 loss of function animal models. While animal model systems do not use language to communicate, they have been important for appreciating the functions of FoxP2 in mammalian brain development and in avian vocal learning.

Strategies for studying Foxp2 loss of function in mice

Several Foxp2 loss of function mouse models have been generated using various techniques (Shu et al., 2005, French et al., 2007, Groszer et al., 2008, Fujita et al., 2008, Usui et al., 2017). For example, the first published Foxp2 loss of function mouse model was a targeted knockout mouse in which homologous recombination was used to replace exons 12 and 13 with a neomycin cassette (Shu et al., 2005). Genetically, this disrupted the forkhead DNA-binding domain; however, no protein was expressed in the full knockout animal suggesting nonsense-mediated decay of the transcript (Shu et al., 2005). Additionally, gene-driven N-ethyl-N-nitrosourea (ENU) mutagenesis screening identified two mutations in Foxp2 that approximated mutations causative of verbal dyspraxia in humans: R552H, which is the mouse version of the KE family mutation, and S321X which causes a premature stop codon close to the human R328X mutation identified in another family with FOXP2-related verbal dyspraxia (Groszer et al., 2008, MacDermot et al., 2005, Lai et al., 2001). Foxp2 protein was detectable in the R552H double positive mutants, but not in the S321X double positive mutants suggesting that this mutation creates a null allele (Groszer et al., 2008). Moreover, Fujita and colleagues published a study using a targeted *Foxp2*-R552H knockin mouse (R552H-KI) (Fujita et al., 2008). Finally, a conditional *Foxp2* null mouse

was created by flanking exons 12 through 14 with *lox*P sites; however, the only published data using this model is a proof of principle cross with a *Sox2-Cre* which leads to *Foxp2* deletion throughout the early embryo (French et al., 2007). All of these full-body, *Foxp2* homozygous loss of function mice die between three and four weeks after birth and weigh less than wild type litter mate controls (Shu et al., 2005, French et al., 2007, Groszer et al., 2008, Fujita et al., 2008). Other phenotypes are described in detail below.

Abnormal cerebellar morphology

The most obvious gross morphological defect across full-body *Foxp2* homozygous null animals is decreased cerebellar size and foliation suggesting that *Foxp2* expression is crucial for proper cerebellar development (French et al., 2007, Groszer et al., 2008, Fujita et al., 2008). In null models on crossed onto pure C57Bl/6 or C3H backgrounds (French et al., 2007, Groszer et al., 2008), no alterations in cerebellar histoarchitecture were observed; however, when mutants were crossed to a mixed background fewer Purkinje cells were present in the Purkinje cell layers, and some existing Purkinje cells were misplaced in the granule cell layer (Shu et al., 2005, Fujita et al., 2008). Moreover, Purkinje cell dendritic arbors were less elaborate suggesting that Foxp2 plays an important role in Purkinje cell development and morphology (Shu et al., 2005, Fujita et al., 2008). Interestingly, *in utero* electroporation of shRNA directed against *Foxp2* specifically in Purkinje cells similarly reduced their dendritic length and branching but not cerebellar size generally (Usui et al., 2017). The *in utero* electroporation was performed by microinjecting shRNAs into the fourth ventricles of embryonic day 12.5 embryos to target Purkinje cells specifically. This reduced the

amount of *Foxp2* expression in the cerebellum by 40% suggesting that either earlier knockdown of *Foxp2* or *Foxp2* knockdown in more cells is required to affect cerebellar size generally (Usui et al., 2017).

Supporting the idea that total Foxp2 loss of function may be necessary to decrease cerebellar size, heterozygous *Foxp2* mutants have normal gross cerebellar morphology (French et al., 2007, Groszer et al., 2008, Fujita et al., 2008). Heterozygotes in the mixed genetic background, however, did display fewer Purkinje cells in the folia, but the defect in dendritic arborization was not as severe as that in the homozygous mutants (Shu et al., 2005, Fujita et al., 2008). While the affected KE family members have decreased gray matter in certain cortical areas and in the caudate nucleus, no overt cortical or striatal structural abnormalities were observed in Foxp2 null mice (Belton et al., 2003, Vargha-Khadem et al., 1998, Watkins et al., 2002b, Shu et al., 2005, French et al., 2007, Groszer et al., 2008, Fujita et al., 2008). All together, these data suggest that at least one copy of *FoxP2* is necessary for development of the cerebellum.

Abnormal thalamic development and cortical barrel morphology

In the developing thalamus between E12.5 and E14, Foxp2 is expressed in a gradient with high expression in the posteriorly and low expression anteriorly (Ebisu et al., 2016), suggesting that controlled levels of Foxp2 expression during development could be important for the proper formation of thalamic nuclei. Indeed, Ebisu and colleagues showed that the ventral posterior nucleus of the thalamus is reduced in size in Foxp2-R552H mice, while the intermediate regions are expanded (Ebisu et al., 2016). Neurons from intermediate regions project to the prefrontal cortex, and in Foxp2-R552H

mice increased numbers of projections from these regions to the prefrontal cortex were observed compared to wild type mice (Ebisu et al., 2016). Conversely, neurons in the posterior nucleus project to the primary somatosensory cortex, and projection neurons in this region were largely absent (Ebisu et al., 2016). Moreover, neurons in the ventral posterior nucleus form barreloid patterns in the thalamus and project into the barrel fields of the primary somatosensory cortex (Van Der Loos, 1976). In Foxp2-R552H mice, both barreloid patterns in the thalamus and barrel patterns in the cortex were disrupted (Ebisu et al., 2016). Taken together, these data suggest an important role for Foxp2 in the development of thalamic nuclei and in the proper targeting of thalamocortical axons (Ebisu et al., 2016).

Abnormal motor and auditory association learning

The cerebellar circuitry has long been known to play a role in motor control (Manto et al., 2012). Perhaps, then, it is unsurprising that all of the Foxp2 loss of function mouse models display severe motor impairments along with cerebellar abnormalities (Shu et al., 2005, French et al., 2007, Groszer et al., 2008, Fujita et al., 2008, Usui et al., 2017). For example, all of the homozygous mutants have impaired righting reflexes as neonates (Shu et al., 2005, French et al., 2007, Groszer et al., 2008, Fujita et al., 2008). Homozygous targeted knockout neonates also underwent the negative geotaxis test and were similarly impaired in this motor task (Shu et al., 2005). Interestingly, *Foxp2* knockdown by shRNA specifically in Purkinje cells also leads to impairment in righting reflex and negative geotaxis, suggesting that Purkinje cell abnormalities drive this motor phenotype (Usui et al., 2017). Moreover, Usui and colleagues found that these phenotypes could be rescued with wild type FOXP2, but not

with a version of FOXP2 that could not be sumoylated at K674, suggesting that this post-translational modification is necessary for FoxP2 function in the cerebellum (Usui et al., 2017).

Heterozygous neonates were able to perform normally in the righting reflex test by at least P15, but as adults ENU generated R552H heterozygotes were impaired in tests for motor learning (Shu et al., 2005, French et al., 2007, Groszer et al., 2008, Fujita et al., 2008). For example, when provided with a tilted voluntary running-wheel, all mice run in short bursts on the first day of exposure, and wild type mice increase running bout length and decrease number of bouts rapidly on the second day (Groszer et al., 2008). While heterozygotes looked the same as controls on day one and eventually reached equal levels of proficiency on the wheel, they were slower to learn, taking a longer time to decrease bout number and increase bout length than wild type animals (Groszer et al., 2008). Similar results were found using the accelerating rotarod task, another test for motor learning. On the first the first trials, heterozygotes and controls had similar performance levels, and while wild type mice progressed as expected, mutant mice improved at significantly slower rates before reaching proficiency (Groszer et al., 2008). Because *Foxp2*-R552H heterozygotes do not have overt motor deficits, these experiments suggest that loss of Foxp2 function plays a role in motor learning.

Because auditory learning is crucial for language formation, Kurt and colleagues tested whether *Foxp2*-R552H and -S321X heterozygotes had reduced ability to make auditory-motor associations (Kurt et al., 2012). The authors had previously shown that these mice had alterations in auditory brainstem response audiometry parameters

which are used to measure sound-evoked bioelectrical potentials and identify hearing deficits (Kurt et al., 2009). While affected members of the KE family have not been shown to have hearing impairment, mice heterozygous for the analogous mutation show evidence of impaired synaptic transmission along auditory pathways that could lead to problems with auditory processing (Kurt et al., 2009). With this in mind, Kurt and colleagues trained *Foxp2*-R552H and -S321X heterozygotes to cross a hurdle separating two sides of a box in response to a 12 Hz tone and to abstain from crossing when a 7 Hz tone was played (Kurt et al., 2012). As in the voluntary wheel running and rotarod tasks (Groszer et al., 2008), both strains of mice took longer to master the motor task of spontaneously crossing the hurdle before an auditory association component was added (Kurt et al., 2012). Wild type mice were able to discriminate between the 12 and 7 Hz tones on day one, while R552H heterozygotes took up to 20 days to learn to distinguish the tones and S321X heterozygotes never reached wild-type levels of proficiency (Kurt et al., 2012). Importantly, while motor learning is clearly affected in Foxp2 loss of function mice, heterozygous knockouts perform normally in another cognitive task, the Morris water maze, implying that loss of Foxp2 does not affect learning generally (Shu et al., 2005). These data support a specific role for Foxp2 in motor learning and further suggest a role for auditory-motor associations that could be relevant for language acquisition in humans (Kurt et al., 2012).

Altered mouse vocalizations

Perhaps the most exciting phenotypes studied in Foxp2 loss of function mouse models involve rodent communication (Castellucci et al., 2016, Chabout et al., 2016, Gaub et al., 2016, Usui et al., 2017, Shu et al., 2005, French and Fisher, 2014, Groszer

et al., 2008, Fujita et al., 2008). While modeling a human-specific trait like language is challenging, many rodents, including mice and rats, communicate using ultrasonic vocalizations (Lepp et al., 2013). For example, rodent pups produce ultrasonic isolation calls when separated from the dam, and adult mice vocalize during mating and other social interactions.

Ultrasonic isolation calls are innate calls emitted by postnatal mice from birth to P14 upon separation from the dam (Ehret, 2005, Hahn et al., 1998). The calls include whistle-like sounds with frequencies between 30 and 90 kHz and clicking sounds that have been shown to be functionally useful in eliciting maternal approach and retrieval (Ehret, 2005, Hahn et al., 1998, Hahn and Lavooy, 2005, Lepp et al., 2013). Notably, homozygous Foxp2 mutant pups produce few spontaneous isolation calls compared to controls (Shu et al., 2005), and in some cases they produce no calls at all, only clicks (Fujita et al., 2008, Groszer et al., 2008). Additionally, as with the neonatal motor deficiencies, spontaneous isolation calls were reduced when *Foxp2* was knocked down by shRNA specifically in Purkinje cells (Usui et al., 2017). Foxp2 sumoylation was also implicated in formation of ultrasonic isolation calls as expression of wild type FOXP2 in Purkinje cells rescued the reduction in calls while expression of a version of FOXP2 that could not be sumoylated at K674 did not (Usui et al., 2017). Thus, expression and proper post-translational modification of Foxp2 in Purkinje cells is critical for the production of ultrasonic isolation calls.

In order to test if the lack of calls was due to reduced arousal or a complete inability to produce calls due to motor deficits, Groszer and colleagues lifted the pups a short distance above the ground in order to increase pup stress and initiate louder,

longer calls (Groszer et al., 2008). Under these conditions, R552H homozygotes were able to generate audible distress calls and complex ultrasonic calls; however, fewer ultrasonic calls with lower sound pressure and shorter duration were emitted by homozygous mutants than heterozygotes or control animals suggesting that while homozygotes are able to produce ultrasounds they seem to be less motivated to do so (Groszer et al., 2008).

Mirroring the Purkinje cell morphology deficit, heterozygous mutants only showed deficits in spontaneous isolation calls on a mixed genetic background, making fewer, shorter calls than control animals (Shu et al., 2005, Fujita et al., 2008). Interestingly, when Fujita-Jimbo and Momoi expressed wild type *Foxp2* specifically in Purkinje cells by using a BAC transgenic mouse in which *Foxp2* expression was under the control of the Pcp2/L7 promoter, they were able to rescue the decrease in call duration exhibited by R552H knockin heterozygotes (Fujita-Jimbo and Momoi, 2014). However, they were unable to rescue the complete loss of calls by the homozygous mutants suggesting that Foxp2 in Purkinje cells alone is not sufficient for call production (Fujita-Jimbo and Momoi, 2014). It would be interesting to see if rescue in Purkinje cells could ameliorate differences in call structure in homozygotes when the pups are under increased stress, a condition in which the homozygotes actually produce vocalizations (Groszer et al., 2008).

The ultrasonic vocalizations of adult mice can also be used to assess communication phenotypes in mouse models. For example, male mice produce ultrasonic calls reminiscent of bird song when exposed to female mice or their urine (Holy and Guo, 2005, Lepp et al., 2013). Although it is believe that these calls are

innate, they contain multiple syllable types repeated in a nonrandom order; thus, they are referred to as mating “songs” (Holy and Guo, 2005, Lepp et al., 2013). Moreover, the songs have functional value during mating as female mice have been shown to prefer vocalizing males to devocalized males and to lose preference for male songs after ovariectomy (Pomerantz et al., 1983, Lepp et al., 2013). Additionally, during playback experiments, female mice exhibited approach behavior when exposed to male songs, but not to artificial control whistles or playbacks of pup isolation calls (Hammerschmidt et al., 2009).

Three separate studies of the vocalizations of adult male mice harboring heterozygous *Foxp2* mutations have been performed, and all three studies exposed male mice to live female mice and/or urine from female mice (Gaub et al., 2016, Castellucci et al., 2016, Chabout et al., 2016). Mice heterozygous for *Foxp2*-R552H (Chabout et al., 2016) or with heterozygous *Foxp2* knockout (Castellucci et al., 2016) on the same C57BL/6J background had calls with normal duration and frequency modulation compared with wild type mice when they were exposed to live females. However, when Gaub and colleagues exposed *Foxp2*-R552H heterozygotes crossed to a different strain (C3H/HenNHsd rather than C57BL6/J) to female urine, they observed increased syllable duration and peak sound pressure (Gaub et al., 2016). Moreover, in response to female urine, their calls had a higher occurrence rate of overtones/harmonics and complex frequency jump types compared to wild type animals, suggesting that more information was carried in each call (Gaub et al., 2016). Because these parameters changed not only in comparison to wild type mice, but also in comparison to exposure to water instead of urine (which was not the case with wild

type mice), the authors suggest that “the (heterozygous) animals either were in a state of higher positive emotion and/or expressed a given emotional state more intensely than the (wild type) group when emitting USVs to female urine” (Gaub et al., 2016).

Conversely, the complexity of the songs of heterozygous Foxp2 loss of function mice on the C57BL6/J background is decreased compared to wild type (Chabout et al., 2016, Castellucci et al., 2016). R552H heterozygotes have shorter sequences, overall, when exposed to female urine or live females compare to wild type (Chabout et al., 2016). Additionally, when exposed to a live female, heterozygous *Foxp2* knockouts produced fewer syllables per minute and per bout than controls (Castellucci et al., 2016). Moreover, the proportion between complex (two or more complex syllables) and simple sequences (one or no complex syllables) is greater with live females than conditions without live females in wild type C57BL6/J mice, but this increase is not seen in R552H heterozygotes (Chabout et al., 2016). Similarly, heterozygous knockouts produced fewer complex syllables than wild type animals when exposed to females (Castellucci et al., 2016). These two studies suggest that heterozygous loss of Foxp2 function decreases song complexity in adult male mice (Chabout et al., 2016, Castellucci et al., 2016).

Differences in the outcomes of the three adult mouse vocalization studies could reflect differences in genetic background, behavioral paradigms, data analysis, and/or statistical methods. Regardless, even though it is thought that these vocalizations are innate, unlike human language (Arriaga and Jarvis, 2013, Arriaga et al., 2012), alterations of the ultrasonic calls emitted by neonatal and adult Foxp2 loss of function

mouse models prove that Foxp2 plays a role in the genetic basis of vocal communication (Lepp et al., 2013).

Abnormal striatal and cerebellar synaptic plasticity

Abnormal striatal and cerebellar physiology caused by loss of Foxp2 function may underlie the motor learning and communication deficits exhibited by mutant animals (Groszer et al., 2008). For example, strongly impaired long-term depression (LTD) was observed in dorsolateral striatum of R552H heterozygotes (Groszer et al., 2008). Moreover, as discussed, the R552H heterozygotes are impaired in the rotarod motor leaning task (Groszer et al., 2008). Importantly, dorsolateral striatum had already been implicated in motor learning on the accelerated rotarod in mice, and the putamen, part of the dorsal striatum in human, is underactive in affected KE family members during language related tasks (Groszer et al., 2008, Liegeois et al., 2003).

Additionally, though the cerebellums of R552H heterozygotes were grossly normal, inputs from the granule neuron parallel-fiber inputs onto Purkinje cells displayed enhanced paired pulse facilitation along with subtle differences suggesting faster induction of parallel-fiber to climbing fiber LTD (Groszer et al., 2008). These results suggest that while the heterozygous mutants display normal brain morphology, changes in cortico-striatal and cerebellar synaptic plasticity caused by Foxp2 loss of function could be responsible for their learning deficits.

Songbirds model the role of Foxp2 in vocal learning

As described above, Foxp2 loss of function mouse models have been used to prove that Foxp2 is important for motor learning and rodent communication, but not to show that Foxp2 is necessary for learning to communicate. This task has proven difficult

in mouse models because there is conflicting evidence on whether or not mice are vocal learners (Arriaga and Jarvis, 2013). Certain species of songbirds, on the other hand, learn songs similarly to how humans learn speech by depending on auditory feedback during a critical period of development (Arriaga and Jarvis, 2013). For example, young male zebra finches, the most studied songbird, learn a song by imitating a tutor and then practicing the memorized tutor song alone until the song is perfected and crystalized (Fisher and Scharff, 2009). This process is accomplished through specialized brain circuits of which, much like in humans, the striatum is a critical component (Fisher and Scharff, 2009).

Localization of FoxP2 expression is largely conserved between birds and mammals, and, as in mouse and humans, FoxP2 is highly expressed in the songbird striatum (Haesler et al., 2004). Interestingly, Foxp2 increases in a particularly critical striatal sub-region in the bird, Area X, during the song learning critical period suggesting that it plays a role in this process (Haesler et al., 2004). Knockdown of FoxP2 specifically in Area X in young zebra finches before the critical song-learning window lead to incompletely replicated tutor songs in adult birds (Haesler et al., 2007). Later, it was found juvenile birds with *FoxP2* knocked down had increased pitch variability which could disrupt the "juveniles' ability to efficiently generate and select those motor programs that produce the best match to the tutor song model" leading to poorly copied tutor songs (Murugan et al., 2013). Importantly, decrease in *FoxP2* levels did not hinder the ability of the birds to form complete syllable repertoires, it only disturbed their ability to copy tutor song, proving that *FoxP2* expression in Area X is necessary for song learning and not just for motor production of syllables (Haesler et al., 2007).

Because *FoxP2* is expressed in the striatum during development and through adulthood, differentiation between the role of FoxP2 in striatal development and in maintaining proper striatal circuitry after development was of interest (Murugan et al., 2013). Crystalized male zebra finch songs have more pitch variability when they are undirected then when they are directed at a female (Murugan et al., 2013). Interestingly, when *FoxP2* is knocked down in Area X after song crystallization this context-dependent song variability is lost suggesting that FoxP2 plays a role in not only in song learning during development but also in song modulation outside of the critical developmental learning window (Murugan et al., 2013).

Electrophysiological experiments suggest that *FoxP2* knockdown in Area X may affect bird song by speeding cortical-striatal signal propagation (Murugan et al., 2013). Moreover, addition of a dopamine receptor 1 (D1R) antagonist into Area X reduced this signal propagation speed in control mice but not in animals with *FoxP2* knocked down in Area X (Murugan et al., 2013). These results suggested an interaction between FoxP2 and dopamine signaling pathways in cortical striatal circuitry. Importantly, *FoxP2* knockdown has been shown to decrease spine density of striatal spiny neurons where D1R is localized (Schulz et al., 2010), and knockdown of *FoxP2* in Area X lead to decreased levels of D1R and DARPP-32, a key component of the D1R signaling cascade (Murugan et al., 2013). This suggests that FoxP2 affects song learning and maintenance by regulating the timing of cortical-striatal signaling through control of modulatory dopamine signaling (Murugan et al., 2013).

Mice provide a genetically tractable model useful for studying the motor aspects of FoxP2 loss of function, but because mice may not be capable of vocal learning,

elucidating the mechanism by which FoxP2 regulates the cognitive aspects language acquisition using this model may be impossible (Arriaga and Jarvis, 2013). Songbirds have given us a much better idea of the role of FoxP2 in vocal learning, especially in the role of FoxP2 in song maintenance in adult animals, but because songbird brains are structurally very different from mammalian brains it has not been possible uncover the role that FoxP2 plays in building communication networks during development. Because humans may be the only animals that use language to communicate, there may never be an acceptable model system for uncovering how FoxP2 sets up human language circuitry during development. Macaques do not use language to communicate but do have more cognitive ability than mice and brains that more closely resemble human brains. Manipulating FoxP2 in macaque using CRISPR would be possible and may lead to a better understanding of the developmental role FoxP2 plays in language learning.

The molecular mechanisms of FoxP2 action

Studies of the behavioral and neurological phenotypes of the affected KE family members and of FoxP2 loss of function animal models have shed light on the importance of FoxP2 in the motor learning pathways that support language formation. However, these studies did not uncover the molecular mechanisms underlying the neural phenomena governed by FoxP2. Because FoxP2 is a transcription factor, interest in finding genes regulated by FoxP2 is high, and several publications have identified direct and indirect targets including those in fetal tissue from mouse and human brain and from several human cell lines (Spiteri et al., 2007, Vernes et al., 2011, Vernes et al., 2007,Consortium, 2012 #453). Moreover, identifying factors that physically interact with FoxP2 in order to influence gene expression has also been a

priority, and multiple FoxP2 cofactors have been identified in various tissues and cell lines (Li et al., 2004, Chokas et al., 2010, Zhou et al., 2008, Wu et al., 2006, Estruch et al., 2016). The studies, detailed below, have brought us a greater understanding of how FoxP2 builds language-learning pathways in the brain.

FOXP family dimerization

The FOXP family of transcription factors is composed of four members, FOXP1-4 three of which, FOXP1, 2, and 4, are expressed in the brain in partially overlapping regions (Ferland et al., 2003, Takahashi et al., 2008). In addition to the conserved winged-helix/Forkhead DNA-binding domain, FOXP family members possess an N-terminal poly-glutamine tract along with zinc-finger and leucine zipper domains (Shu et al., 2001, Li et al., 2004). FOXP monomers homo- and heterodimerize through the leucine zipper, and when this domain is mutated, FOXPs are unable to bind the canonical forkhead motif (Clark et al., 1993) in EMSA assays and less able to repress a luciferase reporter driven by a forkhead promoter in a lung epithelial cell line (Li et al., 2004). Thus, FOXP transcription factors were the first FOX family members shown to act as dimers to repress gene expression (Li et al., 2004). Subsequently, the crystal structure of the FOXP2 DNA-binding domain showed that FOXP2 could bind DNA as a monomer or as a dimer (Stroud et al., 2006), and that when FOXP2 dimerizes several hydrophobic residues that are exposed in the monomer are buried in the dimer causing the dimer to associate more loosely with DNA than the monomer.

While FOXPs must dimerize to repress activity from the FOX motif in a lung epithelial cell line, (Li et al., 2004) the possibility that these proteins can act as monomers *in vivo* has not been ruled out (Stroud et al., 2006). In fact, protein

crystallography has shown that the transcription factor NFAT1 interacts with a FOXP2 monomer to bind a single piece of DNA in a ternary complex, while FOXP family dimers each bind a separate segment of DNA forming a quaternary protein-DNA complex (Wu et al., 2006, Stroud et al., 2006). Moreover, when in complex with NFAT1, FOXP2 binds a separate, lower affinity DNA-binding motif than when it acts as a homodimer (Wu et al., 2006) confirming that DNA shape recognitiion may allow FOXP2 to bind to a broad range of sequences in different contexts (Stroud et al., 2006).

FOXP2 cofactors

In addition to NFAT, other FOXP2 cofactors have been identified indicating that transcriptional regulation by FOXP2 does not depend on FOXP2 expression alone but also on coexpressed factors that specify the action of FOXP2 in various tissues or at different developmental stages (Li et al., 2004, Chokas et al., 2010, Zhou et al., 2008, Wu, 2006 #358, Estruch et al., 2018, Wu et al., 2006). For example, FOXP2 physically interacts with CtBP1 through trans-repressor domain separate from the leucine zipper to synergistically repress gene expression (Li et al., 2004). Additionally, FOXP1/2/4 have been shown to interact with the repressive NuRD/MeCP1 chromatin-remodeling complex, suggesting that FOXP2 may repress target genes by recruiting histone deacetylases (Chokas et al., 2010). Moreover, in a manner independent of its own ability to bind DNA, FOXP2 has been shown to inhibit Nkx2.1-mediated transcription by physically blocking the DNA binding domain of this transcription factor (Zhou et al., 2008). Interestingly, TRB1, a transcription factor implicated in autism spectrum disorder (Deriziotis et al., 2014) and expressed along with FOXP2 in layer 6 cortical neurons (Hisaoka et al., 2010) also physically interacts with FOXP2 (Sakai et al., 2011, Deriziotis

et al., 2014), and other brain development relevant FOXP2 cofactors include SOX5, SATB1, SATB2, NR2F1 and NR2F2 (Estruch et al., 2018). While these specific examples are helpful for understanding the regulatory function of FOXP2, they are unlikely to be the only mechanisms underlying the ability of FOXP2 to specify discrete neuron populations necessary for proper language development

Identification of FOXP2 target genes

While it is important to understand the mechanisms by which FoxP2 regulates downstream targets in different contexts, the key to determining how FoxP2 establishes circuitry necessary for language during development lies in identifying those downstream targets. Several studies have endeavored to locate regions of chromatin where FoxP2 directly binds in a high-throughput manner by performing chromatin immunoprecipitation (ChIP) followed by hybridization to DNA microarrays (ChIP-chip) (Spiteri et al., 2007, Vernes et al., 2011, Vernes et al., 2007) or ChIP followed by next-generation sequencing (ChIP-seq) (Consortium, 2012). ChIP-chip studies looking for human targets of FOXP2 highlighted how experiments performed in human tissue and in human cell lines can compliment one another (Spiteri et al., 2007, Vernes et al., 2007). Obviously, in order to understand the role of FOXP2 in language development, the ultimate goal is to identify FOXP2 targets in human fetal brain. To this end, Spiteri and colleagues performed ChIP-chip on human fetal tissue from the inferior frontal cortex and basal ganglia, two dysfunctional regions in affected KE family members (Vargha-Khadem et al., 2005, Spiteri et al., 2007). To identify cortex-specific, basal ganglia-specific, brain-specific, and general FOXP2 targets, the authors also identified FOXP2 binding sites in human fetal lung, as FOXP2 is highly expressed in lung during

development (Shu et al., 2001). In the fetal brain, FOXP2 targeted genes were found to be involved in neurite outgrowth, calcium signaling, and learning among other developmental categories (Spiteri et al., 2007). At the same time, Vernes and colleagues (Vernes et al., 2007) performed ChIP-chip with a human neuroblastoma cell line, SH-SY5Y, stably expressing FOXP2 and similarly found enrichments of brain development genes, including those involved in neurite development and axon guidance (Vernes et al., 2007). Importantly, even though the two studies used different starting material and different antibodies to immunoprecipitate FOXP2, 29% of bound regions in the basal ganglia and 30% in the inferior frontal cortex were also bound by FOXP2 in cultured neuroblastoma cells suggesting that cultured human cells can be a valuable model for in vivo FOXP2 binding (Vernes et al., 2007).

While the importance of these studies cannot be denied, ChIP experiments depend heavily on the antibody used to immunoprecipitate the protein of interest. *In vivo* ChIP studies benefit from the inclusion of an IGG control immunoprecipitation to account for any noise created by an antibody pulling down non-specific pieces of chromatin; however, these studies did no such controls. The only way to ensure that the binding enrichments identified are not created by random noise or by the specificity of the antibody is incubate the lysates of cells expressing FOXP2 and those not expressing FOXP2 with the same FOXP2 antibody and subsequently eliminate regions of enrichment that appear in both conditions.

Another important note is that the arrays used by these studies only included probes for promoter DNA, and thus, regions outside known promoter regions that were bound by FOXP2 were not analyzed (Spiteri et al., 2007, Vernes, 2007 #175). While it is

still challenging to link a change in gene expression with distal transcription factor binding in a high-throughput manner, it is of interest to know if FOXP2 could be effecting gene expression through long-range interactions. The ENCODE Consortium has performed FOXP2 ChIP followed by next-generation sequencing in PFSK-1 and SK-N-MC cell lines in order to identify all binding events across the genome in these cells (Consortium, 2012). However, this study also failed to include IGG or FOXP2 null control ChIPs in its analysis, and the antibody used to pull down FOXP2 (Abcam Rb 16046) is non-specific in our lab's hands and in published work (Reimers-Kipping et al., 2011, Tsui et al., 2013). Because the antibody likely recognizes both FOXP1 and FOXP2 (Reimers-Kipping et al., 2011), this publically available FOXP2 ChIP-seq data contains areas bound by both proteins.

Moreover, while the human brain and SH-SY5Y ChIP-chip studies were successful in validating expression changes in many of the genes where FOXP2 bound, they did not perform this analysis on a transcriptome-wide scale. However, microarray expression analysis was used to compare the transcriptomes of human neural progenitor cells (hNPs) expressing endogenous *FOXP2*, over expressing *FOXP2*, or with *FOXP2* knocked down (Konopka et al., 2012a). This way, genes that exhibit a change in expression when FOXP2 is increased and/or reduced could be identified in a high-throughput manner (Konopka et al., 2012a). Mirroring the directly bound targets in human fetal cortex, a subset of the FOXP2 differentially expressed genes in this study is enriched for genes involved in neuron projections, synapse, and axonogenesis (Konopka et al., 2012a). Overlapping genes thought to be direct FOXP2 targets based on promoter occupancy with FOXP2 differentially expressed genes can allowed for the

identification of direct and indirect FOXP2 targets; however a study performing both differential gene expression analysis and chromatin occupancy in human neurons has not been published.

Foxp2 direct and indirect targets have been identified in the developing mouse striatum (Vernes et al., 2011). In this study ChIP-chip with a mouse promoter microarray was performed from whole embryonic day 16 brain of both wild type mice and mice homozygous for Foxp2-S321X which have a complete lack of Foxp2 protein (Vernes et al., 2011, Groszer et al., 2008). This allowed robust identification of Foxp2 binding events because non-specific signals produced by the ChIP could be accounted for to reduce false positives (Vernes et al., 2011). Additionally, expression microarrays were performed using RNA harvested from developing striatum of both wild type mice and mice homozygous for *Foxp2*-S321X (Vernes et al., 2011). Subsequently, differentially expressed genes were compared with Foxp2 promoter bound genes, and of the 340 differentially expressed genes identified, 19 genes were found in common with the promoter bound genes including genes with known functions in the brain: *Nrn1*, *Cck* and *Alcam* (Vernes et al., 2011). Interestingly, *Cck* was identified as a FOXP2 target in SH-SY5Y cells and in human fetal brain (Spiteri et al., 2007, Vernes et al., 2007) suggesting that it is a conserved target across species.

Gene ontology analysis identified an enrichment of genes involved in neurite outgrowth among both promoter bound and differentially expressed targets (Vernes et al., 2011). Importantly, when the length of the neurites of differentiated Neuro2a cells expressing wild type Foxp2 was compared to controls, the Foxp2 expressing cells had longer neurites, and the same was true in wild type cells derived from E16 basal ganglia

when compared to cells harvest from *Foxp2*-R552H homozygotes suggesting that this phenotype is not specific to an immortalized cell line (Vernes et al., 2011). This study showed that hypotheses made about the function of Foxp2 from analyzing high-throughput genomic data could be proven experimentally, and implied that regulation of neurite outgrowth by FoxP2 through its downstream targets is a critical function of this transcription factor during brain development (Vernes et al., 2011). Importantly, enrichments for neuron projection development and axon guidance genes among FOXP2 targets identified in human fetal tissue and a human neural cell line indicate an evolutionarily conserved role for FoxP2 in these processes (Vernes et al., 2011).

FOXP2 and evolution

The molecular evolution of FOXP2

Language is a human specific trait, and one of the most intriguing findings in the FOXP2 field involves the molecular evolution of FOXP2 along side the acquisition of language. Although FoxP2 is among the top 5% of the most conserved proteins between human and mouse, outside of the polyglutamine rich region there are only three amino acid differences in the human protein, and two of these three substitutions occurred on the human lineage after separation from the human-chimpanzee shared ancestor (Enard et al., 2002). Thus, these two human-specific amino acid changes, a threonine-to-asparagine change at position 303 and an asparagine-to-serine change at position 325, may have conferred human-specific function to FOXP2 that supported language development (Enard et al., 2002).

If they provided a selective advantage when they arose in the human population, evidence of a recent selective sweep, or the reduction of variation near the beneficial

substitution, should be present surrounding exon 7 where the substitutions are located (Enard et al., 2002,Przeworski, 2002 #472). Indeed, evidence of a selective sweep has been uncovered through studies by three groups using separate methods (Enard et al., 2002, Zhang et al., 2002, Yu et al., 2009). Because the human specific substitutions were fixed in the human population, and because the amino acid sequence of FoxP2 is otherwise so well conserved, the assumption that these particular changes drove the selection of this region seemed sound.

This rational was complicated, however, by evidence from the genome sequences of Neanderthal and Denisovan (Krause et al., 2007, Reich et al., 2010) that these two human-specific amino acids were actually hominid-specific changes. Overrepresentation of low-frequency alleles in a genomic region is a hallmark of a recent selective sweep, but low-frequency alleles are lost over from the population relatively quickly by genetic drift (Coop et al., 2008). Therefore, it is unlikely that evidence of a selective sweep would persist in the approximately 300K years since humans and Neanderthals split from a common ancestor (Coop et al., 2008). One intriguing explanation for this contradiction is that mating between humans and Neanderthals caused the haplotype carrying the substitutions to be passed from humans to Neanderthals before the sweep, and that the sweep occurred in humans after this event in response to a later, human specific mutation elsewhere in the gene (Coop et al., 2008). Indeed, there is evidence that a segment of *FOXP2* flowed from humans to Altai Neanderthals (Kuhlwilm et al., 2016) and that a recent human-specific sequence change in a POU3F2 regulatory site within the positively selected region of *FOXP2* could be the actual cause of the sweep (Maricic et al., 2013). Moreover, linkage

disequilibrium extends across the two hominid-specific substitutions, which would be unlikely if one of those substitutions was being selected for because homologous recombination events occur independently on either side of the beneficial allele breaking down linkage disequilibrium (Ptak et al., 2009).

Functional consequences of hominid-specific changes in FOXP2

Regardless of whether they were the cause of the recent accelerated evolution of the *FOXP2* gene, the amino acid changes at positions 303 and 325 are fixed in the human population and confer human-specific properties to FOXP2 (Konopka et al., 2009, Enard, 2011, Enard et al., 2009). For example, Konopka and colleagues demonstrated differential gene regulation by the human and chimpanzee versions of FOXP2 (Konopka et al., 2009). Human *FOXP2* or the same construct mutated to contain a threonine at position 303 and an asparagine at position 325, representing the chimpanzee version of the gene was exogenously expressed in SH-SY5Y cells and human neural progenitor cells (Konopka et al., 2009). Subsequently, whole-genome expression microarray analysis was used to identify genes differentially expressed by chimp and human FOXP2 in both cells types (Konopka et al., 2009). Human FOXP2 both up-regulated and down-regulated genes compared to chimp FOXP2 in SY5Y cells, and this human specific regulation was consistent in human neural progenitor cells with one third of the differentially regulated genes overlapping in the two cell types (Konopka et al., 2009). Importantly, human and chimpanzee FOXP2 were found to interact with FOXP1 and FOXP4 to the same extent even though the amino acid changes are near the leucine zipper dimerization domain (Konopka et al., 2009, Enard et al., 2002). To validate human specific regulation in *vivo*, microarray analysis was performed with RNA

harvested from adult human and chimpanzee brain tissue, and genes with increased or decreased expression in human brain compared to chimpanzee brain were enriched for genes up- or down-regulated FOXP2 in SY5Y, respectively (Konopka et al., 2009). This result implies that the two amino acid differences between chimpanzee and human FOXP2 lead to differential gene regulation in the brains of the two species, and that these differences in gene expression persist through adulthood (Konopka et al., 2009).

In order to understand the physiological and behavioral consequences of hominid-specific FOXP2, “humanized” FOXP2 mice were created by replacing mouse exon 7 with human exon 7 via homologous recombination (Enard et al., 2009). These mice are extremely well characterized both histologically across many tissues and behaviorally having undergone more than 300 behavioral assessments (Enard et al., 2009). No gross anatomical differences are appreciated between genotypes, but, strikingly, one behavior alone is robustly different when comparing wild type and humanized animals: reduced exploratory behavior in a novel environment (Enard et al., 2009). This result is strengthened by the fact that heterozygous null animals exhibit increased exploratory behavior under the same paradigm (Enard et al., 2009).

By analyzing neurotransmitter levels in multiple brain regions, it was found that dopamine concentration was reduced in humanized mice compared with wild type, while it was increased in *Foxp2* heterozygous null animals. This result was intriguing given that increasing or decreasing dopamine levels in the brain increases or decreases exploratory behavior in rodents accordingly (Viggiano et al., 2003, Enard et al., 2009); however, *Foxp2* is not expressed in dopaminergic neurons suggesting that FoxP2 modulates dopamine levels through an indirect mechanism (Enard et al., 2009). Still,

this result lead to the assessment of *Foxp2* expressing spiny projection neurons, the major targets of dopaminergic neurons (Enard et al., 2009). While the spiny projection neurons of *Foxp2*-R552H heterozygotes show a complete lack of long-term depression after cortical fiber stimulation (Groszer et al., 2008), the spiny projection neurons of humanized animals exhibit long-term depression that is twice as strong as that produced by wild-type animals (Enard et al., 2009). Along with this increase in spiny projection neuron plasticity, the dendrite lengths of spiny projection neurons, layer IV bipolar neurons, and thalamic neurons, which are all neurons expressing *Foxp2* that make up cortico-basal ganglia circuitry, are increased in humanized animals suggesting that human FOXP2 has a specific effect on these language relevant circuits (Enard et al., 2009, Reimers-Kipping et al., 2011). Adding to this conclusion, the humanized mice displayed subtle but reproducible differences in the structure of their ultrasonic isolation calls (Enard et al., 2009).

While adult male humanized animals do not display differences in courtship calls, adult animals learn more quickly in tasks that require a switch from declarative or conscious learning strategies to procedural or non-conscious forms of learning that require repetitive exposure (Hammerschmidt et al., 2015, Schreiweis et al., 2014). Broadly, this could be interpreted as learning to make behaviors habitual more quickly. Moreover, this study demonstrated that dopamine-dependent long-term depression is stronger in spiny projection neurons of the dorsolateral striatum and weaker in the dorsomedial striatum of the humanized mice compared to wild-type animals (Schreiweis et al., 2014). Importantly, the dorsomedial striatum is engaged during declarative learning, while the dorsolateral striatum is active during habitual behaviors, suggesting

that human FOXP2 effects learning by differentially modulating plasticity in these regions (Schreiweis et al., 2014, Yin and Knowlton, 2006).

Based on this, one can speculate that reduced levels of FOXP2 may inhibit the switch from conscious learning to habitual behavior. It is of interest, then, that affected KE family members seem to have trouble generalizing grammar rules across words (Gopnik and Crago, 1991). Affected individuals may be able to remember that the plural form of “fence” is “fences”, but they cannot generalized the rule “add -es” so that when subjects are shown a picture of an imaginary animal and told, for example, that this animal is a “zash”, they are impaired in supplying the expected response, i.e. “zashes” (Gopnik and Crago, 1991). This could reflect a decreased ability to make learned rules about grammar habitual and thus impair expressive language.

FOXP2 in the evolved human subplate

Many lines of evidence support a human-specific role for FOXP2 in cortico-striatal-thalamocortical circuitry. While FOXP2 expression in the striatum is obviously important for the proper function of these pathways, the role of FOXP2 in the human cortex, the evolution of which is thought be critical for higher cognitive function, is less clear. Intriguingly, *FOXP2* expression is enriched in the subplate zone of the developing human cortex (Miller et al., 2014) suggesting that it modulates gene expression in this evolutionarily relevant region.

The subplate is transient region of the developing mammalian cortex that contains some of earliest born neurons in the cortex (Kostovic and Rakic, 1990, Bayatti et al., 2008) and is situated above the intermediate zone but below the cortical plate in all placental mammals (Molnar et al., 2006). In the mouse brain, the subplate and the

marginal zone are formed when their precursor, the preplate, is split by the formation of the cortical plate, which begins at embryonic day (E) 13 in mice (Marin-Padilla, 1978). Mouse subplate cells arrive between E10.5 and E12.5 before the preplate split from the ventricular zone, subventricular zone, rostro-medial telencephalic wall, and ganglionic eminence (Price et al., 1997, Hoerder-Suabedissen and Molnar, 2013, Hoerder-Suabedissen and Molnar, 2015). While subplate cells are born before E13, the subplate layers is largely cyto-architecturally defined and until E16 there is not a clear boundary between the subplate and intermediate zone in mouse (Hoerder-Suabedissen and Molnar, 2015).

Unlike in rodents, there is a minimal preplate in primates (Smart et al., 2002, Bystron et al., 2005, Meyer et al., 2000), and the primate equivalent of the mouse subplate, the presubplate, is "morphologically minimal and is comprised of few neurons" (Smart et al., 2002). Recently, it has been shown that some primate subplate neurons arrive concomitantly with neurons from layer VI (Duque et al., 2016). The subplate proper is distinguishable in human brain by gestational week (GW) 10.5 by an increased GAP34, synaptophysin, and vGABA immunostaining compared with the intermediate zone and overlying cortical plate (Bayatti et al., 2008). Morphologically, it can be distinguished early on by the presence of a cell-sparse band with large extracellular spaces and some large cell bodies (Kostovic and Rakic, 1990), while later it is characterized by its dense, chondroitin sulfate proteoglycan-rich extracellular matrix and incoming afferents (Bicknese et al., 1994, Kostovic and Rakic, 1990, Bayatti et al., 2008). In fact, the subplate acts as a holding compartment for thalamic and cortical afferents that enter the cortex and migrate along the subplate between GW 15 and 18

(Kostovic and Rakic, 1990). During this time, the evolutionary diversity of the subplate becomes clear. The size of the mouse subplate increases only slightly, while the carnivore and primate subplates vastly increase to accommodate incoming afferents (Kostovic and Rakic, 1990, Hoerder-Suabedissen and Molnar, 2015, Molnar et al., 2006). As afferents arrive in the subplate, some of the early born neurons disperse among them, while others are pushed out and form the cell dense, overlying layer VI (Duque et al., 2016). Molecular differences between these two concurrently born cell populations have yet to be assessed (Duque et al., 2016). The increased size of the subplate may serve to support the functions of a more complex brain, as humans have an even larger subplate than carnivores or monkeys (Kostovic and Rakic, 1990).

Thalamocortical and corticocoritcal afferents pause in the subplate layer before making their final connections mostly in layer IV (Kostovic and Rakic, 1990), but the subplate zone is more than just a holding compartment. For example, the subplate guides thalamic afferents to their proper targets (Molnar and Blakemore, 1995a), and when this region is disrupted or misplaced in mouse by knocking out one of several key cortical development genes such as *Reln*, *Gli3*, *Sox5*, *p35* or *Tbr1,* thalamocortical afferents fail to reach their proper target in layer IV (Hoerder-Suabedissen and Molnar, 2015). Moreover, the subplate contains both GABAergic and glutamatergic neurons cells with diverse morphologies and projection patterns (Kostovic and Rakic, 1990, Bayatti et al., 2008, Hoerder-Suabedissen et al., 2009, Marx and Feldmeyer, 2013). In fact, the glutamatergic input from the subplate to early layer IV neurons is critical for the maturation of thalamocortical and cortico-cortical synapses (Kanold et al., 2003, Kanold and Shatz, 2006). Additionally, excitatory synapses from subplate neurons onto

migrating neurons in the intermediate zone have been observed, and this glutamatergic input from the subplate changes the migration pattern of the neurons from multipolar migration in the intermediate zone, to directed, unipolar migration through the subplate and towards there final locations in the upper cortical plate (Ohtaka-Maruyama et al., 2018). Thus, the subplate layer is necessary not only for the proper localization of cortical cells and thalamic projections, but also for the maturation of cortical and thalamocortical circuitry.

As important as the subplate is during development, it is a transient cortical structure that beings to recede after GW 35 when incoming afferents have migrated outward to layer IV (Kostovic and Rakic, 1990); by six months of age the subplate is no longer appreciable in humans (Kostovic and Rakic, 1990). In rodent, the subplate layer, which expands little over development, non the less recedes; however, 10-20% of subplate cells in rodents remain and are identified as layer 6b (Friedlander and Torres-Reveron, 2009). The final vestiges of this layer in humans are interstitial white matter cells (Chun and Shatz, 1989), which, interestingly have been shown to be more abundant in the brains of those with autism or schizophrenia suggesting that aberrations in subplate layer can lead to neurodevelopmental disorders (Eastwood and Harrison, 2003, Hutsler et al., 2007).

Loss of FOXP2 could affect any of the processes governed by the subplate during cortical development. Moreover the subplate specifically supports cortico-basal ganglia-thalamocortical circuitry, which is abnormal in loss of FOXP2 function mouse models and in the affected KE family members. Additionally, the human version of

FOXP2 may have played a role in the evolution of the subplate, which then supported the formation of the neural circuits needed for complex speech and language.

Introduction

FoxP2 plays evolutionarily conserved and human specific roles underlying motor learning pathways in the brain (Spiteri et al., 2007, Vernes et al., 2011, Vernes et al., 2007, Konopka et al., 2009, Enard et al., 2009, Schreiweis et al., 2014), and in humans, heterozygous loss of *FOXP2* perturbs these motor-learning pathways and specifically disrupts proper language formation (Belton et al., 2003, Liegeois et al., 2003, Vargha-Khadem et al., 2005, Watkins et al., 2002b). Understanding the roles that conserved downstream targets of FoxP2 play in communication in mouse may be key to uncovering the pathways that are coopted in humans for the motor aspects of speech formation. Conversely, while conserved FoxP2 targets may be important for some aspects of speech associated motor-learning, human specific FOXP2 targets could play a role in establishing circuitry important for higher cognitive function in primates. Moreover, the mechanisms by which FoxP2 regulates conserved and human gene expression patterns are not well understood, and data explaining how FoxP2 acts both to repress and activate gene expression is lacking.

During my dissertation work I sought to better understand the conserved and human specific functions of FoxP2. To this end, I analyzed the effect that homozygous loss of function of conserved direct target, cholecystokinin (Cck), has on pup ultrasonic isolation calls with the hypothesis that these innate vocalizations would be disrupted. Moreover, intrigued by the enrichment of *FOXP2* in the human subplate layer, I hypothesized that FOXP2 regulates evolutionarily distinct subplate gene expression

patterns. I tested this theory by performing RNA-seq in human differentiating neurons and leveraging publically available developmental expression data from human, macaque, and mouse cortex in order to identified human specific, primate specific, and conserved subplate genes regulated by FOXP2. Finally, I performed ChIP-seq and RNA-seq in human neural progenitor cells and found evidence that FOXP2 may actively modify the chromatin landscape. This lead me to hypothesize that by modifying the chromatin landscape of neural progenitors FOXP2 turns off cellular programs that maintain an undifferentiated state while turning on programs that drive a cell towards a neuronal fate. To test this hypothesis, I identified areas of nucleosomal depletion using an assay for transposase-accessible chromatin using sequencing (ATAC-seq), and correlated epigenetic changes caused by *FOXP2* expression to changes in gene expression in proliferating and differentiating human neurons. Together, these studies push forward our understanding of the function of FoxP2, especially in human neurons, and provide a source of data from which the next hypotheses concerning FoxP2 and human language formation may be derived.

CHAPTER 2: The effect of loss of conserved FoxP2 target, cholecystokinin, on the ultrasonic isolation calls of neonatal mice

Summary

Cholecystokinin (Cck) is a peptide expressed in both the brain and the intestinal tract. In the intestinal tract it is secreted in response to consumption of fat and protein and leads to a reduction in feeding (Dockray, 2014). In the brain, Cck acts as a neurotransmitter and has been implicated in various psychiatric disorders including schizophrenia and panic disorder (Noble and Roques, 2006). Importantly, *Cck* is conserved, direct target of FoxP2 suggesting that it may be necessary for proper language circuitry (Vernes et al., 2011, Vernes et al., 2007, Spiteri et al., 2007). We tested the hypothesis that Cck is involved in mammalian communication by analyzing neonatal isolation ultrasonic vocalizations (USVs) in *Cck* knockout mice and wild type littermates. While initially it appeared that loss of Cck affected various USV properties at P7 and P10, controlling for food intake and recording time in a separate cohort mitigated these phenotypes. These results suggest that while Cck may not be involved in USV production, consistency of food intake and recording time across litters is crucial for assaying USVs in any genotype.

Introduction

FoxP2 has been shown to bind the promoter region of the Cholecystokinin (Cck) gene in embryonic mouse brain, human neuroblastoma culture, and human fetal brain (Vernes et al., 2011, Vernes et al., 2007, Spiteri et al., 2007) suggesting that *Cck* is a conserved, direct target of FoxP2. In the mouse striatum, *Cck* expression is increased in FoxP2 null mice compared to wild type levels, suggesting that Foxp2 binding to the

promoter region of this gene serves to repress its expression (Vernes et al., 2011). In this study, we sought to understand the behavioral consequences of loss of endogenous Cck in mouse, especially the effect on neonatal ultrasonic vocalizations (USVs), which are drastically reduced in FoxP2 null animals (Fujita et al., 2008, Gaub et al., 2010, Shu et al., 2005).

Cck was first characterized as a gut hormone after its discovery in 1928 (Ivy, 1929). The gene encoding the peptide is translated into a 115-amino-acid protein (preproCCK) that is later cleaved into multiple biologically active forms ranging from 58 to 4 amino acids in length (Rehfeld and Nielsen, 1995). In the intestine, Cck is released in response to fat and protein and subsequently acts on vagal afferent neurons to inhibit food intake while also directly simulating processes that increase the delivery of bile salt and digestive enzymes to the intestine (Dockray, 2014).

In 1975, Cck was discovered in the mammalian central nervous system, where it is more abundant than in the gastrointestinal tract (Vanderhaeghen et al., 1975). In fact, it may be the most prevalent neuropeptide in the mammalian brain (Crawley, 1985). In the brain, Cck acts as a neurotransmitter and is co-localized at synapses with dopamine, gamma-Aminobutyric acid (GABA), serotonin and encephalin (Noble and Roques, 2006). Additionally, it is released at corticostriatal synapses potentially with glutamate (Morino et al., 1994). The Cck transcript is produced in neurons in the cortex, thalamus, hippocampus, hypothalamus, substantia nigra pars compacta, ventral tegmental area and amygdala (Dockray, 1976, Calvigioni et al., 2017, Noble and Roques, 2006). Most Cck expressing neurons are GABAergic interneurons; however, a

subset of cortical pyramidal neurons also expresses Cck, albeit at lower levels (Calvigioni et al., 2017).

Two different Cck receptors, Cck_1 and Cck_2, have been characterized as G-protein coupled receptors in the brain and gastrointestinal tract (Sankaran et al., 1980, Innis and Snyder, 1980). Cck_1 is the predominant receptor in the gut, while in the brain Cck_2 is more abundant and widely spread (Honda et al., 1993, Noble et al., 1999). Consistent with this localization profile, mice lacking Cck_1, unlike wild type mice, do not decrease food intake with exogenous Cck administration (Kopin et al., 1999). Cck_2 receptor null mice, on the other hand, did decrease food intake in response to Cck, suggesting that Cck induced satiation is mediated through Cck_1 receptors (Kopin et al., 1999). Interestingly, when Cck is increased endogenously after force feeding or exogenously with Cck administration, USV production by isolated ten-day-old rat pups decreases, and devazepide, a Cck_1 receptor antagonist, mitigates this effect (Blass and Shide, 1993). Because isolated pups may increase calls in response to hunger, these data suggest that Cck, signaling through the Cck_1 receptor in the gut, affects pup to dam communication.

Both Cck receptors have also been implicated in psychiatric disorders, highlighting the important role for Cck as a neurotransmitter in the brain. For example, polymorphisms in Cck_1 have been associated with schizophrenia (Wei and Hemmings, 1999, Sanjuan et al., 2004), and panic disorder has been linked to a polymorphism in Cck_2 (Kennedy et al., 1999). Interestingly, anxiety attacks can be triggered in patients with panic disorder when they are injected with Cck_2 agonists (Bradwejn et al., 1992, Bradwejn et al., 1991). In rodents, exogenous Cck administration also increases

anxious behavior through the Cck_2 receptor (Harro et al., 1993); however, mice that lack Cck_2 display a slight increase in anxiety-like behaviors while an anxiolytic effect would be expected (Noble and Roques, 2006).

Cck and its receptors have also been implicated in addiction, and the interaction between Cck and dopamine signaling has been widely studied (Noble and Roques, 2006). For example, Cck_1 and Cck_2 receptors are known to differentially modulate dopamine release in the nucleus accumbens (Marshall et al., 1991). In the caudal shell, signaling through Cck_1 receptors causes dopamine-agonist-like effects, potentiating dopamine release (Marshall et al., 1991). On the other hand, in the rostral core of the nucleus accumbens, activation of Cck_2 receptors inhibits dopamine release (Marshall et al., 1991). In line with this, Cck_2 null mice show increased D2 receptor sensitivity and dopamine-dependent hyperactivity compared with wild type mice, suggesting increased dopamine signaling (Koks et al., 2003, Dauge et al., 2001).

The majority of the studies of Cck function use exogenous Cck or Cck receptor agonists and antagonists to alter Cck signaling (Noble and Roques, 2006, Crawley and Corwin, 1994). In order to better understand the role of endogenous Cck, *Cck* knockout mice were generated via insertion of a *LacZ* construct into the second exon of the gene which disrupted the transcriptional start site and caused a complete lack of Cck-peptide fragments (Lacourse et al., 1999, Lo et al., 2008). These mice have normal body weight and fat absorption; however, while Cck null mice eat the same amount of food as their wild type littermates, null mice eat more during the light period and less during the dark period (Lo et al., 2008). This suggests a disruption of circadian modulated feeding behavior, and, interestingly, *Cck* has been identified as a direct target of Clock (Arey et

al., 2014). However, circadian rhythms in the null mice are generally normal as demonstrated by running wheel activity that is similar to wild type mice (Lo et al., 2008). In addition to this slight difference in feeding behavior, these mice display increased anxiety-like behaviors and memory deficits (Lo et al., 2008). For example, in the elevated-plus maze they spend more time in the closed arms than their wild type counterparts, and they exhibit increased escape latency in the Morris water maze (Lo et al., 2008). Taken together, these data suggest that while the timing of feeding is disrupted by constitutive lack of Cck, developmental compensatory mechanisms meditate normal food intake, body weight, and fat absorption. In the brain, however, the action of this protein as a neurotransmitter is not fully compensated for in knockout animals, leading to impaired cognitive function (Lo et al., 2008).

Because feeding behavior is relatively normal in *Cck* knockout mice, but they exhibit some behavioral impairment (Lo et al., 2008), we thought this was an appropriate model for studying the potential role of loss of endogenous Cck in the brain on neonatal vocalizations. Cck is a direct, repressed target of Foxp2, therefore knockdown of this target will not tell us how Cck affects vocalizations in relation to Foxp2. However, the role of Cck in modulating dopamine signaling, which is disrupted in Foxp2 null mice and enhanced in humanized mice (Enard et al., 2009), suggests that, like Foxp2, this abundant neuropeptide may also regulate rodent communication in some way.

Results

Expected localization of Cck expression in the mouse brain

In order to confirm loss of Cck transcript in Cck null mice, we harvested the cortex of adult animals, extracted RNA, and performed qRT-PCR. As expected, the wild type mice expressed *Cck* in the cortex, while knockout mice expressed negligible *Cck* transcript (Figure 2.1A). To test that *Foxp2* expression was not altered in Cck null mice, we quantified Foxp2 transcript in the same samples and found the expression levels to be similar between the two genotypes (Figure 2.1A).

In order to confirm the brain regions in which Cck is expressed, we took advantage of the *lacZ* construct disrupting the *Cck* gene in the knockout mice, and performed x-gal staining (Lacourse et al., 1999). Because the endogenous *Cck* promoter drives *lacZ* expression in the knockout animals, the staining revealed regions where *Cck* would normally be expressed, including the cortex, hippocampus, and lower expression in various thalamic nuclei (Figure 2.1B). Importantly, this result is in line with previously published studies of *Cck* transcript localization (Dockray, 1976, Calvigioni et al., 2017, Noble and Roques, 2006).

Cck null animals perform similarly to wild type in the open field

Before recording neonatal USVs, we sought to confirm the previously identified increase in anxiety-like behavior in Cck null animals (Lo et al., 2008). Moreover, we wanted to ensure that these animals did not display hyperactivity, which could potentially confound a phenotype of increased USVs. While *Cck* knockout mice are not more active on the running wheel than wild type animals (Lo et al., 2008), Cck_2 knockout mice do display hyperactivity (Dauge et al., 2001). In order to accomplish both of these, we evaluated adult Cck knockout animals, heterozygotes, and wild type littermates in the open field. Surprisingly, we see no difference in time spent in the

center of the arena among genotypes, suggesting that loss of Cck does not induce and anxiety-like phenotype in the open field (Figure 2.2A). However, because all genotypes traveled the same distance in the open field (Figure 2.2B), we can confirm that loss of Cck does not induce hyperactivity.

Initial evidence that Cck regulates pup USVs

We collected USVs from P4, P7, P10 and P14 Cck knockout mice and wild type litter mates after isolation from the dam and found that both genotypes produced simples calls, calls with frequency jumps, and calls with clicks at all time points suggesting that Cck null animals can produce normal vocalizations (Figure 2.3). When the calls were analyzed further, no parameters considered were significantly different at P4 or P14; however, the number of calls was significantly reduced in knockout animals at P10 (Figure 2.4A). Moreover, when we compared the average call duration between genotypes we found that the knockout animals had significantly shorter calls at P7 (Figure 2.4C), while the maximum duration of the calls was decreased at P10 (Figure 2.4D). This suggests that Cck can regulate call number and duration at specific developmental ages.

Next, we quantified the fraction of calls with frequency jumps, a more complex call type. In wild type mice the fraction of calls with frequency jumps increases at P7 and P10 before decreasing at P14. In Cck knockout mice, however, this fraction remains the same from P7 though P14, and is significantly decreased compared to wild type at P7 and P10 (Figure 2.5A). This suggests that Cck may regulate developmental changes in call structure. Additionally, the mean frequency (pitch) of calls with and without jumps was increased significantly at P7, and calls with frequency jumps were

trending toward a significant increase at P10 (Figure 2.5B-D), suggesting that Cck regulates not only the structure of USVs, but also the pitch at which the calls are delivered.

Controlling for food intake and time of day eliminates the USV phenotype in Cck knockout animals

In order to verify the effect of *Cck* knockout on neonatal USVs, we performed the analysis on a new cohort of animals at P7 and P10 with several changes to the original protocol. While previous studies suggested that *Cck* knockout mice do not have a significant metabolic phenotype (Lacourse et al., 1999, Lo et al., 2008), we remained unsure that differences in food intake, the total amount or the timing, between genotypes were not the cause of the observed phenotype. Therefore, we collected two sets of USVs from this new cohort: one directly after removal from the dam, as before, and one after two hours of isolation from the dam to facilitate fasting. During fasting, the pups were kept in a moist warm container in order to minimize call increases due to a decrease in body temperature. Importantly, pups from all litters were recorded at the same times of day, fed at 10 am and fasted at 2 pm, to control for the potential effects of circadian rhythms as Cck is a known target of the Clock transcription factor (Arey et al., 2014). Moreover, only litters with six pups or fewer were used in these experiments, so each pup would have equal opportunity to feed from the dam based on the “one-half rule” (Gilbert, 1986) in which rodent dams are able to equally feed half the number of pups as they have nipples. In the case of mice, dams have twelve nipples, which means that at most six pups would have equal access to nutrition at any one time. At P0, if litters contained more than 6 pups, n minus 6 pups were chosen randomly and culled.

Interestingly, the above result, a decrease in the number of calls made by Cck null animals at P10, is the opposite of what would be expected if the phenotype were modulated through Cck release in the gut (Blass and Shide, 1993). In that case, we would expect an increase in calls in Cck null animals compared to wild type, as no Cck would be released after feeding (Figure 2.6A) (Blass and Shide, 1993). Upon fasting, we would expect Cck levels in the gut of wild type mice to drop, and their vocalizations to increase to levels similar to wild type (Figure 2.6A). However, if the phenotype is based on levels of Cck in the forebrain, which have not been shown to change with food intake, we would expect the same phenotype in both the fed and fasted states, and possibly a decrease in calls made by *Cck* null mice as exhibited in the previous cohort (Figure 2.6B).

Surprisingly, at P7 pups of both genotypes called less after being fasted, rather than more as expected, and the decrease in wild type calls was statistically significant. At P10, both genotypes called more after fasting, null animals significantly so, suggesting not only that call number may still be regulated by food intake in Cck knockout animals, but also that the response to fasting has a developmental component (Figures 2.7A and 2.8A). The number of bouts of calling after fasting followed the same trend at the total number of calls, decreased at P7 and increased at P10, though not significantly so (Figures 2.7E and 2.8E). These data suggest, as in previous studies, that there is a compensatory mechanism that regulating food intake in Cck null mice (Lacourse et al., 1999, Lo et al., 2008), and, additionally, that this mechanism overrides the need for Cck signaling through the Cck_1 receptor to increase neonatal USVs in response to feeding. There were, however, no significant differences between knockout

and wild type animals in the fasted or fed state on any of the USV parameters measured, suggesting that controlling for food intake and time of day mitigated the phenotype observed in the previous cohort, and that *Cck* does not, in fact, regulate USVs outside of the metabolic context (Figures 2.7 and 2.8).

Discussion

While this study did not show a role for Cck in the production of mouse neonatal isolation USVs, the results highlight the importance of controlling both the food intake of pups and circadian time when studying the affect of any gene on USVs, as both seem to have an impact on the number and structure of USVs. Keeping the number of pups per litter at or below six, in line with the “one-half rule” (Gilbert, 1986), may be especially important for any USV study if food intake affects USV production. However, in our fasting protocol it is impossible to distinguish between changes in vocalizations caused by prolonged separation from the dam aside from feeding. Therefore, repeating the experiment performed by Blass *et al.,* wherein intraoral administration of milk or corn oil increased Cck levels and decreased isolation USVs, after the fasting protocol would be an important control for the effect of this protocol on USVs (Blass and Shide, 1993). If oil or milk administration after fasting rescued the change in vocalizations compared with the fed state then lack of food intake likely caused the change. However, if oil or milk administration failed to rescue the change in USV number, then it is likely that prolonged maternal separation caused the change in calls after our fasting protocol. Either way, feeding has been shown to increase endogenous Cck and decrease USVs (Blass and Shide, 1993), and this study, even ignoring the fasted data, shows that controlling for litter size and circadian time can effect the outcome of USV experiments.

Thus, these controls should be included in future studies of rodent USVs, including those assaying communication deficits in search of an autism-spectrum-disorder-like phenotype.

Future Directions

Clearly, in this study it was difficult to isolate the effects of Cck in the brain and Cck in the intestinal tract on pup USVs. In order to remedy this, it would be necessary to assay USVs in a neuron specific conditional knockout animal, perhaps with the *Cck* gene flanked by *loxP* and a Cre protein driven by the *nestin* promoter. Moreover, to remove the effect of developmental compensatory mechanisms, an inducible forebrain neuron specific Cre-driver could be implemented (Erdmann et al., 2007), and pups could be injected with tamoxifen before recording USVs. Additionally, while Cck_2 receptors are more abundant, both Cck receptors are expressed in the forebrain (Honda et al., 1993). If the conditional knockout mice produced USVs abnormally, it would be interesting to treat the animals with agonists specific to either receptor to see if the phenotype could be rescued. Moreover, analyzing USVs in Cck_1 and Cck_2 receptor knockout animals would provide further evidence of receptor specific contributions to pup USVs.

While the above strategies may provide evidence of a role for Cck in the brain regulating USVs, they will not tell us if the repression of *Cck* by Foxp2 is necessary for proper USV production. Foxp2-Cre mice have been generated (Rousso et al., 2016) and could be crossed with mice driving *Cck* expression with a Cre-dependent FLEX switch (Atasoy et al., 2008). This would allow for the expression of *Cck* in cells that also express *Foxp2*, affectively nullifying the repressive effect of Foxp2 on *Cck*. However, it

would be best if this could be accomplished in a brain specific manner as Foxp2 is also expressed in the intestinal tract (Shu et al., 2001). This strategy may be ineffective, however, if *Foxp2* expressing cells do not express prohormone convertases, the enzymes necessary for cleaving the full length Cck protein into Cck-8, the most abundant, active form of Cck in the brain (Noble and Roques, 2006). Moreover, the sulfated form of Cck-8 binds the Cck_1 receptor with high affinity, while the un-sulfated version binds Cck_2 best (Noble and Roques, 2006). In order for Cck produced in *Foxp2* expressing cells to stimulate both types of receptors, the enzyme that adds a sulfate group to Cck-8 would have to be present. Thus, while expressing *Cck* in cells where Foxp2 is present would be the best experiment for determining the role of Cck repression by Foxp2, many experiments would have to be performed to ensure proper Cck signaling from those neurons.

Figures

Figure 2.1 *Expected localization of Cck expression in the mouse brain*

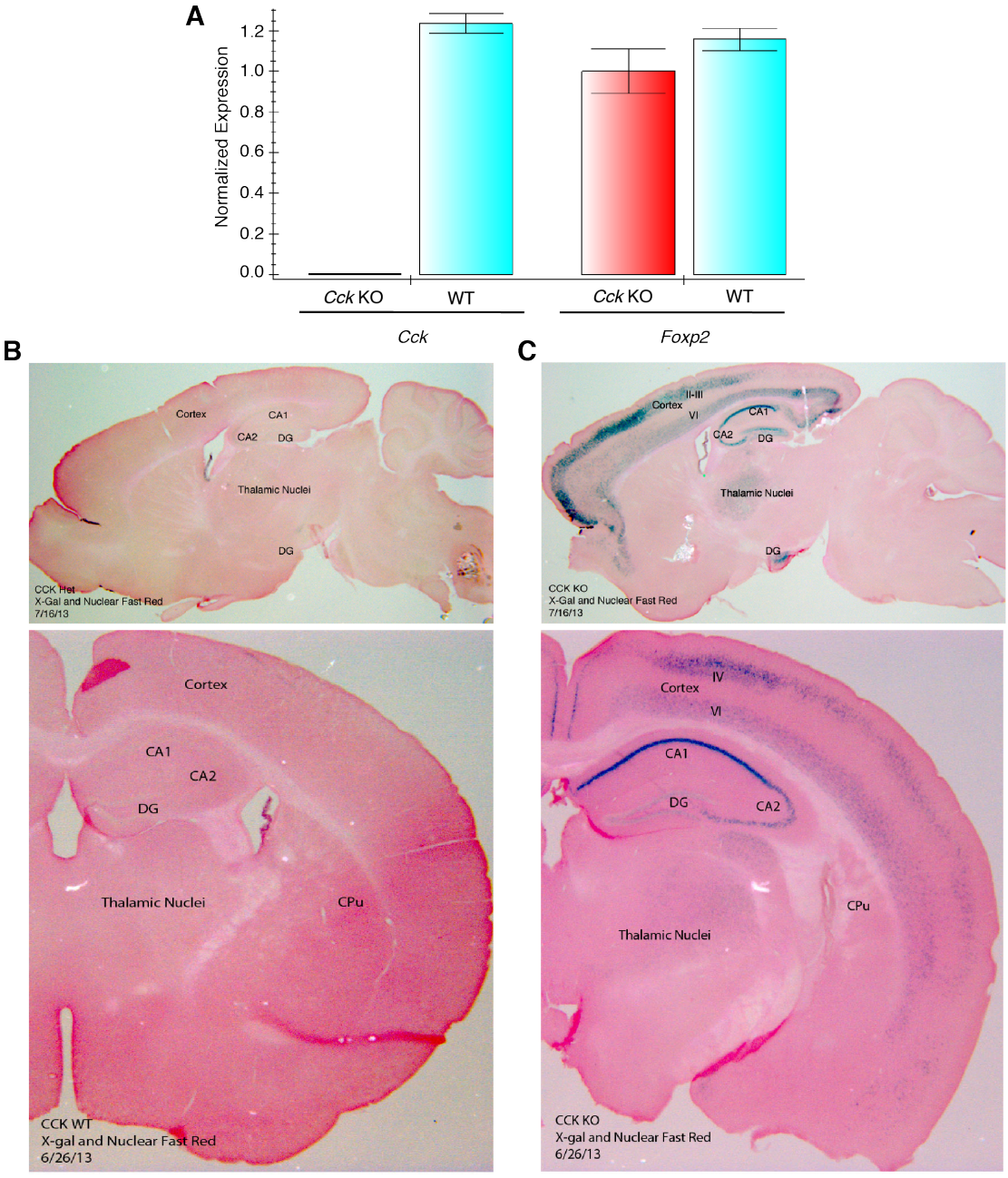

A) Normalized expression of *Cck* and *Foxp2* transcript in adult mouse cortex as determined by qRT-PCR. **B)** Sagittal and coronal sections of wild type adult mouse brains stained with x-gal. **C)** Sagittal and coronal sections of adult *Cck* knockout mouse brains stained with x-gal showing the *lacZ* expression (blue) where *Cck* would normally be expressed.

Figure 2.2 *Cck null animals perform similarly to wild type in the open field*

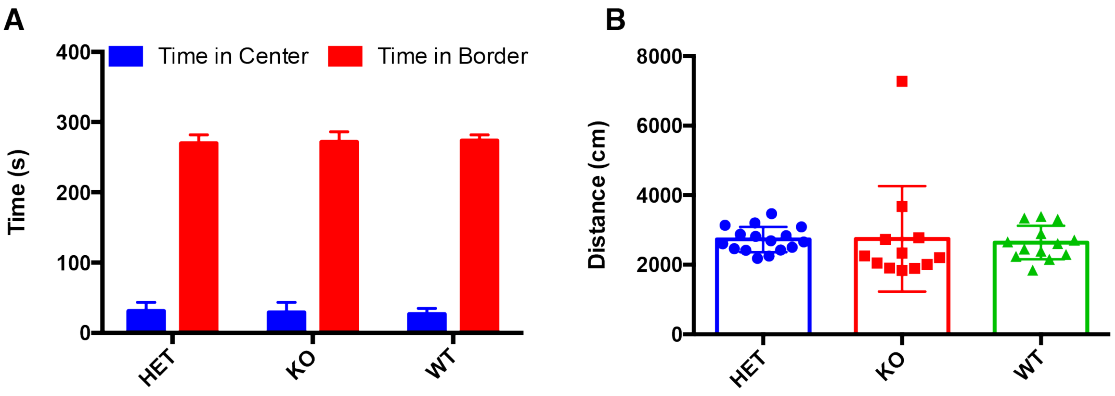

A) Time spent by each genotype in the center or in the border of the open field arena. No significant difference was found comparing time spent in the center or border across genotypes using a one-way ANOVA. **B)** Total distance traveled in the open field across genotypes. No significant difference was found across genotypes using a one-way ANOVA. HET n=16, KO n=12, WT n=13.

Figure 2.3 *Examples of various USV structures*

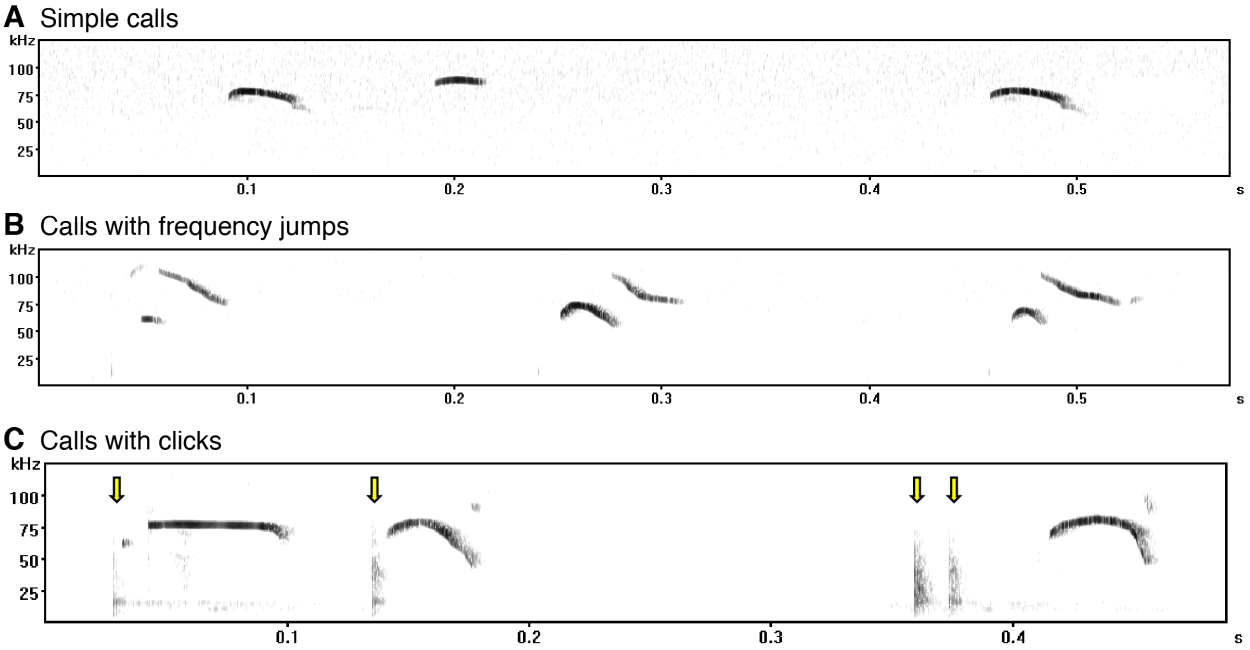

Examples of **A)** simple calls **B)** calls with jumps and **C)** calls with clicks

Figure 2.4 *Initial evidence that Cck regulates the number and duration of pup USVs*

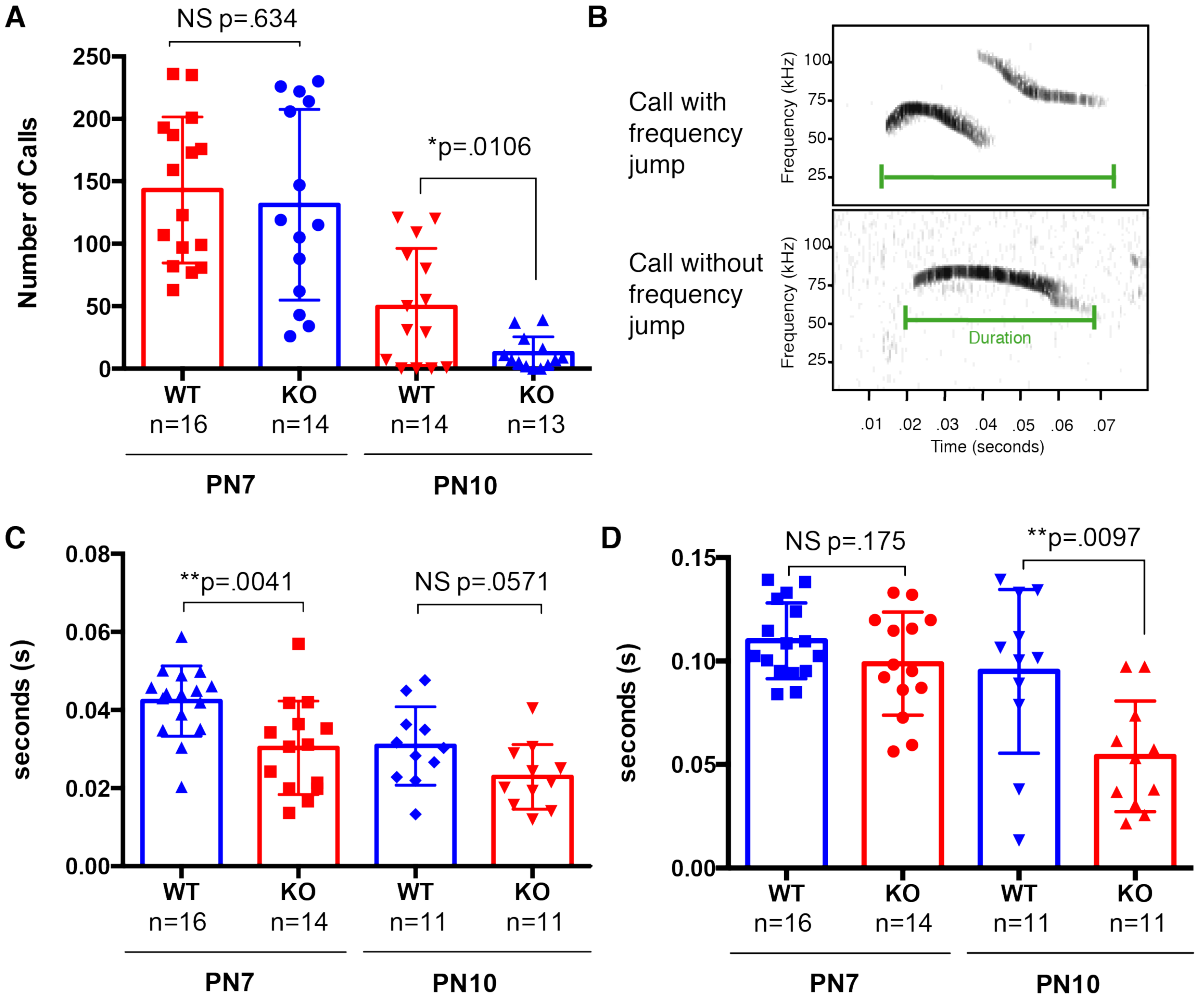

A) Total number of calls. **B)** Examples of how the duration is evaluated for calls with and without frequency jumps **C)** Mean duration of calls **D)** Max duration of calls. Significance calculated with a student's t-test.

Figure 2.5 *Initial evidence that Cck regulates the structure and frequency of pup USVs*

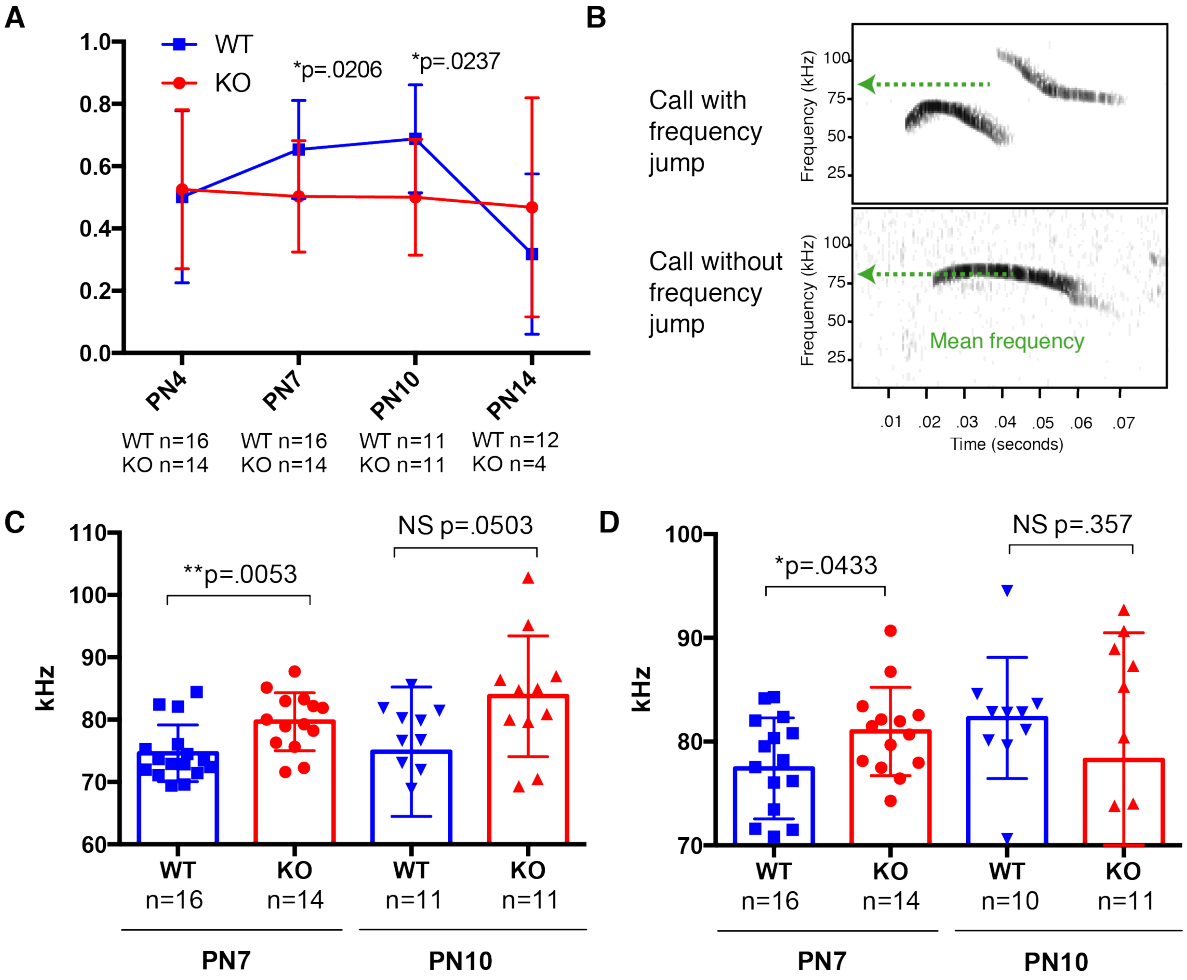

A) Fraction of calls with a frequency jump. **B)** Examples of how the mean frequency is evaluated for calls with and without frequency jumps **C)** Frequency of calls with frequency jumps **D)** Frequency of calls without frequency jumps. Significance calculated with a student's t-test.

Figure 2.6 *Possible outcomes of fasting on pup USVs*

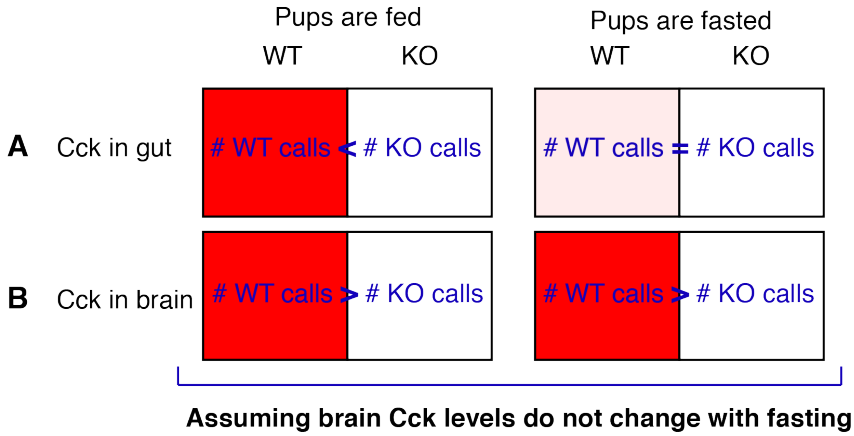

Schematic showing expected outcomes when pups are fasted if call number is related to **A)** gut levels of Cck or **B)** brain levels of Cck. Darker red is representative of higher Cck levels.

Figure 2.7 *No difference between wild type and knockout USVs at P7 in second cohort*

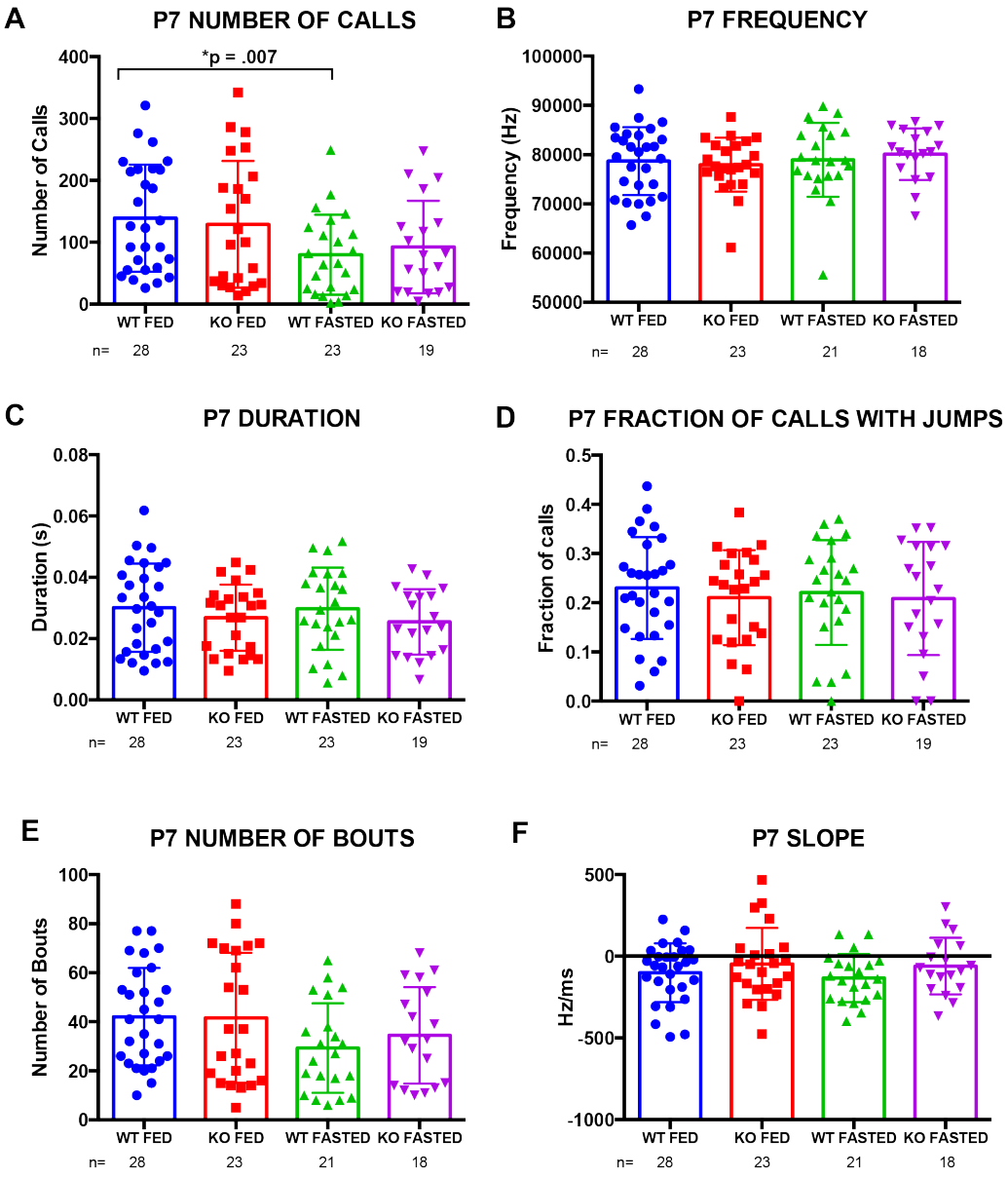

Analysis of USVs in fasted and fed Cck KO and WT animals at P7. **A)** Total number of calls. **B)** Mean frequency of calls. **C)** Mean duration of calls. **D)** Fraction of calls with jumps. **E)** Number of bouts. **F)** Call slope. Significance based on the student's t-test.

Figure 2.8 *No difference between wild type and knockout USVs at P10 in second cohort*

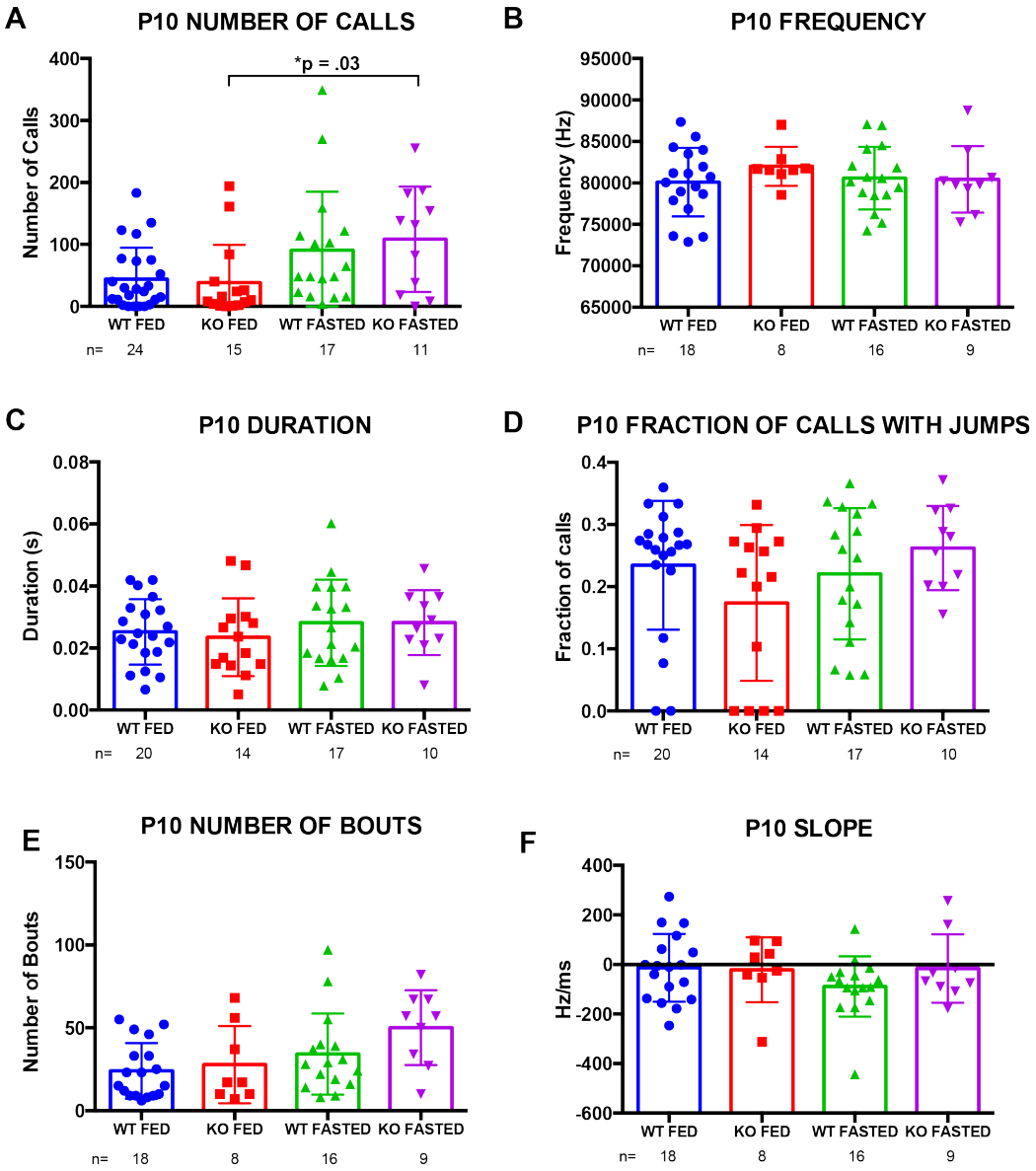

Analysis of USVs in fasted and fed Cck KO and WT animals at P10. **A)** Total number of calls. **B)** Mean frequency of calls. **C)** Mean duration of calls. **D)** Fraction of calls with jumps. **E)** Number of bouts. **F)** Call slope.

CHAPTER THREE: In cultured human neurons, FOXP2 regulates gene expression patterns reminiscent of those in the developing human subplate

Summary

Mammalian brains are highly conserved at both the neuroanatomical and gene expression levels. However, the subplate is a neocortical subregion distinguished by a markedly different developmental trajectory among primates compared to other mammals. Moreover, the molecular mechanisms driving these species differences in subplate development remain mostly unknown. Here, we show that human FOXP2, a transcription factor important for speech and language, regulates gene expression programs consistent with subplate neuron expression patterns. Additionally, we find that FOXP2 regulates conserved, primate-specific and human-specific targets subplate enriched genes. Together, these data highlight FOXP2 as a potential driver of subplate development in the human brain.

Introduction

The subplate is a transient region of the developing mammalian neocortex that contains some of earliest born cortical neurons (Kostovic and Rakic, 1990, Hoerder-Suabedissen et al., 2009). This brain region plays a crucial role in the patterning of cortical circuits by directing thalamocortical afferents to their proper targets (Molnar and Blakemore, 1995b, Molnar and Blakemore, 1995a). While the subplate is present in all mammals, it is greatly expanded in the primate brain, making up a much larger proportion of the developing human cortex compared to the rodent cortex (Hoerder-Suabedissen and Molnar, 2015, Wang et al., 2010). However, the genetic drivers of

subplate development, particularly with regards to human subplate development, remain mostly undiscovered.

A few studies have compared gene expression in the subplate to other regions of the developing forebrain in mouse (Hoerder-Suabedissen et al., 2013, Oeschger et al., 2012, Wang et al., 2009), and at least one study has carried out such comparisons in the developing human fetal brain (Miller et al., 2014). The human fetal brain study noted that expression of the transcription factor *FOXP2* was enriched within the subplate. *FOXP2* has previously been shown to be expressed during human fetal brain development in the cerebellum, thalamus, deep layers of the cortex and striatum (Lai et al., 2003). Mutations disrupting the ability of FOXP2 to bind to DNA, and thus regulate its target genes, have been shown to cause heritable forms of childhood apraxia of speech together with deficits in grammatical function, linking FOXP2 to the development of speech and language (Lai et al., 2000, Lai et al., 2001, Lennon et al., 2007, MacDermot et al., 2005, Vargha-Khadem et al., 1995, Watkins et al., 2002a). Moreover, while FOXP2 is highly conserved among mammals, the hominin version of FOXP2 may have undergone accelerated evolution, resulting in two amino-acid changes that impact transcriptional activity and behaviors (Enard et al., 2002, Zhang et al., 2002, Enard et al., 2009, Konopka et al., 2009). Thus, the enrichment of FOXP2 within a brain region known to be developmentally distinct among primates, suggests that FOXP2 might be important for establishing human subplate identity.

To test this hypothesis, we manipulated *FOXP2* expression in a human cellular system that recapitulates in vivo human brain development (Rosen et al., 2011, Konopka et al., 2012b, Wexler et al., 2011, Palmer et al., 2001, Stein et al., 2014). We

used human neural progenitors (hNPs) that can be induced into post-mitotic neurons (human differentiated neurons or hDNs) and can be genetically modified using viruses. We carried out RNA-sequencing (RNA-seq) in proliferating and differentiated cells in the presence or absence of FOXP2. We compared these data to brain expression data sets from mouse, rhesus macaque and human (Miller et al., 2014, Hoerder-Suabedissen et al., 2013, Bakken et al., 2016), and found that FOXP2 promotes neuronal differentiation into cells with subplate-like expression profiles. Moreover, FOXP2 regulates distinct targets in human subplate, suggesting a species-specific role for human FOXP2 in this region. We further show that FOXP2 represses proliferative, or germinal zone, gene expression patterns, which has never been reported for this transcription factor. Finally, we functionally demonstrate that FOXP2 regulates neuronal maturation and migration *in vitro*, suggesting a potential role for FOXP2 in the transition from a dividing cell in the germinal zone to a mature subplate cell *in vivo*. While we do not claim to have modeled subplate neurons in a dish, these data provide evidence for FOXP2 regulating gene expression programs important for human subplate development.

Results

FOXP2 promotes a subplate-like transcriptional profile

We carried out RNA-seq of hNPs and hDNs expressing either *FOXP2* or a control GFP construct (Figure 3.1A). Importantly, these cells do not endogenously express *FOXP2*, so the GFP expressing control cells provide a null background. We combined these data with human fetal cortex gene expression data (Miller et al., 2014) and first compared the expression of *FOXP2* in human fetal brain to the expression in hNPs and hDNs. *In vivo* the expression of *FOXP2* is about one fold higher than the

mean gene expression level, while *in vitro* expression is close to two folds higher than average (Figure 3.1B). After performing principal component analyses, we found that proliferating hNPs cluster with prenatal samples derived from germinal layers of the developing cortex, while hDNs clustered with samples from post-mitotic cortical layers (Figure 3.1C). Moreover, we calculated the average expression of these layer-correlated genes in hNPs and hDNs and found that genes correlated with the inner and outer subventricular zones and the intermediate zone (SZi, SZo, and IZ) were more highly expressed in proliferating hNPs than in hDNs. In contrast, both control and FOXP2+ hDNs expressed inner cortical plate (CPi)-correlated genes more highly than hNPs, while only FOXP2+ hDNs expressed subplate (SP)-, outer cortical plate (CPo)- and marginal zone (MZ)-correlated genes more highly than hNPs (Figure 3.1D). In line with previous work (Konopka et al., 2012b, Stein et al., 2014), our data support using hNPs and hDNs as models of human cortical neuron development. Additionally, our data show that *FOXP2* expression in hDNs may promote a post-mitotic state.

We performed differential expression analysis comparing cells expressing control virus to *FOXP2* expressing cells in either the hNPs or hDNs (Figure 3.2A, Table 3.1). We found that genes activated by FOXP2 in hDNs are most significantly enriched for genes present in a subplate-correlated gene co-expression network of which *FOXP2* is a member (Figure 3.2B) (Miller et al., 2014). Moreover, as previously reported, *FOXP2* expression is highest in the subplate in all fetal cortex samples analyzed, and in three of four samples this correlation between *FOXP2* expression and the subplate is significant when compared to other layers (Figure 3.2C) (Miller et al., 2014). To more directly test whether FOXP2 activates genes that are relevant to the subplate, we next overlapped

hDN FOXP2 activated genes with individual layer-correlated genes from human fetal brain (Miller et al., 2014) (Table 3.1). We found that the subplate-correlated genes contained the greatest percentage of genes activated by FOXP2 in all samples (Figure 3.2D), while subpial granular layer-correlated genes overlapped best with genes repressed by FOXP2 (Figure 3.2E). Together, these data demonstrate that FOXP2 positively regulates genes that are expressed in human fetal subplate.

FOXP2 activates subplate genes in a species-specific manner

Next, we sought to determine whether FOXP2 activates subplate genes specifically in the human brain. In order to accomplish this we selected microarray expression data from tissue laser microdissected from embryonic day (E) 70, 80, and 90 rhesus macaque cortices made publically available through the NIH Blueprint non-human primate atlas (Bakken et al., 2016). These fetal macaque developmental ages were chosen because they, like the developmental ages surveyed in the human fetal cortex microarray (Miller et al., 2014), correspond to the “subplate stage” of primate cortical development (Kostovic and Rakic, 1990). We identified samples from the human fetal cortex microarray (Miller et al., 2014) that were from analogous regions to those assayed in the macaque microarray and calculated significant layer correlated genes for each species. The human 15 and 16 pcw samples and both 21 pcw samples were combined for this analysis and renamed 16 pcw and 21 pcw, respectively. Comparing layer specific genes with hDN FOXP2 targets again revealed a significant overlap between human VZ correlated genes and genes repressed by FOXP2 at 16 pcw. Importantly, this relationship was conserved in macaque (Figure 3.3A; Table 3.2). Moreover, subplate correlated genes from both species at all stages overlapped

significantly with genes activated by FOXP2 in hDNs (Figure 3.3A; Table 3.3). This suggests that repression of VZ genes and activation of SP genes is a conserved function of FOXP2 in primates. We next compared VZ genes repressed by FOXP2 in human and macaque at any developmental stage. While species specific VZ FOXP2 repressed genes were identified, we found that VZ genes repressed by FOXP2 were significantly more likely to be conserved between species than VZ correlated genes generally (Fisher's exact test $p = 9.2 \times 10^{-06}$, odds ratio 0.51, 95 percent confidence interval 0.34-0.69) (Figure 3.3B). Similar results were found when comparing human and macaque subplate genes activated by FOXP2 (Fisher's exact test $p = 7.5 \times 10^{-04}$, odds ratio 0.36, 95 percent confidence interval 0.20 - 0.66) (Figure 3.3B). These data suggest that while the role of FOXP2 in subplate development between these species is partially conserved, species-specific FOXP2 targets may still differentiate human and macaque VZ and subplate during development.

Since the primate subplate is much larger in proportion to cortical plate than the rodent subplate, and the subplate is hypothesized to have evolved in order to support the more complex cortex of higher mammals (Montiel et al., 2011), we compared human and macaque subplate enriched FOXP2 hDN activated targets with those in mouse. Because of the unavailability of a mouse genome-wide expression data set that includes and distinguishes all of the developing cortical layers including the subplate, we made use of expression data collected from embryonic day (E) 15 and E18 mouse primary somatosensory (S1) subplate and cortical plate that was used previously to identify mouse subplate enriched genes (Hoerder-Suabedissen et al., 2013, Oeschger et al., 2012). We compared genes expressed more highly in mouse subplate compared

to cortical plate with genes expressed more highly in human or macaque fetal subplate compared to cortical plate (Miller et al., 2014). As in the mouse data, only human and macaque samples from S1 were used in this analysis. Because there are few human and macaque S1 samples per developmental stage, we combined data from multiple stages before differential expression analysis was performed in order to more confidently identify subplate-enriched genes. In the developing human brain, *FOXP2* is more highly expressed in subplate compared to cortical plate, while macaque *FOXP2* expression is similar across these layers (Figure 3.4A). Interestingly, in the mouse *FOXP2* is more highly expressed in cortical plate than subplate (Figure 3.4A), suggesting that *FOXP2* expression in the subplate correlates with subplate size (Kostovic and Rakic, 1990). These results are consistent with previously published *in situ* hybridization experiments showing that *FOXP2* expression is enriched the human subplate but in the mouse cortical plate (Vernes et al., 2008, Teramitsu et al., 2004, Takahashi et al., 2003). Significantly SP and CP enriched genes were identified in all three species (Figure 3.4B); however, the largest numbers of significant SP and CP enriched genes were present in human suggesting that the human SP and CP transcriptomes are more distinct than those of macaque and mouse. We compared the SP enriched genes of each species and identified species specific, primate specific, and conserved SP enriched genes (Figure 3.4C). Supporting the results shown in Figure 3.3, the overlap between human and macaque subplate genes was the most significant of any pairwise overlap (Figure 3.4D). However, mouse SP genes are more significantly enriched in macaque than human subplate genes (Figure 3.4D) suggesting that while human and macaque SP are developmentally similar, the mouse SP transcriptome is

more similar to the macaque than to the human SP transcriptome. We next calculated the enrichment of FOXP2 hDN activated genes among the SP genes of each species and found that all species were significantly enriched for these genes (Figure 3.4 E). However, when we compared SP enriched FOXP2 hDN activated genes across species, human specific genes formed the largest group with 56 genes (Figure 3.4F; Table 3.4). Additionally, we identified 18 primate specific and 13 conserved FOXP2 hDN activated subplate enriched genes (Figure 3.4F; Table 3.4). We next constructed a simple network to visualize the shared and specific SP enriched FOXP2 hDN activated genes among the three species. Darker red nodes represent a higher gene expression fold change by FOXP2 compare to control in hDNs, and the top four FOXP2 hDN activated SP genes (*PAPPA*, *TGM2*, *NGB*, and *RASGRF1*) are all human specific (Figure 3.4G; Table 3.4). Interestingly, copy number variants containing *PAPPA* and *TGM2* have been shown to cause speech and language delays and other neurological phenotypes (Firth et al., 2009). Importantly, conserved SP FOXP2 target, *CDH18,* and mouse SP specific target, *RCAN2,* were previously confirmed to be subplate specific in mouse by in *situ hybridization* (Oeschger et al., 2012). In addition, conserved SP target *SLC1A2 and* mouse specific SP target *NR3C1* are both enriched in the SP compared to CP as shown by *situ hybridization* in E18 mouse cortex performed by the Allen Institute (Figure 3.5B-C). Conversely, primate specific SP target, *PLXNA2,* and human specific target *GPR37* are not SP enriched in the mouse (Figure 3.5D-E). Comparing the FOXP2 activated subplate enriched genes of human, macaque, and mouse allowed us not only to identify primate specific FOXP2 SP targets, but also emphasized the influence of FOXP2 in the human subplate specifically.

FOXP2 promotes migration in a cell-non-autonomous manner and facilitates neuron differentiation

Because FOXP2 has been previously implicated in neuronal migration (Tsui et al., 2013), and because subplate neurons are involved in the switch of migrating upper layer neurons from multipolar to bipolar migration (Ohtaka-Maruyama et al., 2018), we tested whether expression of FOXP2 affected the migration capacity of hNPs in culture. We generated neurospheres from proliferating hNPs by mixing equal quantities of cells expressing CTRL-GFP or FOXP2-WT or mixing equal quantities of cells expressing CTRL-GFP or FOXP2-KE as previously described (Usui et al., 2017, Fontenot et al., 2017) (Figure 3.6A-B). FOXP2-KE contains a single point mutation in the DNA-binding domain of FOXP2 that mimics the mutation in a family known as the “KE” family with verbal dyspraxia (Lai et al., 2001) (Figure 3.6C). FOXP2-KE has been shown to localize less efficiently to the nucleus (Vernes et al., 2006), and immunohistochemistry of hNPs expressing FOXP2 showed that the KE mutant was expressed in both the cytoplasm and the nucleus while the WT protein had almost entirely nuclear expression (Figure 3.6D). Importantly, electron mobility shift assays have shown that this altered form of FOXP2 is unable to bind to DNA (Vernes et al., 2006). Thus, FOXP2-KE was used as an additional control. The migration distance of the nucleus of every cell from the center of the sphere was measured. Compared to control cells within the same neurospheres, both FOXP2-KE and –WT expressing cells traveled significantly further from the center of the sphere on average (Figure 3.7A); however, FOXP2-WT cells migrated further from their GFP positive counterparts than FOXP2-KE expressing cells (Figure 3.7B). These data suggest that FOXP2 increases neuronal migration in a DNA-binding

independent manner, but that the ability of the WT gene to robustly activate target genes increases the cells' migration capacity over the DNA-binding mutant. Surprisingly, the CTRL-GFP cells cultured with FOXP2-WT expressing cells migrated significantly further than the CTRL-GFP cells cultured with FOXP2-KE expressing cells (Figure 3.7C). These results suggest that non-cell-autonomous factors regulated by FOXP2-WT play some role in the observed increase in cell migration.

Together with confirming the role of FOXP2 in neuron migration, Foxp2 has been shown to regulate the transition between proliferating radial glia and post-mitotic intermediate progenitors in developing mouse cortex (Tsui et al., 2013). To confirm that FOXP2 plays a pro-neurogenic role in hNPs, we performed immunostaining for FOXP2 and the early post-mitotic neuron marker, doublecortin or DCX (Figures 3.6A-B), and quantified the percent of CTRL-GFP, FOXP2-KE and FOXP2-WT expressing cells in the neurospheres that were also positive for DCX. There was no significant difference within spheres between the percent of CTRL-GFP and FOXP2-KE expressing cells that were DCX positive (Figure 3.7D, left). FOXP2-WT expressing cells, on the other hand, exhibited a significant increase in the percent of cells co-labeled with DXC compared to CTRL-GFP cells in the same sphere (Figure 3.7D, right). These data together with our RNA-seq data, these findings suggest that FOXP2 promotes neuron maturation.

Discussion

The subplate is an understudied part of the neocortex with potentially important evolutionary adaptations as, relative to overall neocortical size, the subplate is much larger in human and non-human primates than in lissencephalic mammals such as rodents (Hoerder-Suabedissen and Molnar, 2015). *FOXP2* is enriched within the

subplate in the developing human fetal neocortex (Miller et al., 2014), its function has been linked to the ability to develop proper language skills (Lai et al., 2001), Moreover, FOXP2 contains two amino acid changes that are specific to the human lineage (Enard et al., 2002). These observations led us to hypothesize that FOXP2 plays a role in establishing human subplate identity**.**

Subplate neurons are among the first mature neurons in the developing cortex (Kostovic and Rakic, 1990, Hoerder-Suabedissen et al., 2009, Rakic, 1974), and in embryonic mouse cortex, Foxp2 has been shown to regulate the transition from radial glia to more mature intermediate neuronal progenitors (Tsui et al., 2013). *In utero* electroporation of shRNAs targeting Foxp2 in the germinal layers of E13-14 cortex lead to a decrease in the number of cells expressing the intermediate progenitor marker Tbr2 and an increase in the number of cells expressing the radial glia marker Pax6 at E16, suggesting that Foxp2 plays a proneurogenic role in the developing cortex (Tsui et al., 2013). Consistent with this finding in mouse, we show that in human neurons exogenous expression of *FOXP2* leads to repression of genes expressed in germinal layers of developing human cortex. While several studies of FOXP2 targets have highlighted the regulation of genes related to a mature neuronal phenotype (Vernes et al., 2011, Vernes et al., 2007), ours is the first to suggest a role for FOXP2 in the repression of genes involved in maintenance of a germinal state. Moreover, we show that cells expressing FOXP2-WT, but not the DNA-binding deficient KE mutant, are more likely than control cells to express doublecortin, a marker of newborn neurons. This strengthens the finding that FOXP2 inhibits proliferation and increasing the number of post-mitotic neurons.

Interestingly, we showed that FOXP2-WT promoted cell migration in a cell-non-autonomous manner, and previous work has shown that *in utero* electroporation of shRNAs targeting Foxp2 in the germinal layers of E13-14 mouse cortex decreases neuronal migration into the cortical plate (Tsui et al., 2013). Since the generation of *Foxp2* expressing subplate and layer VI neurons occurs at E11.5 and E12.5, respectively (Angevine and Sidman, 1961, Custo Greig et al., 2013), reducing *Foxp2* expression at E13-14 is unlikely to impede the migration of early born *Foxp2* expressing cells into the cortical plate. Moreover, knockdown of *Foxp2* at E13-14 reduced the number of neurons migrating into the upper cortical plate, where *Foxp2* is not typically expressed (Tsui et al., 2013). These observations, along with the data from the neurosphere migration assays presented here, suggest that *FoxP2* expression in the subplate is playing a non-cell-autonomous role to affect migration of later-born neurons.

This role may be facilitated by regulation of extracellular matrix (ECM) components by FoxP2. Mouse, human and non-human primate subplate zones are rich in ECM (Derer and Nakanishi, 1983, Kostovic et al., 2002), which acts as a scaffold for migrating neurons (Franco and Muller, 2011). In this study, we find that Hyaluronic Acid Synthase 3 (*HAS3),* which is involved in the synthesis of a major constituent of the ECM (Arranz et al., 2014, Fraser et al., 1997) is an activated target of FOXP2 specifically enriched in human and macaque subplate. Perturbation of primate specific subplate enriched targets like *HAS3* may explain the loss of cortical grey matter in KE family members (Belton et al., 2003) when no analogous cortical volume loss has been shown in mouse (French et al., 2007, Shu et al., 2005, Groszer et al., 2008).

Cell non-autonomous effects by FOXP2 on migration could also be facilitated by an increase in neuronal activity in *FOXP2* expressing cells. Recently, it was shown that mouse subplate neurons enable the multipolar to bipolar transition of migrating excitatory cortical neurons, and that this transition is essential for the formation of the mouse six-layer cortex (Ohtaka-Maruyama et al., 2018, Tsai et al., 2005). Specifically, it was found that glutamatergic inputs from the subplate neurons onto the migrating multipolar neurons we necessary for this multipolar to bipolar transition (Ohtaka-Maruyama et al., 2018). Activated FOXP2 targets are enriched for genes involved in chemical synaptic transmission including *synaptotagmin-4* and *-7*. Synaptotagmins detect calcium influx during action potentials and trigger neurotransmitter release (Sudhof, 2012). By activating of targets involved in synaptic transmission, FOXP2 could regulate migration non-cell-autonomously by increasing neurotransmitter release from cells in which it is expressed onto non-*FOXP2* expressing multipolar neurons. While it would not elucidate a human-specific role of FOXP2 in subplate neurons, it would, nonetheless, be fascinating to see if subplate regulation of the multipolar to bipolar transition of migrating cortical neurons was preserved in cortical *Foxp2* knockout mice.

Another activated FOXP2 target enriched in the subplate at pcw 15 that may play a role in cortical neuron migration is *Contactin Associated Protein Like 2* (*CNTNAP2*). Mutations in this gene are associated with epilepsy, autism spectrum disorder, schizophrenia, and language impairment (Rodenas-Cuadrado et al., 2014). Histological analysis of tissue from patients harboring a homozygous point mutation in *CNTNAP2* showed, among other abnormalities, aberrant thickening of areas of the cortex, blurring of the boundary between gray and white matter, and many ectopic neurons within the

white matter itself (Strauss et al., 2006). Because interstitial white matter neurons are thought to be the final vestiges of the subplate, boundary blurring and ectopic cells in the white matter and could indicate subplate abnormalities (Kostovic and Rakic, 1980). Moreover, observations of thickened cortical layers and neurons with inappropriate orientation could suggest problems with cell migration including the multipolar to bipolar transition of migrating neurons (Strauss et al., 2006). Importantly, this study and others identify *CNTNAP2* as a downstream target of FOXP2 (Vernes et al., 2008, Adam et al., 2017, Usui et al., 2017). Therefore, alteration of the expression of *CNTNAP2* by FOXP2 maybe one mechanism by which FOXP2 effects subplate development and cortical neuron migration in humans. That the heterozygous FOXP2 loss of function phenotype (Hurst et al., 1990, Vargha-Khadem et al., 1998) is less severe than the phenotype exhibited by those with homozygous mutations in *CNTNAP2* (Strauss et al., 2006) is unsurprising given that *CNTNAP2* expression would be not be totally ablated by partial loss of FOXP2 function.

Future directions

In addition to the subplate, *FOXP2* is expressed in thalamic neurons that project to the cortex. The expansion of the subplate zone between 15 and 18 pcw in human is thought to be largely due to the increase of invading afferent fibers (Kostovic and Rakic, 1990, Kostovic and Judas, 2002). In fact, the subplate acts as a holding compartment for thalamocortical, basal forebrain, and callosal and ipsilateral cortico-cortical afferents during cortex development (Kostovic and Goldman-Rakic, 1983, Kostovic and Judas, 2002). When the subplate is ablated, the circuits formed by these neurons are disrupted (Kanold and Luhmann, 2010). Because the *in vivo* RNA-seq data used in this study was

derived from a bulk dissection of the subplate layer, transcripts present in the waiting afferents were likely represented. Thus, both targets of FOXP2 expressed in subplate neurons, and targets of thalamic FOXP2 destined to be translated in axons migrating through the subplate were potentially identified in this study. It would be of interest to perform single cell sequencing to determine which genes are regulated by FOXP2 in subplate neurons alone. Moreover, subplate cells are morphologically and molecularly diverse (Kostovic and Rakic, 1990, Hoerder-Suabedissen and Molnar, 2013). Single cell transcriptomic analysis throughout human subplate development would increase our understanding of subplate cell types, their origin, and the involvement of FOXP2 in the regulation of their identities.

Moreover, single cell transcriptomic analysis of mouse and macaque subplate at similar developmental stages would allow us to identify conserved and species-specific subplate cell transcriptional profiles. Additionally, sequencing the overlying cortical plate in parallel in all three species would allow us to compare the amount of FoxP2 transcript along with the number of *FoxP2* expressing cells in the subplate and cortical plate. This way, we could determine if the proportion of *FoxP2* expressing cells in the subplate compared to the cortical plate was highest in human, followed by macaque and mouse causing the expression differences seen in bulk expression data (Figure 3.4). Alternatively, the proportion of *FoxP2* expressing cells could be the same across species, but the expression levels in those cells could differ. Furthermore, this analysis would enable us to identify transcriptomic differences between *FoxP2* expressing cells in the subplate and cortical plate, which would help us to determine whether *FoxP2* expressing cells in the subplate are simply layer VI cells whose migratory routes were

impeded by incoming afferents, or whether they are a different cell type. Importantly, we could compare these differences across species. Even outside of the FoxP2 context, an evolutionary single-cell transcriptomic analysis of the subplate and cortical plate would be of incredible value to the cortical development field.

While our study provides evidence of a role for FOXP2 in subplate development, in particular maturation of subplate neurons and, potentially, the migration of neurons traversing the subplate zone to upper cortical layers, and highlights two human subplate specific FOXP2 targets implicated in language delay (Firth et al., 2009), we have yet to discover the role that FOXP2 plays in establishing the early subplate circuitry that leads to proper thalamocortical connections and, thus, proper language circuitry. It is known that subplate neurons are some of the first physiologically active neurons in the cortex, forming one of the first functional cortical circuits connecting early thalamic inputs to layer IV, relaying early oscillatory activity into the developing cortical plate (Kanold and Luhmann, 2010). Subplate correlated genes activated by FOXP2 in hDNs are enriched for post-synaptic and voltage gated channel genes. Regulation of these genes by FOXP2 may lead to the mature physiological phenotype of subplate neurons.

It is impossible, however, to prove a relationship between FoxP2 and subplate neuron maturation and function without knocking down *FoxP2* in a model that includes developing cortical circuits. Our lab is currently characterizing mice with cortex-specific loss of *Foxp2*, but we have yet to identify any morphological differences in these mice compared to wild type animals (Co *et al.,* unpublished). The lack of an overt morphological phenotype could suggest that FoxP2 plays a primate specific role in this region; however, we have yet to analyze the effect of cortical *Foxp2* knockout on

thalamocortical afferent targeting which is known to require the subplate layer in mice (Hoerder-Suabedissen and Molnar, 2015). Along these lines, *Foxp2*-R552H null animals have abnormally organized cortical barrels in primary somatosensory cortex where thalamic afferents form circuits with layer IV pyramidal neurons (Ebisu et al., 2016). While this could be due to loss of Foxp2 in the thalamus alone, it will be important to observe barrel structure in the cortex-specific null animals as the subplate is critical for proper barrel formation (Piñon et al., 2009, Tolner et al., 2012). Additionally, even if thalamocortical axon path finding and barrel structure are morphologically normal in cortex specific null animals, the circuitry could still be abnormal because subplate neurons are required for the maturation of thalamocortical circuits in layer IV (Kanold et al., 2003). It would be necessary to probe these circuits electrophysiologically in cortical knockout and wild type animals. These experiments would help to prove a conserved role for FoxP2 in the subplate.

Human forebrain organoids could potentially help us uncover the human specific role of FOXP2 in the subplate. Derived from human embryonic stem cells or induced pluripotent stem cells, 3D forebrain organoids have been shown to recapitulate human early cortical development, especially as they form of proliferative zones and lower layer neurons in a spatially organized way (Camp et al., 2015, Lancaster et al., 2013, Lancaster et al., 2017). One group has even shown evidence of a preplate-like layer splitting into marginal zone and presubplate-like layers (Lancaster et al., 2017), suggesting that they could be useful for studying genes involved in early subplate formation. In an attempt to study the role of Foxp2 in human cortical development, our lab has successfully generated FOXP2-null, human induced pluripotent stem cells and

is in the process of generating knockout and wild type forebrain organoids (Park *et al.*, unpublished). One caveat in using forebrain organoids to study FOXP2 function is that *FOXP2* positive cells are not abundant in previously published forebrain organoid models, making up fewer than 3% of the total cells as assayed by single-cell RNA-sequencing (Camp et al., 2015, Quadrato et al., 2017). Observing a phenotypic difference between wild type and knockout organoids when so few *FOXP2* expressing cells are present in wild type may prove challenging. Even if we are able to increase the number of *FOXP2* expressing cells, it is, at present, not possible to model thalamocortical circuitry in cerebral organoids, which is crucial as a defining feature of the human subplate is the vast number of incoming thalamic afferents (Kostovic and Rakic, 1990). However, organoids with dorsal and ventral identities have been fused to model human interneuron migration from the medial ganglionic eminences to the cortex (Bagley et al., 2017, Xiang et al., 2017) suggesting that in the future we will be able to study connections between different brain regions in human organoids.

In the mean time, CRISPR/Cas9 gene editing tools have made it possible to genetically engineer ferrets and cynomolgus monkeys, animals with cortices larger than mice that are gyrencephalic (Johnson et al., 2018, Niu et al., 2014). As carnivores and non-human primates both have expanded subplate layers compared with rodents, studying the effects of loss of FoxP2 in these model systems could prove fruitful as it has for disorders like microcephaly and autism spectrum disorders (Johnson et al., 2018, Liu et al., 2016).

Figures

Figure 3.1 *FOXP2 promotes a subplate-like transcriptional profile*

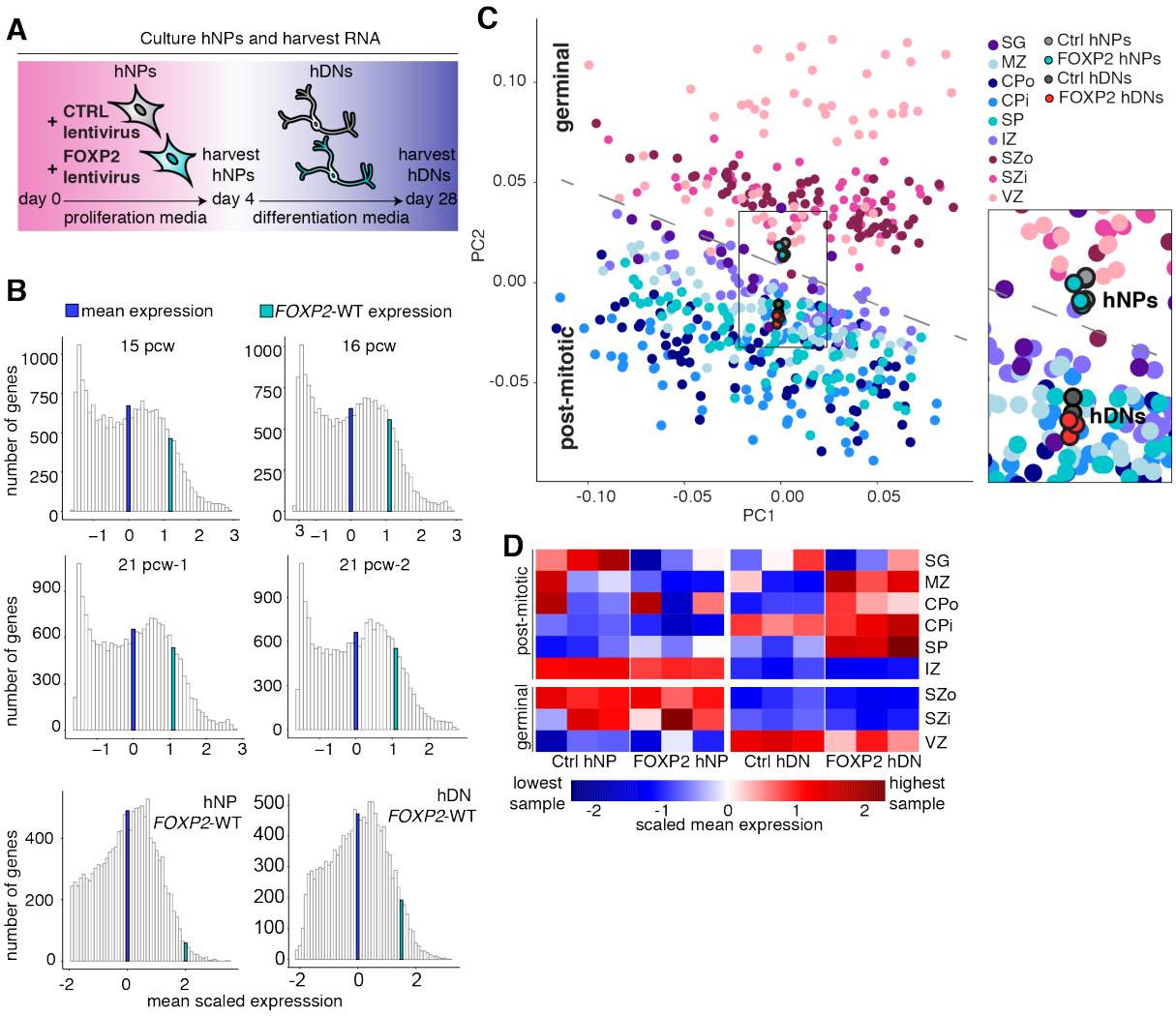

A) Schematic representation of the human cell culture and RNA collection timeline. **B)** Number of expressed genes *in vivo*, in hNPs and hDNs binned by average mean-scaled expression. The expression of FOXP2 relative to all other genes is highlighted in turquoise. **C)** A PCA plot comparing human fetal brain transcriptomes (Miller et al., 2014) with hNP and hDN RNA-seq transcriptomes. Samples from all four brains analyzed in Miller et al. are represented. Inset: Enlarged image of rectangle containing hNP samples. Subpial granular zone (SG), marginal zone (MZ), outer and inner cortical plate (CPo, CPi), subplate (SP), intermediate zone (IZ), outer and inner subventricular zone (SZo, SZi), ventricular zone (VZ). **D)** Heat map representing the mean expression in the hNP and hDN transcriptomes of the layer correlated genes identified in 21 pcw-2 human fetal brain. Red corresponds to higher mean expression, while blue represents lower mean expression compared to other hNP or hDN samples. White is the average of the mean layer expression across samples.

Figure 3.2 *FOXP2 positively regulates genes expressed in human fetal subplate*

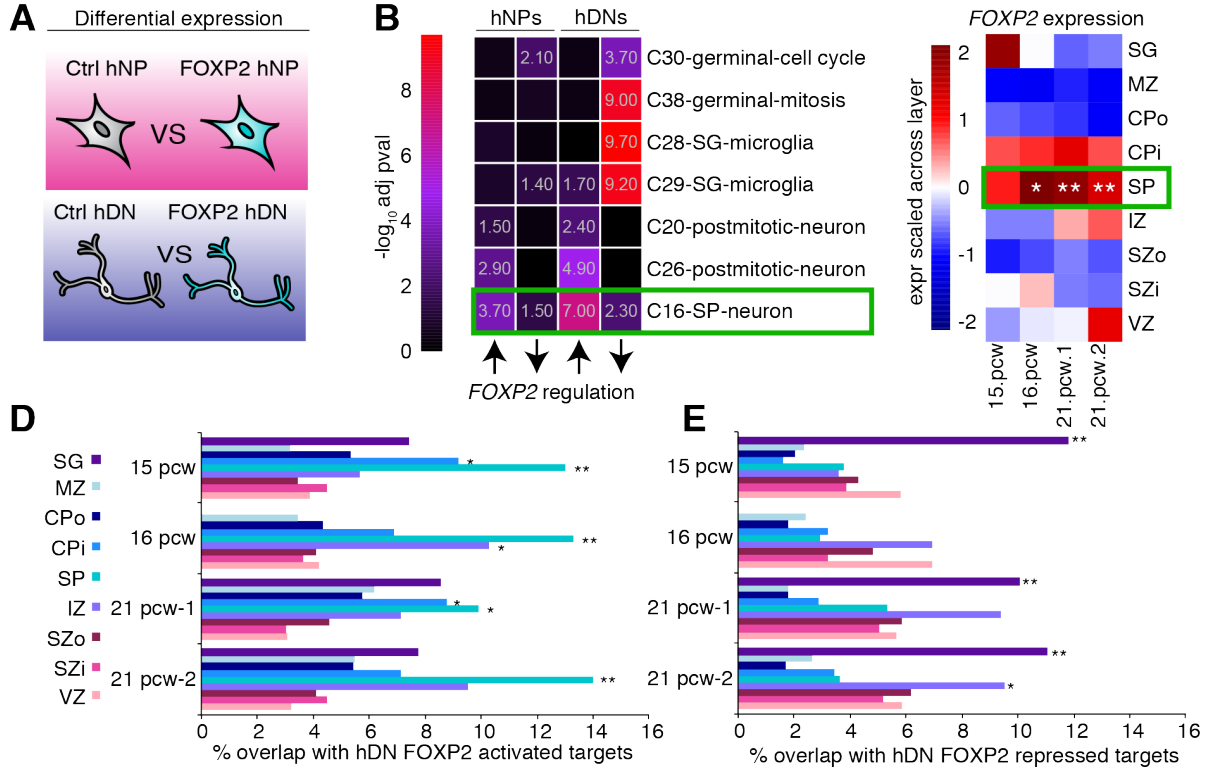

A) Schematic showing the groups compared for differential expression (DE) analysis. **B)** Overlap between WGCNA modules from human fetal cortical layers identified by Miller et al. and FOXP2 DE genes. Only modules with a significant overlap with at least one group of DE genes are shown. The p-value was corrected for comparison to all identified modules. Color corresponds to –log10 BH adjusted p-value with red being most and black being least significant. Green box highlights the overlap between DE genes and the subplate specific module. **C)** FOXP2 expression in fetal brain from Miller et al. Green box highlights high expression in the subplate (ANOVA test of Pearson correlations of FOXP2 expression in each layer from Miller et al., *$p < 0.01$, **$p < 0.05$) **D)** A bar plot showing the percent overlap of human fetal layer correlated genes with genes repressed by FOXP2 in hDNs. **E)** A bar plot showing the percent overlap of human fetal layer correlated genes with genes activated by FOXP2 in hDNs (for D and E: *$p < 0.05$, ** $p < 0.01$, hypergeometric test BH corrected for comparisons across layers within subject).

Figure 3.3 *FOXP2 regulates similar gene expression profiles in human and macaque*

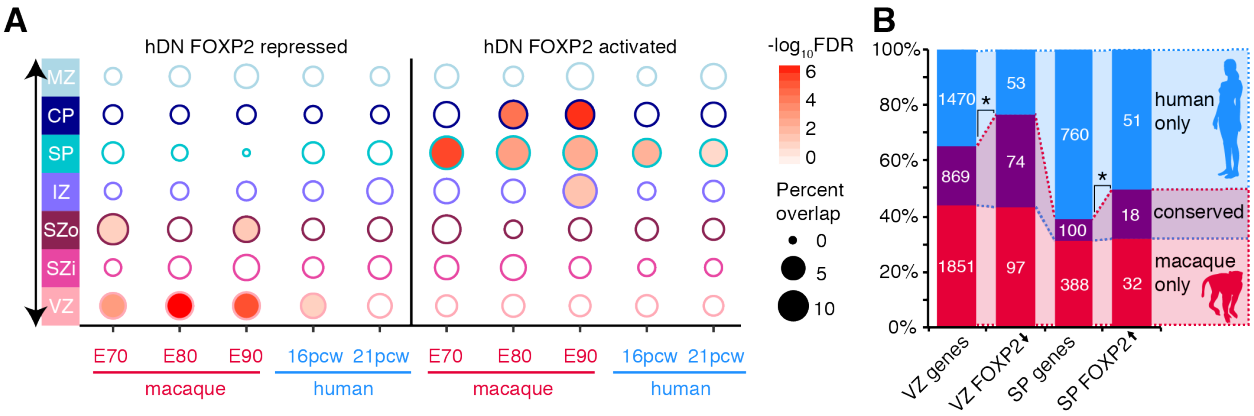

A) Bubble plot showing the overlaps between human or macaque genes significantly correlated with each layer when compared to all others and genes repressed or activated by FOXP2 in hDNs. The size of each bubble represents the percentage of layer-correlated genes that are FOXP2 targets. Darker shading indicates a lower BH corrected hypergeometric test p-value of the overlap. **B)** Bar plot showing the overlap between human and macaque VZ genes, VZ genes repressed by FOXP2 in hDNs, SP genes, and SP genes activated by FOXP2 in hDNs (* $p < 1x10^{-3}$ fisher exact test comparing the prevalence of species specific and conserved genes between FOXP2 targets and non-targets).

Figure 3.4 *FOXP2 activates subplate genes in a species-specific manner*

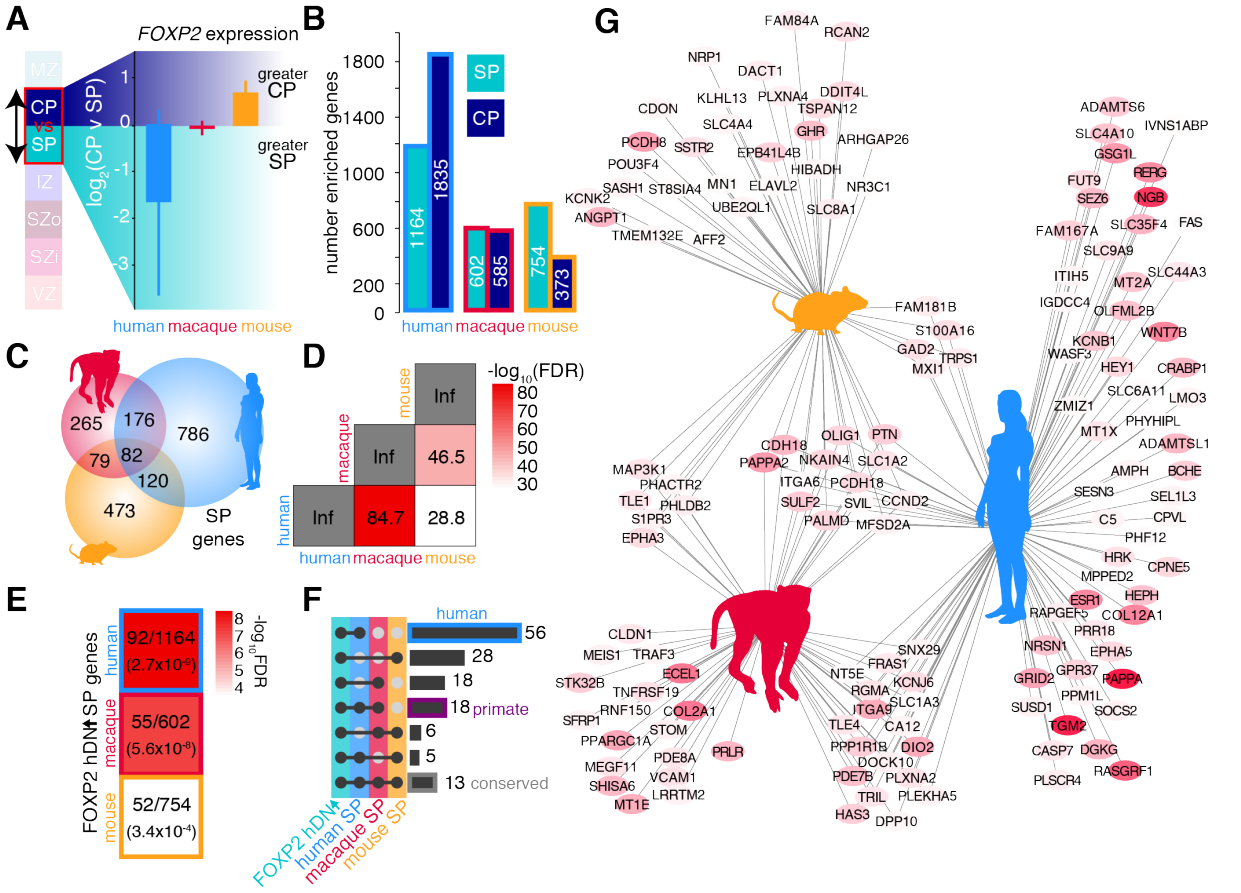

A) Comparison of FOXP2 expression levels between CP and SP in human, macaque, and mouse. A positive log2 fold change indicates enrichment in CP, while negative a value indicates enrichment in SP. **B)** Number of SP and CP enriched genes in all three species. **C)** Venn diagram showing the overlaps among human, macaque, and mouse SP enriched genes. **D)** Hypergeometric overlap between human, macaque, and mosue SP enriched genes. Color corresponds to –log10 BH adjusted p-value with red being most and white being least significant. **E)** Number of SP enriched genes activated by FOXP2 compared to total SP enriched genes. The hypergeometric test derived p-value of the overlap is in parentheses. Darker shading represents a more significant p-value. **F)** Upset plot showing the number of overlapping hDN FOXP2 activated subplate genes among human, macaque, and mouse. **G)** A network connecting FOXP2 hDN activated genes to species for which the genes are subplate enriched. Node color represents the log2 fold change of the gene expression in FOXP2 expressing hDNs compared to control.

Figure 3.5 *Example in situ hybridizations of conserved and species-specific subplate enriched FOXP2 targets in mouse cortex*

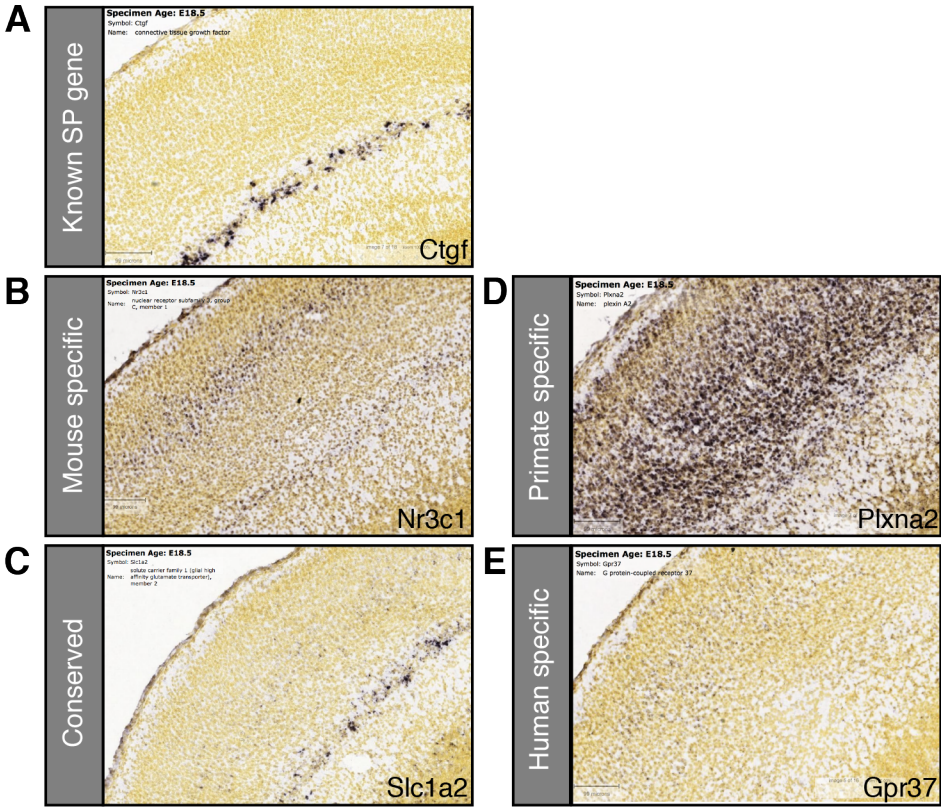

Image credit: Allen Institute

In situ hybridization in mouse E18 cortex showing: **A)** Expression of known SP gene, *Ctgf*. **B)** Expression of mouse specific SP enriched FOXP2 target, *Nr3c1*. **C)** Expression of conserved SP enriched FOXP2 target, *Slc1a2*. **D)** Expression of primate specific SP enriched FOXP2 target, *Plxna2*. **E)** Expression of human specific SP enriched FOXP2 target, *Gpr37*.

Figure 3.6 *Neurospheres expressing FOXP2-WT and –KE hNPs*

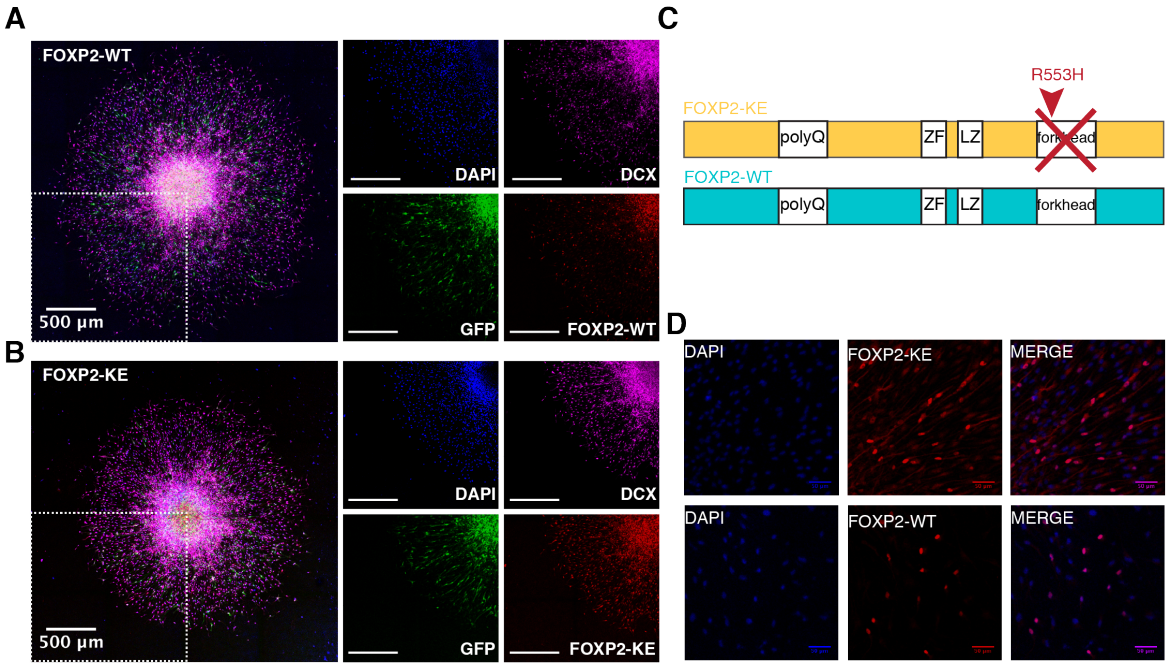

A) IHC of example neurosphere composed of hNPs expressing FOXP2-WT and CTRL-GFP (FOXP2 (red) and DCX (magenta)). GFP fluorescence is shown in green, and DAPI blue. Left: whole sphere, channels merged. Right: Separate channels; lower left quadrant shown. **B)** Same as A showing an example neurosphere composed of hNPs expressing FOXP2-KE and CTRL-GFP. **C)** Schematic representation of the R553H mutation in FOXP2-KE. **D)** Examples of hNPs exogenously expressing FOXP2-WT or –KE probed with an anti-FOXP2 antibody that recognizes both.

Figure 3.7 *FOXP2 promotes migration in a cell-non-autonomous manner and facilitates neuron differentiation*

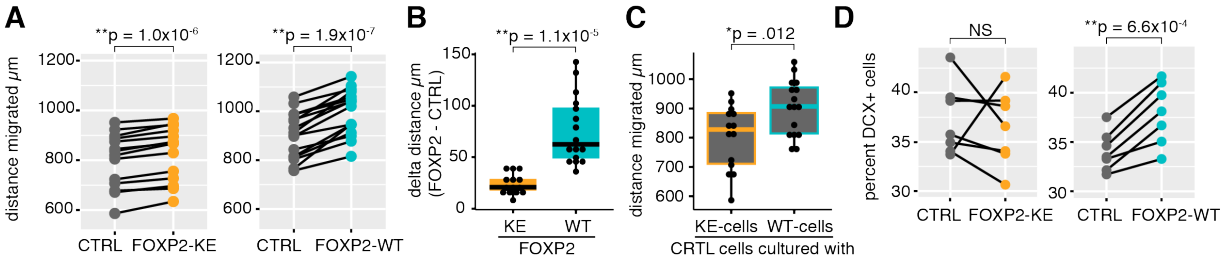

A) Left: average distance migrated by CTRL-GFP or FOXP2-KE positive cells from the center of the neurosphere. Each pair of points represents CTRL-GFP and FOXP2-KE positive cells cultured in the same neurosphere (n = 14 neurospheres with hundreds of cells counted per sphere; paired student's t-test). Right: average distance migrated by CTRL-GFP or FOXP2-WT positive cells from the center of the neurosphere. Each pair of points represents CTRL-GFP and FOXP2-WT positive cells cultured in the same neurosphere (n = 16 neurospheres; paired student's t-test). **B)** Box plot showing delta average distance traveled between FOXP2-KE or FOXP2-WT cells and the respective CTRL-GFP positive cells (n = 7 neurospheres per condition, student's t-test, two-sided, non-parametric). **C)** Average distance traveled by CTRL-GFP positive cells cultured with FOXP2-KE or FOXP2-WT expressing cells (n= 7 neurospheres per condition; student's t-test, two-sided, non-parametric). **D)** Left: Percent of CTRL-GFP or FOXP2-KE positive cells that are also positive for the newborn post-mitotic neuron marker DCX. Right: Percent of CTRL-GFP or FOXP2-WT positive cells that are also positive for DCX. Each pair of points represents CTRL-GFP and FOXP2-WT or FOXP2-KE positive cells cultured in the same neurosphere (n = 7 neurospheres per condition; paired student's t-test).

Tables

Table 3.1 *Layer correlations of differentially expressed genes*

The differentially expression genes are from the first round of hNP and hDN RNA-sequencing later described here and later in chapter 4.

Table 3.1	log2 Fold Change - First round - CMP filtered		Significantly correlated layer			
Gene	hNP	hDN	15 pcw	16 pcw	21a pcw	21b pcw
MARCH1		0.73		CPi	CPo	CPo
MARCH2	-0.49		CPo	MZ	CPi	CPi
MARCH4	1.11	0.69	SP	SP	SP	CPi
SEPT4	-0.65		SP	SP	SP	SP
SEPT9	-0.60		VZ	SZo	SZo	SZo
SEPT11	0.42		VZ	VZ	CPo	SZo
A2M	-0.72	-2.19			SZi	VZ
ABCA5	0.51	0.51		CPo	CPi	CPi
ABCA8	-0.59	-0.95				
ABCB1		-0.84				
ABCC3	1.08					
ABCC4		0.82	VZ	VZ		
ABCC9		0.97	VZ	VZ	IZ	VZ
ABL2	0.44		MZ	CPo	CPi	CPo
ABLIM1		-0.31	MZ	CPo	CPo	CPo
ABTB2		0.75	VZ	VZ	SG	SZo
ACADL		0.79	VZ	VZ		
ACER3	-0.46			VZ	SZo	IZ
ACKR1		0.74				
ACP6	0.49		VZ	VZ	VZ	SZo
ACSL3		-0.53	CPo	SP	CPi	CPi
ACSL6	-0.84		CPi			
ACTN2	-0.73		CPi	CPi	CPi	CPi
ACTN4		-0.54	IZ		IZ	SZo
ACVR1C		0.75			CPi	VZ
ADAM19	0.53		CPo	CPo	CPi	CPi
ADAM9		-0.45	VZ	VZ	SZi	VZ
ADAMTS15	1.27	-0.80				
ADAMTS16		-1.85	CPo			CPo
ADAMTS18	0.93	-2.33	VZ	IZ		
ADAMTS3	0.36	-0.92		SP		CPi
ADAMTS4	0.78		SG	SZi	VZ	VZ
ADAMTS6	0.71	1.26		VZ	SZo	SZi

Table 3.1	log2 Fold Change - First round - CMP filtered		Significantly correlated layer			
Gene	hNP	hDN	15 pcw	16 pcw	21a pcw	21b pcw
ADAMTS8		1.10	SP		CPi	SP
ADAMTS9	0.79		SG	CPi	CPi	CPi
ADAMTSL1	0.81	1.66			SG	
ADARB2		1.21				
ADCY1		0.87	SP	SP	SP	CPi
ADCY2	-0.43					
ADCY9		-0.80	CPo	CPo	CPi	CPi
ADCYAP1R1		1.69				
ADD2		0.49	CPo	CPo		CPo
ADGRA1		0.99				
ADGRA2	0.80					
ADGRB3		0.64				
ADGRG1		0.77				
ADGRG6	0.73					
ADGRL2	0.80					
ADGRL3		1.18				
ADGRL4	0.75					
ADM	-0.85	-1.94	SG	IZ	IZ	IZ
ADORA1		0.74	SP	SP	SP	SP
ADORA2B	-0.93	-0.81	SG	SZo		SZo
ADRA2C		1.89	MZ	MZ	MZ	MZ
ADRBK2	0.68		IZ	SP	SP	SP
AFAP1L1	0.70		SG	IZ		IZ
AFP		-1.04	IZ	IZ		
AGAP2		0.49	IZ	MZ	MZ	MZ
AGBL4		0.84		IZ	MZ	
AGL		0.45	SP	SP		
AGPAT4		-0.58	CPo	CPi	CPi	CPi
AHCYL2		-0.73				
AHI1		0.40	VZ	VZ		
AHNAK		-0.50	SG	VZ		SG
AHNAK2		-1.68	MZ	CPo	CPi	MZ
AHSA1	-0.44					
AIM1		1.23				
AIM2		0.73	MZ	MZ	SG	MZ
AJAP1	-1.11	-1.63			CPi	CPi
AKAP14		-3.06	IZ			
AKAP6		0.64	SP	SP	SP	
AKAP7		0.51	SP	SP	SP	SP
AKR1C1		-0.80	CPo	CPo	CPi	CPi

Table 3.1	log2 Fold Change - First round - CMP filtered		Significantly correlated layer			
Gene	hNP	hDN	15 pcw	16 pcw	21a pcw	21b pcw
ALCAM		-0.60			CPi	CPi
ALDH1A1		-1.41	SG	CPo	SG	
ALDH1B1	-0.59	-0.69	SZi			
ALDH1L2	0.42		CPo			VZ
ALDH3A2		-0.45	VZ	VZ	VZ	VZ
ALDH3B1		-1.30	IZ			
ALDH9A1	0.49		VZ	VZ	SZo	SZo
ALPK2	-0.79		VZ			
ALPK3		0.86	IZ	IZ		
AMBN	1.13	0.57			VZ	VZ
AMIGO2		-0.43	CPo	CPi	SG	CPi
AMOTL1	0.30			SZi	IZ	SZi
AMOTL2		-0.79	SZi	SZi	CPo	VZ
AMPH		0.53	SP	SP		SP
AMZ1		1.33	VZ	VZ	IZ	
ANG		-0.98	VZ	VZ	VZ	VZ
ANGPT1		1.60	SG	VZ		VZ
ANK1	0.68		IZ		IZ	MZ
ANKFN1	-0.64		VZ	VZ	VZ	SZo
ANKRD1		-0.89			CPi	
ANKRD13A		-0.41	VZ	VZ	SG	VZ
ANKRD29		0.91	VZ	VZ		
ANKRD40		-0.31				
ANKRD44	0.62	1.02	CPi	CPo	CPo	CPo
ANKRD66		1.61				
ANKS1B		0.51	SP	SP	CPo	CPi
ANKUB1		-0.84				
ANO4	-0.65		CPo	CPi	CPi	CPi
ANO6		-0.36	SG	VZ	SG	VZ
ANXA1	-0.39	-0.61	SG	VZ	VZ	VZ
ANXA3		-1.20		SZo		
ANXA6		1.07	VZ	VZ	SZo	SZo
AP1S3	0.85		IZ	MZ	CPi	
APBA1	-0.61	0.54	SP	CPi		
APBA2		0.55	CPo	CPo		CPo
APCDD1	-0.63		SG	IZ	SG	SG
APLN	0.81		IZ	IZ	IZ	IZ
APLP2		-0.39				
APOBEC3C		-0.74	SZo	SZi	SZi	VZ
APOD	-0.75		IZ		MZ	

Table 3.1	log2 Fold Change - First round - CMP filtered		Significantly correlated layer			
Gene	hNP	hDN	15 pcw	16 pcw	21a pcw	21b pcw
APOE		0.79		SZi	SZi	VZ
APOL4	0.80		SZo	SZo	VZ	VZ
AQP1		1.64		VZ		VZ
ARAP2		-0.35	VZ	VZ	CPi	CPi
ARAP3	0.70		VZ	SZi	SZo	SZi
ARHGAP1		0.44	MZ	CPo		CPo
ARHGAP10		0.81				
ARHGAP20		0.81	SP	CPi	CPi	CPi
ARHGAP21	0.32		SZi			
ARHGAP22	-0.96	-0.85			SG	MZ
ARHGAP26	0.82		IZ	SP		
ARHGAP29		-0.82				
ARHGAP32	0.43					
ARHGAP36	1.03					
ARHGAP42		-0.43				
ARHGAP44	-0.74					
ARHGEF3	0.57		CPo	CPo	CPi	CPi
ARHGEF37	0.76					
ARL2		-0.72		SP	CPi	CPo
ARL4C	0.68		CPo	MZ	SG	MZ
ARL4D	-0.72	-0.76				
ARMC2	0.47		IZ	MZ	IZ	
ARPP21	0.62	1.25	IZ	CPi	IZ	IZ
ARSE		-0.89	VZ	VZ	SZo	SZo
ARSF		2.33			MZ	MZ
ASIC4		0.91				
ASPH		-0.44	VZ	VZ	VZ	VZ
ASTN1		0.55	SP			
ASTN2		-1.31	SP			
ATAD2		-0.57	VZ	VZ	SZo	SZi
ATOH8		-0.47	VZ	VZ		
ATP10B	1.05					
ATP13A5		1.58			MZ	
ATP1A2		-0.80	VZ	VZ	SZo	SZo
ATP1A3		0.45	SP	CPi	CPi	CPi
ATP2B1		0.62	CPo	CPo	CPi	CPo
ATP2B2	-0.69					
ATP2B3		0.84	SP	SP	SP	CPi
ATP6V0E2		0.56	CPo	CPi		CPi
ATP8B1		-0.63				

Table 3.1	log2 Fold Change - First round - CMP filtered		Significantly correlated layer			
Gene	hNP	hDN	15 pcw	16 pcw	21a pcw	21b pcw
B3GALNT1		0.50	CPo	CPi	CPi	CPi
B3GALT1	0.47		IZ	CPo		MZ
B3GALT5		-0.45				
B3GNT2	0.68		IZ	MZ	IZ	
B4GALT1	0.50		SG	VZ	SG	VZ
B4GALT5		0.53	CPo	CPo	CPo	CPo
BAALC	-0.48		SP	MZ	CPi	MZ
BACH2	0.58	0.50	CPo	CPo	CPi	CPi
BAIAP3		0.62			VZ	
BAMBI		-1.47	SG	IZ		
BBC3	-0.84		SP	CPi	CPo	CPo
BBOX1	-0.82		VZ	VZ	VZ	SG
BCAM		-0.72	MZ	MZ	MZ	MZ
BCAT1	1.15		SP	SP	CPi	IZ
BCAT2		-0.86	SP	CPo	CPo	CPo
BCHE		1.24	VZ	VZ		MZ
BCKDHB		-0.49	VZ	VZ	VZ	VZ
BCL11A	0.76		IZ	SP		
BCL2	0.35		CPi	CPi	SP	SP
BCL2L11	0.45		VZ	IZ	MZ	
BCL6	0.95		CPo	CPo	CPo	CPo
BCO2		0.85				
BEAN1		0.59				
BEND5		0.60	CPo	CPo		VZ
BEST3	-0.85				VZ	VZ
BICC1	0.48		VZ	VZ	SG	SZi
BIN1		0.81				
BMF		-0.72	SZi	SZi	VZ	VZ
BMP2		-1.17	SG	CPi	SG	MZ
BMP4		0.90		IZ	SG	VZ
BMP6	-0.75	-2.28		VZ	SG	SG
BMP8B		-1.17	MZ	MZ	MZ	MZ
BNC2		-0.47		MZ		
BRINP1		0.87				
BRINP2		1.57				
BRINP3		0.85				
BRS3		2.07	CPi	MZ		
BTG1	0.66		SZi	SZi	VZ	VZ
BTG3	0.33		VZ	VZ	SZo	VZ
BTNL9		0.88	SG	CPo	CPi	SP

Table 3.1	log2 Fold Change - First round - CMP filtered		Significantly correlated layer			
Gene	hNP	hDN	15 pcw	16 pcw	21a pcw	21b pcw
C10orf105		1.47	VZ	SZo	VZ	SZo
C10orf54		-1.59	SP	SP		VZ
C11orf87		0.64		CPo	CPo	CPi
C11orf96	-1.02					
C12orf49	-0.34				VZ	
C15orf59	-0.71		SZo	SP	SP	SP
C1orf115		0.44	SP	IZ	CPo	CPo
C1orf21	0.33	0.74	IZ	CPo	CPo	CPo
C1orf226		0.61	VZ	VZ	SZo	SZo
C1orf95		1.03	SP			
C1QL4		2.37			IZ	VZ
C1QTNF4		1.54	MZ	MZ	MZ	MZ
C1R		-0.65	VZ	VZ	SG	VZ
C21orf91		-0.35	SZi		VZ	VZ
C2CD2	0.54			MZ	MZ	CPi
C2orf50	0.99					
C2orf72		0.80	VZ	VZ	SZo	
C2orf80	-1.01		SP	SP	SP	SP
C2orf88		0.93			SG	SZi
C3		1.32			SZi	VZ
C3orf52		-2.18	VZ	VZ		
C3orf58		-0.50	VZ	VZ		SZi
C3orf70	-0.41		SP			
C4orf19	-0.71		VZ	VZ		
C5		0.49	VZ	VZ	SZi	SZi
C7orf57		0.61	CPo			
C8orf34	3.34	1.03	CPo	SP	CPi	CPi
C8orf37	0.38	0.34	VZ	VZ	SZo	VZ
C9orf3		-0.80		VZ		
CA4		0.91				MZ
CABLES1	-0.54	-0.99	SP	SP	SP	SP
CABYR	0.63		SP	SP	CPi	CPi
CACNA1A	0.74	1.46		IZ		
CACNA1D		1.09				
CACNA1G		1.22		CPi	CPi	CPi
CACNA2D2		0.94	CPo	SP	SP	
CACNA2D3		1.05	SP	SP	SP	SP
CACNB2	-0.41		SP	SP	CPi	SP
CACNG4		0.44		IZ		
CADM2		0.88	SP	SP	SP	IZ

Table 3.1	log2 Fold Change - First round - CMP filtered		Significantly correlated layer			
Gene	hNP	hDN	15 pcw	16 pcw	21a pcw	21b pcw
CADM3		1.16	CPo	CPi	CPi	CPi
CADPS	0.96	0.82	SP	SP	CPi	CPi
CALB1		0.90	CPo	CPo	CPi	CPo
CALB2		-0.75			SG	
CALD1		-0.88	VZ	VZ	VZ	VZ
CALN1	0.50	1.31	SP	SP	CPi	MZ
CALU		-0.54	VZ	VZ	SG	SZo
CAMK1G		1.72	SP	SP	MZ	SP
CAMK2B	-0.50		SP	SP	CPo	CPo
CAMK2D		-0.53	SP		SP	
CAMK2N1	0.49		MZ	MZ	MZ	MZ
CAMK4		0.50	SP	SP	CPi	
CAMKV		1.95	SP	CPi	CPi	CPi
CAMTA1		0.42	VZ	SZo	VZ	VZ
CAPN2	0.34		VZ	VZ	SZo	SZo
CASP1		1.08	VZ	VZ	SZi	VZ
CASP6		-0.65	VZ	VZ	VZ	VZ
CASP7		0.76	VZ	VZ	SZo	VZ
CASQ1		0.78	VZ	SZo	SZo	SZo
CAT		0.52	VZ	VZ	VZ	VZ
CAV2	0.64		CPi	SP	CPo	CPi
CBLN2		1.21	CPo			
CBLN4		1.41			CPo	
CBX4	-0.53		IZ	CPi		
CCBE1	-0.73	2.28	SP	CPi	CPo	CPo
CCDC109B		-0.37	VZ	VZ	VZ	VZ
CCDC136	0.59					SG
CCDC173		0.60				
CCDC175	-0.70					
CCDC178		1.22				
CCDC184		1.16				
CCDC39		0.85				
CCDC50	0.34		IZ	IZ		
CCDC69		1.01	CPi	MZ		CPo
CCDC80	0.35				IZ	IZ
CCNB3	0.74		CPi			
CCND1		-1.36				
CCND2		0.62	SZo	SZo	SZo	SZo
CCNE2		-0.54	VZ	VZ	VZ	SZi
CCS		-0.55	VZ	VZ	SZo	SZo

Table 3.1	log2 Fold Change - First round - CMP filtered		Significantly correlated layer			
Gene	hNP	hDN	15 pcw	16 pcw	21a pcw	21b pcw
CCSER1		1.31				
CCT6B	0.60		VZ	VZ	VZ	VZ
CD164		-0.35	VZ	VZ	SZi	VZ
CD34	1.09					MZ
CD38		1.41			VZ	VZ
CD44	0.80		VZ	VZ	VZ	VZ
CD47		-0.46	VZ	VZ	VZ	SZo
CD59	-0.61	-0.75	SZo	SZo		SG
CD83		0.74	CPo	CPo	CPo	CPo
CD8A		2.63	CPo	CPo	CPi	CPi
CDC14A	0.56		VZ	VZ	SZo	VZ
CDC42EP2		1.91	CPo	CPo	CPi	CPi
CDH1		-1.10	SG	SP	SP	
CDH13	-0.79	-1.48	SP	SP	CPo	CPo
CDH18		1.49	SP	SP	SP	SP
CDH20	-0.90		VZ	VZ		
CDH23		1.59	VZ	VZ		SZi
CDH5		-1.07	SG			
CDH6	0.54		SP			
CDH8		-0.70			CPo	CPo
CDK1		-0.51				
CDK14		0.33				
CDK5R1	-0.43		CPo	MZ		
CDK6		-0.69	VZ	SZo	SZi	SZi
CDKL1	-0.52		SG	MZ	CPi	CPi
CDKN1A		-0.71				
CDKN1C		-0.61	SG	CPi	CPi	CPi
CDO1		-0.59	VZ	VZ	VZ	VZ
CDR2		-0.57	CPo	SP	CPi	CPi
CELF4		0.94				
CELSR1		-0.56	VZ	VZ	VZ	SZo
CENPE		-0.57	VZ	VZ	SZo	SZi
CENPN		-0.50			IZ	
CENPU		-0.50				
CEP55		-0.66	VZ	VZ	SZo	SZo
CERKL		1.36	VZ	SZo	VZ	
CERS2		-0.47				
CFAP52		0.83				
CFAP69		0.56				
CFI	-0.55	-0.62	SG	SZo		VZ

Table 3.1	log2 Fold Change - First round - CMP filtered		Significantly correlated layer			
Gene	hNP	hDN	15 pcw	16 pcw	21a pcw	21b pcw
CGNL1	0.71					SG
CHCHD10	-0.64					
CHDH		0.63		VZ	IZ	
CHGA		0.71	SP	SP	SP	SP
CHL1	0.95		CPo	CPi	CPi	SP
CHMP4B		0.35	VZ			
CHN1		-0.56	CPo	CPo		CPo
CHPF		-0.50				
CHRDL1		-1.61	SZi	SZi	SZo	SZo
CHRFAM7A	0.77	1.29				
CHRM3		1.02	IZ	SP	SP	CPo
CHRNA7		1.04		SP	MZ	MZ
CHRNA9	0.75		MZ		MZ	
CHST1		0.96		SP		SP
CHST2	0.77		CPo		CPi	CPi
CHST7	-0.64					
CHST9		-0.69	VZ	VZ	VZ	VZ
CKB	-0.75		VZ		VZ	SZo
CLDN1	1.10		CPo	SP		CPo
CLDN11	-0.75	-1.10	SG	IZ	MZ	SG
CLDN2		-1.00		IZ		
CLGN		0.52	VZ	VZ	VZ	VZ
CLIC6		1.70				
CLINT1		0.38		SP	CPo	
CLMP		1.38				
CLSPN		-0.49				SZi
CMPK2		0.54			SZo	VZ
CNGA3	0.45		VZ	VZ		SZo
CNIH3		-0.81	SP	SP		
CNKSR2		0.45				
CNN1	0.93		SG			
CNNM4		-0.60	IZ	CPo	CPi	CPo
CNR1	1.28	1.84	SZi		MZ	
CNRIP1		0.49	CPi	CPi	CPo	CPo
CNTN2		0.71	IZ			
CNTN6	1.01				CPo	IZ
CNTNAP2	0.70	1.01	SP		SG	MZ
COBLL1	-0.49			SZo		MZ
COL11A1	-0.51	-1.11	VZ	VZ	VZ	VZ
COL12A1		2.53	SG	SP	SG	

Table 3.1	log2 Fold Change - First round - CMP filtered		Significantly correlated layer			
Gene	hNP	hDN	15 pcw	16 pcw	21a pcw	21b pcw
COL14A1		-1.29	SG	MZ		
COL16A1	-0.76		SP	VZ	SP	SP
COL1A1		-1.54	SG		SG	
COL1A2		-0.60		VZ		SG
COL24A1		1.16		IZ	CPi	CPo
COL28A1	-0.85					
COL2A1	-0.66	2.85		VZ		SG
COL4A1		-0.88		IZ		IZ
COL4A2		-0.76				IZ
COL4A3		-1.07				
COL4A5		-0.68	VZ	VZ	SG	VZ
COL4A6		-0.60	VZ	VZ	VZ	VZ
COL5A3		-0.74				
COL6A6		1.21	CPi	MZ		
COL8A1		-1.43	MZ	MZ		
COL8A2	-0.99	-1.37			SZi	IZ
COL9A3		-1.21	SZo			CPo
COLCA2		1.28				
COLGALT2	-0.47	-0.69				
COMMD5	-0.65					CPi
COPRS	-0.51					
CP		-2.16	SG			
CPD		-0.44	VZ	VZ		
CPEB3		0.55	CPi	SP	CPi	CPi
CPNE4		-0.50	CPi	CPi		CPi
CPNE5		1.07	SP	SP	SP	SP
CPXM2	0.76	0.95			IZ	
CPZ		-2.31			MZ	
CRABP1		1.62	SG			
CREB3L2		-0.54	SG	VZ	SG	VZ
CREB5	0.46		VZ	VZ	SZo	VZ
CRHBP		-1.87	SP	IZ		
CRHR2		1.01	CPo			
CRIM1	1.21	-0.74	VZ		MZ	CPo
CRISPLD1		-0.94	VZ	VZ	VZ	SG
CRTAP		-0.50	VZ	VZ		SZo
CRYAB	0.65	-0.94		VZ	VZ	
CSF1		-0.70	IZ	CPi		
CSGALNACT1		1.09	SP	SP	CPi	CPi
CSMD1		1.64	IZ	SP	CPi	CPo

Table 3.1	log2 Fold Change - First round - CMP filtered		Significantly correlated layer			
Gene	hNP	hDN	15 pcw	16 pcw	21a pcw	21b pcw
CSMD2	1.06			CPi		
CSPG4	0.83					
CSPG5	-0.37	1.36	VZ	VZ	CPi	CPi
CSRP2	-0.60	-0.87	CPo	CPo		CPo
CST3	-0.67		SZo	SZo	IZ	SZo
CTDNEP1	-0.48					
CTGF	0.82	-0.85	VZ	VZ	VZ	IZ
CTH	-0.85		VZ	VZ	VZ	VZ
CTNNA2		1.31	CPo	MZ	CPi	CPi
CTNNAL1	0.50		VZ	VZ	SZo	SZi
CTSD		-0.48				
CTSV		-1.17				
CUBN		-0.83				
CXCL16		-0.58	SG		SZi	VZ
CXCL2		1.44	SG			SG
CXCL5		1.14		SP	CPo	CPi
CXCR4		-0.60	SG	MZ		VZ
CXXC4		0.90	CPo		CPi	CPo
CYFIP2		0.33	IZ	SP	SP	CPo
CYP1B1	0.81		SG	MZ	SG	
CYP27C1		0.81	VZ	VZ	CPo	CPo
CYP2J2	-0.84		SZo	VZ		
CYR61	0.64		VZ	VZ	VZ	VZ
CYTL1		-0.92	SG	MZ	SZi	SZi
DAB1		1.68				
DAB2	-0.61	-0.74	SG		SG	
DACT1		0.62	SP	CPo	CPo	CPo
DAPL1	1.00		SZi	SZi	SG	VZ
DAW1		0.71				
DCBLD2	0.43		VZ	VZ		
DCDC2		-0.80	SG	VZ		
DCHS2		0.94				
DCLK1	-0.33		CPo	CPo	CPi	CPi
DDIT4	-0.71		VZ	VZ	VZ	IZ
DDIT4L		0.98	VZ	VZ	SZo	SZo
DDO		-0.99	SG			
DENND2A	0.52		VZ	VZ	SP	
DENND2C		-0.62	SG		IZ	
DEPTOR	0.76					
DFNA5	0.51	0.51	SP	SP		

Table 3.1	log2 Fold Change - First round - CMP filtered		Significantly correlated layer			
Gene	hNP	hDN	15 pcw	16 pcw	21a pcw	21b pcw
DGKE	0.64		CPo	CPo	CPi	CPi
DGKG		1.53	CPi	SP		
DGKH		0.55	CPo	SP	CPi	CPi
DIAPH3		-0.62	VZ	VZ	VZ	SZi
DIEXF		-0.37				
DIO2	2.35	1.79	VZ	SZo	SG	
DIRAS2	0.82	1.32	SP	SP	SP	SP
DIRAS3		0.50	SP	CPi	CPi	CPi
DIXDC1		-0.41		CPi	CPi	CPi
DKK3		-0.74	VZ	SP		
DLC1	-0.37		SG	SP		
DLG2	-0.79		CPo	CPo	CPo	CPo
DLGAP2	0.73		CPo	CPi	CPi	CPo
DLGAP5		-0.49	VZ	VZ	SZo	SZo
DLK1	0.96					
DMD		-0.62	SP			
DMKN		-0.89	SG			
DMRT2	-0.92			SP	SP	SP
DNA2		-0.49	VZ	SZo		
DNAH11		1.06	VZ	VZ	SZi	VZ
DNAH12		0.71				
DNAH5		0.82	SP	SP		CPi
DNAH9		0.97				
DNAJC1		-0.44	VZ	VZ	VZ	VZ
DNAJC10		-0.32	VZ	VZ	IZ	
DNER	0.49	0.77		CPo	CPo	CPo
DNM1		0.48	SP	CPi	CPi	CPi
DOC2B	0.81	1.49	CPi	SP	CPo	CPo
DOCK10		0.57	CPi	SP	MZ	
DOCK4	-0.56		SP	SP		SP
DOPEY2		0.37	CPo	IZ	CPo	CPo
DPP10		0.49	SP	SP	CPi	SP
DPP4	0.82	1.24				
DPP6		0.69	CPo	CPo	CPi	CPo
DPYD		-0.77		CPo		
DPYSL3	0.72	0.48	CPo	CPo		
DRD1		1.64	SP	SP		
DRP2		1.39		IZ		
DSC3		0.89	VZ	VZ	VZ	VZ
DSCAM		0.94	IZ	IZ		

Table 3.1	log2 Fold Change - First round - CMP filtered		Significantly correlated layer			
Gene	hNP	hDN	15 pcw	16 pcw	21a pcw	21b pcw
DSTN		-0.51	CPo	CPo	CPi	CPi
DTX1		0.46	CPo	CPo	CPo	CPo
DTX4		0.93	CPi	CPo	CPo	CPo
DTYMK		-0.45	VZ	VZ	SZo	SZo
DUSP10	0.72	0.74	VZ	VZ	SZo	SZi
DUSP18		0.50	MZ	CPo	CPi	CPo
DUSP4	-0.45		CPo	CPo		
E2F8	0.56		VZ	VZ	SZo	SZi
EBF3		0.88	SG		SG	SG
ECE1		-0.56	VZ			
ECEL1		1.85	CPo	SP	SG	SP
ECM2		-1.48				
EDA		0.97				
EDN1		-1.38			IZ	SG
EDN3		5.86	SG	IZ		
EDNRB		0.72	VZ	VZ		MZ
EFCC1	-0.78					
EFEMP1		-1.33			SG	
EFHC2		0.43	VZ	VZ	VZ	SZo
EFHD1		1.51	VZ	VZ	SZo	SZo
EFNB2		-0.46	VZ	SZi		
EGF		-0.83		MZ		
EGLN2		-0.56	CPo	CPo	CPo	CPi
EGLN3		-0.49		VZ	VZ	VZ
EHBP1	0.50		IZ	SP	IZ	
EHD3		0.95	SP	SP		SP
EHD4		-1.04	SG			IZ
EHF		0.96				
ELAVL2		0.42				
ELAVL4		0.91	CPo	CPi		
ELF4	0.78		SG	SZo	SZi	SZo
ELMO1		0.65	CPi	CPo		CPo
ELMOD1		0.59	CPi	CPi	CPi	CPi
ELOVL1		-0.62	VZ	SZo	SZo	
ELOVL6	0.43		MZ	CPo	MZ	MZ
EMC6	-0.62					
EMILIN3		0.73	VZ	VZ	VZ	VZ
EML4	0.49		SP	SP	SP	
EMP1		-0.91			SG	
EMP2		-0.67	VZ	VZ	SZo	SZo

Table 3.1	log2 Fold Change - First round - CMP filtered		Significantly correlated layer			
Gene	hNP	hDN	15 pcw	16 pcw	21a pcw	21b pcw
EN1		1.34	SZo			
ENAH		-0.34			IZ	VZ
ENC1		-0.54				
ENDOD1	0.47		SP	SP	SP	SP
ENO1		-0.41	VZ		VZ	SZi
ENOX1	0.65	0.65	CPo	CPo		CPo
ENPP2	-1.12	-0.98	VZ	VZ	MZ	
ENPP5		-0.66			SP	SP
ENTPD1		0.45			SZi	SG
EOGT		-0.59				
EPAS1	2.23					
EPB41L1		0.43	SP	CPi	CPi	CPo
EPB41L4B	1.68	1.11	SG	IZ	SG	CPo
EPHA3		1.01			SZo	SZo
EPHA4		0.88		CPo		
EPHA5		1.00				
EPHB2		0.52	SZo			
EPHB3		-0.76	VZ	VZ	VZ	VZ
EPHX1		-0.59				
ERBB2		0.64	VZ	VZ	SZo	VZ
ERCC6L		-0.53	VZ	VZ	SZo	SZo
ERICH2	-0.51					
ERMN		-0.85	MZ		MZ	MZ
ERRFI1		-0.45	SG	CPi	SG	CPo
ESCO2		-0.62	VZ	VZ	SZo	SZo
ESR1		1.85		IZ		IZ
ESYT2		-0.50	CPo	IZ	CPo	CPo
ESYT3		1.26	CPi	CPo		
ETNPPL		2.37				
ETV1		-0.52	CPo	CPo	CPi	VZ
ETV5		-0.56	VZ	SZo		
EVC		0.59	VZ	VZ	VZ	SZi
EXPH5	0.64		VZ	VZ		
F11R		-0.80				
F2R	-0.58		VZ	VZ	SZo	SZo
F2RL2		-1.04	IZ	IZ	IZ	VZ
F3	0.60		SZo	SZo	SZo	SZo
FABP5		0.69	VZ	VZ	SZo	SZo
FAM101A		1.27	CPo	CPo	SP	SP
FAM107A	-0.93	-0.61	VZ	SZo		SZo

Table 3.1	log2 Fold Change - First round - CMP filtered		Significantly correlated layer			
Gene	hNP	hDN	15 pcw	16 pcw	21a pcw	21b pcw
FAM110C		0.67	VZ	CPo		CPo
FAM111B		-0.59	VZ	VZ	SZo	SZi
FAM122A		-0.64		VZ		
FAM127A	-0.52					
FAM129A	0.68			VZ		SG
FAM133A		-0.71	SP	SP	MZ	MZ
FAM135B	-0.63		SP	SP	SG	SG
FAM13C	0.70		CPo	SP	CPi	CPi
FAM155B		1.36	IZ	CPo	CPo	MZ
FAM167A		1.20	VZ	VZ	SG	
FAM180B		2.38				
FAM181B		0.66	SP	SP	IZ	IZ
FAM184B	0.83	0.68	VZ			CPo
FAM189A2		1.89	VZ	VZ	SZo	SZo
FAM196A	1.62	1.06	SP	SP	CPi	SP
FAM198B		0.53		VZ	VZ	VZ
FAM19A5	-0.85	-1.03	SZo	SZo		
FAM216B		-1.89				
FAM221A		-0.48				
FAM43B		0.94	SP	SP	SP	SP
FAM45A	-0.46		IZ	CPo	CPi	CPo
FAM69A		0.79	SP	SP	CPo	CPo
FAM69C	-0.62		VZ	VZ	VZ	VZ
FAM72A		-0.81	SZi	SZo	SZo	SZi
FAM81B		-1.30			VZ	
FAM83G		-1.22				
FAM84A	0.94	0.66				
FAM84B	0.46			VZ	VZ	VZ
FAT1		-0.48	VZ	VZ	SZo	SZo
FAT2		1.30	IZ	MZ		IZ
FAT4	1.16		CPo	SP	CPo	CPo
FBLN1		1.03	SZo	SZo		SZo
FBLN5	0.66	-0.70	SG			SG
FBN1		-0.78		VZ		
FBN2		-0.86	VZ	SZo		SZo
FBXL7		0.34	VZ	VZ	VZ	VZ
FBXO32	1.61	-0.70	VZ	VZ	CPi	CPi
FCHO2		0.34	CPo	CPi		
FCHSD2		0.44	SP	SP	CPi	CPi
FEZ1	-0.46		CPo	CPo		CPo

Table 3.1	log2 Fold Change - First round - CMP filtered		Significantly correlated layer			
Gene	hNP	hDN	15 pcw	16 pcw	21a pcw	21b pcw
FGF11	-0.61					
FGF13		0.46	CPo	CPo	CPo	CPo
FGF18		2.30	SP	SP		SP
FGF5		-0.77	CPi			
FGF7	-0.81		SP	SP	CPi	
FGFR1		-1.09	VZ	VZ	SZo	SZo
FGFR2		-0.83	VZ	VZ	SZo	SZi
FGL2	-0.70	-1.19	SG			SG
FHDC1	0.66			SZi	SZo	SZo
FHOD3	0.34	-0.52	VZ	VZ		
FIBIN	-0.94		MZ			
FIGN		0.69	VZ	VZ	SZi	VZ
FILIP1		-0.92	VZ	VZ	VZ	VZ
FKBP1A		-0.43	IZ	CPo	CPo	CPo
FKBP5	0.48			SP		
FLNB		-0.63	VZ	VZ	VZ	SZo
FLRT1		0.78	IZ	IZ	SG	MZ
FLRT2		1.89	CPo	CPi	CPi	CPo
FLRT3	0.97		SZi	SZi	CPo	
FLVCR1	0.42				MZ	MZ
FMN2		0.48	SP	SP	CPi	SP
FMNL2	0.34		SP	SP	SZo	SZo
FMNL3	0.85		CPi	SZo		
FMO1		1.30				
FMO4		0.62		VZ	SZo	
FNDC1		-3.80		VZ		CPi
FNDC3B		-0.70		VZ	SZi	SZi
FNDC5		1.17			SG	SP
FOLH1	0.58		VZ	VZ	SZo	SZi
FOS		-0.71	SG	VZ	VZ	
FOSL2	1.02		SP			IZ
FOXO1		-0.69		VZ		
FOXP2	1.15	5.95			SP	SP
FRAS1		0.73	SP	SP	SP	SP
FREM1		1.83	SG		SG	
FREM2	0.47			VZ		
FRMD3		-1.00	CPo	CPi	CPo	CPo
FRMD4A	0.84	0.66		SP		
FRMD4B		-0.45	CPo	CPi	SZo	
FRMD6		-0.63	SG	SZi		SG

Table 3.1	log2 Fold Change - First round - CMP filtered		Significantly correlated layer			
Gene	hNP	hDN	15 pcw	16 pcw	21a pcw	21b pcw
FRMD7		0.90	SG	MZ		SZi
FRMPD1	-0.82		SZi	CPo	CPi	CPo
FRMPD4		-2.18	SP	CPi	CPi	CPi
FRRS1	0.97					
FRRS1L	0.65	0.89				
FRZB		-0.86		CPo	CPo	CPo
FSD1L		0.40	CPo	CPi	CPo	
FST	-0.53		SZo	SZo	CPi	SZo
FSTL1		-1.10	VZ	VZ	VZ	VZ
FSTL4		1.45	SG			
FUT8	0.44		VZ	VZ		
FUT9		0.84	SP	SP	CPi	SP
FZD2	-0.49		VZ	VZ	VZ	VZ
FZD5		-0.79	SG	VZ	VZ	VZ
G0S2		0.99		IZ		
GAB3	1.27					SG
GABBR1	0.83		SP	CPi	SP	SP
GABBR2	-0.91		SP	CPi	CPi	CPi
GABPB2		-0.38	IZ	IZ		
GABRA3		1.14				
GABRA4	1.18			CPi	CPi	CPi
GABRB2		-0.51			SP	SP
GABRB3		0.52	CPo	CPi	CPi	CPo
GABRG2		1.07	CPo	CPo	CPi	CPo
GABRG3	-1.02		SP	SP	SP	SP
GAD1	-0.65		IZ	MZ	MZ	
GAD2	0.75	0.84			VZ	VZ
GAL		1.02		IZ		
GALC		-0.40				
GALNT10		-0.44	IZ	CPi	IZ	
GALNT18		-1.84				
GALNT5		-1.45	SG			
GAP43		0.72	CPo	CPo	CPo	CPo
GAR1		-0.58	VZ	VZ	SZo	
GAREML		0.57				
GAS6		-0.62	CPo	CPi	CPo	CPo
GATM		-0.69	VZ	VZ	SZo	VZ
GBP3		0.61				
GBP4		1.26		IZ		SZi
GCH1	0.79		SG	VZ		

Table 3.1	log2 Fold Change - First round - CMP filtered		Significantly correlated layer			
Gene	hNP	hDN	15 pcw	16 pcw	21a pcw	21b pcw
GCNT1		-1.04	IZ		IZ	IZ
GCOM1		1.17	VZ	SZi	SG	VZ
GDA		0.88	SP	SP	CPi	CPi
GDF10		0.93	SG	SP	CPo	CPi
GFAP		-0.66	SZo	IZ	VZ	VZ
GFRA1		1.30		IZ		
GHR		1.56	SG		CPi	CPi
GJA1		-0.62		MZ		
GLCE	0.46			SP	VZ	VZ
GLI3		0.63	VZ	VZ	SZo	SZo
GLRB		0.49	SP	CPi		
GLT8D2	-0.71		SG		VZ	VZ
GLTSCR1L	0.54					
GLUD1		0.43	VZ	VZ		
GLUL	-0.54		SZo	SZo	SG	VZ
GMPR	-0.81		SG			
GNAO1	-0.63		MZ	CPi	CPi	CPi
GNAS		0.36	MZ	MZ	MZ	MZ
GNB2	-0.62			CPo		
GNG11		-0.48	SG	SZo	SG	IZ
GNG12	0.60		VZ	VZ	SZo	SZi
GNG3		1.03		SZi	CPo	
GNS		-0.56				
GPAT3		-0.93				
GPATCH4		-0.49	IZ	IZ	SG	CPi
GPC3	0.92			SP		SZo
GPC4		-0.85	VZ	VZ	VZ	VZ
GPC6	-1.02		VZ	VZ	SZo	SZo
GPD1L		0.53	SP	SP	SP	SP
GPM6A		0.48	CPo	SP		
GPNMB	-0.70	-1.19	SG	SZi	SZi	VZ
GPR12	-0.66	0.87	SP	SP	CPo	SP
GPR158	0.58			IZ	CPi	CPi
GPR19		0.85	CPo	CPo	CPo	
GPR37		1.14	SP	SP	CPi	SP
GPR37L1	-0.56			IZ		
GPR39		0.74	SZi	SZi	SZo	SZi
GPR50	1.15		IZ	IZ		
GPR63		0.53	IZ			
GPR78		-1.66				

Table 3.1	log2 Fold Change - First round - CMP filtered		Significantly correlated layer			
Gene	hNP	hDN	15 pcw	16 pcw	21a pcw	21b pcw
GPR83		-1.89	IZ		SG	MZ
GPRC5B	-0.51		SZi	SZi	VZ	VZ
GPRIN3		0.94	SP	SP	CPi	CPi
GPX3	-0.96	-0.53	VZ	VZ	SZo	VZ
GRAMD1B		0.84		SZi	SZo	SZi
GRAMD4		0.64	CPo		SZo	
GRHL3	0.76					
GRIA1	-0.46	-0.91	CPo	CPi	CPo	CPo
GRIA3	-0.46		CPi	CPi		
GRIA4	-0.64		CPo	CPo	CPo	CPo
GRID2		1.84	SP	SP	SG	
GRIK1	-0.67	1.48	SG	IZ		
GRIK2		1.67				
GRIK3		-0.73				
GRIK4	-1.07		SP	MZ	MZ	MZ
GRIN2B	-0.84		SP	SP	CPi	MZ
GRIP1	-0.48	0.53	SP	SP	CPo	CPi
GRM3		2.22	CPi	SP		
GRM5	-0.90	0.74	IZ	MZ		
GRM7	-1.58	0.72	CPo	CPi	CPi	CPi
GSG1L		2.18	SG	SP		
GSX1	-1.41			IZ		
GTF2F2		-0.68		VZ	VZ	
GUCY1A3	0.64		SP	SP	CPi	CPi
GUCY1B3		-0.86	SP	CPi	CPi	CPi
GYG2		0.49	VZ	VZ	SZo	
GYPC		-0.57	VZ	VZ	VZ	VZ
HAPLN3	0.66					
HAS3	1.04	1.14	SP	SP		
HBEGF		-1.10			CPo	CPo
HCN1		-0.89	SP	CPi	CPi	CPi
HEG1		-0.45	VZ	VZ	SZo	SZo
HEPH	0.78	1.40	VZ	VZ	VZ	VZ
HERPUD1		-0.50				
HEXB		-0.51	VZ	VZ	SZi	SZo
HEY1		1.05	VZ	VZ	SP	SP
HEY2	0.53	0.71	SG	SZo	SG	
HIBADH	0.42	0.50				VZ
HIF1A	0.35					
HIGD1A		-0.40	VZ			

Table 3.1	log2 Fold Change - First round - CMP filtered		Significantly correlated layer			
Gene	hNP	hDN	15 pcw	16 pcw	21a pcw	21b pcw
HILPDA		0.76				
HIP1	-0.40				IZ	
HIST1H3E	-0.69				VZ	VZ
HIST3H2A		1.33	SZi	SZi	VZ	VZ
HIST3H2BB		1.76	SZi	SZi	SZi	VZ
HIVEP3	0.78		IZ	MZ	MZ	MZ
HK1		-0.40	CPo	CPo	CPo	CPo
HK2	0.53		VZ	SZi	SZi	SZi
HKDC1	-0.77		VZ	VZ	SZo	SZi
HLA-DMB		-0.99			SZi	VZ
HLA-DOA		-0.96			VZ	
HLA-DRA	-0.71			VZ	VZ	VZ
HLA-DRB1		-0.92	SG	SP		CPi
HLF		2.04	SG		CPo	SG
HMMR		-0.72	VZ	VZ	SZo	SZo
HN1L		-0.40	VZ	VZ	SZo	SZo
HNMT	-0.62		VZ	VZ	SZo	
HOMER2	0.57		CPi	MZ	CPo	CPi
HOPX		-1.38	VZ	SZo	SZo	SZo
HOXB5		0.91				
HPCAL1		0.56				
HPSE		-1.46		SZi	SZi	VZ
HRK		0.73	IZ	IZ		
HS3ST1	-0.89		SZo		SZo	SZo
HS3ST5	-0.78	-2.01	SP	SP	SP	SP
HS6ST3		1.11	SP	MZ		IZ
HSD11B1		1.09			MZ	
HSD17B14		-0.73	VZ	SZi	VZ	VZ
HSPB8	0.91	1.62			VZ	VZ
HSPG2		-0.89				
HTR1D	1.00		MZ		MZ	
HTR1F		1.13	SG		MZ	
HTR2A		1.11	IZ	MZ		
HTRA1	0.44	-0.57	VZ	VZ	SZo	SZo
HVCN1		0.89	VZ	VZ	SZi	VZ
ICA1		1.00	SP	CPo	CPi	CPi
ICA1L		0.40	IZ	CPo	CPo	CPo
ICMT		-0.40	VZ	VZ		CPi
ID1		-2.24			SG	
ID3	0.66	-1.74	SG	CPo	SG	

Table 3.1	log2 Fold Change - First round - CMP filtered		Significantly correlated layer			
Gene	hNP	hDN	15 pcw	16 pcw	21a pcw	21b pcw
IDH2		0.40	SZo	SZo	VZ	SZo
IFI27		1.01				
IFIT3	-0.50					SZo
IGDCC4		0.46	VZ	VZ	SZi	
IGF1R	0.38		CPo	CPi		VZ
IGFBP2		-1.29	CPo	CPo	CPi	
IGFBP3	1.03	-2.12	SP	SP	SP	
IGFBP4		0.87	SG	IZ		
IGFBP7		-0.77	SG			IZ
IGSF1	0.54					
IGSF10		1.25	SG			
IGSF3		0.39	IZ	SP		
IL18	1.03		MZ		SZi	VZ
IL1RAPL1		0.87	CPo	SP	SP	SZi
ILDR2		-0.47	VZ			
IMMP2L	0.58		VZ	VZ	VZ	SZi
INF2		-0.77		SZo	SZo	VZ
INHBA		1.25	IZ	CPo	CPo	CPo
INPP5D	0.76				SZi	VZ
IQCD		0.62	VZ	VZ	VZ	VZ
IQGAP1		-0.40	VZ	VZ	SZo	VZ
IQGAP2		0.74	VZ	VZ	VZ	VZ
IQSEC2		0.63	SP	SP	SP	SP
IRF2BP2	0.50	0.46	SP			SP
IRS4		0.83				
IRX2		1.00				
IRX3	1.79					
ISLR2		0.95	IZ	CPo		CPi
ITGA2		-1.34	VZ	VZ	VZ	VZ
ITGA3	0.73		SP	SP	CPi	CPi
ITGA6		0.40	VZ	VZ	SZi	VZ
ITGA7		-0.50	VZ	SZo	SZo	SZo
ITGA9		1.85	SP	SP	SP	CPo
ITGAV	-0.52		VZ	VZ	SZo	SZi
ITGB1		-0.51	VZ	VZ	SZi	VZ
ITGB3		-0.94	SP			
ITGB5	-0.90		VZ	VZ	SZo	SZo
ITGB6	-0.93			IZ		
ITPR1		-0.71	CPo	CPo	CPo	CPo
ITPR2	0.51		SG	VZ	SZo	SZi

Table 3.1	log2 Fold Change - First round - CMP filtered		Significantly correlated layer			
Gene	hNP	hDN	15 pcw	16 pcw	21a pcw	21b pcw
ITPR3	-0.74					
ITPRIPL2		-0.54		IZ		SG
ITSN1		-0.58	SP	SP	SP	SP
IVNS1ABP		0.36	SZi	SZi	SP	SZo
JADE1		-0.51				
JADE3	0.54					
JUN	0.44	-0.56	VZ	VZ	VZ	SG
JUP		-0.56	CPo	CPo		
KANK2		-0.70	SG	SZo		SG
KCNA1		-1.69	IZ	SP		
KCNA4		0.99	SP	SP		SP
KCNB1		1.22	SP	SP	SP	SP
KCNB2		1.73	SP	SP		
KCND2		0.83	SZi	CPo	CPo	MZ
KCNG1	0.82	-1.26		SP	SP	
KCNH7	-0.66					
KCNIP1	-0.56		CPi	SP	SP	SP
KCNIP3		0.57	VZ	VZ		
KCNJ13	-1.12	-1.92	VZ	VZ	VZ	
KCNJ16	1.11		CPo	SP	SP	MZ
KCNK10		0.84	VZ	VZ	CPi	
KCNK2		0.57	CPo	IZ	CPo	
KCNMA1	0.69		SP	SP	SP	SP
KCNQ3	0.96					SZi
KCNQ4		1.03	SG			CPo
KCNS3		1.32	SP	IZ	SG	
KCTD21		-0.51	MZ	CPo		
KDELR3		-0.88	SG	VZ		
KDM7A	0.50					
KDR	1.66			IZ		
KIAA0040		1.10				
KIAA0319	0.89	0.72	SP	CPo	CPo	CPi
KIAA0355		-0.49	IZ			
KIAA1161	-0.66	-0.99		VZ	VZ	SZo
KIAA1211L	0.84					
KIAA1217		-1.06	SP		SP	SP
KIAA1324L		0.65			CPo	CPo
KIAA1549L	-0.55					
KIAA1614		-0.75				
KIAA1644		-1.25	SP	CPi	SP	CPi

Table 3.1	log2 Fold Change - First round - CMP filtered		Significantly correlated layer			
Gene	hNP	hDN	15 pcw	16 pcw	21a pcw	21b pcw
KIAA1671	0.41			SP		
KIAA2012		0.99				
KIF26B		1.49	VZ	VZ		SZi
KIF5A		0.41	CPo	CPo	CPi	CPi
KIF5C		0.59	IZ	MZ	IZ	SP
KIRREL		-0.60	SZi	SP	CPi	MZ
KIRREL3		0.77	CPo	CPi	CPi	CPi
KITLG		-0.56		CPo	MZ	
KLF17	0.81					
KLF5		-0.76			CPi	
KLHL13		0.45		SP	CPi	MZ
KLHL14		1.21	CPi	CPi	CPi	CPi
KLHL32		1.91	CPi	SP	CPi	SP
KLHL4		0.70		CPo	CPo	CPo
KLHL42		0.43				
KY		1.03	MZ			
L1CAM		0.65				CPo
L3MBTL3		0.48	CPo	CPo	CPo	CPo
LAMA2	1.35	2.01	SG	MZ	SG	SG
LAMA3		0.93	VZ	VZ	VZ	SZi
LAMB1		-0.98	SG	IZ	SG	
LAMC1		-0.62	SZi	SZo		IZ
LAMP1		-0.42			SZo	
LAMP5		-0.61				
LANCL3	1.44	0.96			SG	
LAYN		-1.46				
LBH	1.18		CPo	IZ	SG	
LCA5		-0.45	SZi	SZi	SZi	VZ
LDB2		1.07	CPi	SP		CPi
LDLRAD3		-0.40	VZ	VZ	VZ	
LDLRAD4	0.61					
LEF1	-0.58	-0.61	SG	IZ		
LFNG		0.67	VZ	VZ	SZi	VZ
LGALS12		1.11			SG	
LGALS3		-0.73	VZ	VZ	SZo	SZi
LGALS3BP		-0.59	VZ	VZ	SZo	SZo
LGALS8	-0.50		SG	CPi	CPi	CPi
LGI1	-0.81	-0.87	SP	SP	CPi	CPi
LGI2	0.79	0.90	SP	CPo	CPi	CPi
LGMN		-0.66	CPo			

Table 3.1	log2 Fold Change - First round - CMP filtered		Significantly correlated layer			
Gene	hNP	hDN	15 pcw	16 pcw	21a pcw	21b pcw
LHCGR		-0.72				
LHFPL3	-0.70					
LIMCH1		0.42	CPo	MZ	CPo	CPo
LIMK2		1.14				
LIMS1	0.40		SG	VZ	SG	VZ
LINGO1		0.92	CPo	CPo	CPi	CPi
LIPG		-0.62	VZ	VZ	VZ	VZ
LIX1		-0.62	VZ	VZ	IZ	SG
LMAN2L		-0.42		VZ	SZo	SZo
LMCD1		-0.47	VZ	SZo		
LMO2	-0.43	-0.75	SG	IZ		MZ
LMOD1		-1.13	MZ			
LNPEP	0.47				SG	
LNX1	1.06		IZ	CPi	CPi	IZ
LNX2		-0.43	CPo	SP	CPi	CPi
LOXL1	-0.56		VZ	VZ	VZ	VZ
LPCAT2		-1.21				
LPL	-1.25	-1.09	CPi	CPi	CPi	CPi
LPP	0.38		VZ		CPo	MZ
LRAT		-0.63				
LRFN1		0.89	IZ	IZ		
LRIT3		-1.27				
LRP1B		0.50	SP	SP		CPi
LRRC10B		1.19	VZ	SZo		
LRRC15	1.37		MZ	CPo		
LRRC2		-2.20	IZ	IZ	IZ	CPi
LRRC3B	-1.24		VZ	VZ	SZo	SZo
LRRC4C		0.92		CPi	CPi	CPi
LRRC55		1.09	IZ	IZ		
LRRC7		0.85	IZ	CPi	CPo	CPo
LRRC8C		-0.47	VZ	SZo		SZi
LRRN1		0.57	VZ	VZ		
LRRN2		0.43	CPo	CPo		CPo
LRRTM1		1.29	CPo	CPo	CPo	CPi
LRRTM2	-0.40	0.58	SP	SP	SP	
LSAMP		0.88	CPi	CPi	CPi	CPi
LTBP2	0.62	-0.86				
LTBP4		-1.14		VZ	MZ	MZ
LUM	-0.98		SG		SG	
LURAP1L		0.77				

Table 3.1	log2 Fold Change - First round - CMP filtered		Significantly correlated layer			
Gene	hNP	hDN	15 pcw	16 pcw	21a pcw	21b pcw
LUZP2	-1.08		MZ	CPo	CPo	CPo
LY6H	-0.94		CPo	CPo	CPi	CPi
LYPD6B	0.88			CPi	CPi	CPi
LYST	0.47		CPo	SP	CPi	MZ
LZTS1		-0.74	MZ	SP	SP	SP
MAATS1	0.68	0.47				
MAB21L1		-0.76	SG	MZ	SG	MZ
MACROD2		0.91	SP	SP	CPi	CPi
MAFB	0.44		IZ	IZ	SG	MZ
MAGEE1		0.48	CPo	CPo	CPi	CPi
MAGEE2		-0.94	SP	CPi		
MAN1C1		-0.52	SG	CPo	CPo	CPo
MAN2B2		-0.50	CPo			CPi
MAP1B	0.43		MZ	MZ	CPi	CPo
MAP1LC3C		-1.52		IZ		
MAP3K1		0.86	VZ	VZ	SZi	IZ
MAP3K3		0.54	IZ	IZ	SG	CPo
MAP4		-0.57	CPo	CPo	CPo	CPo
MAPT		0.67	CPo	CPo	CPo	CPo
MARVELD3		-1.20				
MASP1		1.00	CPo	CPi		CPi
MAST4	-0.48		VZ	VZ		
MATN2		-0.95				
MB21D2		0.69				
MCHR1	0.89	1.62	SG		MZ	SP
MCTP1	-0.45		SP	SP	SP	SP
MDGA2		1.05	SP	SP	CPi	CPi
MDM1		0.35	VZ	VZ	VZ	SZi
MEF2C		0.49	CPo	CPo	CPo	CPo
MEGF11		0.73	SP	CPi		
MEGF9		-0.47	CPo	CPi	CPo	CPi
MEIS1		0.59	VZ	VZ	VZ	VZ
MERTK		-0.67	VZ	IZ	SZi	VZ
MET	-0.72	-1.31		CPi	CPo	CPo
METRNL	-0.61	-0.89	SG	CPi		CPi
METTL21B		-0.56				
METTL7A	-0.82		VZ	VZ	SZo	VZ
METTL7B		-1.27	SG			
MEX3B		0.67				VZ
MFAP4		-1.65	VZ	VZ	VZ	VZ

Table 3.1	log2 Fold Change - First round - CMP filtered		Significantly correlated layer			
Gene	hNP	hDN	15 pcw	16 pcw	21a pcw	21b pcw
MFAP5		1.12				
MFGE8		-0.38	VZ	SZo	SZo	SZo
MFSD10	-0.76					
MGAT3		0.90	CPo	MZ	MZ	MZ
MGAT4A	0.49	0.56	SP	SP	CPi	SP
MGAT4C	-0.72	-0.95	VZ	VZ		
MGST1		-0.48	SP	SP	SP	
MGST3	-0.51		MZ		MZ	MZ
MLIP		-1.37				
MMP15		-0.84	VZ		SZo	SZo
MMP16		-0.48	CPi	SP	CPi	SP
MMP17		0.83	IZ	IZ	CPi	CPo
MMP19		-1.22	SZo	SZi	IZ	VZ
MNS1	0.68		VZ	VZ	VZ	SZi
MOGS		-0.49	SP			
MORN3		-0.60	SP	SP		SP
MOXD1	-0.71		VZ	VZ	SZo	SZi
MPC1	-0.32					
MPPED2		0.38	VZ	VZ	VZ	VZ
MRAS		0.41	CPo	CPo	CPo	CPo
MREG	1.20		SZi	VZ	VZ	SZi
MRPS12		-0.67				
MRPS6		-0.99	SP	SP	SP	SP
MRVI1		1.36				
MSTN		0.79		VZ	VZ	VZ
MSX1		1.22	SG	MZ	SG	SG
MT1F		0.92	SZo		VZ	SZi
MT1X		0.75	VZ	SZo	VZ	VZ
MT2A		1.43	VZ	SZo	VZ	SZi
MT3		1.19	VZ	SZo		
MTSS1L	-0.52					
MTTP		-0.62	VZ	VZ	VZ	VZ
MTURN		0.64				
MTUS2	1.77		SP	SP	SP	SP
MXI1		0.67			VZ	VZ
MXRA5		1.00		MZ	SG	SG
MYCL		0.80				
MYH14		-0.90				
MYH7		0.65			VZ	SP
MYH9		-0.69				VZ

Table 3.1	log2 Fold Change - First round - CMP filtered		Significantly correlated layer			
Gene	hNP	hDN	15 pcw	16 pcw	21a pcw	21b pcw
MYLK		-1.11	SG	SP	SG	
MYLK3		1.03				
MYO10	-0.42		VZ	VZ	SZo	SZi
MYO16		2.17	SP	CPo	CPi	CPi
MYO1B	0.73		SG	SZi		
MYO1E		-1.08				SZi
MYO3A	1.41		SZo	VZ	SZo	SZo
MYO5B	-0.43		SP	SP	CPo	SP
MYO5C		-0.61	VZ	VZ		IZ
MYO6		0.30	SZi	VZ	SZo	VZ
MYO7A		1.98	IZ	IZ		
MYOC		-1.21	SG	MZ	SG	
MYOM1		-0.89				
MYOZ3		0.72			SG	SG
MYZAP		1.62				
NAALAD2		0.81			SP	
NAALADL2		-0.54	VZ			
NACC2	-0.36	-0.61	VZ	VZ		
NALCN	-1.06	-0.85				
NAV2	1.16		SP	CPi	CPo	CPo
NCALD	0.65	0.75	CPo	CPo		CPi
NCAM1		0.45	CPo	SP	MZ	
NCAN	-0.48				SZo	VZ
NCAPG		-0.56	VZ	VZ	SZo	SZo
NDC80		-0.50	VZ	VZ	SZo	SZo
NDRG4		0.56		MZ	IZ	
NDUFA7	0.70		VZ	SZo	VZ	VZ
NEB	-1.00					
NEBL	1.02				CPo	CPi
NEDD9		-0.87	CPi		SZo	SZi
NEGR1		1.26	SP	SP		
NEK5		1.26				
NELL2	0.90	2.50	CPo	CPo	CPo	CPo
NES	0.36		MZ	MZ	SG	SZo
NET1		-0.53				VZ
NETO1	0.35	0.74	CPi	CPo	CPo	CPo
NETO2		0.47	IZ	IZ	MZ	MZ
NFASC	0.76	1.29	SP	SP		
NFE2L1		-0.56	SG			CPi
NFIX		0.38	MZ	MZ		

Table 3.1	log2 Fold Change - First round - CMP filtered		Significantly correlated layer			
Gene	hNP	hDN	15 pcw	16 pcw	21a pcw	21b pcw
NFKBIZ	0.90				SG	
NGB		2.14	SP	SP	SP	SP
NHS		-0.64				
NHSL2		-0.98	VZ	SZo	SP	VZ
NID1		-0.48		VZ	VZ	SG
NID2		-0.58				
NIPAL2	0.88	0.74	SG	VZ	SP	SP
NIPAL3		-0.51	SP		SP	SP
NKAIN1		0.53	CPo	CPo	CPo	CPo
NKAIN2	0.75	2.36	CPo	CPo	CPi	CPo
NKAIN4		1.06	VZ	SZo	SZo	SZo
NMB		1.91	SZo		CPi	CPi
NME9		0.75				
NMRK1	-0.44					
NNAT		-0.68			VZ	VZ
NNMT		1.43	VZ	SZi	VZ	VZ
NOMO1		-0.40	CPo	CPi	CPo	CPo
NOMO2		-0.71				
NOS1AP		0.67	IZ	IZ		SP
NOVA1		0.68	SP	SP		
NPAS3		0.71	VZ	VZ	MZ	
NPC2	-0.54		SG	SZo	SZi	SZo
NPFFR1		1.13	CPi		IZ	
NPM3		-0.66	CPo	CPo	CPo	CPo
NPR3		-1.13	SP			
NPTXR	1.21	0.64	SG	IZ	CPo	CPo
NPY	0.80		VZ	CPo	SP	
NQO1		-0.74	SG	VZ	SG	SZo
NR3C1		0.36			SG	
NR4A2		-0.76	SP	SP		
NRCAM	0.49		SP	SP	SP	
NRG4		0.80	CPi			
NRIP1		0.60				
NRL	-0.82		SP	SP		
NRP1		0.51	SZi	SZo	SZo	SZo
NRP2	0.85				CPo	CPo
NRSN1		1.47	SP	SP		
NRXN2		0.76	IZ	CPi	SP	CPi
NT5DC3	0.98	1.84	SP	CPi	CPi	SP
NTM		2.39	CPi	CPi		

Table 3.1	log2 Fold Change - First round - CMP filtered		Significantly correlated layer			
Gene	hNP	hDN	15 pcw	16 pcw	21a pcw	21b pcw
NTNG1	-0.87	-2.26	VZ	MZ	CPi	CPi
NTRK2		1.12	SG			
NUAK1		-0.60	SP	SP		
NUDT11		0.47	CPo	CPo	CPo	CPo
NUF2		-0.50	VZ	VZ	SZo	SZi
NUPR1	-1.22	-1.53		MZ		
NWD1		-0.62				
NXPH3		-0.85	SP	SP	SP	
OAF		1.11	VZ	VZ	SZo	SZo
OGN		-0.74	SG	MZ	SG	SG
OLFM3	-0.71		SP	SP	SP	SP
OLFML2A		-0.93				
OLFML2B	1.40	0.98				
OLFML3	0.81				SG	SG
OLIG1		0.84		IZ	IZ	IZ
OLIG2	-0.34				IZ	IZ
OMG	-0.91				SP	
OPCML		1.82	SP	SP	CPi	SP
OPRK1		-0.86	CPi	CPi	CPi	CPi
OSBPL10	0.41		SP	SP	SP	SP
OSBPL1A		0.36	VZ		CPi	CPi
OSGIN2		-0.40		VZ		
OTOL1		1.89				
OTUD1		0.50				
OTX2	-0.33					
P2RX7	-0.58		MZ		IZ	IZ
P2RY1		0.58				
P3H2	0.57					
P3H3		-1.17				
P4HA2		-0.76	SG	MZ	SG	
P4HB		-0.42	VZ	VZ	SZo	SZo
PADI2		3.16		CPi		
PALD1		0.99				
PALM2	0.76	1.32	SP	SP	CPi	SP
PALMD		1.08			SZo	SZo
PAM		0.32	VZ	VZ	SZo	VZ
PAMR1		-0.72				
PAPPA		4.59				
PAQR3	0.74			CPo		CPo
PAQR8	-0.86	-0.86	VZ	SZo	SZo	SZo

Table 3.1	log2 Fold Change - First round - CMP filtered		Significantly correlated layer			
Gene	hNP	hDN	15 pcw	16 pcw	21a pcw	21b pcw
PARD3	0.32		VZ	VZ	VZ	VZ
PARD3B		-0.30	VZ	VZ	VZ	SG
PARD6B	0.67					
PARD6G	-0.37		SG	CPo		
PBK		-0.60	VZ	VZ	SZo	SZi
PBX3		0.70	SZi	SZi	VZ	VZ
PCDH1		0.99	IZ	CPo	SP	CPo
PCDH18		1.01	SG	VZ		
PCDH7	0.88	0.66	SP	CPo	SP	CPi
PCDH8		2.17	CPo	CPo	MZ	
PCDHA1		0.81	SP	SP	CPi	CPi
PCLO	0.70		CPo	CPo	CPi	CPi
PCP4L1	-0.80		IZ	IZ	SG	SP
PCSK1		-0.78	SZi	SZo	MZ	
PCSK5		-0.64	SP	SP	SP	SP
PCSK9		1.04	CPi	CPi	CPi	CPi
PDCD1LG2	0.96					
PDE1B		1.17	SP	SP	MZ	CPi
PDE1C		-0.92	SZi	SZi	SZo	SZi
PDE4B	-0.42		IZ	CPo	CPo	IZ
PDE4DIP	-0.37		CPi	MZ	SG	SG
PDE7B	0.69	1.56				
PDE8A		0.79	SG	SZo		
PDE8B	1.87			SP		
PDGFB		-1.87				VZ
PDGFRB	-0.77	-0.47	VZ	VZ	SG	VZ
PDIA3		-0.52		VZ	SZo	SZo
PDIA4		-0.52	VZ	VZ	VZ	SZi
PDIA6		-0.33	VZ	VZ	VZ	SZo
PDK3		-0.60		IZ	SG	VZ
PDLIM4		-0.71	VZ	VZ		
PDLIM5	0.54		VZ	VZ	SZo	VZ
PDP1	0.55		CPo	SP	CPi	CPi
PEA15		0.41	VZ	VZ	SZo	SZo
PELI2		-0.86			VZ	VZ
PGM1		0.58	VZ	VZ	SZo	SZo
PGRMC2		-0.36	SZi	SZi	SZo	VZ
PHACTR3	0.88	0.72	SP	MZ	CPi	SP
PHF12		0.37	IZ	IZ		
PHKA1	-0.47		VZ	VZ	SZo	SZo

Table 3.1	log2 Fold Change - First round - CMP filtered		Significantly correlated layer			
Gene	hNP	hDN	15 pcw	16 pcw	21a pcw	21b pcw
PHLDA1	-0.56		SZi	SZo	SZo	SZi
PHLDB2		0.65	SG	VZ		SG
PI15		-2.73	IZ	CPo		
PIEZO1		-0.96				
PIGH		-0.42	SZi	SZi	VZ	SZi
PIGT		-0.46	SG			
PIK3C2A		-0.38	VZ	VZ	SZi	SZi
PIK3C2B	-0.67		CPo	CPo	CPi	CPi
PIP5K1B		-1.24	VZ	SZi		VZ
PIRT	0.54					
PITPNC1	-0.53		SP	SP	SP	SP
PITPNM3		0.95				
PKIB		0.91	VZ			
PKP2		1.43			CPo	CPi
PLA2G12A		-0.84	CPo	MZ	SG	
PLA2R1	0.65					
PLAG1		-0.90	VZ	VZ	SZi	VZ
PLAU		-0.68		IZ	VZ	IZ
PLBD2		-0.67		SP		
PLCB4		0.32	IZ	SZi	SP	MZ
PLD5		-1.99	VZ	VZ		
PLEKHA1	0.75		IZ	IZ	CPi	IZ
PLEKHA4		-0.45	SG	IZ	VZ	VZ
PLEKHA5		0.55				
PLEKHA6		1.11	CPo	CPi	CPi	CPi
PLEKHA7		-0.69	VZ	VZ	VZ	VZ
PLEKHG3		-0.58	SZo	SZo		VZ
PLEKHG5	0.70	0.49		CPo	CPo	MZ
PLEKHH2	-0.63	-0.95				SP
PLPP1		-0.39				
PLPP4		1.07				
PLPP5		-0.41				
PLPPR5		0.63				
PLS1	0.99		SZi	SZi	SZo	SZi
PLXDC2	0.63	-0.65	SP		SZi	VZ
PLXNA2		0.80			IZ	IZ
PLXNA4		0.60	IZ	CPo	CPo	CPi
PLXND1		-0.75	SG	MZ	MZ	
PNMA2	0.54		CPo	CPi	CPo	CPo
PNOC		-1.20	SG	MZ	SG	MZ

Table 3.1	log2 Fold Change - First round - CMP filtered		Significantly correlated layer			
Gene	hNP	hDN	15 pcw	16 pcw	21a pcw	21b pcw
POPDC3		-1.01				
PPARG		1.04	SP	SP		
PPARGC1A		2.06			SG	
PPDPF		-0.48				
PPFIA3		1.06	CPo	CPo	CPi	CPo
PPFIA4		0.76	SP	SP	SP	SP
PPFIBP2	-0.55		SZi		SZo	SZo
PPIF		-0.84			VZ	
PPM1L		0.55	SP	SP		
PPP1CC		1.19	VZ	SZi		VZ
PPP1R14C		-0.78	CPo	CPo	CPo	CPo
PPP1R1A		1.74	IZ	IZ		IZ
PPP1R1B		1.08	SP	SP		
PPP1R1C	-0.40		VZ	VZ	SZi	SG
PPP1R3C	-0.77		SG	SZo		VZ
PPP1R9A	0.51	0.40	SP	SP		CPo
PPP2R2C		1.92	SP	SP	CPi	CPi
PPP2R5A	-0.45					CPi
PQLC3	0.77		SG	SP	SP	SP
PRAF2		-0.55	IZ	CPo	CPo	CPo
PRDM1	-0.54			SZo		
PRDX1	-0.51		SZi	SZi	SZo	SZo
PRDX6		-0.48	VZ	VZ	SZo	SZo
PRELID2	0.74	0.71	VZ	VZ	SZi	SZi
PRELP	-1.16					SZo
PRICKLE1	-0.63			SP		
PRIMA1		1.42				
PRKAA2		0.49	CPo	SP	CPi	CPo
PRKAB2		0.32	CPo	CPi	CPo	CPo
PRKCD	0.63	0.89				
PRKCE	0.48	0.73	SP	SP	SP	SP
PRLR		1.38				MZ
PRMT6		-0.71	VZ	VZ		CPo
PRNP	-0.33	-0.47	SG	MZ	IZ	
PROB1		-0.95				
PROCR		-1.81		IZ		SG
PROKR1	1.18	0.78				SZi
PROS1		-0.54				
PROX1	0.39			SZi		
PRR18		0.75			VZ	

Table 3.1	log2 Fold Change - First round - CMP filtered		Significantly correlated layer			
Gene	hNP	hDN	15 pcw	16 pcw	21a pcw	21b pcw
PRR29		0.83				
PRR32		1.37				
PRR5		1.55				
PRR5L	0.60		VZ	SZo	SZo	SZo
PRRG3		0.80	SP	CPi	CPo	
PRRT3	-0.49		SP	SP	SP	CPi
PRRT4		1.17				
PRSS23		-0.90	CPo	CPi	CPi	CPo
PRUNE2		-0.33	VZ	VZ	SP	SP
PRX		-0.83			MZ	MZ
PSAP		-0.38	VZ	VZ	VZ	SZo
PSAT1		0.94	VZ	VZ	SZo	SZo
PSD3	-0.43	-0.43	CPo	CPi	CPi	CPi
PTBP3	0.50					
PTCHD1		1.10	IZ	IZ	CPi	CPo
PTCHD4	0.36	-0.61				
PTGDS	-0.87		SG	MZ	SG	SG
PTGFR		0.79	SG		MZ	MZ
PTHLH		1.05				
PTK2	0.43					
PTK2B	-0.66	-0.93	CPi	VZ	CPo	CPo
PTN		1.30	VZ	VZ	SZo	SZo
PTPN3	0.87		CPo	CPo	CPo	CPo
PTPRD		0.87	CPo	CPi		
PTPRQ		1.14				
PTPRT	-0.63		CPo	CPo	CPi	CPi
PTPRU		-0.79	SP		MZ	
PTRF		-0.68				SG
PUM3		-0.35				
PUS7		-0.41	VZ			
PXDNL		-1.26			SG	
PXYLP1	0.40	0.67				
PYGM		1.88	SG			
QPCT		1.15			IZ	
QTRTD1		-0.53	VZ	VZ	SZo	SZi
RAB11FIP1		-1.34	SG			
RAB27A		-0.46	VZ	SZi	SZi	VZ
RAB29	-0.31					
RAB30		0.70	CPi			SZi
RAB3B	0.94		SP	MZ	SP	SP

Table 3.1	log2 Fold Change - First round - CMP filtered		Significantly correlated layer			
Gene	hNP	hDN	15 pcw	16 pcw	21a pcw	21b pcw
RAB3GAP2		-0.41	VZ	VZ		SZo
RAB6B	-0.53	0.47	SP	MZ	CPi	CPi
RAD9A		0.64	VZ	VZ		CPi
RAI2	1.32		IZ	IZ	CPo	CPi
RALGAPA2	-0.42			SZi	SZo	
RALGPS1		0.41	CPo	CPo	CPo	CPo
RAMP1		-1.11	SG	SZo		
RAP1GAP	-0.50		SP	CPo	CPo	CPo
RAPGEF5	0.93		SP	SP	CPi	CPi
RARB		1.54	SG	MZ	CPo	CPo
RARRES3	-0.81			IZ	SZi	VZ
RASA3		-0.44	IZ	CPi	IZ	
RASD1		0.83			SZi	CPo
RASD2		0.84	IZ			
RASGEF1B		0.54	SZi	SZi	SZo	SZi
RASGRF1		3.14	SP	SP		
RASGRF2		-0.81	IZ	IZ	CPo	CPo
RASGRP1	1.33	1.10	SZi	SZi	SZi	SZi
RASGRP2		0.80	SP	SP	CPi	CPi
RASGRP3		0.61				
RASL10B		0.48	MZ	MZ	MZ	MZ
RASSF5		0.85	SP	SP		VZ
RASSF9		-0.45	SG			
RAVER2		-0.43	VZ	VZ		SZi
RBBP8		-0.55	VZ	VZ	SZo	SZi
RBFOX1		0.96				
RBMS2	-0.43		VZ	VZ	SZi	SZi
RBMX2	-0.31			CPo		
RBPMS		-0.74				
RCAN2		0.92	SG	CPi	MZ	MZ
RCAN3		-0.72	SZo			
RDH10	0.94		SG	VZ	SG	VZ
RELL1		-0.67	VZ	VZ	SG	VZ
RELN		0.90	MZ	MZ	SG	MZ
RERG		1.37	SP	SP	SG	SP
RET	-0.74		CPi	SP	CPi	CPi
RFFL	1.05		VZ	SZo	SZi	VZ
RFTN1		-0.82			VZ	VZ
RFX3		0.32		CPi	CPo	CPo
RGCC		1.44				

Table 3.1	log2 Fold Change - First round - CMP filtered		Significantly correlated layer			
Gene	hNP	hDN	15 pcw	16 pcw	21a pcw	21b pcw
RGMA		0.82	SP	SP	IZ	SP
RGPD8	0.83					
RGS11		-1.02	SG			
RGS16	0.73		VZ	VZ	SG	SP
RGS19		-0.85		CPi		CPi
RGS20	-0.67		VZ	VZ	CPi	
RGS3		1.03	VZ	VZ	SG	SZi
RGS4		-1.06	SP			IZ
RGS5	0.76	-2.15			MZ	
RGS7BP	-0.75		SP	SP	CPi	CPi
RGS8	0.95	1.49				
RGS9	-1.05		SP	SP		SP
RHBDF1		-0.80				
RHBDL3		0.64	SP	SZo	SZo	SZo
RHOU		1.08	CPo	CPo	CPo	CPo
RHPN2		-0.78	VZ	VZ	SZo	SZi
RIMKLA		0.40	CPo	IZ	MZ	MZ
RIMS3		1.00	MZ	MZ	MZ	MZ
RIPPLY1		1.10				
RIPPLY2		0.91	SP	SP	MZ	
RNASE1		-2.55	SG			SG
RNASE4		-1.09	VZ	VZ	SZi	SZi
RND1		0.74	IZ		CPi	
RNF122		0.50	SZi	SZi	VZ	VZ
RNF144A		0.47				
RNF150		0.47	IZ	IZ	CPo	CPo
RNF152		0.61	CPo	CPo	CPo	CPo
RNF165		0.62	MZ	CPo	MZ	
RNF182		0.50	CPo	IZ	CPo	IZ
RNF187		0.47	SP	CPi	CPi	SP
RNF19A	0.33			CPi		CPi
RNF207		-0.78	IZ	IZ		
RNF5	-0.54			CPo		
ROBO1		0.90	SZi			
ROBO2	-0.57				SZo	SZo
ROMO1	-0.65					
RP11-511P7.5		0.85				
RP11-849H4.2		-0.75				
RP6-24A23.6		1.14				
RPE65		-1.01	SZo		MZ	

Table 3.1	log2 Fold Change - First round - CMP filtered		Significantly correlated layer			
Gene	hNP	hDN	15 pcw	16 pcw	21a pcw	21b pcw
RPL10A	-0.34		IZ	MZ		
RPL13	-0.45		IZ	MZ		
RPL27	-0.36		IZ	MZ		
RPLP2	-0.49		IZ	MZ		
RPN2		-0.43	VZ	SZo	VZ	SZo
RPRM		-0.84	CPo	CPi	CPi	CPi
RPS28	-0.97		IZ	MZ		
RPS6KA1		-1.01				VZ
RPS6KA2		-0.52	MZ	MZ	SP	MZ
RRBP1		-0.71				SZi
RRM2		-0.70	VZ	VZ	SZo	SZo
RSPH1		0.53	VZ	VZ	VZ	VZ
RSPH4A		0.54	CPo			
RTN1	-0.96		CPo	CPi		
RTN2		0.59	CPo	CPo	CPo	CPi
RTN3		0.35	CPo	CPo	CPi	CPo
RTP1		0.96	VZ	VZ	VZ	
RUNX1T1		0.85	CPo	CPi	CPi	CPi
RYR2		0.90	CPi	CPi	CPi	CPi
RYR3	-0.59	0.76	SP	SP	SP	SP
S100A10	0.85		SG	IZ	CPi	
S100A16		0.75	VZ	SZo	SZo	SZo
S100B		-0.52	IZ			
S1PR1		0.50	VZ	VZ	SZo	SZi
S1PR3		0.59				
SALL4	0.97					SG
SAMD11		-1.85	SG			
SAMD5	1.00		CPi	CPi	CPi	CPi
SAPCD2		-0.76				
SASH1		0.55				
SAT1	-0.77		VZ	SZo	SZi	VZ
SATB1		0.44	SP	SP		IZ
SATB2	0.36		IZ	CPo	CPo	CPo
SBSPON	2.34	1.19				
SCARB1		-0.54	IZ	SP	SP	SP
SCD5		0.52	CPi	CPi	CPi	CPi
SCG3	-0.59		CPo	CPo	SP	SP
SCN3B		0.75	SP	SP	CPi	CPi
SCN7A		1.73	VZ	VZ	CPo	MZ
SCN9A		0.81	CPo	CPi	CPo	CPi

Table 3.1	log2 Fold Change - First round - CMP filtered		Significantly correlated layer			
Gene	hNP	hDN	15 pcw	16 pcw	21a pcw	21b pcw
SCNN1B		1.16				
SCPEP1		-0.57	SG	VZ	SG	VZ
SCUBE1	1.22	3.99				
SCYL2	0.43		CPo	CPo	CPi	CPi
SDC2		-1.51	VZ	VZ	SZo	SZi
SDC3		1.41	CPo	CPi	IZ	CPo
SDC4	1.01		VZ	VZ	VZ	VZ
SDK1		-1.00	CPo	CPo	CPo	CPo
SEL1L3	0.77		VZ	VZ	SZo	SZo
SELENBP1	-0.66	-0.82	SG	VZ	VZ	VZ
SEMA3A	0.47	-0.68	CPo	CPi	CPi	CPi
SEMA3B		-1.02	SG		SG	
SEMA3C		-1.26	SP	SP	SZo	
SEMA3D		-1.85	SG	MZ		
SEMA4B	-0.59					
SEMA5A		-0.71	VZ	VZ		IZ
SEPP1	-0.96	-1.68	VZ	VZ	VZ	VZ
SEPSECS		-0.51	VZ	SZi	SZi	
SERPINA3		-1.27	SG		SZi	
SERPINB8	0.61					
SERPINB9		-1.32	SG			
SERPINE2	-0.75		CPo	CPo		IZ
SERPINH1	-0.38		VZ	VZ	VZ	SZo
SERPINI2		-1.01	VZ	VZ		VZ
SERTAD4	0.72	0.99	VZ	VZ		
SESN3		0.35	IZ	IZ		
SESTD1	0.39		SP	SP	CPi	CPi
SEZ6		1.57	SP	SP	SP	
SEZ6L	0.61		SZo		CPi	
SFRP1		0.54	VZ	VZ	SZo	SZi
SFRP2		0.96	VZ	VZ	VZ	VZ
SFT2D2	0.32		VZ	VZ	SZi	SG
SGCD	-1.30	-0.49	SG	VZ		
SGK1	0.88	1.36	SG	CPi	CPi	MZ
SH3BGRL2		-0.43		MZ	IZ	
SH3BP5	0.67	0.37	CPo	CPi	CPo	CPi
SH3GL2	0.59		SP	SP	SP	SP
SH3PXD2A	0.53		MZ	MZ		
SH3RF1		0.54	VZ	VZ		VZ
SH3RF3		-0.54		CPi	MZ	MZ

Table 3.1	log2 Fold Change - First round - CMP filtered		Significantly correlated layer			
Gene	hNP	hDN	15 pcw	16 pcw	21a pcw	21b pcw
SHCBP1		-0.66	VZ	VZ	SZo	SZi
SHISA3		-1.00	SZo	SZo		
SHISA6		1.55	IZ	IZ		
SHISA7	-0.87			IZ		
SHROOM3		-0.59	VZ	VZ	SZo	SZi
SHTN1		0.32				
SIDT1		1.18	SG		SG	
SIPA1L2	0.33		SZi	SZi	SG	VZ
SIPA1L3	-0.51		IZ	CPo	IZ	MZ
SIX3		1.42				VZ
SKAP1		0.95				
SLA		0.94	IZ	IZ		CPo
SLC12A5		0.78	SP	SP	SP	SP
SLC12A8	-0.64	-0.59	IZ			
SLC16A12		-1.59		VZ	VZ	VZ
SLC16A2		-0.51	SP	CPi	CPi	CPi
SLC16A6	0.74			VZ	SZo	SZi
SLC17A6		0.92	SZi	SZi	SZi	SZi
SLC17A8	0.83	1.02			IZ	IZ
SLC1A1	0.66		CPo	CPo	CPi	CPi
SLC1A2		0.90	SZo	SZo	SZo	SZo
SLC1A5		-1.26				
SLC22A15		0.73	SP	SP	SG	SP
SLC22A3		2.62	SG		CPo	SG
SLC24A4	2.58				CPo	
SLC25A43		-0.46	VZ	VZ	SZo	SZo
SLC26A4	-0.70		SP	SP	CPi	CPi
SLC26A7	0.72		VZ	VZ		SG
SLC29A1		-1.31	SG	SP	SP	CPi
SLC2A5		0.96	SZi	SZi	SZi	VZ
SLC34A2		1.01	IZ	IZ		
SLC35B4		-0.41	VZ		SZo	
SLC35F2	1.01		CPi	CPi	CPi	CPi
SLC35F4		1.44	SP		MZ	SP
SLC39A12		0.75	VZ	VZ	SZo	SZo
SLC44A1		-0.49	CPo	CPo		
SLC44A3		0.69				
SLC44A5		0.60	CPo	CPi	CPo	CPo
SLC47A1		-0.97		VZ	VZ	SG
SLC47A2		-1.11	CPi		VZ	

Table 3.1	log2 Fold Change - First round - CMP filtered		Significantly correlated layer			
Gene	hNP	hDN	15 pcw	16 pcw	21a pcw	21b pcw
SLC4A10	0.75	1.50				
SLC5A1		-1.54	IZ	MZ		
SLC5A3		-1.48	IZ	IZ		
SLC6A20	-1.95		SG	MZ	SG	SG
SLC7A11	-0.58			VZ	SG	SG
SLC7A7		0.89		IZ	SZi	VZ
SLC8A1	0.77	0.70	CPo	CPo		CPo
SLC9A9		0.76	SG	VZ	SZi	SZo
SLC9B2	0.43	0.47				
SLCO1A2	-1.64		IZ	SP		
SLCO1C1	-0.67		VZ	VZ	SZo	SZo
SLCO5A1		0.49		CPo	MZ	MZ
SLF2	-0.42	-0.71				
SLIT3		-1.54	SP			
SLITRK2		0.90	VZ	VZ		
SLITRK4	0.75		CPi	CPi	CPo	CPo
SLITRK5		0.50	SP	CPi	CPi	CPi
SMAD6		-0.81	SG	VZ		
SMAD9		-0.51	SZi	SZi		VZ
SMC4		-0.35	VZ	VZ	SZo	SZo
SMC5		-0.50	VZ	VZ	VZ	VZ
SMIM18		0.70				
SMIM4		-0.82				
SMOC2		-1.09	CPo	CPo		
SMPD2	-0.69				VZ	CPi
SMTNL2		0.87	SG	CPo	CPo	CPo
SNAI2		-1.01			CPo	CPo
SNTG1		-0.36	VZ	VZ		
SNTG2	-0.87		IZ	IZ	SP	CPo
SNX29		0.52	CPo	CPo	MZ	MZ
SNX5		-0.35				
SOBP	-0.74		SP	SP	SP	SP
SORBS2	0.45				SZo	SZo
SORCS1	0.39		SP	SP	SP	SP
SORCS3	0.70	0.53	CPo	CPo	MZ	MZ
SOX21	-0.55	-0.43	VZ	VZ	VZ	VZ
SPAG5		-0.49	VZ	VZ	SZo	SZo
SPARCL1	-1.06		SG	SZo	MZ	MZ
SPATA2L		-0.77	IZ		IZ	
SPC24		-0.51	VZ	SZo	SZo	SZo

Table 3.1	log2 Fold Change - First round - CMP filtered		Significantly correlated layer			
Gene	hNP	hDN	15 pcw	16 pcw	21a pcw	21b pcw
SPOCK1		0.74	SP	SP	CPi	CPi
SPON1		0.79	CPo		CPo	CPo
SPSB1	0.87					
SPSB4		0.58	VZ			
SPTLC3		0.41	SG	VZ	SG	VZ
SPTSSB	1.04					
SQRDL		0.78		IZ	SG	SG
SRD5A1		-0.42	CPo	CPi	CPo	CPo
SREBF1		-0.66	VZ	VZ	VZ	VZ
SRRM4	0.74		MZ	CPi	SP	
SSC5D		-0.76				
SSFA2	-0.37		VZ	VZ	SZi	VZ
SSR1		-0.33	SP	SP		
SST		1.87	IZ	IZ		
SSTR2		0.81	SZi	SZi	SP	CPi
ST3GAL6	0.61				CPo	CPo
ST6GAL1	1.10	0.79	CPi	CPi	CPo	CPi
ST6GAL2	-0.68		SZo	CPi		CPo
ST6GALNAC3		0.45	SP	SP	SG	SG
ST8SIA2		0.50	CPo	CPi		CPo
ST8SIA6		1.78	CPi	SP	CPo	CPo
STAC		-0.99	VZ		CPo	CPo
STAC2		-1.42				
STC1	0.50					
STC2	1.56					CPi
STEAP2	0.42	0.68	VZ	VZ	MZ	
STIM1		-0.33	VZ	VZ		
STK17A	-0.74		VZ	SZo	SZo	SZo
STK26		0.94				
STK32A	0.79		SZi		SG	
STK32B		1.19	CPo	CPo	CPo	CPo
STKLD1		1.04				
STMN4		0.57	CPo	CPo	CPo	CPo
STOM	0.50		VZ	SZo	SZo	SG
STOML3		-1.67				MZ
STON1		-0.88	VZ	VZ	SZo	SZi
STX11		-0.73				
STX3	0.75	-0.70	CPo	CPo	CPo	CPo
STXBP5L	0.45		SP	SP	SG	MZ
SUCLG1	-0.42		CPo	CPo		

Table 3.1	log2 Fold Change - First round - CMP filtered		Significantly correlated layer			
Gene	hNP	hDN	15 pcw	16 pcw	21a pcw	21b pcw
SULF1		0.86			SP	
SULF2	0.57	1.27	CPi	SP	SP	SP
SUMF1		-0.73	VZ	VZ	VZ	SZo
SUSD5		-0.56			CPi	MZ
SV2B		1.59	SG	CPi	CPi	SP
SVEP1		-1.78				
SWAP70		-0.84	VZ	VZ	SZi	VZ
SYN2		2.11	SP	SP	SP	CPi
SYNE2	0.59		VZ	VZ	SZi	SZi
SYNJ2		0.43	SP	SP	CPi	CPi
SYNM		-0.82	VZ	VZ		
SYNPO		0.81	SG			
SYT1		0.76	IZ	IZ	SP	IZ
SYT12	0.71			IZ		SP
SYT5		0.91	CPo	CPi	CPi	CPi
SYT7		1.91				
TADA1	0.33					
TAF4B	-0.62	-0.72	IZ	MZ		
TARBP1	0.53				SP	
TBC1D9		-0.52	CPo	MZ	CPi	CPi
TBX2		-1.18				
TCEAL7	0.52				CPi	
TCF7L2	0.54		VZ	VZ	IZ	IZ
TEK		-1.15				
TENM3		-0.57				
TENM4	0.96					
TF		1.24			IZ	
TFCP2L1		0.87			VZ	
TFPI2		-0.92	VZ	VZ		SG
TGFB2		-0.58	VZ	CPi	CPi	CPi
TGFBI	0.84				SG	VZ
TGM2		3.92				SZi
TGOLN2		-0.30	IZ	SP		
THAP8	-0.75				VZ	VZ
THBS1		-1.69			CPo	CPo
THBS2	-0.55	0.40	VZ	VZ	SZo	SZo
THBS3		-0.56				
THBS4		-0.64			SZo	SZi
THRB		1.18	CPo	CPo	CPo	CPi
THSD1	-0.50	-0.57	VZ	VZ	SZo	VZ

Table 3.1	log2 Fold Change - First round - CMP filtered		Significantly correlated layer			
Gene	hNP	hDN	15 pcw	16 pcw	21a pcw	21b pcw
THSD7B	-0.55	1.01	MZ	CPi	MZ	MZ
TIAM1	0.33		IZ	IZ		
TIMP2		-0.49	SG	VZ	SZi	VZ
TIMP3	0.35		VZ	VZ	SZo	SZo
TIMP4	-0.72					
TKTL1		2.04	VZ	VZ	SZo	SZo
TLE1		0.78	VZ		SZo	
TLE2	-0.71		MZ	MZ	MZ	
TLE4		0.82	SP	SP		
TLR3		-0.79	VZ	VZ	SZi	SG
TLR5		1.12	CPo	IZ		
TM4SF1	-0.63					
TMED10		-0.32			VZ	VZ
TMEM106C		0.68	VZ	VZ	CPi	CPi
TMEM132B	1.28	1.93	VZ	VZ	SZo	SZi
TMEM132C		1.45		VZ		
TMEM132E		0.47	IZ		MZ	MZ
TMEM133	0.42		VZ	VZ		MZ
TMEM150C		0.75	CPo	CPi		CPo
TMEM163		-0.68	VZ			
TMEM178B		0.51				
TMEM179	-0.78		IZ			
TMEM185B		-0.32				
TMEM2	0.70		SG		SG	VZ
TMEM200A		1.20	CPo	CPo	CPi	CPo
TMEM205	-0.67			VZ		
TMEM221		-0.84				
TMEM229B	0.90	0.62	SP	SP	SG	MZ
TMEM233	2.09					
TMEM257		1.33				
TMEM266		1.34				
TMEM47		-0.57	VZ	VZ	VZ	VZ
TMEM51		1.07	SG	VZ	IZ	IZ
TMEM63C		1.38	SP	SP	CPi	CPi
TMOD1		-0.59		IZ		CPo
TMPRSS7		-1.93				IZ
TMTC1	0.74			CPo	CPo	CPo
TMTC2	-0.70		VZ	VZ	SZo	VZ
TNFAIP2		1.30	SP	CPi	CPi	CPi
TNFRSF11B	-0.64	-1.09	VZ	VZ	IZ	IZ

Table 3.1	log2 Fold Change - First round - CMP filtered		Significantly correlated layer			
Gene	hNP	hDN	15 pcw	16 pcw	21a pcw	21b pcw
TNFRSF19		0.85	VZ	VZ	SG	VZ
TNN	1.48		SG		SG	SG
TNR	-0.78	1.05			CPi	
TNS1	0.76					
TNS3	-0.61	-0.63	IZ	IZ		
TOP1MT		-0.58			SZo	
TPD52L1		1.59	SG	VZ	SG	
TPM1		-1.22			SG	SG
TPP1		-0.60	VZ	SZi	SZo	VZ
TPPP		-1.29	SP	CPi	CPi	CPi
TPPP3		0.86	SP		VZ	
TRAF3		0.48	CPi	MZ	MZ	MZ
TRAF4	-0.57		CPo	CPo		CPo
TRAF5		-0.79	VZ		CPi	CPi
TRAM2	-0.63	-0.70	VZ	VZ	VZ	SZo
TRIB1	0.79		SP	SP		
TRIL		0.76	SP	SP		
TRIM14	0.60					
TRIM22		-0.44	VZ	VZ		VZ
TRIM36	0.44		CPo	CPi		CPo
TRIM47		1.05	VZ	SZo	SZo	SZo
TRIM5		-0.38		VZ	VZ	VZ
TRIM56		-0.43	VZ	SZo	SZi	SZo
TRIM66		-0.55				
TRIP6		-0.57	VZ	VZ	VZ	SZo
TRPC3	1.03		VZ	VZ		IZ
TRPC6	-1.60				MZ	
TRPM1		1.13				
TRPM8	-1.06				MZ	
TRPS1		0.74	VZ	VZ	SZo	VZ
TSC22D3	-0.67		SP	CPi	SG	MZ
TSHZ1		0.41	VZ	VZ		VZ
TSHZ2		0.72	IZ			
TSKU		-0.51	CPi	CPi		
TSPAN12		0.93	VZ	VZ	VZ	VZ
TSPAN33		0.59	VZ	VZ	SG	VZ
TSPAN7	-0.92	0.61				
TTC29		0.83	VZ	VZ	VZ	
TTC39A	0.67		CPi			
TTC39C		-0.42	IZ	CPo	MZ	MZ

Table 3.1	log2 Fold Change - First round - CMP filtered		Significantly correlated layer			
Gene	hNP	hDN	15 pcw	16 pcw	21a pcw	21b pcw
TTLL4		0.65	VZ	VZ	SZo	SZo
TTYH2		-0.70	SZi	SZi	SZo	SZi
TUB		0.37	CPo	MZ	CPi	CPi
UAP1L1		-0.66	SG			IZ
UBALD2	-0.48					
UBE2E2		0.69	CPo	CPo	CPo	CPo
UHRF1		-0.54	VZ	VZ	SZo	SZo
ULBP3		-1.13				
UNC5B		-0.84				VZ
USP2	-0.60		CPi	SP		
USP51		0.73			CPi	SG
USP53	0.49			VZ	SZo	VZ
UTRN	0.32		SG	IZ		IZ
UXS1		-0.42	CPo			CPi
VAMP3		-0.36	VZ	VZ	VZ	SZo
VASH2	3.14		IZ	IZ	MZ	MZ
VASN		-0.75	SG	VZ	VZ	VZ
VAT1L	0.96	-1.03	VZ	VZ	SP	SP
VAV2		-0.52	VZ	VZ	MZ	
VAV3	0.48		SG	SZi	IZ	SZo
VCAM1	-0.46	0.78	VZ	VZ	VZ	VZ
VCL		-0.71	VZ	VZ	SZo	SZo
VDR		1.61				
VEGFA		-0.98	VZ	VZ	IZ	IZ
VEPH1		1.02	VZ	VZ	SZo	SZo
VIM		-0.57	VZ	VZ	SZo	SZo
VSTM2L		0.88	CPo	CPo	CPo	CPo
VSTM4		0.70				
VWC2L		0.94	SP		CPi	MZ
WASF3		0.43	SP	SP		
WBP2		0.42				
WBP5	0.71		VZ	VZ	SZi	VZ
WDR63		0.54				
WEE1		-0.60	VZ	VZ	SZo	SZi
WFDC1		-1.04	SP	SP		
WIPF3		1.07	VZ	SZi	MZ	SZi
WNT7B		1.77	SP	SP	SP	SP
WWC1	-0.52	-0.57		CPo		CPi
WWP1		0.62			CPi	CPi
WWTR1	0.37		SG	VZ	CPo	VZ

Table 3.1	log2 Fold Change - First round - CMP filtered		Significantly correlated layer			
Gene	hNP	hDN	15 pcw	16 pcw	21a pcw	21b pcw
XAF1	0.64		MZ	IZ		
XKR4		0.85	SP	SP	CPi	SP
ZAR1		-0.90	VZ			
ZBTB44		0.37		SP	CPo	IZ
ZCCHC12		0.69	CPi	CPi	SP	SP
ZDHHC13	0.92		VZ	VZ		
ZDHHC22		1.09			SP	SP
ZDHHC23		-0.44	CPo		CPi	CPi
ZFPM2		0.84	SP			
ZGRF1		-0.42				
ZMIZ1		0.45			SZo	SZi
ZMYND10		0.73	VZ			
ZNF106	-0.40					
ZNF385B	-1.07	-0.93	SP	CPi	CPi	CPi
ZNF385D		-0.49	IZ	MZ	IZ	
ZNF436	-0.46		CPo	CPo	CPi	CPo
ZNF483	0.87		VZ	VZ	SZo	VZ
ZNF488		1.24			CPo	CPo
ZNF503	-0.73		SG	MZ	CPi	CPi
ZNF521		0.96	VZ	VZ	SP	SP
ZNF550		0.52				
ZNF556		0.94	IZ	CPi	IZ	IZ
ZNF695	0.65		SZo			
ZNF70		0.45				
ZNF704	0.51		SZi	SZi	VZ	
ZNF727		-0.66	MZ	MZ	MZ	
ZNF804A		0.88			MZ	
ZNRF2	0.48				CPo	MZ
ZRANB3		-0.44	VZ	VZ		CPo

Table 3.2 *FOXP2 hDN repressed VZ genes in macaque and human at various developmental stages (Corresponds to figure 3.3)*

Table 3.2

FOXP2 hDN repressed	human VZ correlated	macaque VZ correlated			species specific or conserved
ADAM9	pcw16	E70	E80	E90	conserved
AHNAK	pcw16	E70	E80	E90	conserved
ALDH3A2	pcw16	E70	E80	E90	conserved
ANO6	pcw16	E70	E80	E90	conserved
CD164	pcw16	E70	E80	E90	conserved
CD63	pcw16	E70	E80	E90	conserved
CHST9	pcw16	E70	E80	E90	conserved
COL4A5	pcw16	E70	E80	E90	conserved
COL4A6	pcw16	E70	E80	E90	conserved
CREB3L2	pcw16	E70	E80	E90	conserved
DKK3	pcw16	E70	E80	E90	conserved
DNAJC1	pcw16	E70	E80	E90	conserved
E2F7	pcw16	E70	E80	E90	conserved
FGFR2	pcw16	E70	E80	E90	conserved
FILIP1	pcw16	E70	E80	E90	conserved
FLNA	pcw16	E70	E80	E90	conserved
FLNB	pcw16	E70	E80	E90	conserved
FSTL1	pcw16	E70	E80	E90	conserved
GATM	pcw16	E70	E80	E90	conserved
GPC4	pcw16	E70	E80	E90	conserved
HEG1	pcw16	E70	E80	E90	conserved
IQGAP1	pcw16	E70	E80	E90	conserved
ITGA2	pcw16	E70	E80	E90	conserved
LGALS3BP	pcw16	E70	E80	E90	conserved
MTTP	pcw16	E70	E80	E90	conserved
PARVA	pcw16	E70	E80	E90	conserved
PDIA4	pcw16	E70	E80	E90	conserved
RELL1	pcw16	E70	E80	E90	conserved
RNASE4	pcw16	E70	E80	E90	conserved
SHROOM3	pcw16	E70	E80	E90	conserved
SLC15A4	pcw16	E70	E80	E90	conserved
SPARC	pcw16	E70	E80	E90	conserved
SREBF1	pcw16	E70	E80	E90	conserved
STON1	pcw16	E70	E80	E90	conserved
TAGLN2	pcw16	E70	E80	E90	conserved
TMEM47	pcw16	E70	E80	E90	conserved
TNFRSF11B	pcw16	E70	E80	E90	conserved

Table 3.2

FOXP2 hDN repressed	human VZ correlated	macaque VZ correlated			species specific or conserved
TNFRSF12A	pcw16	E70	E80	E90	conserved
TPM1	pcw16	E70	E80	E90	conserved
VIM	pcw16	E70	E80	E90	conserved
ATP1A2	pcw16	E70	E80		conserved
CALD1	pcw16	E70	E80		conserved
CENPF	pcw16	E70	E80		conserved
EMP2	pcw16	E70	E80		conserved
EPHB3	pcw16	E70	E80		conserved
ITGB1	pcw16	E70	E80		conserved
MKI67	pcw16	E70	E80		conserved
SCPEP1	pcw16	E70	E80		conserved
SERPINH1	pcw16	E70	E80		conserved
SEPP1	pcw16	E70		E90	conserved
AIF1L	pcw16	E70			conserved
DTL	pcw16	E70			conserved
HTRA1	pcw16	E70			conserved
KIF20A	pcw16	E70			conserved
KIF23	pcw16	E70			conserved
LGALS3	pcw16	E70			conserved
LIMA1	pcw16	E70			conserved
MYO5C	pcw16	E70			conserved
NTNG1	pcw16	E70			conserved
POLQ	pcw16	E70			conserved
SDC2	pcw16	E70			conserved
SLC10A4	pcw16	E70			conserved
SMC5	pcw16	E70			conserved
APOBEC3C	pcw16		E80	E90	conserved
FOXO1	pcw16		E80	E90	conserved
SOX9	pcw16		E80		conserved
PLEKHG4B	pcw16			E90	conserved
AMOTL2	pcw16				human specific
BRIP1	pcw16				human specific
C1R	pcw16				human specific
C3orf52	pcw16				human specific
CASP6	pcw16				human specific
CCNE2	pcw16				human specific
CD47	pcw16				human specific
CDK6	pcw16				human specific
CDO1	pcw16				human specific
COL1A2	pcw16				human specific

Table 3.2

FOXP2 hDN repressed	human VZ correlated	macaque VZ correlated	species specific or conserved
ESCO2	pcw16		human specific
FAM111B	pcw16		human specific
FAT1	pcw16		human specific
FGFBP3	pcw16		human specific
FZD5	pcw16		human specific
GNG11	pcw16		human specific
HLA-DPA1	pcw16		human specific
HMMR	pcw16		human specific
IFIT2	pcw16		human specific
ITGA7	pcw16		human specific
KIF15	pcw16		human specific
MFAP4	pcw16		human specific
NUSAP1	pcw16		human specific
P4HB	pcw16		human specific
PAQR8	pcw16		human specific
PBK	pcw16		human specific
PGRMC2	pcw16		human specific
PLEKHA4	pcw16		human specific
PLEKHA7	pcw16		human specific
PRDX6	pcw16		human specific
QTRTD1	pcw16		human specific
RRM2	pcw16		human specific
SLC47A1	pcw16		human specific
SOX21	pcw16		human specific
SUMF1	pcw16		human specific
TFPI2	pcw16		human specific
TLR3	pcw16		human specific
TMTC2	pcw16		human specific
TRAM2	pcw16		human specific
TRIM22	pcw16		human specific
VCL	pcw16		human specific
VEGFA	pcw16		human specific
ADAMTS6		pcw21	human specific
BAIAP3		pcw21	human specific
BMP4		pcw21	human specific
C10orf105		pcw21	human specific
C1orf226		pcw21	human specific
C5		pcw21	human specific
CAMTA1		pcw21	human specific
CASP1		pcw21	human specific

Table 3.2

FOXP2 hDN repressed	human VZ correlated	macaque VZ correlated			species specific or conserved
CD38	pcw21				human specific
CLGN	pcw21				human specific
DNAH9	pcw21				human specific
DSC3	pcw21				human specific
ERBB2	pcw21				human specific
FAM198B	pcw21				human specific
GAD2	pcw21				human specific
GLI3	pcw21				human specific
HSPB8	pcw21				human specific
IDH2	pcw21				human specific
ITGA6	pcw21				human specific
KCNQ4	pcw21				human specific
NDRG2	pcw21				human specific
NNMT	pcw21				human specific
SFRP2	pcw21				human specific
SLC44A3	pcw21				human specific
SUSD1	pcw21				human specific
SYNPO	pcw21				human specific
VCAM1	pcw21				human specific
AKAP12		E70	E80	E90	macaque specific
ARHGAP29		E70	E80	E90	macaque specific
ARL4A		E70	E80	E90	macaque specific
C1QL1		E70	E80	E90	macaque specific
CD151		E70	E80	E90	macaque specific
COBLL1		E70	E80	E90	macaque specific
COL5A2		E70	E80	E90	macaque specific
CRISPLD1		E70	E80	E90	macaque specific
DCDC2		E70	E80	E90	macaque specific
DLGAP5		E70	E80	E90	macaque specific
EFNB2		E70	E80	E90	macaque specific
ENO1		E70	E80	E90	macaque specific
FGFR1		E70	E80	E90	macaque specific
FNDC1		E70	E80	E90	macaque specific
FNDC3B		E70	E80	E90	macaque specific
GNS		E70	E80	E90	macaque specific
GPC1		E70	E80	E90	macaque specific
ICMT		E70	E80	E90	macaque specific
IFITM3		E70	E80	E90	macaque specific
ITGB5		E70	E80	E90	macaque specific
KCTD21		E70	E80	E90	macaque specific

Table 3.2

FOXP2 hDN repressed	human VZ correlated	macaque VZ correlated			species specific or conserved
KIAA0355		E70	E80	E90	macaque specific
LEFTY2		E70	E80	E90	macaque specific
LTBP2		E70	E80	E90	macaque specific
MATN2		E70	E80	E90	macaque specific
MMP15		E70	E80	E90	macaque specific
PDK3		E70	E80	E90	macaque specific
PDLIM4		E70	E80	E90	macaque specific
PI15		E70	E80	E90	macaque specific
PLEKHG3		E70	E80	E90	macaque specific
RASSF8		E70	E80	E90	macaque specific
SLC15A2		E70	E80	E90	macaque specific
SYNM		E70	E80	E90	macaque specific
TGFB2		E70	E80	E90	macaque specific
TPBG		E70	E80	E90	macaque specific
VASN		E70	E80	E90	macaque specific
WEE1		E70	E80	E90	macaque specific
ASPH		E70	E80		macaque specific
CALU		E70	E80		macaque specific
CAMK2D		E70	E80		macaque specific
CHODL		E70	E80		macaque specific
CRTAP		E70	E80		macaque specific
FBN1		E70	E80		macaque specific
FHOD3		E70	E80		macaque specific
HIST1H2AC		E70	E80		macaque specific
IGFBP2		E70	E80		macaque specific
IGFBP7		E70	E80		macaque specific
MFSD1		E70	E80		macaque specific
MGST1		E70	E80		macaque specific
NFE2L1		E70	E80		macaque specific
PDIA3		E70	E80		macaque specific
PLOD1		E70	E80		macaque specific
RAI14		E70	E80		macaque specific
RPN2		E70	E80		macaque specific
SCD		E70	E80		macaque specific
SEMA5A		E70	E80		macaque specific
SORT1		E70	E80		macaque specific
ANGPTL1		E70		E90	macaque specific
MID1		E70		E90	macaque specific
NAALADL2		E70		E90	macaque specific
SYT14		E70		E90	macaque specific

Table 3.2

FOXP2 hDN repressed	human VZ correlated	macaque VZ correlated		species specific or conserved
DIAPH3		E70		macaque specific
DSTN		E70		macaque specific
ENPP2		E70		macaque specific
FAM107A		E70		macaque specific
HOPX		E70		macaque specific
ID1		E70		macaque specific
IGF2R		E70		macaque specific
IGFBP5		E70		macaque specific
KLF5		E70		macaque specific
LMO2		E70		macaque specific
MELK		E70		macaque specific
MERTK		E70		macaque specific
MYBL1		E70		macaque specific
MYH9		E70		macaque specific
NCAPG		E70		macaque specific
PIK3C2A		E70		macaque specific
PNOC		E70		macaque specific
PPIF		E70		macaque specific
PRMT6		E70		macaque specific
RAB3GAP2		E70		macaque specific
RAVER2		E70		macaque specific
RBBP8		E70		macaque specific
SDK1		E70		macaque specific
SFRP4		E70		macaque specific
SMAD3		E70		macaque specific
TRAF5		E70		macaque specific
ANXA1		E80	E90	macaque specific
BMP6		E80	E90	macaque specific
KCNJ13		E80	E90	macaque specific
LMOD1		E80	E90	macaque specific
SNTB1		E80	E90	macaque specific
CTSD		E80		macaque specific
PLD5		E80		macaque specific
SEMA3B		E80		macaque specific
TIMP2		E80		macaque specific
ABCA8			E90	macaque specific
AKAP14			E90	macaque specific
ALDH3B1			E90	macaque specific
C10orf54			E90	macaque specific
JUN			E90	macaque specific

Table 3.2

FOXP2 hDN repressed	human VZ correlated	macaque VZ correlated	species specific or conserved
MYH14		E90	macaque specific
PTRF		E90	macaque specific
SLC47A2		E90	macaque specific

Table 3.3 *FOXP2 hDN activated SP genes in macaque and human at various developmental stages (corresponds to figure 3.3)*

Table 3.3

FOXP2 hDN activated	human SP correlated			macaque SP correlated		species specific or conserved
LRRTM2		pcw21	E70	E80	E90	conserved
KCNK2		pcw21	E70			conserved
NOS1AP		pcw21	E70			conserved
TMEM63C		pcw21	E70			conserved
PPM1L		pcw21		E80	E90	conserved
DPP10	pcw16		E70	E80	E90	conserved
DSCAM	pcw16		E70	E80	E90	conserved
ADCY1	pcw16		E70			conserved
ANKS1B	pcw16		E70			conserved
PALM2	pcw16		E70			conserved
PPP2R2C	pcw16		E70			conserved
SPOCK1	pcw16		E70			conserved
ITGA9	pcw16			E80	E90	conserved
KCNB2	pcw16	pcw21	E70		E90	conserved
GPR37	pcw16	pcw21	E70			conserved
NGB	pcw16	pcw21	E70			conserved
NRSN1	pcw16	pcw21	E70			conserved
WNT7B	pcw16	pcw21	E70			conserved
CAMK4		pcw21				human specific
CHL1		pcw21				human specific
CXADR		pcw21				human specific
DGKG		pcw21				human specific
FRAS1		pcw21				human specific
GSG1L		pcw21				human specific
HRK		pcw21				human specific
KCNB1		pcw21				human specific
KLHL32		pcw21				human specific
LRRTM3		pcw21				human specific
NT5E		pcw21				human specific
PAPPA2		pcw21				human specific
PHACTR3		pcw21				human specific
PPP1R1A		pcw21				human specific
PRKAR2B		pcw21				human specific
SLC6A11		pcw21				human specific
SYN2		pcw21				human specific
TRIL		pcw21				human specific
ARHGAP26	pcw16					human specific
CPNE5	pcw16					human specific
CRABP1	pcw16					human specific
CSGALNACT1	pcw16					human specific
CSMD1	pcw16					human specific
DGKH	pcw16					human specific
DRD1	pcw16					human specific
EHD3	pcw16					human specific
FAM181B	pcw16					human specific

Table 3.3

FOXP2 hDN activated	human SP correlated		macaque SP correlated			species specific or conserved
FAM196A	pcw16					human specific
FMN2	pcw16					human specific
FUT9	pcw16					human specific
GPRIN3	pcw16					human specific
IGSF10	pcw16					human specific
IGSF3	pcw16					human specific
KCNJ6	pcw16					human specific
MEGF11	pcw16					human specific
NDP	pcw16					human specific
NRIP1	pcw16					human specific
NTRK2	pcw16					human specific
PHYHIPL	pcw16					human specific
PPARG	pcw16					human specific
PRKCE	pcw16					human specific
RERG	pcw16					human specific
SEZ6	pcw16					human specific
SLC44A3	pcw16					human specific
WASF3	pcw16					human specific
FREM1	pcw16	pcw21				human specific
GPD1L	pcw16	pcw21				human specific
LMO3	pcw16	pcw21				human specific
PLEKHA5	pcw16	pcw21				human specific
RAPGEF5	pcw16	pcw21				human specific
SLC4A10	pcw16	pcw21				human specific
AMPH			E70	E80	E90	macaque specific
LRRC55			E70	E80	E90	macaque specific
RNF150			E70	E80	E90	macaque specific
DIRAS2			E70	E80		macaque specific
NRXN2			E70	E80		macaque specific
PLXNA2			E70	E80		macaque specific
ZNF550			E70		E90	macaque specific
AKAP7			E70			macaque specific
CDC42EP2			E70			macaque specific
ENOX1			E70			macaque specific
FAT2			E70			macaque specific
HMP19			E70			macaque specific
KIF5A			E70			macaque specific
L1CAM			E70			macaque specific
NEGR1			E70			macaque specific
PPP1R1B			E70			macaque specific
PRLR			E70			macaque specific
RNF187			E70			macaque specific
SNX29			E70			macaque specific
XKR4			E70			macaque specific
ZMIZ1			E70			macaque specific
PPARGC1A				E80	E90	macaque specific
CAMTA1				E80		macaque specific
CASP7				E80		macaque specific
CLDN1				E80		macaque specific
FAM101A				E80		macaque specific
GABRA3				E80		macaque specific
QPCT				E80		macaque specific
GRIA3					E90	macaque specific
NRG4					E90	macaque specific
RASGRP1					E90	macaque specific
SHISA6					E90	macaque specific

Table 3.4 *FOXP2 hDN activated genes differentially expressed between the subplate and cortical plate across species (Corresponds to figure 3.4)*

Table 3.4

Gene	human SPvCP log2 FC	human layer	macaque SPvCP log2 FC	macaque layer	mouse SPvCP log2 FC	mouse layer	hDN FOXP2 log2 FC
ABCA5			-0.51	CP			0.56
ABR			-0.28	CP			0.44
ADAMTS 6	2.49	SP					1.48
ADAMTS 8	-0.50	CP					1.72
ADAMTS L1	1.31	SP			-0.259	CP	1.86
ADD2	-0.71	CP	-0.39	CP			0.51
AFF2	-1.03	CP	-0.15	CP	0.246	SP	0.37
AMPH	0.60	SP					0.56
ANGPT1					0.441	SP	1.91
ANKRD44			-0.41	CP			1.06
APBA1					-0.266	CP	0.57
APBA2	-0.31	CP					0.58
AQP1			-0.63	CP			2.09
ARHGAP 26			-0.74	CP	0.615	SP	0.52
ARPP21			-0.56	CP	-0.506	CP	1.49
ASXL3	-0.28	CP					0.57
ATP2B1	-0.85	CP					0.65
B4GALT5	-0.47	CP					0.59
BCHE	1.15	SP					1.37
BCL11B					-0.314	CP	0.63
BMP4					-0.236	CP	1.07
C5	0.96	SP					0.52
CA12	1.24	SP	0.53	SP			0.57
CAMK4					-0.437	CP	0.54
CAMKV			-0.85	CP	-0.294	CP	2.34
CASP7	2.17	SP					0.85
CCND2	0.55	SP	0.51	SP	0.880	SP	0.66
CCNG1					-0.192	CP	0.50
CDC42EP 2	-0.53	CP					2.12
CDH18	4.59	SP	0.69	SP	0.766	SP	1.89
CDON					0.589	SP	0.52
CLDN1			0.36	SP			0.84
CNKSR2			-0.62	CP			0.48
CNR1	-0.69	CP					1.90
CNRIP1			-0.27	CP			0.52
COL12A1	1.99	SP			-0.127	CP	3.01
COL2A1			0.21	SP			3.33
CPNE5	1.48	SP			-0.225	CP	1.18
CPVL	2.00	SP	-0.12	CP			0.50
CRABP1	2.10	SP					1.85
CSRNP3	-0.76	CP					0.44
CTNNA2			-0.73	CP			1.39
DAB1					-0.253	CP	1.96
DACT1					0.541	SP	0.72
DDIT4L					0.421	SP	1.13
DGKG	2.12	SP					1.97
DIO2	1.69	SP	0.43	SP			2.20
DOCK10	1.62	SP	0.58	SP			0.63
DPP10	1.88	SP	0.96	SP			0.51
DPYSL3	-0.60	CP	-0.38	CP	-0.218	CP	0.49
DTX4	-0.55	CP					1.01
ECEL1			0.15	SP			3.34

Table 3.4

Gene	human SPvCP log2 FC	human layer	macaque SPvCP log2 FC	macaque layer	mouse SPvCP log2 FC	mouse layer	hDN FOXP2 log2 FC
ELAVL2					0.192	SP	0.44
ELAVL4	-0.61	CP					0.98
ELMO1	-1.75	CP			-0.366	CP	0.71
ENOX1	-0.35	CP					0.68
EPB41L4B					0.264	SP	1.33
EPHA3			0.37	SP	1.009	SP	1.10
EPHA4					-0.443	CP	0.93
EPHA5	0.93	SP					1.13
ESR1	0.94	SP					2.93
FAM167A	1.29	SP					1.33
FAM181B	1.56	SP			0.376	SP	0.71
FAM196A					-0.541	CP	1.18
FAM84A	-2.08	CP			0.879	SP	0.72
FAS	3.50	SP					0.41
FAT4			-0.61	CP	-0.345	CP	0.56
FBLN1					-0.456	CP	1.21
FGF13	-0.42	CP	-0.50	CP			0.49
FLRT1	-0.84	CP					0.84
FLRT2	-1.65	CP	-0.74	CP			2.03
FOXP2					-0.788	CP	7.33
FRAS1	1.06	SP	0.29	SP			0.80
FUT9	1.29	SP					1.03
GAD2	0.45	SP			0.371	SP	0.97
GAP43	-0.48	CP	-0.32	CP	-0.274	CP	0.76
GHR					0.318	SP	1.72
GLRB			-0.59	CP			0.53
GPM6A			-0.37	CP			0.52
GPR37	1.66	SP					1.28
GRIA3			-0.59	CP	-0.496	CP	0.42
GRID2	1.28	SP					2.35
GSG1L	2.63	SP					2.58
HAS3	4.68	SP	0.89	SP			1.39
HEPH	2.37	SP					1.67
HEY1	0.79	SP					1.13
HIBADH					0.234	SP	0.53
HLF	-1.63	CP			-0.196	CP	2.38
HMGCR	-0.75	CP					0.42
HRK	0.88	SP					0.94
HSD11B1	-1.08	CP					1.29
ICA1L	-0.67	CP					0.42
IDH2	-0.44	CP					0.41
IGDCC4	0.52	SP					0.48
INHBA	-5.44	CP	-2.95	CP			1.40
ITGA6	1.60	SP	0.36	SP	0.353	SP	0.42
ITGA9	1.48	SP	0.40	SP			2.15
ITIH5	0.75	SP					0.53
IVNS1ABP	0.63	SP					0.37
KCNB1	0.75	SP					1.52
KCND2	-1.00	CP					1.07
KCNJ6	0.60	SP	0.72	SP			1.07
KCNK2					0.496	SP	0.64
KLHL13					0.467	SP	0.48
KLHL14	-1.33	CP	-1.43	CP	-0.333	CP	1.53
L1CAM					-0.241	CP	0.72
L3MBTL3	-1.97	CP					0.51
LIMCH1	-1.03	CP	-0.51	CP			0.45
LMO3	1.39	SP					0.57
LMO4	-1.46	CP	-0.66	CP			0.40
LRRC4C			-0.48	CP			1.01
LRRTM2			0.58	SP			0.61

Table 3.4

Gene	human SPvCP log2 FC	human layer	macaque SPvCP log2 FC	macaque layer	mouse SPvCP log2 FC	mouse layer	hDN FOXP2 log2 FC
LSAMP	-1.23	CP					0.95
MACROD2	-1.70	CP					0.98
MAP3K1			0.93	SP	0.452	SP	0.91
MAPK8IP1	-0.40	CP					0.51
MARCKS	-0.26	CP					0.35
MASP1	-1.14	CP					1.11
MEF2C	-1.04	CP	-0.84	CP	-0.238	CP	0.52
MEGF11			0.62	SP			0.85
MEIS1			0.43	SP			0.62
MFSD2A	0.72	SP	0.23	SP	0.553	SP	0.60
MN1	-0.58	CP			0.244	SP	0.40
MPPED2	0.76	SP					0.39
MRAS	-0.28	CP					0.43
MT1E			0.81	SP			2.08
MT1X	0.61	SP					0.87
MT2A	1.34	SP					1.60
MXI1	0.21	SP			0.371	SP	0.72
MYO16			-1.40	CP	-0.334	CP	2.28
NCALD	-0.71	CP			-0.225	CP	0.81
NCAM1					-0.161	CP	0.47
NELL2			-0.50	CP			2.87
NFIX					-0.157	CP	0.40
NGB	1.83	SP					4.77
NKAIN4	1.13	SP	0.45	SP	0.241	SP	1.20
NMB	-0.06	CP					2.17
NR2F1	-0.46	CP	-0.41	CP			0.53
NR3C1					0.378	SP	0.37
NRP1					0.755	SP	0.53
NRSN1	1.04	SP					1.64
NT5E	1.32	SP	0.14	SP			0.41
NTRK2					-0.360	CP	1.30
OLFML2B	1.71	SP					1.63
OLIG1	2.34	SP	1.38	SP	0.651	SP	1.21
PALMD	1.15	SP	0.49	SP	0.801	SP	1.20
PAPPA	1.15	SP					5.43
PAPPA2	3.03	SP	0.28	SP	0.362	SP	2.51
PCDH18	1.13	SP	0.51	SP	0.596	SP	1.13
PCDH8					0.493	SP	2.42
PDE7B	2.07	SP	0.44	SP			1.74
PDE8A			0.34	SP			0.85
PHACTR2			0.40	SP	0.258	SP	0.55
PHACTR3			-0.35	CP			0.80
PHF12	0.57	SP					0.39
PHLDB2			0.17	SP	0.360	SP	0.69
PHYHIPL	0.95	SP					0.36
PKIA	-0.70	CP	-0.42	CP			0.47
PLEKHA5	1.34	SP	1.30	SP			0.58
PLEKHA6	-0.82	CP					1.24
PLSCR4	1.90	SP					0.68
PLXNA2	1.70	SP	0.86	SP			0.89
PLXNA4	-1.05	CP	-0.43	CP	0.411	SP	0.68
POU3F4	-1.28	CP			0.471	SP	0.48
PPARGC1A			0.43	SP			2.27
PPM1L	1.41	SP			-0.209	CP	0.57
PPP1R1B	2.04	SP	0.36	SP	-0.347	CP	1.43
PRKAR2B					-0.369	CP	0.52
PRLR			0.26	SP			1.95
PRR18	0.98	SP					0.83
PTBP2					-0.151	CP	0.42

Table 3.4

Gene	human SPvCP log2 FC	human layer	macaque SPvCP log2 FC	macaque layer	mouse SPvCP log2 FC	mouse layer	hDN FOXP2 log2 FC
PTN	0.99	SP	1.00	SP	0.336	SP	1.40
PTPRD	-0.73	CP			-0.358	CP	0.95
RAB3C			-0.37	CP			0.71
RAPGEF5	0.78	SP					0.66
RARB	-3.08	CP					1.64
RASGRF1	2.62	SP			-0.523	CP	3.88
RCAN2	-1.24	CP			0.776	SP	0.99
RERG	2.43	SP			-0.221	CP	2.85
RGMA	1.21	SP	0.29	SP	-0.409	CP	0.88
RGMB	-0.85	CP					0.37
RIMKLA	-0.54	CP					0.41
RIMS3	-0.75	CP					1.06
RNF150			0.37	SP			0.50
RUNX1T1	-1.13	CP	-0.53	CP			0.89
RYR2			-1.06	CP			1.14
S100A16	1.01	SP			0.576	SP	0.98
S1PR3			0.33	SP	0.641	SP	0.64
SAMD5	-1.30	CP					0.40
SASH1					0.449	SP	0.57
SATB1					-0.264	CP	0.47
SCN3B					-0.210	CP	0.80
SCN7A	-0.48	CP					2.44
SCN9A	-0.72	CP	-0.23	CP			0.90
SEL1L3	1.72	SP					0.56
SESN3	0.64	SP					0.36
SEZ6	0.93	SP					1.79
SFRP1			0.67	SP			0.58
SGK1	-0.32	CP					1.59
SHISA6			0.77	SP			1.87
SLA			-0.41	CP	-0.408	CP	3.66
SLC1A2	1.07	SP	0.93	SP	0.589	SP	0.92
SLC1A3	1.21	SP	0.53	SP			0.36
SLC24A3	-2.20	CP	-1.65	CP			0.63
SLC35F4	1.41	SP					1.99
SLC44A3	2.49	SP					0.80
SLC4A10	1.44	SP					1.59
SLC4A4					0.397	SP	0.55
SLC6A11	1.04	SP					0.41
SLC8A1	-1.36	CP			0.345	SP	0.73
SLC9A9	1.03	SP					0.85
SLITRK5	-0.26	CP	-0.39	CP			0.53
SNX29	0.29	SP	0.16	SP			0.55
SOCS2	1.43	SP					0.62
SPOCK1					-0.432	CP	0.80
SRI	-0.69	CP					0.37
SSTR2					0.368	SP	0.94
ST6GAL1	-0.36	CP					0.86
ST6GALNAC3			-0.68	CP			0.47
ST8SIA2					-0.298	CP	0.52
ST8SIA4					0.294	SP	0.43
STK32B			0.59	SP	-0.125	CP	1.37
STMN2	-0.32	CP	-0.38	CP			0.50
STMN4	-0.65	CP	-0.59	CP			0.61
STOM			0.28	SP			0.63
SULF1			-0.81	CP			1.10
SULF2	1.48	SP	0.40	SP	0.524	SP	1.45
SUSD1	0.40	SP					0.62
SVIL	0.77	SP	0.50	SP	0.577	SP	0.44
SYNPO					-0.312	CP	0.93
TGM2	1.70	SP					5.27

Table 3.4

Gene	human SPvCP log2 FC	human layer	macaque SPvCP log2 FC	macaque layer	mouse SPvCP log2 FC	mouse layer	hDN FOXP2 log2 FC
TLE1			0.41	SP	0.820	SP	0.83
TLE4	2.23	SP	0.32	SP			0.84
TMEM106C	-0.66	CP					0.73
TMEM132E					0.284	SP	0.51
TMEM200A	-3.66	CP					1.42
TNFRSF19			0.23	SP			0.96
TRAF3			0.28	SP			0.49
TRIL	3.15	SP	0.84	SP			0.87
TRPS1	1.13	SP			1.063	SP	0.76
TSPAN12					0.364	SP	1.05
UBE2E2	-0.84	CP	-0.37	CP			0.76
UBE2QL1			-0.58	CP	0.171	SP	0.56
VCAM1			0.49	SP			0.94
WASF3	0.42	SP					0.45
WNT7B	4.34	SP					3.03
ZMIZ1	0.37	SP					0.47

CHAPTER FOUR: Separable mechanisms for activation and repression of FOXP2 target genes

Summary

FOXP2 is the only gene to be implicated in a heritable form of verbal dyspraxia (Fisher et al., 1998). Because the encoded transcription factor is expressed in the brain during development (Lai et al., 2003), its role in speech and language has been of particular interest. By analyzing FOXP2 whole-genome binding and gene regulation in human neural progenitors (hNPs), we have found evidence that FOXP2 increases chromatin accessibility globally. While it is known that FOXP2 can act as both an activator and a repressor (Spiteri et al., 2007, Vernes et al., 2011, Vernes et al., 2007, Konopka et al., 2009), functional studies have only focused on the repressive action of FOXP2 (Shu et al., 2001, Li et al., 2004, Zhou et al., 2008) and the question of how FOXP2 activates gene expression is still unanswered. In this study we use RNA- and ChIP-seq in human neural progenitor cells to show that FOXP2 down-regulates the expression of genes encoding transcriptional repressors or co-repressors. Activated targets, however, are enriched for neuronal differentiation genes. Moreover, we use an assay for transpose assessable chromatin followed by sequencing (ATAC-seq) (Buenrostro et al., 2015a) to show that FOXP2 turns off cellular programs that maintain an undifferentiated state by closing chromatin in a DNA-dependent manner while opening chromatin to turn on programs that drive a cell towards a neuronal fate in a DNA-binding independent manner. Additionally, this DNA-binding independent chromatin opening may be mediated through interactions with NFI transcription factors.

Thus we have identified a novel mechanism by which FOXP2 activates gene expression and promotes neuron maturation.

Introduction

The forkhead box, or FOX, family of transcription factors is comprised of thirteen subfamilies related by a conserved winged helix DNA binding domain. FOX proteins have been shown to regulate transcription both positively and negatively, and are involved in processes such as embryonic development, organogenesis, and immunoregulation (Wijchers et al., 2006a). While some FOX proteins act as canonical transcription factors, directing regulatory protein complexes to specific target sequences within already accessible chromatin, others, such as FOXA1 in liver precursor cells (Cirillo et al., 2002), have been shown to act as pioneer factors. Pioneer factors are transcription factors that access target sequences on compacted chromatin and nucleosomes without the help of large transcription factor complexes. Additionally, pioneer factors are the first proteins to bind cell-fate-specific regulatory regions during development (Zaret and Carroll, 2011). Thus, pioneer factors have the ability to independently destabilize nucleosomes giving other regulatory complexes access to specific target sequences. The forkhead domain structurally resembles linker histone H1, which condenses chromatin and represses gene activity (Cirillo et al., 1998). FOXA1 likely activates genes by binding chromatin directly, replacing H1, and de-compacting chromatin (Cirillo et al., 1998).

FOXP2 is among the few genes implicated in heritable forms of verbal dyspraxia (Fisher et al., 1998). Because FOXP2 is expressed in the brain during development (Lai et al., 2003), its role in regulating developmental pathways that might be important for

speech and language has been of particular interest. Mice with mutated *Foxp2* lack neonatal ultrasonic vocalizations and exhibit severe motor impairments, reduced cerebellar size, and impaired neurite outgrowth (Shu et al., 2005, Groszer et al., 2008, Fujita et al., 2008, French et al., 2007). Indeed, genome-wide FoxP2 binding and expression microarray studies in mouse and human cells imply that FoxP2 regulates genes involved in neuron outgrowth and other neuronal functions (Vernes et al., 2007, Vernes et al., 2011, Spiteri et al., 2007), but the mechanism by which FoxP2 does so remains unclear.

While the above gene expression studies suggest that FoxP2 acts to repress and activate gene expression, only the repressive actions of this protein have been studied functionally. For example, FOXP1/2/4 have been shown to interact with the repressive NuRD/MeCP1 chromatin-remodeling complex, suggesting that FOXP2 may repress target genes by recruiting histone deacetylases (Chokas et al., 2010). Additionally FOXP2 has been shown to heterodimerize with homologs FOXP1 and FOXP4 and physically interact with CtBP1 to synergistically repress gene expression (Li et al., 2004). Moreover, the ability to homo- or heterodimerize, a trait specific to the FOXP family of forkhead transcription factors, seems to be necessary to facility gene repression (Li et al., 2004), even though FOXP2 can bind DNA as a monomer (Stroud et al., 2006). While these specific examples are helpful for understanding the regulatory function of FOXP2, they are unlikely to be the only mechanisms underlying the ability of FOXP2 to specify discrete neuron populations necessary for proper language development, and they do not explain the ability of FOXP2 to regulate gene activation.

FOXP2 could activate gene expression via several mechanisms. For example, it could activate targets indirectly by down-regulating the expression of transcriptional repressors (Figure 4.1A). Additionally, FOXP2, like FOXA1 could act as a pioneer factor by binding DNA as a monomer and independently de-compacting chromatin (Figure 4.1B). It could also be recruited to already open chromatin on its own, or through interaction with a cofactor, which may, or may not, also act as a pioneer factor (Figure 4.1C). Using genome-wide DNA-binding and transcriptome-wide expression analysis we found that FOXP2, indeed, down-regulates a network of transcriptional repressors in human neural progenitor cells. Additionally, using chromatin accessibility assays we determined that FOXP2 binds DNA directly to condense chromatin and repress genes involved in maintaining a germinal state while opening chromatin in conjunction with co-activating NFI transcription factors to activate genes that promote neuronal maturation.

Results

FOXP2 directly down-regulates transcriptional repressors in hNPs

While gene promoter regions occupied by FOXP2 have been identified in human fetal brain and in a human neuroblastoma cell line (Spiteri et al., 2007, Vernes et al., 2007), regions of chromatin bound by FOXP2 across the genome have not been assayed in normal human neuronal cells. Moreover, while direct and indirect targets of FOXP2 could be identified by integrating genome-wide occupancy data with transcriptome-wide gene expression changes mediated by FOXP2, such experiments have yet to be performed in tandem on a human genomic background. In an attempt to identify direct and indirect targets of FOXP2 in a system that better approximates normal neural progenitors we performed ChIP-seq and RNA-seq in human neural

progenitor cells (hNPs) derived from normal human fetal forebrain (Svendsen et al., 1998, Palmer et al., 2001). Importantly, this system is an extensively characterized model of human neuronal development (Konopka et al., 2012b, Wexler et al., 2011, Rosen et al., 2011, Palmer et al., 2001, Stein et al., 2014). For example when the hNPs are differentiated into human developing neurons (hDNs) they have been shown to better recapitulate cortical development than neurons derived from both induced pluripotent stem cells and embryonic stem cells (Stein et al., 2014). Additionally, these cells are genetically tractable, and because they do not express *FOXP2* endogenously we induced expression of FOXP2 or a control GFP construct via lentiviral transduction and compared these two conditions.

ChIP-seq was performed in one line of hNPs under *FOXP2* expressing and control conditions. FOXP2 bound regions significantly enriched for immunoprecipitated and sequenced DNA fragments over input compared to control and were annotated to potentially regulated genes using the GREAT algorithm (McLean et al., 2010). RNA-seq was performed in the same hNP line as the ChIP experiment as well as in one additional line (Table 6.1). Four replicates per condition per line were used to identify differentially expressed (DE) genes. By overlapping DE genes identified in both cell lines with genes annotated to regions of the genome bound by FOXP2, we identified 258 direct FOXP2 targets (Figure 4.21A; Table 4.1). Repressed direct targets were enriched for genes involved in negative regulation of transcription, while activated direct targets were enriched for neuronal differentiation genes as described previously (Spiteri et al., 2007, Vernes et al., 2007) (Figure 4.2B).

Weighted gene co-expression network analyses (WGCNA) of the RNA-seq data from both hNP lines identified a co-expression module negatively correlated with samples expressing *FOXP2* (Figure 4.3A). This module is enriched for genes repressed by FOXP2 and the module's hub genes include known FOXP2 binding partner *NFATC3* as well as direct targets *RYBP* and *GADD45A* (Figure 4.3B; Table 4.1). These and other direct targets in the module were confirmed as repressed FOXP2 targets in a third hNP line (Figure 4.3C; table 6.1), confirming the robustness of our assays. Moreover, this module is enriched for gene ontology terms such as "chromatin", "repressor", and "regulation of transcription", suggesting that FOXP2 regulates a network of genes involved in epigenetic control in hNPs (Figure 4.4A). Remarkably, the nuclei of hNPs expressing FOXP2 have increased levels of H3K27 acetylation, a marker of active promoter and enhancer regions, compared with FOXP2 null nuclei (Figure 4.4B). These data imply that by down-regulating transcriptional repressors, FOXP2 has a large effect on transcriptional activation at the chromatin level. Taken together, these data suggest that in proliferating hNPs, FOXP2 can activate genes indirectly by repressing repressors (Figure 4.1A).

FOXP2 opens chromatin at NFI motifs specifically in hDNs

In the human cortex, *FOXP2* is expressed in intermediate progenitor cells and in layer VI neurons (Nowakowski et al., 2017). In conjunction with our data, this expression pattern suggests that progenitors expressing *FOXP2* mature into *FOXP2* expressing layer VI neurons. In order to better understand how FOXP2 activates genes during the course of neuronal development, and to ascertain whether FOXP2 acts as a pioneer factor in this context, we performed RNA-seq and ATAC-seq in both proliferating hNPs

and in progenitors cells that were differentiated into neurons (human differentiated neurons, hDNs) with or without exogenous *FOXP2* expression (Figure 4.5A). Tens of thousands of open chromatin regions (OCRs) were detected in each condition (Figure 4.5B), and while thousands of those were more open in hNPs than hDNs or vice versa (Figure 4.5C), few regions were differentially accessible when hDN and hNP samples were combined and FOXP2 and CTRL conditions were compared (Figure 4.5D). This suggests that our differentiation protocol causes gross changes in chromatin structure while expression of *FOXP2* may only alter chromatin structure in a manner that is dependent on the state of maturation.

In order to determine the effect of FOXP2 on the chromatin landscape in a condition specific manner, we identified regions of chromatin that are open in an individual condition (hNP CTRL, hNP FOXP2, hDN CTRL, hDN FOXP2) but closed in the other three conditions. We called these areas condition specific differentially accessible regions (DARs) (Figure 4.6A). Surprisingly, only two DARs were present in CTRL hDNs only (Figure 4.6A), suggesting either that FOXP2 closes most regions of chromatin that it is capable of closing in hNPs before differentiation, or that there is some technical reason for the inability to detect regions closed during differentiation. Importantly, there are regions of chromatin opened in hDNs only when *FOXP2* is expressed during differentiation (Figure 4.6A), supporting the possibility that FOXP2 can act as a pioneer factor. Compared to all open chromatin regions, fewer DARs are annotated as being in transcription start sites (TSS) (Figure 4.6B). However, areas of differentially open chromatin in CTRL hNPs (closed when FOXP2 is expressed) are closer to transcription start sites than areas differentially open in hNPs or hDNs

expressing FOXP2 (Figure 4.6C). This suggests that FOXP2 may open chromatin at distal enhancers, which have been shown to be important for cell identity (Neph et al., 2012, Thurman et al., 2012), and close chromatin at regions distal and proximal to TSS.

Accessible sites closed by FOXP2 in hNPs are enriched for forkhead motifs, pointing toward direct repression of genes near these regions (Figure 4.7A). FOXP2 opens sites that are enriched for activator protein 1 (AP1) motifs in hNPs (Figure 4.7A). AP1 is a transcription factor complex composed of various Jun, Fos and ATF protein dimers that is implicated in the proliferation and differentiation of various cell types (Hess et al., 2004). Moreover, JUN is most highly expressed in FOXP2 hNPs and is significantly repressed by FOXP2 in hDNs (Figure 4.7B). This modulation of JUN expression by FOXP2 might explain the AP1 motif enrichment in FOXP2 hNP DARs. FOXP2 opens sites enriched for nuclear factor I (NFI) motifs in hDNs (Figure 4.7A). If FOXP2 acted similarly to pioneer factor FOXA1, binding to chromatin directly to replace linker histone H1 and de-compact chromatin, a FOX motif would likely be enriched in these regions. There is evidence that FOXP2 may have less affinity to the canonical FOX motif than FOXA1 and may, instead, bind to a certain chromatin shape regardless of the underlying motif (Stroud et al., 2006); however, the strength of the NFI motif enrichment in the hDN open regions and the fact that NFI genes are highly expressed in our system (Figure 4.7C) support the notion that FOXP2 and NFI factors interact in some way to open chromatin. For instance, NFIX is activated by FOXP2 in hDNs, implying that this specific NFI protein may be binding FOXP2 hDN DARs (Figure 4.7C). Moreover, NFI transcription factors are expressed in the brain and are involved in neuronal migration, differentiation, and neurite outgrowth (Heng et al., 2012, Martynoga

et al., 2013, Betancourt et al., 2014), functions that FOXP2 has also been shown to regulate (Tsui et al., 2013, Vernes et al., 2011, Usui et al., 2017).

In order to strengthen the results of the motif analysis, we overlapped condition specific DARs with transcription factor ChIP peaks made available by the ENCODE project (Consortium, 2012). One thousand groups of randomly selected OCRs from across all conditions and containing the same number of regions as the condition specific DAR group were also overlapped with ENCODE peaks in order to assess the number of overlapping regions expected by chance. Each of the randomly generated sets of control regions and condition specific DARs were overlapped with all FOX, AP1 factor, and NFI ChIP peaks available from the ENCODE project. The number of regions bound by each transcription factor that overlapped with DARs was compared with the average number of bound regions overlapping the 1000 randomly generated sets of control regions. If the actual overlap was greater than or less than the average of the random overlaps, then the DARs were considered enriched or under-enriched for regions bound by the assayed transcription factor, respectively (Figures 4.7E-F). CTRL hNP DARs are enriched for FOXA1 bound regions, and contain an average number of FOXP2 bound regions, while FOXP2 DARs in hNPs and hDNs are under-enriched for regions bound by both factors further suggesting that FOXP2 binds DNA directly to closed, but not open, chromatin (Figure 4.7D-E). The lack of enrichment for CTRL hNP DARs in FOXP2 bound regions could be explained by the use by the ENCODE consortium of an antibody that also recognizes FOXP1. Except for ATF2 and AFT3, FOXP2 hNP DARs are more enriched for peaks bound by AP1 factors than CTRL hNP of FOXP2 hDN DARs (Figure 4.7D, F), as expected given the AP binding motif

enrichment in these regions. Surprisingly, while the enrichment for the NFI binding motif is very strong in FOXP2 hDN DARs, these regions are under-enriched for NFIC bound regions identified by ChIP. NFIC is the only NFI family member for which ChIP-seq was performed by the ENCODE project, thus, this result could suggest that another NFI factor opens chromatin at these sites. Indeed, NFIC is the least expressed NFI factor in hDNs (Figure 4.7C). Additionally, the cell lines used by the ENCODE consortium were largely proliferating cancer cells lines. Given the overt difference between the chromatin landscapes of hNPs and hDNs (Figure 4.5C), one may not expect to see much overlap between accessible chromatin regions in differentiating neurons and proliferating cancer cells, regardless which transcription factor is assayed. Overall, comparing regions of chromatin made differentially accessible by expression of *FOXP2* to regions bound by specific transcription factors strengthened the results of the motif analysis in hNPs but not in hDNs.

Next, we performed RNA-seq in hNP and hDNs in the same conditions in parallel with the ATAC-seq. In order to compare changes in gene expression downstream of FOXP2 with changes in chromatin accessibility, all DARs were annotated to the gene with the closest transcription start site, and only genes near DARs from one condition, not genes annotated to DARs from multiple conditions, were considered (Figure 4.8A). Genes identified as differentially expressed in hNPs were largely distinct from those differentially expressed in hDNs, highlighting differential roles for FOXP2 in neural progenitors and differentiating neurons (Figure 4.8B; Table 4.3). A significant overlap was found in hNPs between genes near sites closed by FOXP2 and genes repressed by FOXP2 Figure 4.8C; Table 4.2). Similarly in hNPs, genes near sites open by FOXP2

overlap significantly with genes activated by FOXP2, and in hDNs, genes near sites open by FOXP2 significantly overlap with genes activated by FOXP2 (Figure 4.8C; Table 4.2). This implies that changes in chromatin accessibly due to *FOXP2* expression are related to gene expression changes mediated by FOXP2.

Moreover, weighted gene co-expression network analysis (WGCNA) identified gene co-expression networks enriched for both condition-specific open chromatin regions and differentially expressed genes, suggesting that FOXP2-dependent epigenetic changes are driving specific transcriptional programs (Langfelder and Horvath, 2008) (Figure 4.9A). For example, module 1 (M1) is enriched both for genes activated by FOXP2 in hDNs and genes near FOXP2 hDN DARs (Figure 4.9A). The eigengene of M1 is not correlated with gene expression in hNPs, but is negatively correlated with genes expression in CTRL hDNs and positively correlated with gene expression in FOXP2 hDNs, suggesting that the member genes are regulated positively by FOXP2 in a coordinated fashion (Figure 4.9B). Importantly, the most connected genes within this network include genes near FOXP2 hDN DARs and hDN activated genes (Figure 4.9C). Gene ontology analysis of M1 member genes shows enrichments for ontological categories relevant for mature neurons including genes involved in synaptic transmission and neuron projection formation (Figure 4.9D). Together, these data imply that FOXP2-dependent epigenetic changes are driving transcriptional programs relevant for neuronal maturation.

FOXP2 regulates gene expression through DNA-binding dependent and independent mechanisms

Analysis of the areas of chromatin differentially open when *FOXP2* is expressed during neuronal differentiation shows that, while FOXP2 does open chromatin in hDNs that is not open in hNPs, it does so in regions enriched for the NFI factor binding motif, not a canonical FOX motif (Figure 4.7C). Several possibilities could explain this finding. For example, FOXP2 could be binding DNA directly at an alternative motif, or it could be forming an activating complex with NFI. Alternatively, FOXP2 could be activating the transcription of an NFI gene in hDNs that, after translation, goes on to activate FOXP2 targets indirectly. Discerning the relationship between FOXP2 and NFI could elucidate the mechanism by which FOXP2 regulates neuron maturation.

In order to uncover the mechanism by which FOXP2 regulates neuronal gene expression, we again performed ATAC-seq (Buenrostro et al., 2015a) to identify differentially accessible regions of chromatin with expression of *FOXP2* in proliferating and differentiated cells. Because changes in chromatin structure could be a consequence of FOXP2 directly binding chromatin or of FOXP2 interacting with chromatin through a cofactor independent of its ability to bind DNA, we performed ATAC-seq in cells expressing either wild-type FOXP2 (FOXP2-WT) or FOXP2 with a DNA-binding mutation (FOXP2-KE). As discussed in chapter 3, FOXP2-KE contains a single point mutation in the DNA-binding domain of FOXP2 that mimics the mutation in a family known as the “KE” family with verbal dyspraxia (Lai et al., 2001). FOXP2-KE has been shown to localize less efficiently to the nucleus (Vernes et al., 2006), further supporting its use as a non-chromatin interacting mutant. As demonstrated in Figure 3.5B, immunohistochemistry of hNPs expressing FOXP2 showed that the KE mutant was expressed in both the cytoplasm and the nucleus while the WT protein had almost

entirely nuclear expression. Importantly, electron mobility shift assays have shown that this altered form of FOXP2 is unable to bind to DNA (Vernes et al., 2006).

In order to confirm that the KE mutant is unable to regulate gene expression in our system, we performed a second round of RNA-seq in hNPs and hDNs expressing *FOXP2*-WT, *FOXP2*-KE, or CTRL-GFP (Table 4.2). Compared with the first round of RNA-seq (Figure 4.8B, Table 4.2), *FOXP2*-WT was expressed at much lower levels in this experiment (Figure 4.10A, Table 4.2). Moreover, approximately twice as much *FOXP2*-KE is expressed compared with the second round expression of *FOXP2*-WT (Figure 4.10A). In order to identify differentially expressed genes in the second round of RNA-seq, we compared the transcriptomes of cells expressing *FOXP2*-WT and *FOXP2*-KE pairwise with the transcriptomes of CTRL-GFP cells (4.10B, Table 4.2). In accordance with the decreased *FOXP2* expression in the second round, there are fewer *FOXP2*-WT differentially expressed genes compared with the first round (Figure 4.10C; Table 4.2); however, the *FOXP2*-WT repressed and activated genes in hNPs and hDNs significantly overlap between the first and second experiment with more than half of the second round hDN differentially expressed genes confirming first round differentially expressed genes (Figure 4.10D; Table 4.2). Importantly, only one gene in hNPs and one gene in hDNs were differentially expressed with the expression of *FOXP2*-KE, even though twice as much of the mutant was present compared with the wild-type condition (Figure 4.10C). This confirms that FOXP2-KE has little to no ability to regulated gene expression.

For this experiment, differentially accessible regions (DARs) were determined by calculating the fold-difference between normalized reads in regions accessible in

FOXP2-WT or -KE expressing cells relative to CTRL cells in a pairwise manner (Figure 4.11A). We identified regions made differentially accessible with only FOXP2-WT expression (DNA-binding dependent DARs) and regions differentially accessible if either FOXP2-WT or FOXP2-KE was expressed (DNA-binding independent DARs) in hNPs or hDNs (Figure 4.11B). In contrast with the first ATAC-seq experiment (Figure 4.6A), in this experiment we were able to identify regions of chromatin closed by FOXP2 specifically in hDNs (Figure 4.11B) suggesting that the previous finding was the result of a technical error.

In order to determine the functional significance of the DNA-binding dependent and independent DARs, we compared DAR locations to the locations of genomic regions with defined functional chromatin states imputed from epigenetic marks in human fetal brain (Roadmap Epigenomics et al., 2015, Ernst and Kellis, 2015) (Figure 4.11C; Table 6.4). DARs do not significantly overlap with inactive regions of chromatin such as heterochromatin and regions repressed by the polycomb complex, suggesting FOXP2 alters chromatin structure in regulatory regions of the genome (Figure 4.11C; Table 6.4). FOXP2 DARs are also not enriched in actively transcribed regions marked by H3K36me3, H4K20me1, and H3K79me2 (Ernst and Kellis, 2015) consistent with ATAC-seq data from human fetal brain (de la Torre-Ubieta et al., 2018) (Figure 4.11C; Table 6.4). Interestingly, Most DAR types were significantly enriched for enhancer regions, suggesting that FOXP2 exerts its effects through long-range interaction with promoter regions.

To elucidate how the DNA-binding dependent and independent DARs influence gene expression, we compared genes with the closest transcriptional start sites to

DARs in each group with FOXP2-WT differentially expressed (DE) genes from the second round of RNA-seq (Tables 4.2 and 4.3). Importantly, the cells from which the RNA was harvested for this experiment were transduced, differentiated and collected in parallel with those used for ATAC-seq (Figure 4.10C). Interestingly, the only DAR types that significantly overlapped with DE genes were those with the most significant enrichment for enhancer states (Figure 411C, outlined in green). Genes near closed, hDN DNA-binding dependent DARs overlapped significantly with genes repressed by FOXP2 in hDNs, while genes near open, hDN DNA-binding independent DARs overlapped significantly with hDN FOXP2 activated genes (Table 4.3). These data suggest that FOXP2 directly binds DNA to facilitate chromatin compaction in enhancer regions that control target gene repression. Conversely, FOXP2 activates gene expression by opening chromatin in enhancer regions independent of direct DNA binding, perhaps in conjunction with a cofactor or cofactors.

In order to confirm that FOXP2 closed chromatin at regions enriched for FOX motifs and opens chromatin in conjunction with NFI factors as shown previously (Figure 4.7), we performed *de novo* motif analysis (Heinz et al., 2010) on hDN closed DNA-binding dependent and hDN open DNA-binding independent DARs. A Forkhead motif was among the most significantly enriched motifs identified in hDN closed DNA-binding dependent DARs ($p = 1x10^{-16}$), while hDN open DNA-binding independent DARs were most significantly enriched with an NF1 half-site motif ($p = 1x10^{-16}$). Next, we performed a known motif enrichment analysis to compare the prevalence of the *de novo* identified motifs in all DAR types compared to background regions normalized for sequence bias (Heinz et al., 2010). The Forkhead motif was significantly enriched above background in

hDN closed DNA-binding dependent and independent DARs (Figure 4.12A). Closed hDN DNA-binding dependent DARs likely represent areas of chromatin condensed by FOXP2 homodimers, while hDN closed DNA-binding independent DARs may be areas bound by heterodimers of FOXP2 and FOXP1 or P4 which are both expressed in hDNs and are able to interact with FOXP2-KE, albeit with slightly decreased affinity (Estruch et al., 2016). As expected, hDN open DNA-binding independent DARs were highly enriched with NFI half-sites, and hDN open DNA-binding dependent DARs were enriched to a lesser extent (Figure 4.12B). These data suggest that FOXP2 directly binds its consensus sequence in order to close chromatin and repress nearby gene expression. Because FOXP2-WT directly closes sites that significantly overlap with enhancer regions (Figure 4.11C), it may be displacing activator complexes present in the control condition and destabilizing enhancer-promoter loops to repress gene expression (Figure 4.12C). FOXP2-KE cannot bind DNA; thus, when it is present the activator complexes remain intact and gene expression is not repressed (Figure 4.12C).

Because the regions of chromatin that align with activated gene expression are open in a DNA-binding independent manner by FOXP2-WT and FOXP2-KE alike, and because FOXP2-KE is unable to bind to DNA (Vernes et al., 2006), it is unlikely that FOXP2 is directly binding a non-canonical motif similar to the NFI motif to activate gene expression. Moreover, because the KE mutant is largely unable to regulate gene expression (Figure 4.10C), the regions of chromatin open in the presence of FOXP2-WT and FOXP2-KE are not likely to be opened because FOXP2 increases the expression of an NFI factor which then acts independently to open chromatin, or decreases the expression of a repressor that competes with NFI factors for binding

sites. Thus, these data allow us to determine that FOXP2 likely forms a complex with an NFI cofactor to open inaccessible chromatin and activate gene expression. Additionally, regions of chromatin open in a DNA-binding dependent manner overlap significantly with transcription start sites (TSS), but do not correlate with gene activation, while regions of chromatin open in a DNA-binding independent manner overlap significantly with enhancer regions and do correlate with gene activation (Figure 4.11C). This suggests a model in which a FOXP2-NFI complex forms promoter-enhancer loops, and while FOXP2-KE is able to complex with NFI to facilitate chromatin opening at the enhancer, it is unable to promote looping and open chromatin at the promoter region (Figure 4.12D).

FOXP2 target genes coordinate subplate and germinal zone co-expression networks

To identify networks of genes coordinated by alterations in chromatin accessibility governed by FOXP2, we performed weighted gene co-expression network analysis (WGCNA) (Langfelder and Horvath, 2008). Moreover, to better understand how the gene networks we identified contributed to *in vivo* human cortical development, we looked in the modules for enrichment of genes correlated with specific human developmental cortical layers (Figure 4.13) (Miller et al., 2014). The module most enriched for hDN FOXP2 activated genes (M7) was also enriched for genes correlated with the subplate layer, a transient developmental cortical layer which is expanded in primates and plays a role in corticothalamic circuit formation and maturation, among other things (Kostovic and Rakic, 1990, Ghosh et al., 1990, Kanold et al., 2003, Kanold and Shatz, 2006) (Figure 4.13, 4.14A). The eigengene of M7, which represents the gene expression profiles of the genes within M7, was positively correlated with *FOXP2*-

WT expressing hDN samples and negatively correlated with CTRL and *FOXP2*-KE expressing hDN samples (Figure 4.14B), and the genes in M7 were enriched for genes involved in chemical synaptic transmission (Figure 4.14C). M7 was not enriched for genes near DARs; however, the most highly connected hub gene of this module, *NKAIN2*, is near an hDN open DNA-binding independent DAR in this module and in module M1 from the previous analysis (Figure 4.14A, Figure 4.9A). While few subplate correlated genes are near hDN open DNA-binding independent DARs, these data suggest that FOXP2 dependent chromatin opening influences subplate gene expression by modulating network hub genes and drives FOXP2 expressing cells to a more mature state.

The module most enriched with hDN FOXP2 repressed genes (M13) was also enriched for germinal zone layer genes across human fetal time points, including VZ genes at 16 pcw (Figure 4.15A). The eigengene of M13 was negatively correlated with *FOXP2*-WT expressing and CTRL samples, and not correlated with *FOXP2*-KE expressing samples (Figure 4.15B). The genes in M13 were enriched in gene ontology categories for cell proliferation, adhesion, and locomotion (Figure 4.15C). Similar to the activated gene module, M13 was not enriched for genes near DARs, but the most highly connected hub gene, *NEDD9*, was near an hDN closed DNA-binding dependent DAR. This suggests that FOXP2 dependent chromatin condensation drives the repression of a network of genes necessary for maintaining proliferative capacity.

Discussion

By performing ChIP- and RNA-seq in human neural progenitors (hNPs) we found that FOXP2 directly represses repressors of transcription. Moreover, by differentiating

hNPs into human differentiating neurons (hDNs) in the presence or absence of FOXP2 and comparing chromatin accessibility between the two stages, we found that expression of *FOXP2* does, in fact, open regions of chromatin in hDNs that were closed in hNPs. While this suggested putative pioneering activity, performing the same assay using the DNA-binding deficient FOXP2-KE mutant (Vernes et al., 2006) showed that this chromatin opening is independent of the ability of FOXP2 to bind DNA. Additionally, while some form of FOXP2 is necessary for the de-compaction, motif analysis of the open regions identified a putative FOXP2 co-activator, NFI transcription factors. Moreover, comparing the locations of regions of chromatin made differentially accessible with expression of *FOXP2* with known promoter and enhancer regions in human fetal brain (Roadmap Epigenomics et al., 2015) suggests that the FOXP2-NFI complex acts to open chromatin at enhancers, and perhaps, facilitates enhancer-promoter looping, in order to activate genes expressed in mature neurons. On the other hand, FOXP2 binds directly to DNA to close chromatin at enhancers, reducing the expression of genes involved in cell proliferation. Thus, we identified separable mechanisms for activation and repression of FOXP2 target genes involved with maintaining proliferative capacity and promoting neuronal maturation, respectively.

FOXP2 can bind DNA as a homodimer, can heterodimerize with other FOXP proteins, and has been shown to interact with NFAT, TBR1, and CTBP among other DNA-binding proteins (Wu et al., 2006, Deriziotis et al., 2014, Li et al., 2004). We identified Nuclear Factor 1 (NFI) transcription factors, which are essential for proper forebrain development (Betancourt et al., 2014, das Neves et al., 1999, Campbell et al., 2008), as potential, novel, co-regulators of FOXP2 activated genes. While NFI-A, -B,

and –X are highly expressed in the neocortex during mouse development, NFI-A is more correlated with the human subplate than other NFI factors (Miller et al., 2014). Importantly, a co-expression module enriched for FOXP2 activated targets is also enriched for subplate-correlated genes. Mice with *Nfia* loss of function mutations exhibit hydrocephalus and lack the corpus callosum (das Neves et al., 1999). Interestingly, whole brain gene expression analysis of E16 Nfia deficient mice shows that NFIA and FOXP2 share activated targets including NCAM1, a human subplate correlated gene, and GAP43, a known subplate marker (Miller et al., 2014, Honig et al., 1996, Wong et al., 2007). This suggests that FOXP2 and NFIA may work together to regulate human subplate gene expression.

Other evidence of the relationship between Foxp2, Nfia, and chromatin accessibility comes from an analysis of accessible chromatin regions across layers of the adult mouse visual cortex (Gray et al., 2017). Forkhead motifs were present in areas of chromatin that were less accessible in layer VI where Foxp2 is expressed compared with other cortical layers devoid of Foxp2; in contrast, an enrichment of Nfi motifs was seen in regions of chromatin that were comparably more accessible in layer VI, where Nfia is highly expressed (Gray et al., 2017). Moreover, Gray et al. suggest Nfia as a putative activator of Foxp2 based on the presence of an Nfi motif in a differentially accessible region near Foxp2. It is remarkable that our motif enrichment analysis in hDNs exogenously expressing FOXP2 also shows that Forkhead motifs are present in differentially closed chromatin, while NFI motifs are present in differentially open chromatin. While we cannot confirm the regulation of FOXP2 by NFIA in our overexpression system, we suggest that because these NFIA motifs are present in

regions of chromatin that are more open when FOXP2-WT or the DNA-binding deficient FOXP2-KE are expressed, that FOXP2 and NFIA may physically interact to open chromatin in the subplate. Importantly, NFI factors have already been shown to interact with the Forkhead transcription factor FOXA1 in JEG-3 choriocarcinoma cells expressing HA-tagged NFIA-C or NFIX (Grabowska et al., 2014).

The consistency between results from our study in human hDNs and those from mouse visual cortex suggests a conserved mechanism for FoxP2 regulatory control in the cortex; however, our gene expression analysis identified conserved, primate specific, and human specific FOXP2 regulated subplate genes (Figure 3.2D). This implies that while FoxP2 functionally controls gene expression in a conserved way, it can regulate species-specific targets along with NFI, likely by binding at DNA-sequences that are not conserved between species. Significantly, the regions of chromatin made differentially accessible by FOXP2 that predicted gene expression in hDNs were located in human fetal brain enhancer regions, which are less conserved than mammalian promoters (Villar et al., 2015). Taken together, these data provide evidence of a novel relationship between FOXP2 and NFI transcription factors whereby these factors physically interact to open chromatin at enhancer regions and promote neuronal maturation.

Future directions

In order to prove a physical interaction between an NFI family transcription factor and FOXP2, we performed co-immunoprecipitations (co-IPs) of FOXP2-V5 and NFIA and -B. However, we were unable to detect FOXP2-V5 via immunoblot following SDS-PAGE after immunoprecipitating NFIA or -B. There are several potential explanations

for this result. First, although the antibodies used to detect NFIA and –B have been validated using NFIA and NFIB double knockout mice via immunohistochemistry (Chen et al., 2017), they may not be suitable for co-IPs followed by western blotting. Moreover, the interaction between FOXP2 and NFI could be transient or weak, making it difficult to detect via co-IP. Therefore, it may be useful to employ in-cell co-IP using proximity ligation, which allows for the detection and localization of endogenous protein complexes *in situ* with a strong signal-noise-ratio (Soderberg et al., 2006). Alternatively, there may be no physical interaction between FOXP2 and NFI transcription factors suggesting either that FOXP2 interacts with another protein with a binding motif to the NFI motif, or that the DNA-binding independent regions of open chromatin enriched for NFI-motifs are artifacts of the ATAC-seq assay that happen to significantly overlap with genes activated by FOXP2 in two separate experiments. Because proximity ligation is such a sensitive tool, a negative result using this immunohistochemistry-based assay would be highly suggestive of a lack of interaction.

If FOXP2 and NFI factors are shown to interact physically, it would be of interest to determine the regions of FOXP2 required for this interaction by mutagenizing FOXP2. Potential interacting regions include the leucine-zipper and trans-repressor domains of FOXP2, which have been shown mediate homo- and heterodimerization of FOXP proteins and interactions with CtBP1, respectively (Li et al., 2004). The polyglutamine track is another potential cofactor binding domain that has yet to be functionally characterized in FOXP2. Importantly, polyglutamine repeat regions are thought to stabilize protein-protein interactions (Schaefer et al., 2012). Proximity ligation followed by transduction of mutant FOXP2 constructs containing deletions of these domains into

hDNs could determine the domains critical for forming a FOXP2-NFI complex. Once the interaction domain is identified, the ATAC-seq experiments could be repeated in hDNs expressing FOXP2-WT, FOXP2-KE or the NFI binding deficient FOXP2. If a physical interaction between FOXP2 and an NFI factor is necessary for DNA-binding independent chromatin opening we would see a loss of regions open by FOXP2-WT and –KE in the hDNs expressing FOXP2-NFI binding deficient mutant.

Figures

Figure 4.1 *Potential mechanisms by which FOXP2 opens chromatin to activate gene expression*

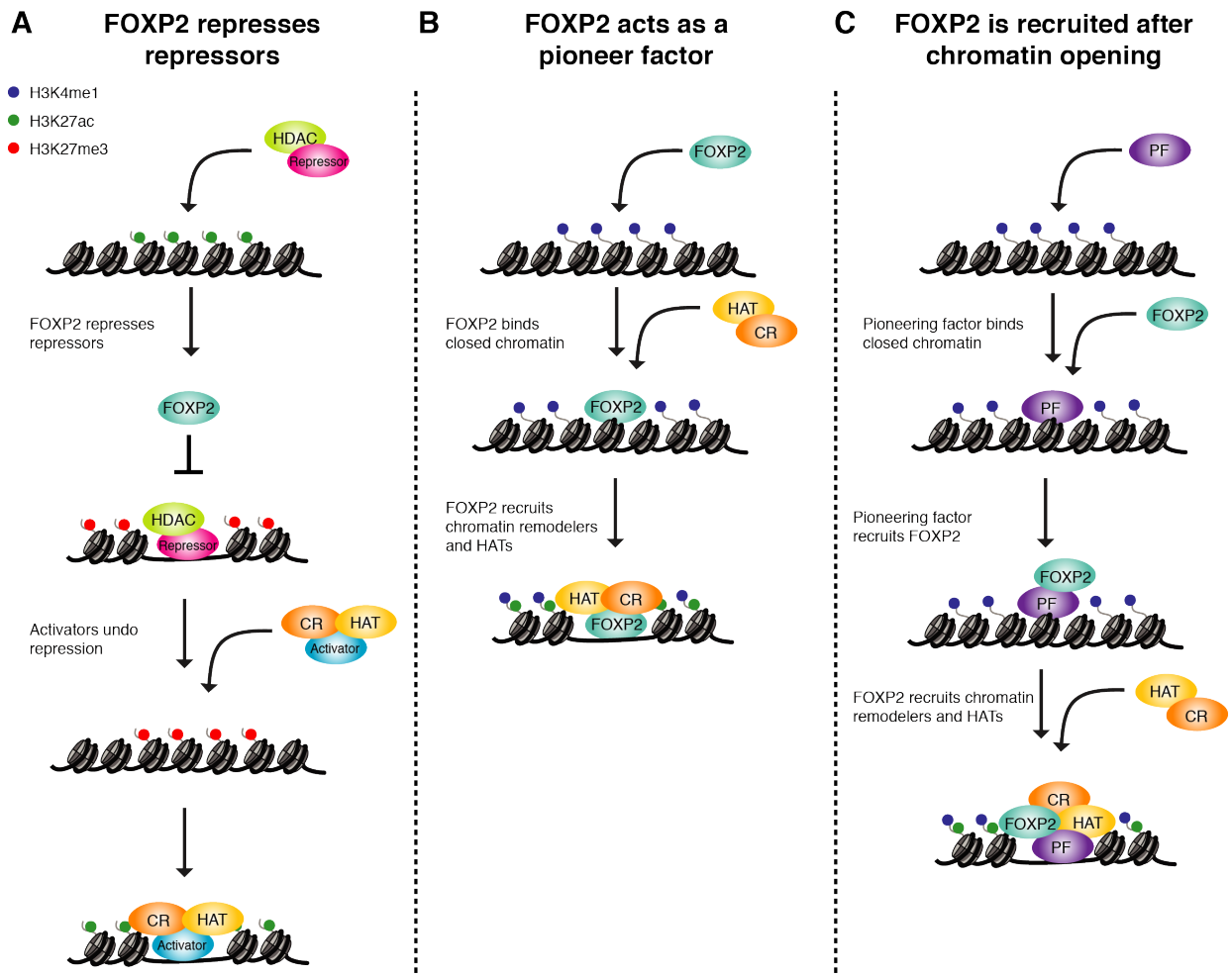

A) FOXP2 represses transcriptional repressors. **B)** FOXP2 acts as a pioneer factor. **C)** FOXP2 is recruited after chromatin opening. HDAC – histone deacetylase, HAT – histone acetyltransferase, CR – chromatin remodeler, PF – pioneering factor.

Figure 4.2 *Identification of direct and indirect FOXP2 targets in hNPs*

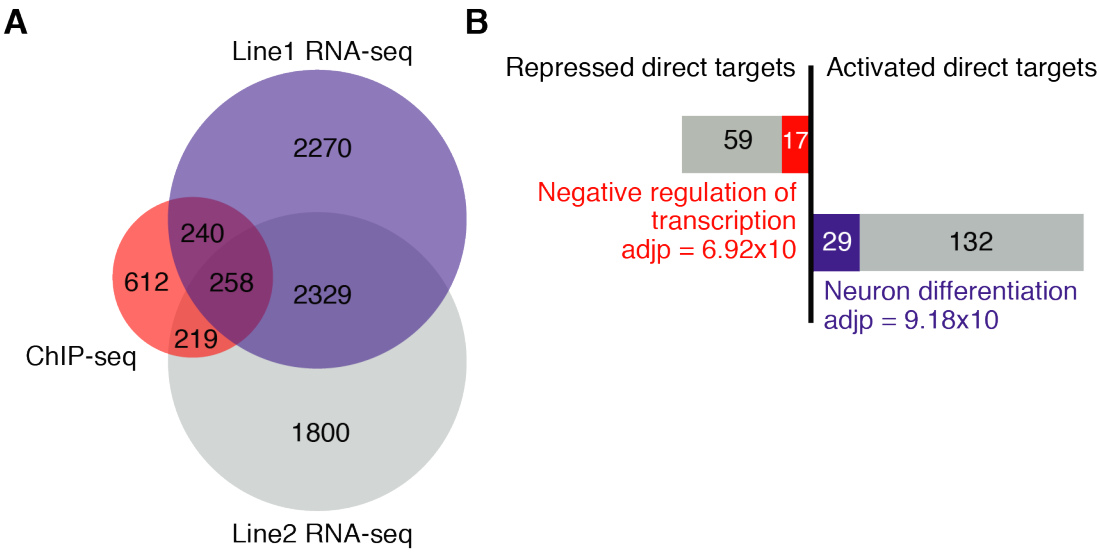

A) Overlap between genes bound by FOXP2 and genes differentially expressed in two independent hNP lines expressing FOXP2. Genes that are bound and differentially expressed are defined as direct FOXP2 targets. **B)** Gene ontology analysis of repressed and activated direct FOXP2 targets.

Figure 4.3 *FOXP2 repressed direct targets are hubs in a module whose eigengene is negatively correlated with FOXP2 expression*

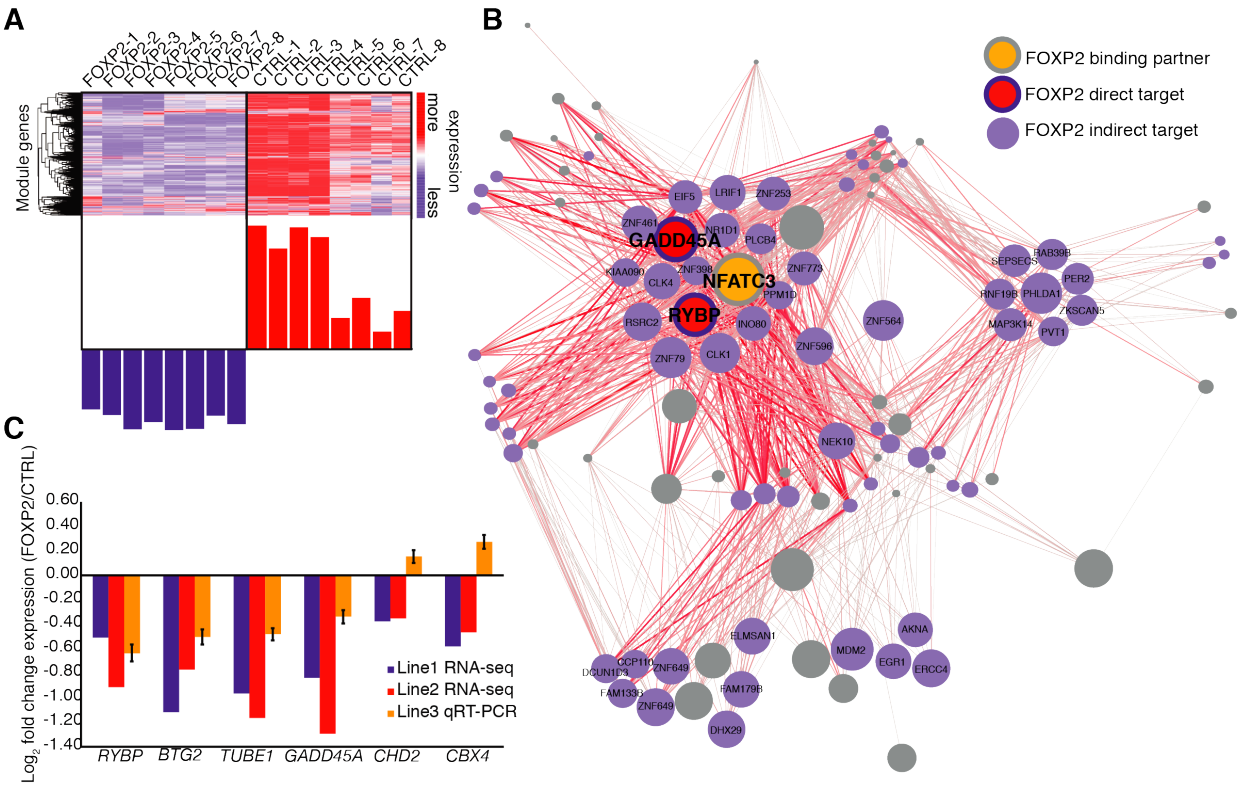

A) The average gene expression profile across samples indicates a module whose eigengene is negatively correlated with FOXP2 expression. **B)** Hub genes of the FOXP2 correlated network include direct targets *RYBP* and *GADD45A* and known FOXP2 binding partner NFATC3. Size of the nodes is correlated to kwithin, the distance between nodes is force directed by edge-betweenness, and the color of the edges is correlated with weight, red lines having larger weights. **C)** Confirmation by qRT-PCR of repression of direct FOXP2 targets contained in the module in a third line of HNPs.

Figure 4.4 *FOXP2 down-regulates a network of transcriptional repressors*

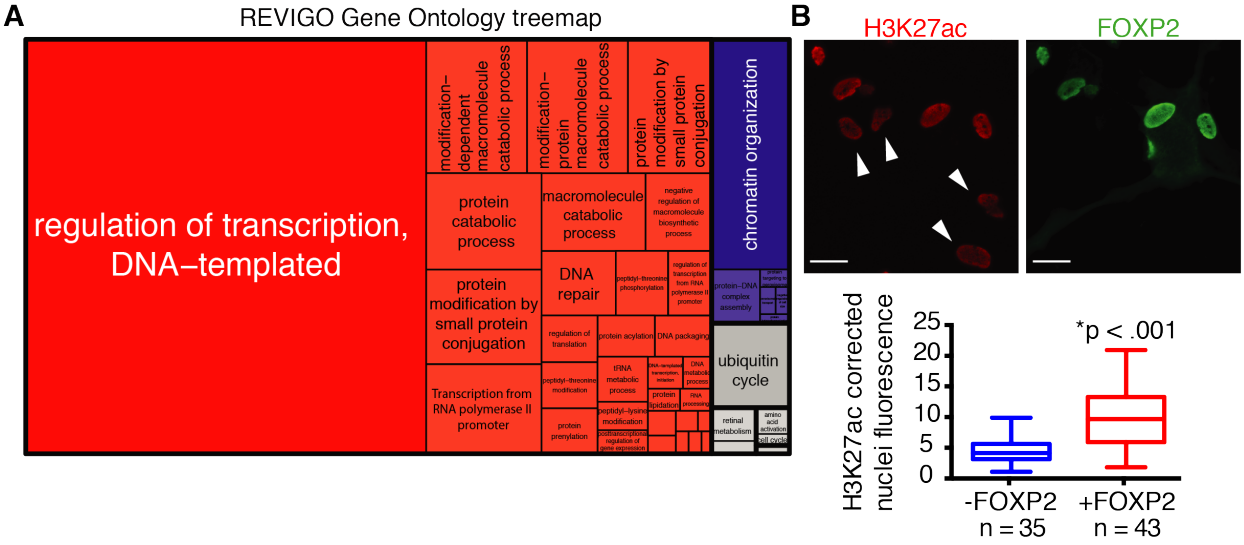

A) Gene ontology of the negatively correlated module. The size of the box is proportional to the –log of the adjusted p-value of the enrichment. The colors represent related gene ontology categories. **B)** Top: hNPs exogenously expressing FOXP2-FLAG immunostained for H2K27ac and FLAG. H3K27ac positive, FOXP2 negative nuclei are marked by arrowheads. Bottom: Quantification of H3K27ac fluorescence intensity in FOXP2+ and FOXP2- nuclei. Significance calculated using the Mann-Whitney test.

Figure 4.5 *FOXP2 down-regulates a network of transcriptional repressors*

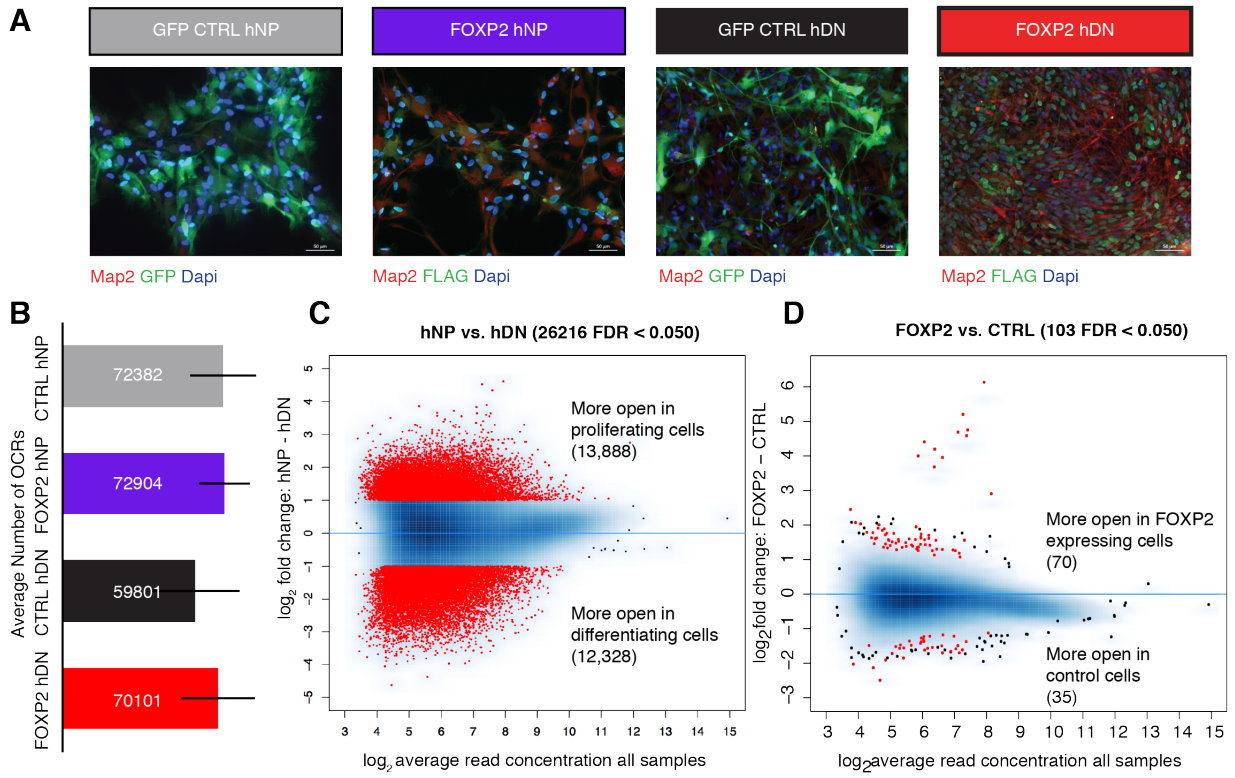

A) Immunocytochemistry showing hNPs and hDNs expressing FOXP2 or control GFP **B)** Average number of open chromatin regions (OCRs) per condition as called by MACS2 (all peaks fold enrichment > 4). **C)** Comparing open chromatin regions between hNPs and hDNs (CTRL hNPs + FOXP2 hNPs vs. CTRL hDNs + FOXP2 hDNs) reveals 13,888 OCRs more open in proliferating cells and 12,328 OCRs more open in differentiating cells. **D)** In contrast, comparing all FOXP2 expressing cells to all control cells (FOXP2 hNPs + FOXP2 hDNs vs. GFP hNPs + GFP hDNs) shows only 70 OCRs more open in FOXP2 expressing cells and 35 OCRs more open in CTRL cells.

Figure 4.6 *Localization of condition specific differentially open chromatin regions*

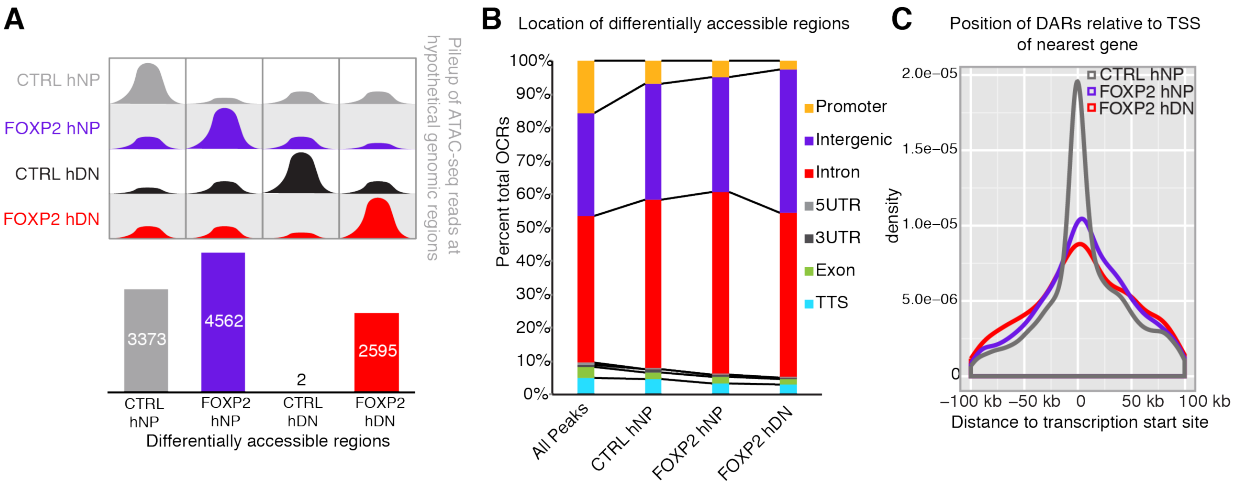

A) Top: Schematic representation of condition-enriched ATAC peaks. Bottom: Number of differentially accessible regions identified using EdgeR to calculate fold difference between normalized reads in one condition relative to the other three. **B)** Compared to all OCRs, fewer DARs are present in promoter regions and more DARs are present in introns and intergenic regions. **C)** Compared with CTRL hNP DARs, a higher proportion of FOXP2 DARs are located more than 25kb from the transcription start site (TSS) of the nearest gene. This suggests that FOXP2 is making distal enhancer regions accessible, and, according to the ENCODE project, these regions are important for cell identity.

Figure 4.7 *FOX, AP1, and NFI motifs are enriched in DARs*

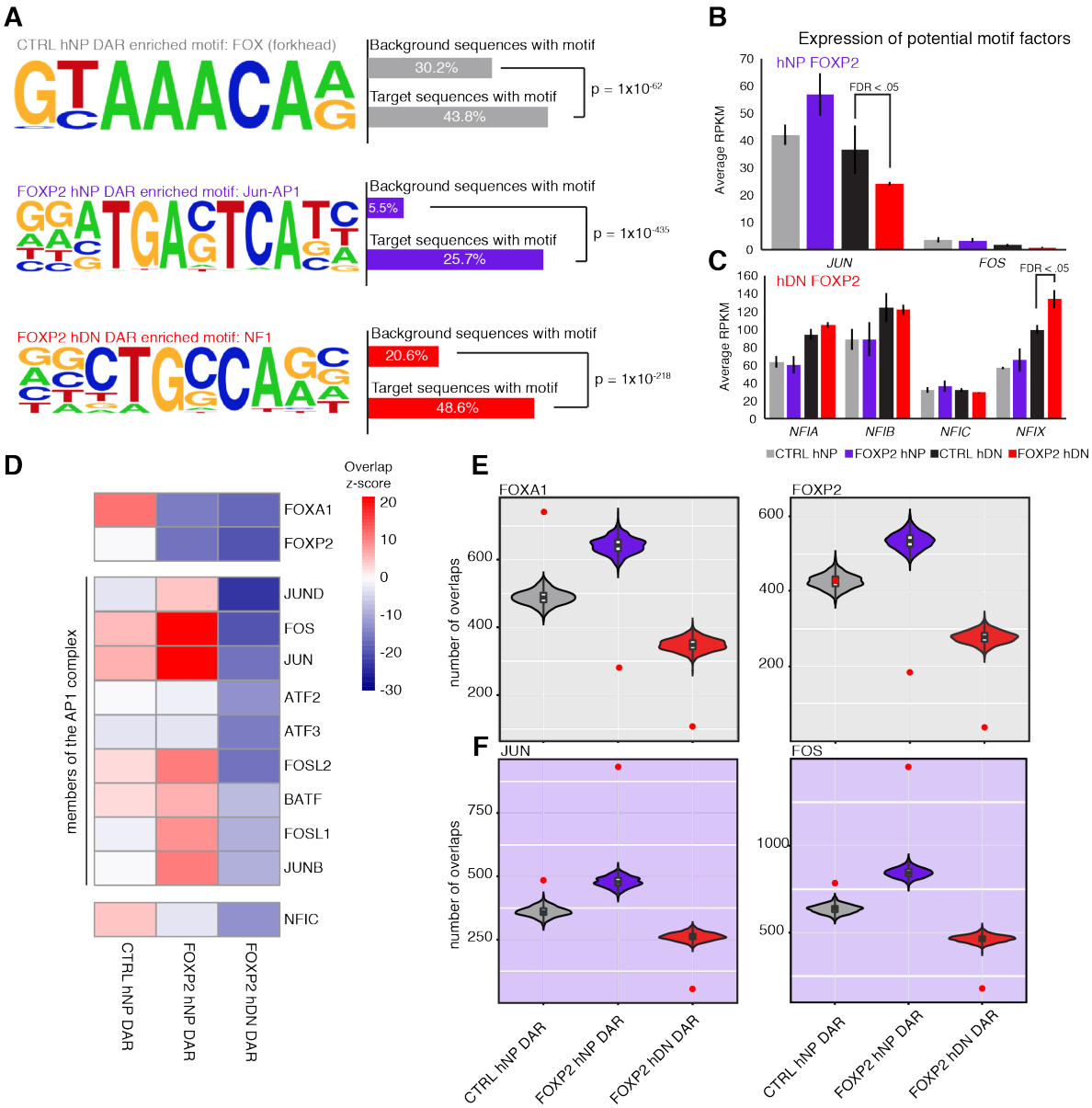

A) Motifs enriched in DARs foud by Homer motif analysis. **B)** JUN is most highly expressed in FOXP2 expressing hNPs and is significantly repressed by FOXP2 in hDNs. The modulation of JUN expression by FOXP2 might explain the motif enrichment shown in A. **C)** NFI genes are highly expressed in hNPs and hDNs, and NFIX is activated by FOXP2 in hDNs. **D)** One thousand random peak sets with the same number of peaks and location profile as the DAR peak set of interest were generated using all OCRs across all conditions. Each of these random peak sets was overlapped with all FOX, AP1 factor, and NFI ChIP peaks available from the ENCODE project. POLR2 peaks were also analyzed. The heatmap represents the z-score of the actual number of ENCODE transcription factor peaks overlapping DARs when compared to the average of the number of ENCODE transcription factor peaks overlapping the 1000 random peaks sets. Red represents positive z-scores (highly enriched in DARs vs. random) and blue represents negative z-scores (under-enriched in DARs vs. random). **E)** Violin plots of the distribution of FOXA1 and FOXP2 peak overlaps with the 1000 random peak sets. The red point represents the actual number of overlaps. **F)** Same as E. with FOS and JUN peak overlaps.

Figure 4.8 *FOXP2 DARs correspond to FOXP2 differentially expression genes*

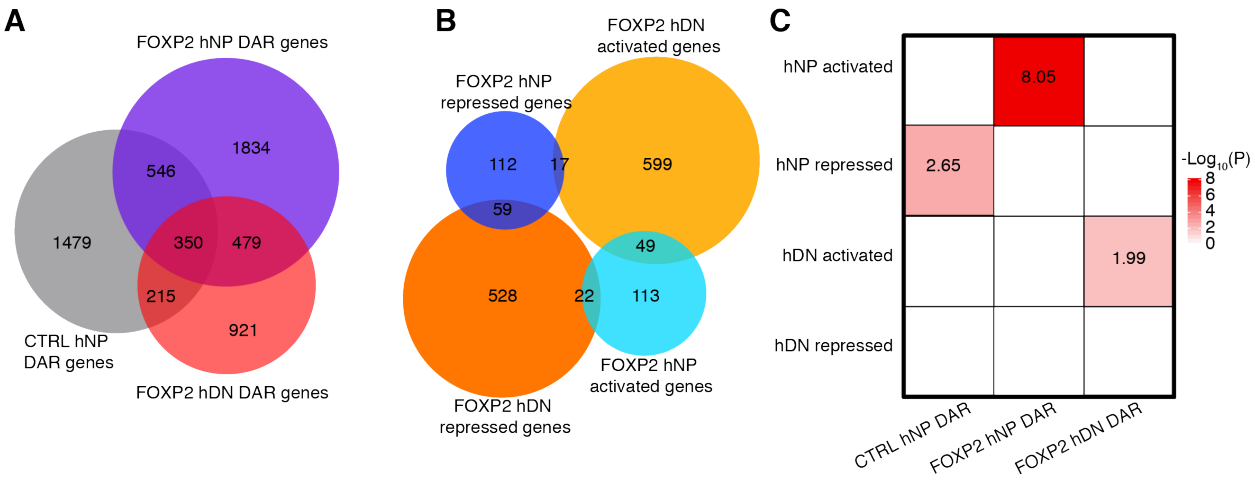

All DARs were annotated to the gene with the closest transcription start site. **A)** Venn diagram showing overlapping and specific genes annotated to DARs. DARs from each condition can be associated with the same gene (overlapping groups), or different genes (non- overlapping groups). The non-overlapping groups are used for all further analyses. **B)** Genes differentially expressed with expression of FOXP2 in hNPs of hDNs. **C)** Hypergeometric test to calculate the significance of the overlap between differentially expressed (DE) genes and DAR associated genes. Darker red corresponds to smaller B&H adjusted p-value.

Figure 4.9 *Genes near FOXP2 hDNs DARs are hubs of a FOXP2 correlated module enriched for synaptic genes*

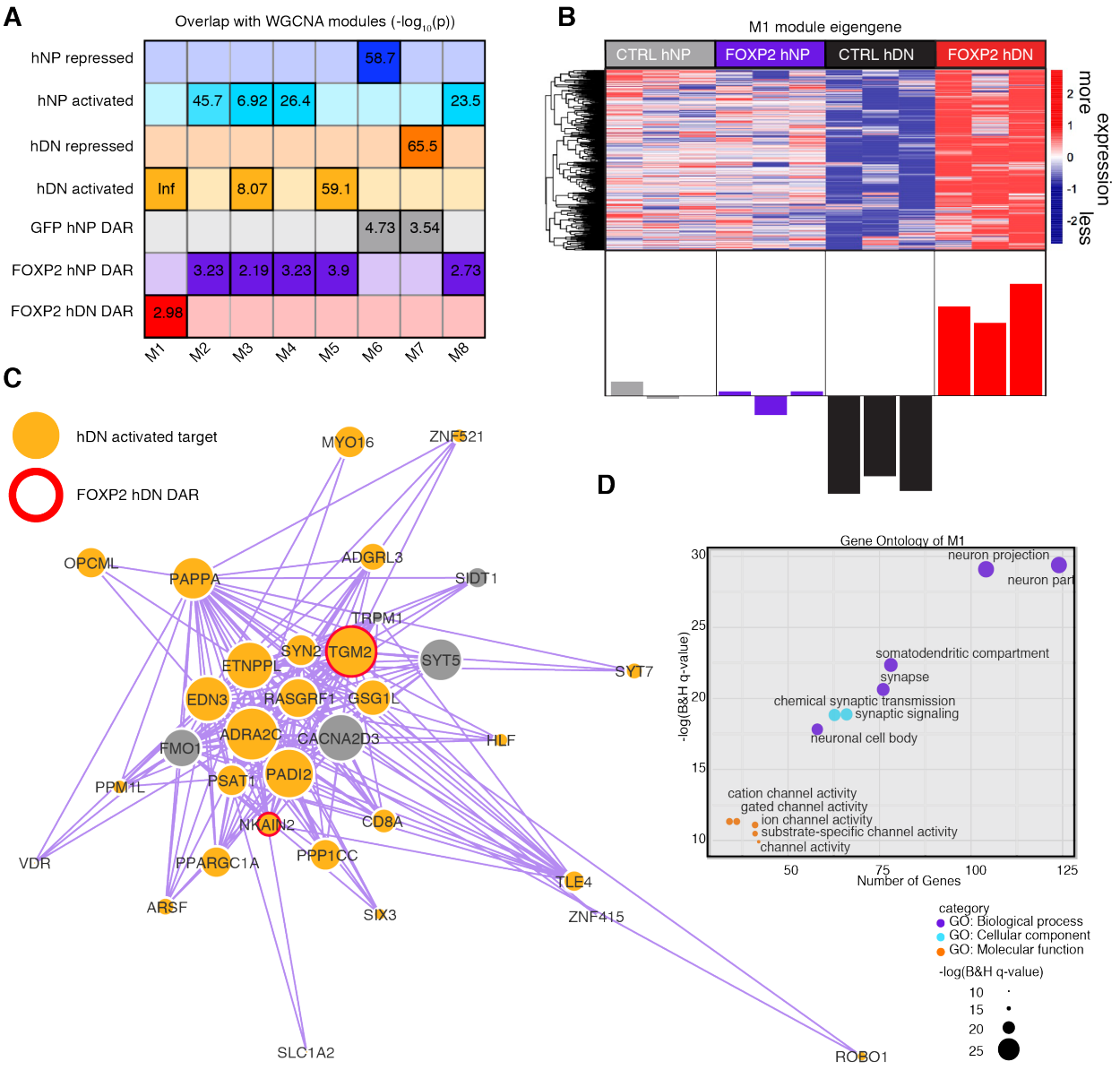

A) WGCNA reveals several modules enriched for DAR associated and DE genes. Numbers within the boxes are -log10(B&H p-val). **B)** M1 (enriched for 4W activated targets and FOXP2 hDN DARs) is positively associated with FOXP2 in hDNs. Top: a heatmap representing expression of genes in module M1. Each row is one gene, and each column is one replicate of the associated condition. Bottom: Bar plot showing the module eigengene correlation with each replicate of the associated condition. **C)** Representation of the 200 strongest connections in M1. Edge length corresponds to the weight of the interaction with nodes closer together being more strongly co-expressed. Node size corresponds to kWithin, a measurement of how highly connected the node is to all other nodes. hDN activated genes are hubs in M1. **D)** Gene ontology analysis (ToppFunn) shows enrichment for categories associated with mature neurons.

Figure 4.10 *A second round of RNA-seq shows that FOXP2-KE does not regulate gene expression in hNPs and hDNs*

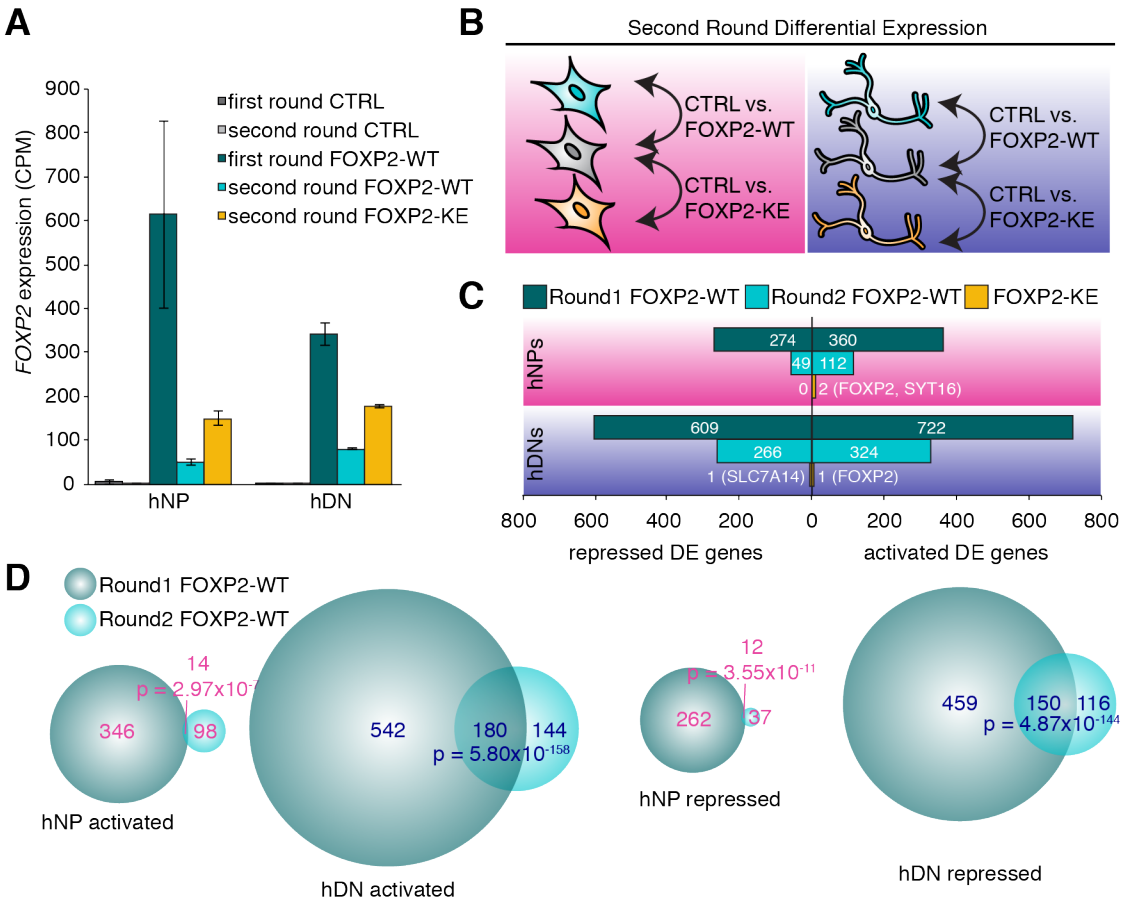

A) Bar plot showing the mean expression of FOXP2 in the first and second RNA-seq experiments across conditions. Samples expressing FOXP2-KE were only included in the second experiment. Error bars represent standard deviation. Three replicates were performed per condition. **B)** Schematic representation of the groups compared for differential expression analysis in the second RNA-seq experiment. **C)** Numbers of DE genes in the first (Round1) and second (Round2 FOXP2-WT and FOXP2-KE) RNA-seq experiments. **D)** Venn diagrams showing the overlap between FOXP2 activated and repressed genes in hNPs and hDNs with more or less exogenous FOXP2 expression. P-values are derived from hypergeometric overlap tests.

Figure 4.11 *ATAC-seq including FOXP2-KE identifies DNA-binding dependent and independent DARs differentially effect gene expression*

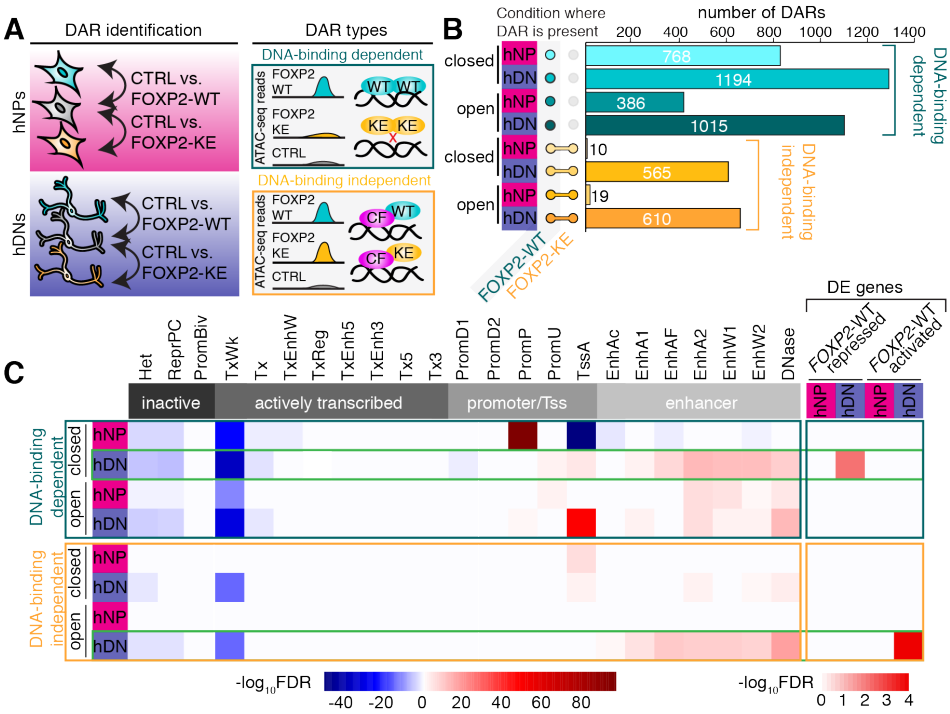

A) Schematic showing pairwise comparison of ATAC-seq samples for identification of differentially accessible chromatin regions (DARs) and examples of open DNA-binding dependent and independent DARs. FOXP2-WT (WT), FOXP2-KE (KE), hypothetical cofactor (CF). **B)** Bar plot showing number of DARs open or closed compared to CTRL and the conditions in which they are present. DARs represented by green bars occur only when FOXP2-WT is expressed (DNA-binding dependent), while DARs represented by yellow bars co-occur with expression of FOPX2-WT or FOXP2-KE (DNA-binding independent). **C)** Heatmap representing the adjusted p-value of the overlaps between DARs and regions of the genome defined by 24 imputed chromatin states in human fetal brain (Roadmap Epigenomics et al., 2015, Ernst and Kellis, 2015) and the hypergeometric overlap between genes near DARs and FOXP2 DE genes. For the chromatin states, darker blue corresponds to –log10 BH adjusted p-value of significantly under-enriched groups while red corresponds to significantly enriched groups. For the DE gene overlaps color corresponds to –log10 BH adjusted p-value with red being most and white being least significant. DAR types significantly overlapping with DE genes are outlined in green.

Figure 4.12 *FOX and NFI motifs are enriched in closed DNA-binding dependent and open DNA-binding independent DARs, respectively*

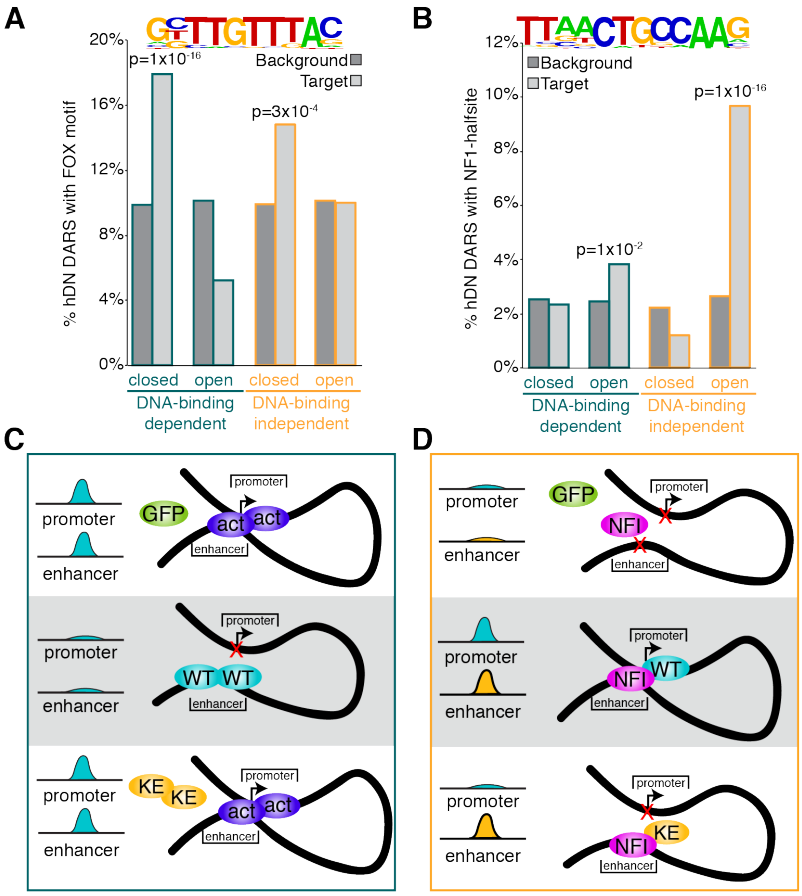

A) Top: Significantly enriched FOX motif identified in closed DNA-binding dependent DARs by de novo motif analysis. Bottom: Percent of DARs with previously identified FOX motif compared to background regions. **B)** Top: Significantly enriched NFI-half site identified in open DNA-binding independent DARs by de novo motif analysis. Bottom: Percent of DARs with previously identified NFI-half site compared to background regions. P-value calculated using hypergeometric test. **C)** Model of DNA-binding dependent chromatn closing by FOXP2. **D)** Model of DNA-binding depndent and independent opening of chromatin by a FOXP2-NFI comple

Figure 4.13 *Overlap of differentially expressed and layer correlated genes with WGCNA modules*

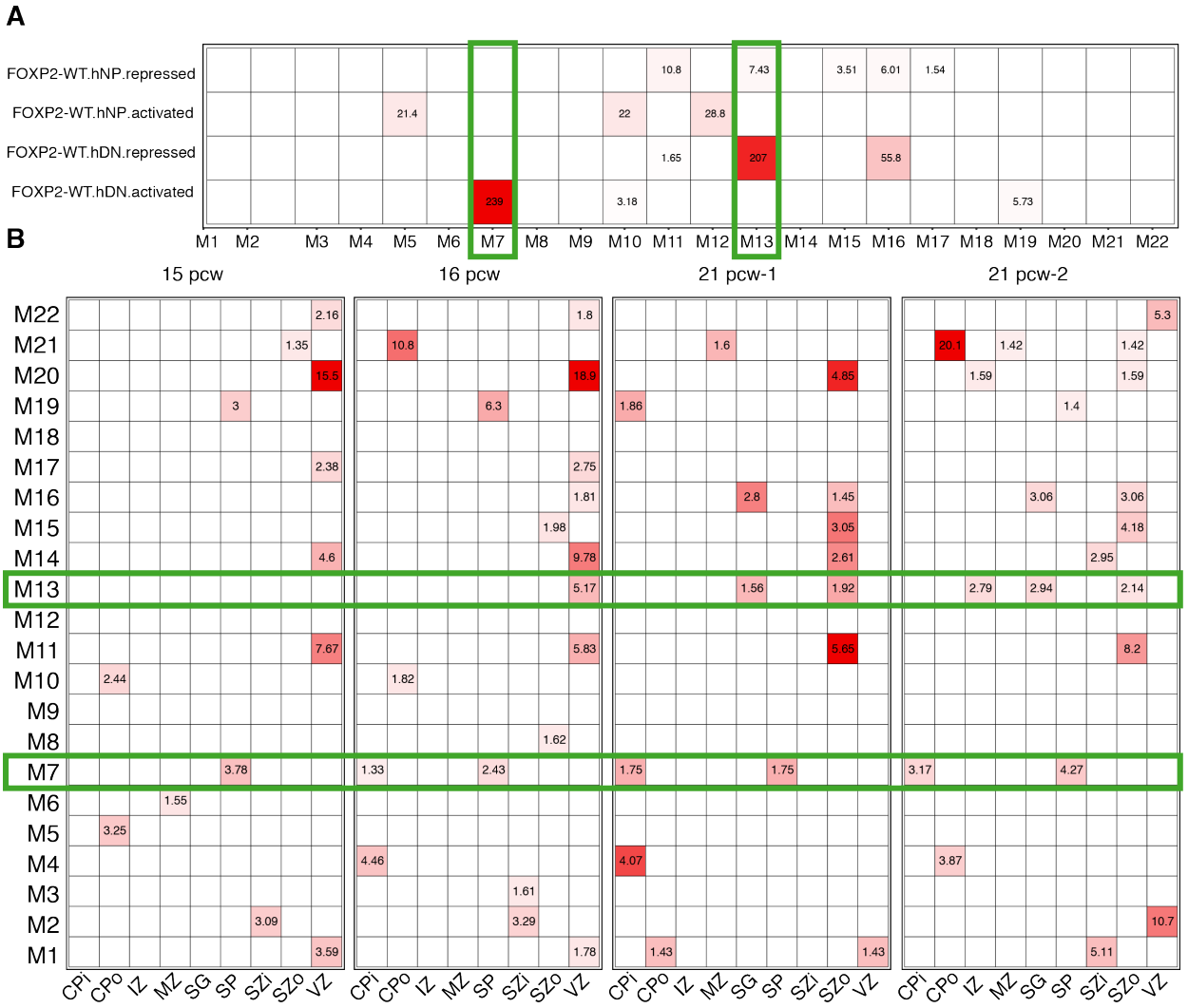

A) Heat map showing significant hypergeometric test –log10 BH adjusted p-values of the overlaps between FOXP2 DE genes from the second RNA-seq experiment with WGCNA modules derived from the same samples. M7 and M13 (outlined in green) have the most significant overlaps between hDN repressed and activated genes, respectively. **B)** Heat map showing significant hypergeometric test –log10 BH adjusted p-values of the overlaps between WGCNA modules and significantly layer-correlated genes across four samples (Miller et al., 2014).

Figure 4.14 *Activated FOXP2 target genes coordinate a subplate layer co-expression module*

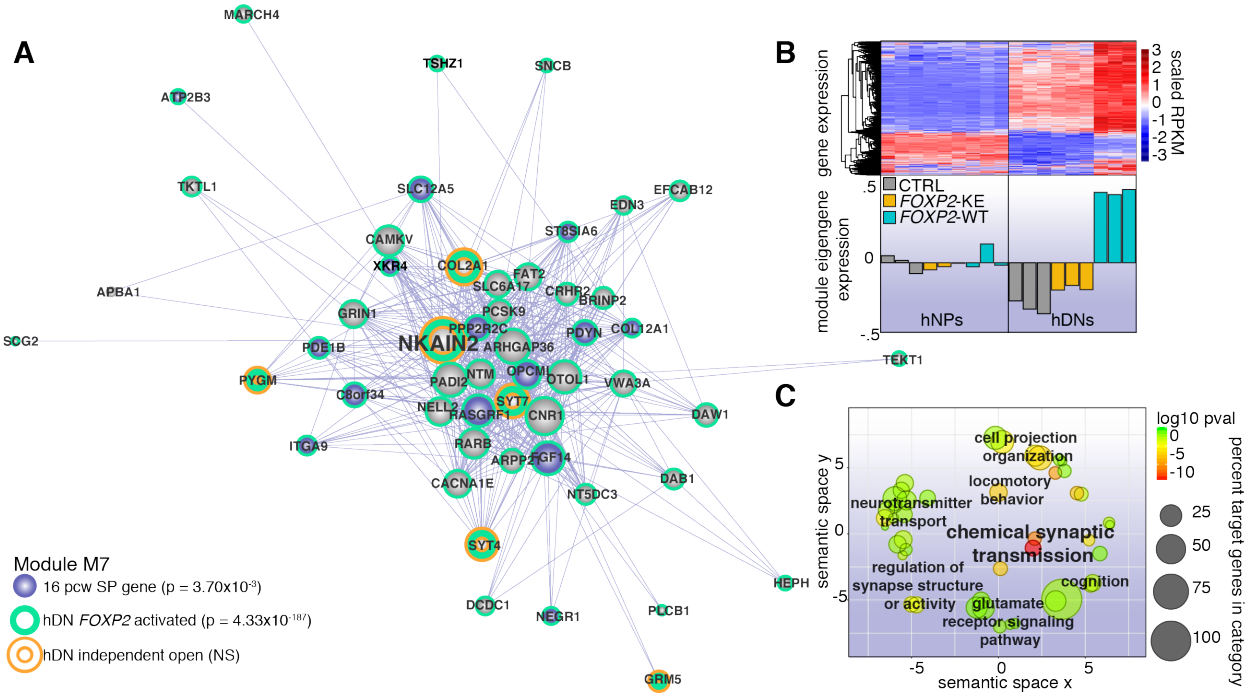

A) Top 500 connections in the WGCNA module most significantly enriched for hDN FOXP2 activated genes. The p-value of the enrichment of 16 pcw layer correlated genes, DE genes, and DAR gene is listed (hypergeometric test, BH corrected for comparison across all modules in the network) (See also Figure S5). Node size represents kwithin or the degree of connectivity within the module. Edge length represents the strength of the correlation between two nodes. **B)** Top: Heat map showing the expression of module genes across samples. Bottom: Expression of the module eigengene in each sample. **C)** Modified Revigo plot of module gene ontology. The relationship between ontological categories is represented in semantic space on the x- and y-axes. The size of the node represents the percent of module genes present in each category. The color of the node represents the enrichment p-value (BH corrected).

Figure 4.15 *Repressed FOXP2 target genes coordinate germinal layer co-expression module*

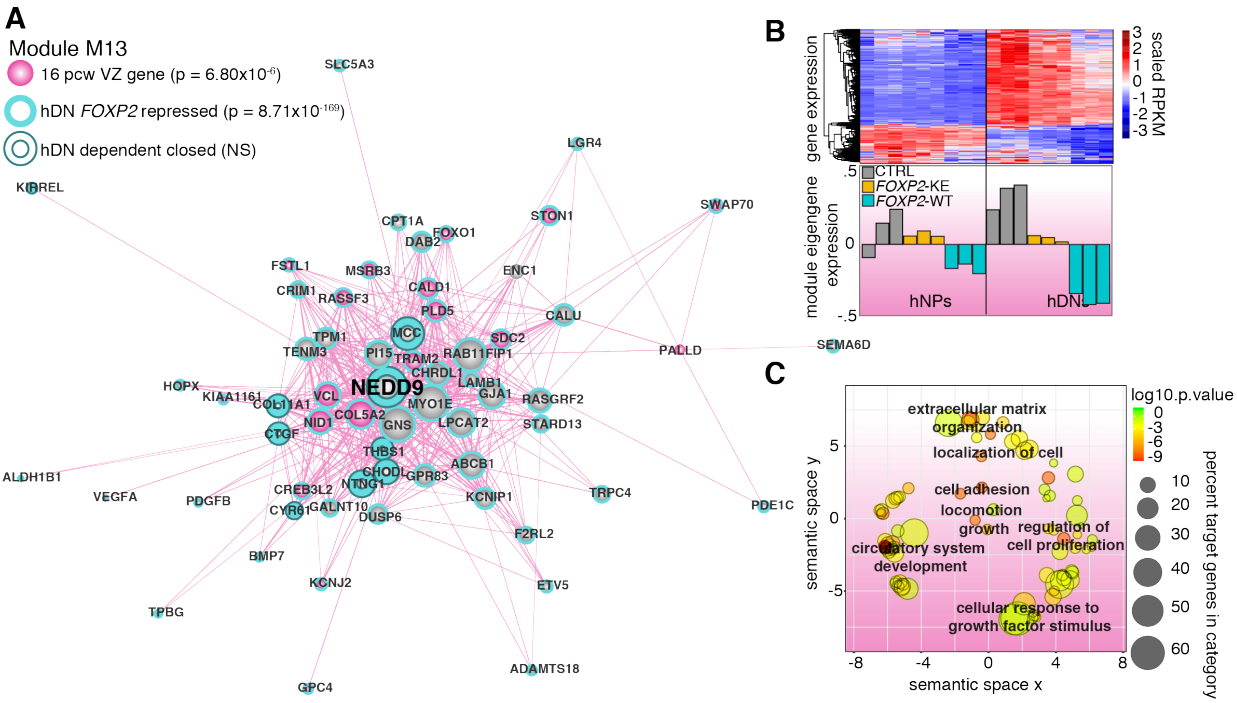

A) Top 500 connections in the WGCNA module most significantly enriched for hDN FOXP2 repressed genes. The p-value of the enrichment of 16 pcw layer correlated genes, DE genes, and DAR gene is listed (hyper-geometric test, BH corrected for comparison across all modules in the network) (See also Figure S5). Node size represents kwithin or the degree of connectivity within the module. Edge length represents the strength of the correlation between two nodes. **B)** Top: Heat map showing the expression of module genes across samples. Bottom: Expression of the module eigengene in each sample. **C)** Modified Revigo plot of module gene ontology. The relationship between ontological categories is represented in semantic space on the x- and y-axes. The size of the node represents the percent of module genes present in each category. The color of the node represents the enrichment p-value (BH corrected).

Tables

Table 4.1 *Direct targets of FOXP2 in hNPs (Corresponds to figure 4.2)*

Table 4.1	Line1 log2 fold change		Line2 log2 fold change		ChIP-seq binding position		
Gene	**DESeq**	**EdgeR**	**DESeq2**	**EdgeR**	**Chr**	**start**	**end**
ABCD4	0.621	0.618	0.444	0.437	chr14	74790800	74800899
ADA	1.657	1.649	0.470	0.470	chr20	43210500	43211399
ADAM9	0.476	0.470	0.849	0.841	chr8	38851900	38857099
ADAMTS16	-1.018	-1.019	-1.319	-1.339	chr5	6092200	6096999
ADAMTS3	0.454	0.448	1.365	1.356	chr4	73282000	73287899
ADAMTS9	0.573	0.567	2.434	2.426	chr3	64669900	64672999
ADAMTSL1	1.584	1.583	1.528	1.520	chr9	17613300	17617399
AFF3	-0.638	-0.651	-1.120	-1.123	chr2	100896900	100899399
AK4	1.532	1.522	1.275	1.268	chr1	65613300	65615499
ALDH9A1	1.206	1.200	1.095	1.088	chr1	165663200	165667999
ALK	0.533	0.528	1.960	1.952	chr2	29504200	29505099
ANO1	-0.314	-0.319	-0.939	-0.949	chr11	69982600	69985799
APOLD1	0.555	0.547	0.640	0.657	chr12	12877500	12879499
APP	0.926	0.921	0.694	0.686	chr21	27540400	27544499
ARID5A	-0.466	-0.468	-0.681	-0.690	chr2	97068200	97085799
ASPH	0.433	0.427	0.442	0.434	chr8	62747500	62755099
ATF3	-1.699	-1.705	-1.398	-1.403	chr1	212838300	212843099
ATP10A	0.593	0.594	0.594	0.584	chr15	25929300	25935899
ATP2B1	0.422	0.415	0.875	0.867	chr12	90276500	90278399
BATF3	-0.376	-0.376	-0.400	-0.410	chr1	212838300	212843099
BBC3	-0.631	-0.635	-0.438	-0.443	chr19	47757900	47761999
BCL6	0.467	0.464	0.784	0.778	chr3	187768700	187771399
BCOR	-0.347	-0.349	-0.477	-0.483	chrX	39872800	39874099
BMP7	1.114	1.108	0.842	0.836	chr20	55321800	55324999
BOC	0.611	0.607	0.921	0.913	chr3	112892500	112893599
BTG2	-0.771	-0.775	-1.116	-1.123	chr1	203291600	203297399
C12orf65	-0.435	-0.441	-0.371	-0.373	chr12	123751500	123755799
C21orf62	0.314	0.308	0.518	0.509	chr21	34289000	34293399
C3orf38	-0.472	-0.481	-0.348	-0.354	chr3	88960800	88962599
CACNA1E	-0.537	-0.499	1.184	1.180	chr1	181063400	181067099
CALR	0.879	0.874	0.688	0.681	chr19	13047700	13051099
CBLN1	2.712	2.700	1.747	1.737	chr16	49727700	49737799
CBLN4	-0.752	-0.760	-0.876	-0.893	chr20	54790000	54796399
CBX4	-0.464	-0.469	-0.579	-0.588	chr17	77810600	77812599
CCDC66	-0.961	-0.971	-0.678	-0.685	chr3	57079800	57083499
CCND1	-1.201	-1.224	1.138	1.131	chr11	69256300	69259099
CDCA7	0.410	0.401	-0.888	-0.900	chr2	174114600	174116299

Table 4.1	Line1 log2 fold change		Line2 log2 fold change		ChIP-seq binding position		
Gene	**DESeq**	**EdgeR**	**DESeq2**	**EdgeR**	**Chr**	**start**	**end**
CECR2	0.309	0.304	0.357	0.349	chr22	17744700	17749999
CGNL1	0.811	0.806	-0.572	-0.581	chr15	57508600	57513799
CHD2	-0.352	-0.357	-0.375	-0.383	chr15	93340000	93356899
CHEK2	0.687	0.673	1.193	1.184	chr22	29136800	29139099
CHL1	0.549	0.544	0.364	0.356	chr3	112500	117099
CHN2	-0.394	-0.417	-1.179	-1.216	chr7	28722000	28728599
CHODL	0.664	0.658	-1.111	-1.127	chr21	19191500	19192399
CITED2	-0.498	-0.504	-0.655	-0.662	chr6	139693700	139697399
CLU	1.020	1.015	0.352	0.344	chr8	27467900	27470299
CNTN3	0.867	0.876	0.704	0.694	chr3	73773300	73775399
COL1A2	0.592	0.598	0.447	0.440	chr7	93869000	93870299
COL22A1	1.127	1.123	0.382	0.374	chr8	140287800	140290699
COPZ2	0.565	0.553	-1.181	-1.204	chr17	46078700	46084499
CREB5	-0.474	-0.483	0.373	0.366	chr7	28722000	28728599
CRLF3	-0.331	-0.346	0.398	0.395	chr17	29033700	29036199
CRYAB	1.314	1.312	1.020	1.013	chr11	111780900	111789099
CSPG4	4.095	4.088	1.926	1.921	chr15	75984100	75990999
CSRP1	0.849	0.845	1.023	1.016	chr1	201534200	201535999
CTNND1	0.393	0.375	0.741	0.737	chr11	57545100	57548199
DACH1	-0.540	-0.599	-0.377	-0.387	chr13	72332300	72335899
DAP	0.735	0.732	0.540	0.532	chr5	11407700	11408399
DDX20	-0.506	-0.510	-0.349	-0.357	chr1	112276100	112282799
DFNA5	0.747	0.741	1.008	1.001	chr7	24930500	24931599
DIRAS3	1.079	1.066	1.548	1.539	chr1	68638000	68640499
DKK3	1.387	1.382	0.601	0.594	chr11	11997900	12002199
DOCK4	-0.718	-0.726	-1.310	-1.320	chr7	111843500	111846999
DPY19L1	0.772	0.766	1.646	1.639	chr7	34758700	34764899
DUSP4	-0.577	-0.583	-0.695	-0.703	chr8	29887300	29893699
EEF1A1	0.668	0.663	0.417	0.410	chr6	74287400	74292299
EGF	0.726	0.731	1.004	0.989	chr4	111008100	111013699
EIF2S2	-0.624	-0.631	-0.402	-0.409	chr20	32580900	32588699
ELOVL2	0.311	0.305	1.472	1.467	chr6	11043300	11044099
ELOVL6	0.414	0.407	1.832	1.825	chr4	111008100	111013699
EMID1	1.497	1.493	2.717	2.701	chr22	29546800	29552399
EPHA3	-0.422	-0.441	-1.714	-1.725	chr3	88960800	88962599
EVA1C	0.330	0.327	0.629	0.619	chr21	33892800	33898099
EXTL3	0.503	0.498	0.322	0.314	chr8	28510600	28520799
F3	0.806	0.801	0.396	0.387	chr1	95055700	95059999
FAM107A	0.964	0.959	1.773	1.767	chr3	58565700	58571299
FAM110B	-0.710	-0.716	-0.826	-0.831	chr8	59167500	59172599
FAM150B	0.838	0.819	-0.682	-0.699	chr2	393300	395999

Table 4.1	Line1 log2 fold change		Line2 log2 fold change		ChIP-seq binding position		
Gene	**DESeq**	**EdgeR**	**DESeq2**	**EdgeR**	**Chr**	**start**	**end**
FAM49B	0.484	0.477	0.612	0.604	chr8	130994300	130998899
FAM84B	0.726	0.719	1.635	1.628	chr8	127640000	127645899
FASTKD3	-0.772	-0.780	-0.380	-0.388	chr5	7760500	7763999
FBLN2	1.917	1.914	1.967	1.972	chr3	13567500	13571899
FGFBP3	0.609	0.601	0.484	0.477	chr10	93641600	93653799
FNBP4	-0.676	-0.683	-0.341	-0.349	chr11	47789200	47791499
FOXP1	-1.071	-1.080	-0.761	-0.767	chr3	71630900	71636099
FOXP2	11.893	11.894	11.170	11.163	chr7	114267400	114268799
FRMD4A	0.818	0.813	1.019	1.011	chr10	13875800	13878599
FUT10	0.597	0.590	0.685	0.674	chr8	32640700	32641399
GAD1	-0.510	-0.515	-1.080	-1.088	chr2	171673700	171679599
GADD45A	-1.290	-1.296	-0.837	-0.844	chr1	68110100	68114599
GALC	0.318	0.310	0.370	0.360	chr14	88094500	88098199
GALNT2	0.646	0.641	0.476	0.469	chr1	230288300	230291499
GLI3	0.563	0.559	0.610	0.602	chr7	42190100	42196799
GNG12	0.630	0.625	1.293	1.286	chr1	68296100	68298999
GRB14	0.534	0.523	2.347	2.339	chr2	165461700	165464099
GRID1	0.381	0.378	0.949	0.937	chr10	88124700	88126599
GSE1	-0.596	-0.603	-0.410	-0.418	chr16	85239900	85241099
HDAC11	0.536	0.538	0.515	0.515	chr3	13567500	13571899
HIVEP3	0.355	0.350	0.718	0.709	chr1	42414100	42422899
HMGA2	-0.757	-0.810	1.478	1.471	chr12	66289500	66292099
IGFBP2	0.894	0.889	1.048	1.041	chr2	217508100	217511599
IL17RD	0.667	0.661	0.844	0.836	chr3	57193900	57195899
INTS6	-0.777	-0.786	-0.516	-0.523	chr13	52026700	52027999
IRS2	-0.525	-0.531	-0.468	-0.476	chr13	110773700	110777799
JAG1	-0.422	-0.428	0.597	0.590	chr20	11330400	11333199
KAT6B	-0.307	-0.312	-0.673	-0.681	chr10	76177200	76180699
KCTD15	-0.576	-0.577	-0.303	-0.309	chr19	34287400	34288899
KDM4B	-0.395	-0.400	-0.332	-0.339	chr19	5192200	5199599
KIAA0922	0.711	0.705	0.339	0.336	chr4	154455300	154458399
KIF16B	0.525	0.522	0.320	0.310	chr20	16002600	16009199
KLF10	-1.169	-1.176	-1.538	-1.544	chr8	103816000	103822199
KLF12	0.488	0.481	0.425	0.418	chr13	74706100	74709199
KREMEN1	1.048	1.043	3.171	3.158	chr22	29546800	29552399
LDB2	0.499	0.497	-0.475	-0.486	chr4	16591800	16594299
LDLRAD3	0.566	0.560	0.430	0.423	chr11	36126100	36127799
LFNG	2.356	2.354	1.763	1.756	chr7	2559900	2564099
LIPG	0.885	0.879	0.496	0.488	chr18	47091500	47093099
LMCD1	-0.491	-0.493	1.660	1.656	chr3	8538500	8543699
LMO4	-0.377	-0.384	-0.434	-0.441	chr1	88164500	88166699

Table 4.1	Line1 log2 fold change		Line2 log2 fold change		ChIP-seq binding position		
Gene	**DESeq**	**EdgeR**	**DESeq2**	**EdgeR**	**Chr**	**start**	**end**
LPP	-0.404	-0.411	0.674	0.667	chr3	187768700	187771399
LRRC4	0.335	0.334	0.446	0.440	chr7	127614200	127618999
LYPD1	-1.883	-1.883	-0.352	-0.359	chr2	133560600	133562499
LZTS1	-0.995	-0.999	-1.172	-1.180	chr8	20165200	20169599
MAML3	1.346	1.329	0.908	0.905	chr4	141069500	141074099
MAN1A1	-0.399	-0.411	0.348	0.340	chr6	119467200	119472899
MAN2A1	-0.880	-0.891	-0.593	-0.601	chr5	108786700	108787899
MAP2	0.333	0.328	0.366	0.358	chr2	210304200	210312099
MAP6	0.713	0.708	0.439	0.431	chr11	75349800	75351699
MAPK4	0.986	0.982	0.728	0.720	chr18	48202900	48208499
MARCKS	0.385	0.379	0.368	0.360	chr6	114172200	114180699
MBOAT7	0.405	0.401	0.386	0.379	chr19	54692500	54695299
MDFIC	0.713	0.704	1.193	1.184	chr7	114267400	114268799
MEF2C	0.395	0.384	0.488	0.480	chr5	88080400	88082499
MFSD6	0.682	0.660	1.627	1.622	chr2	191331100	191335099
MGST3	0.744	0.741	0.502	0.495	chr1	165663200	165667999
MKX	-2.441	-2.427	-2.889	-2.858	chr10	28033100	28034399
MNT	-0.500	-0.505	-0.354	-0.359	chr17	2301700	2306499
MR1	0.710	0.688	0.575	0.569	chr1	181063400	181067099
MRO	1.599	1.556	0.471	0.459	chr18	48202900	48208499
MXI1	0.673	0.666	1.323	1.318	chr10	111966400	111972099
MYO16	-0.478	-0.486	-0.598	-0.609	chr13	109926600	109929199
MYO1E	-0.468	-0.473	-0.587	-0.594	chr15	59581800	59593299
MYOZ3	1.330	1.327	1.561	1.551	chr5	150014900	150023799
NAB2	0.305	0.301	0.528	0.522	chr12	57478700	57484999
NAV1	0.411	0.406	0.884	0.876	chr1	201662800	201667499
NDFIP1	0.484	0.479	0.458	0.451	chr5	141433900	141449999
NHLRC3	0.569	0.560	1.120	1.115	chr13	40088400	40092199
NIN	0.726	0.719	0.759	0.752	chr14	51248400	51253399
NLGN1	0.310	0.303	0.854	0.845	chr3	173918500	173920999
NR4A3	-1.421	-1.422	-0.714	-0.717	chr9	102577600	102587599
NRP1	0.345	0.339	0.841	0.834	chr10	33640500	33645399
NRP2	0.579	0.573	0.974	0.966	chr2	206575500	206587299
NUAK2	0.348	0.345	-0.921	-0.934	chr1	205322100	205331799
PCDHGC5	0.675	0.671	0.638	0.630	chr5	140872600	140877299
PDGFRA	-0.416	-0.422	-1.273	-1.282	chr4	54968300	54977399
PDLIM1	0.488	0.482	0.341	0.335	chr10	97173000	97177599
PDZRN3	0.417	0.412	0.394	0.388	chr3	73773300	73775399
PEX2	0.454	0.448	0.375	0.368	chr8	77598100	77602199
PGBD5	1.575	1.592	0.727	0.723	chr1	230288300	230291499
PHF17	-1.456	-1.463	-0.515	-0.519	chr4	129305600	129311199

Table 4.1	Line1 log2 fold change		Line2 log2 fold change		ChIP-seq binding position		
Gene	**DESeq**	**EdgeR**	**DESeq2**	**EdgeR**	**Chr**	**start**	**end**
PHF21B	-1.099	-1.106	-0.925	-0.930	chr22	45400000	45403999
PHLPP1	0.512	0.507	0.307	0.301	chr18	60413300	60420999
PIGN	0.348	0.336	0.394	0.384	chr18	59614600	59619999
PKM	0.308	0.303	0.548	0.540	chr15	72522700	72525799
PLXNA1	0.937	0.932	1.036	1.028	chr3	127140200	127148599
PLXNA2	0.386	0.381	-0.371	-0.371	chr1	208686000	208690299
PLXNA4	0.731	0.726	0.528	0.520	chr7	131749800	131754399
POC5	-0.540	-0.558	-0.334	-0.340	chr5	74954600	74962099
POU3F3	0.306	0.301	0.338	0.334	chr2	105020500	105023399
PPP1R14C	-0.669	-0.685	-0.848	-0.855	chr6	150411700	150415999
PRCP	0.698	0.692	0.778	0.770	chr11	82464400	82469499
PSAP	0.567	0.562	0.360	0.353	chr10	73619500	73622499
PTGFRN	0.866	0.861	0.574	0.567	chr1	117416200	117422299
PTK2	0.653	0.647	1.217	1.210	chr8	142047200	142051299
RAB11A	0.366	0.360	0.454	0.447	chr15	66314800	66318199
RAB11FIP1	0.833	0.827	0.801	0.793	chr8	37747300	37751399
RAB30	0.317	0.306	1.009	1.006	chr11	82780700	82785999
RAB31	0.620	0.614	0.429	0.421	chr18	9740600	9745199
RALY	0.427	0.423	0.469	0.462	chr20	32580900	32588699
RBL2	0.443	0.436	0.392	0.384	chr16	53122600	53125399
RFC3	0.804	0.795	0.435	0.425	chr13	35163900	35170099
RGMA	1.633	1.629	1.148	1.141	chr15	94472200	94473799
RGMB	0.322	0.316	0.398	0.391	chr5	97331400	97336599
RNASEH2B	-0.404	-0.416	-0.398	-0.409	chr13	50693500	50700799
RPE65	-0.913	-0.922	-0.587	-0.597	chr1	68849600	68851599
RPL23A	0.662	0.657	0.397	0.389	chr17	27044500	27047699
RPN2	0.656	0.651	0.490	0.482	chr20	35857500	35861999
RPS6KA5	-0.741	-0.758	-0.462	-0.457	chr14	91105000	91112099
RRAS	0.541	0.544	0.582	0.579	chr19	50141200	50147899
RUNX1T1	-0.543	-0.566	-0.641	-0.650	chr8	93285100	93286199
RYBP	-0.912	-0.921	-0.509	-0.517	chr3	72706000	72711399
SARNP	-1.175	-1.157	-1.132	-1.111	chr12	56138300	56140399
SCAMP1	0.426	0.419	0.564	0.556	chr5	77932700	77945899
SCARA3	1.458	1.453	1.667	1.660	chr8	27521800	27523999
SCGN	0.702	0.687	-0.504	-0.513	chr6	25446600	25450999
SCRN1	0.479	0.473	0.535	0.527	chr7	30015100	30018099
SEMA6A	0.728	0.722	1.224	1.216	chr5	115907300	115913099
SEMA6B	1.681	1.678	3.613	3.601	chr19	4580700	4582199
SEPN1	0.830	0.825	0.690	0.682	chr1	26021800	26026099
SESN3	0.853	0.847	0.348	0.340	chr11	95068600	95073199
SHB	-0.523	-0.525	-0.405	-0.411	chr9	38284300	38286299

Table 4.1	Line1 log2 fold change		Line2 log2 fold change		ChIP-seq binding position		
Gene	**DESeq**	**EdgeR**	**DESeq2**	**EdgeR**	**Chr**	**start**	**end**
SLC17A5	0.891	0.879	0.993	0.989	chr6	74287400	74292299
SLC1A3	0.465	0.460	0.446	0.439	chr5	36657000	36666999
SLC22A4	-0.755	-0.704	-0.766	-0.779	chr5	131594700	131595599
SLC24A3	1.025	1.020	1.159	1.134	chr20	19738200	19741499
SLC39A11	0.493	0.495	0.647	0.636	chr17	70146000	70150199
SLC44A1	0.649	0.642	0.828	0.820	chr9	108069700	108070699
SLC44A3	0.889	0.879	0.752	0.736	chr1	95055700	95059999
SLC4A4	0.321	0.315	1.251	1.257	chr4	71993600	71997899
SLC6A1	0.708	0.702	-0.555	-0.564	chr3	10943000	10945899
SLC6A11	1.782	1.772	1.001	0.974	chr3	10943000	10945899
SLC6A6	-2.375	-2.340	-1.441	-1.450	chr3	14370700	14372099
SMYD3	-0.732	-0.737	-0.464	-0.471	chr1	245762200	245765499
SOBP	-0.460	-0.468	-0.768	-0.776	chr6	108140400	108142599
SOX13	-0.732	-0.733	0.500	0.494	chr1	203963900	203968199
SOX21	-1.303	-1.311	-1.253	-1.258	chr13	95780200	95781399
SOX5	-0.536	-0.542	-0.848	-0.857	chr12	24713600	24718199
SOX6	-0.621	-0.628	-0.826	-0.835	chr11	16624300	16631299
SPEG	0.564	0.560	0.347	0.340	chr2	220314700	220320299
SPOCK2	0.539	0.535	-0.652	-0.667	chr10	73738700	73745799
SRI	0.790	0.785	0.605	0.597	chr7	87846600	87850699
ST3GAL5	0.313	0.301	0.688	0.680	chr2	86261300	86264799
ST8SIA2	1.090	1.090	1.199	1.191	chr15	92885600	92890799
STC1	0.653	0.639	0.579	0.570	chr8	23779400	23787499
STIM2	0.549	0.544	0.749	0.742	chr4	26786200	26788999
STRA6	0.781	0.778	1.083	1.077	chr15	74512100	74518699
SUB1	0.422	0.415	0.432	0.425	chr5	32501500	32509099
TAPT1	-0.403	-0.411	-0.563	-0.571	chr4	16591800	16594299
TCF7L2	0.515	0.509	0.488	0.481	chr10	114706800	114711099
TENM3	0.754	0.745	0.723	0.715	chr4	183305400	183307099
TLE1	-0.320	-0.326	-0.508	-0.516	chr9	84299500	84305099
TLN2	0.445	0.442	0.847	0.840	chr15	62836300	62839199
TMEM107	0.482	0.481	0.501	0.488	chr17	8090700	8093099
TMEM200C	-0.512	-0.511	-0.384	-0.387	chr18	5673100	5675099
TMEM51	1.084	1.080	1.535	1.531	chr1	15080500	15087199
TNRC18	0.358	0.352	0.375	0.368	chr7	5461200	5467299
TNRC6C	-0.431	-0.429	-0.315	-0.322	chr17	75464800	75475599
TNS1	1.705	1.702	2.537	2.526	chr2	218874000	218881299
TPM4	0.408	0.402	1.019	1.011	chr19	16197700	16198499
TRPM8	-0.519	-0.524	-1.199	-1.213	chr2	234881600	234885199
TTYH3	1.178	1.173	0.439	0.432	chr7	2653700	2658999
TUBB2A	0.755	0.751	0.757	0.750	chr6	3191400	3198499

Table 4.1	Line1 log2 fold change		Line2 log2 fold change		ChIP-seq binding position		
Gene	**DESeq**	**EdgeR**	**DESeq2**	**EdgeR**	**Chr**	**start**	**end**
TUBB2B	0.702	0.697	0.832	0.824	chr6	3340800	3344499
TUBE1	-1.165	-1.167	-0.964	-0.964	chr6	112526000	112531899
VEGFA	-1.190	-1.196	-1.201	-1.209	chr6	44016600	44024099
VIM	0.423	0.417	0.364	0.357	chr10	17268200	17278599
WLS	0.871	0.866	1.137	1.129	chr1	68849600	68851599
XPC	-0.862	-0.864	-0.765	-0.773	chr3	14370700	14372099
ZBTB7B	-0.385	-0.390	-0.332	-0.339	chr1	154970400	154977199
ZFP36L2	-0.454	-0.461	-0.853	-0.859	chr2	43448000	43450299
ZIC1	0.353	0.347	0.312	0.305	chr3	147124500	147127799
ZIC4	0.921	0.912	0.852	0.847	chr3	147124500	147127799
ZNF140	-0.889	-0.894	-0.376	-0.380	chr12	133656300	133658199
ZNF414	-0.396	-0.393	-0.474	-0.474	chr19	8589200	8592699
ZNF462	0.310	0.306	0.619	0.612	chr9	109622600	109628999
ZNRF2	0.654	0.643	0.615	0.610	chr7	30211900	30216299

Table 4.2 *DARs near differentially expressed genes (corresponds to figure 4.8)*

Table 4.2							
Gene	**DAR Type**	**Differential expression**	**Chr**	**Start**	**End**	**Annotation**	**BPs to TSS**
SEPT9	hNP repressed	CTRL hNP DAR	chr17	77470834	77473296	intron 1 of 2	-3178
ABCA1	hDN repressed	FOXP2 hNP DAR	chr9	104873146	104873746	intron 5 of 7	54800
ACSL3	hDN repressed	FOXP2 hNP DAR	chr2	222939231	222939657	intron 4 of 4	78430
ACSL3	hDN repressed	FOXP2 hNP DAR	chr2	222866187	222866651	intron 1 of 3	5405
ACTN4	hDN repressed	CTRL hNP DAR	chr19	38642991	38645579	Intergenic	-3342
ADAM9	hDN repressed	FOXP2 hNP DAR	chr8	39038027	39038507	intron 11 of 19	41281
ADAMTS8	hDN activated	CTRL hNP DAR	chr11	130403140	130404020	TTS	25064
ADAMTSL1	hDN activated	FOXP2 hNP DAR	chr9	18045303	18045709	Intergenic	-428575
ADAMTSL1	hDN activated	FOXP2 hNP DAR	chr9	18268322	18268852	Intergenic	-205494
ADAMTSL1	hDN activated	FOXP2 hNP DAR	chr9	18490552	18491175	intron 1 of 28	16782
ADAMTSL1	hDN activated	FOXP2 hNP DAR	chr9	18478594	18479245	intron 1 of 28	4838
ADAMTSL1	hDN activated	FOXP2 hNP DAR	chr9	18472847	18473463	promoter-TSS	-926
ADCY9	hDN repressed	CTRL hNP DAR	chr16	4109067	4109914	intron 1 of 3	6695
ADD2	hDN activated	CTRL hNP DAR	chr2	70746053	70747170	intron 1 of 3	21104
ADGRB3	hDN activated	FOXP2 hNP DAR	chr6	68826288	68826993	intron 3 of 31	190900
ADGRL3	hDN activated	CTRL hNP DAR	chr4	61506033	61506678	intron 1 of 23	9234
ADGRL3	hDN activated	CTRL hNP DAR	chr4	61336272	61337413	intron 1 of 24	-160279
ADGRL4	hNP activated	FOXP2 hNP DAR	chr1	79006523	79007046	promoter-TSS	26
ADORA2B	hNP repressed	CTRL hNP DAR	chr17	15965460	15967269	intron 1 of 1	21447
AGL	hDN activated	FOXP2 hDN DAR	chr1	99843828	99844103	Intergenic	-6119
AIM1	hDN activated	CTRL hNP DAR	chr6	106517668	106518062	intron 1 of 19	6010

Table 4.2

Gene	DAR Type	Differential expression	Chr	Start	End	Annotation	BPs to TSS
AMPH	hDN activated	FOXP2 hNP DAR	chr7	38506882	38507158	intron 2 of 19	124547
AMPH	hDN activated	FOXP2 hNP DAR	chr7	38584238	38584907	intron 1 of 19	46995
AMPH	hDN activated	FOXP2 hNP DAR	chr7	38520744	38521094	intron 2 of 19	110648
ANGPTL1	hDN repressed	CTRL hNP DAR	chr1	178870842	178871593	promoter-TSS	-137
ANK3	hDN activated	FOXP2 hNP DAR	chr10	60222052	60222383	intron 8 of 43	-81201
ANK3	hDN activated	FOXP2 hNP DAR	chr10	60384613	60385341	intron 2 of 43	4899
ANK3	hDN activated	FOXP2 hNP DAR	chr10	60611409	60611777	intron 2 of 2	-38637
ANK3	hDN activated	FOXP2 hNP DAR	chr10	60677757	60678096	intron 1 of 43	55600
ANK3	hDN activated	FOXP2 hNP DAR	chr10	60668142	60668653	intron 1 of 43	65129
ANO6	hDN repressed	FOXP2 hNP DAR	chr12	45343227	45343599	intron 1 of 1	50730
ANOS1	hDN activated	CTRL hNP DAR	chrX	8688686	8689306	intron 2 of 13	43190
ANXA6	hDN activated	FOXP2 hDN DAR	chr5	151121587	151122391	TTS	19666
APBA1	hDN activated	FOXP2 hNP DAR	chr9	69546216	69546643	intron 1 of 12	125930
APBA2	hDN activated	FOXP2 hNP DAR	chr15	29034097	29034708	intron 3 of 14	112765
APLP2	hDN repressed	CTRL hNP DAR	chr11	130037027	130037432	Intergenic	-32592
ARHGAP1	hDN activated	FOXP2 hDN DAR	chr11	46694620	46695164	TTS	5773
ARHGAP29	hDN repressed	FOXP2 hNP DAR	chr1	94266001	94266448	intron 3 of 4	-28473
ARL4C	hNP activated	FOXP2 hNP DAR	chr2	234285532	234285911	Intergenic	211328
ASTN2	hDN repressed	FOXP2 hNP DAR	chr9	116628761	116629076	intron 17 of 22	58297
ASXL3	hDN activated	FOXP2 hDN DAR	chr18	33572068	33572862	intron 1 of 1	-6112
ATP13A5	hDN activated	FOXP2 hNP DAR	chr3	193344317	193345015	intron 8 of 29	34059
BASP1	hDN activated	FOXP2 hNP DAR	chr5	17278637	17278932	Intergenic	61223
BASP1	hDN activated	FOXP2 hNP DAR	chr5	17118701	17119068	intron 2 of 3	-97939
BASP1	hDN activated	FOXP2 hNP DAR	chr5	17106119	17106469	intron 2 of 3	-110529
BIN1	hDN activated	FOXP2 hNP DAR	chr2	127067573	127068385	intron 6 of 14	39348
BIN1	hDN activated	FOXP2 hNP DAR	chr2	127064491	127065287	promoter-TSS	42438
BMP4	hDN activated	FOXP2 hDN DAR	chr14	54165558	54167018	Intergenic	-209452
BNC2	hDN repressed	CTRL hNP DAR	chr9	16709828	16710283	intron 2 of 5	160733
BRINP3	hDN activated	FOXP2 hNP DAR	chr1	189939982	189940398	Intergenic	537439
BRS3	hDN activated	FOXP2 hDN DAR	chrX	136469542	136470132	Intergenic	-18129
C2orf80	hNP repressed	CTRL hNP DAR	chr2	208183833	208184573	intron 1 of 6	5846
C2orf88	hDN activated	FOXP2 hDN DAR	chr2	190137474	190138074	promoter-TSS	14
CACNG4	hDN activated	FOXP2 hNP DAR	chr17	66925937	66926574	Intergenic	-38609
CADM3	hDN activated	FOXP2 hNP DAR	chr1	159163503	159164097	Intergenic	-7787
CALN1	hDN activated	FOXP2 hNP DAR	chr7	72539834	72540298	Intergenic	-127691
CAMK1G	hDN activated	FOXP2 hDN DAR	chr1	209595694	209596383	intron 2 of 12	12338
CASP6	hDN repressed	FOXP2 hDN DAR	chr4	109661965	109664256	intron 3 of 7	40363
CCND1	hDN repressed	CTRL hNP DAR	chr11	69638810	69639640	Intergenic	-1880
CCSER1	hDN activated	CTRL hNP DAR	chr4	90833685	90834071	intron 9 of 9	598847
CD44	hNP activated	CTRL hNP DAR	chr11	35180239	35180757	intron 3 of 4	41628
CD47	hDN repressed	FOXP2 hNP DAR	chr3	108009022	108009517	Intergenic	81819

Table 4.2

Gene	DAR Type	Differential expression	Chr	Start	End	Annotation	BPs to TSS
CDC42EP2	hDN activated	FOXP2 hDN DAR	chr11	65297929	65299823	TTS	-15942
CDH18	hDN activated	FOXP2 hNP DAR	chr5	19930067	19930373	intron 2 of 3	-43948
CDH18	hDN activated	FOXP2 hNP DAR	chr5	19929088	19929437	intron 2 of 3	-42990
CEMIP	hDN repressed	CTRL hNP DAR	chr15	80750507	80751049	intron 2 of 2	-28565
CENPF	hDN repressed	FOXP2 hDN DAR	chr1	214636218	214636757	intron 10 of 19	33298
CHRM3	hDN activated	FOXP2 hNP DAR	chr1	239124951	239125411	Intergenic	-503892
CHRM3	hDN activated	FOXP2 hNP DAR	chr1	239418680	239419107	intron 1 of 2	-210180
CHRM3	hDN activated	FOXP2 hNP DAR	chr1	239538034	239538641	intron 2 of 3	-90736
CHRM3	hDN activated	FOXP2 hNP DAR	chr1	239571436	239571783	intron 3 of 8	-57464
CHRM3	hDN activated	FOXP2 hNP DAR	chr1	239392308	239392620	intron 1 of 3	-236609
CHST7	hNP repressed	CTRL hNP DAR	chrX	46582511	46583862	intron 1 of 1	9499
CHST7	hNP repressed	CTRL hNP DAR	chrX	46649174	46650302	intron 10 of 16	76051
CLDN1	hDN activated	FOXP2 hNP DAR	chr3	190231529	190232377	Intergenic	90493
CLINT1	hDN activated	FOXP2 hNP DAR	chr5	157978042	157978499	Intergenic	-119095
CLINT1	hDN activated	FOXP2 hNP DAR	chr5	158013322	158013753	Intergenic	-154362
CLSTN1	hDN repressed	FOXP2 hDN DAR	chr1	9839994	9840721	Intergenic	-15831
CLSTN2	hNP repressed	FOXP2 hDN DAR	chr3	140073159	140073764	intron 1 of 16	138276
CLSTN2	hNP repressed	FOXP2 hDN DAR	chr3	140086644	140087119	intron 1 of 16	151696
CNKSR2	hDN activated	CTRL hNP DAR	chrX	20857509	20858517	Intergenic	-516405
CNTN6	hNP activated	FOXP2 hNP DAR	chr3	1092485	1093311	promoter-TSS	240
COL2A1	hDN activated	CTRL hNP DAR	chr12	47995697	47996758	intron 7 of 52	8275
COL4A2	hDN repressed	FOXP2 hDN DAR	chr13	110322837	110324876	intron 3 of 47	16572
COL4A6	hDN repressed	CTRL hNP DAR	chrX	108415729	108416245	intron 2 of 44	22443
COLGALT2	hDN repressed	FOXP2 hNP DAR	chr1	183942969	183943642	intron 10 of 11	94465
CPNE4	hDN repressed	FOXP2 hNP DAR	chr3	132064092	132064470	intron 2 of 19	-24675
CPNE4	hDN repressed	FOXP2 hNP DAR	chr3	132083573	132083924	intron 2 of 19	-44142
CPNE4	hDN repressed	FOXP2 hNP DAR	chr3	132135828	132136485	intron 2 of 19	-96550
CPNE5	hDN activated	CTRL hNP DAR	chr6	36786082	36786584	intron 9 of 13	-28924
CPXM2	hDN activated	FOXP2 hDN DAR	chr10	123868418	123869648	intron 3 of 19	22951
CRISPLD1	hDN repressed	CTRL hNP DAR	chr8	75094918	75095386	Intergenic	94998
CSPG4	hNP activated	FOXP2 hNP DAR	chr15	75695059	75695681	intron 1 of 9	17478
CTH	hNP repressed	CTRL hNP DAR	chr1	70442245	70442884	Intergenic	31346
CTH	hNP repressed	CTRL hNP DAR	chr1	70422011	70422580	intron 4 of 10	11077
CTNNA2	hDN activated	FOXP2 hDN DAR	chr2	80306620	80306928	intron 1 of 11	1669
DAB1	hDN activated	FOXP2 hNP DAR	chr1	58340164	58340668	intron 4 of 20	-89877
DCT	hDN activated	CTRL hNP DAR	chr13	94390812	94391371	intron 3 of 4	88591
DDIT4L	hDN activated	FOXP2 hDN DAR	chr4	100343280	100343587	Intergenic	-152935
DEGS1	hDN repressed	FOXP2 hDN DAR	chr1	224196799	224197460	Intergenic	13921
DFNA5	hDN activated	FOXP2 hDN DAR	chr7	24665593	24666006	intron 8 of 12	91665
DGKG	hDN activated	FOXP2 hNP DAR	chr3	186383173	186384052	Intergenic	-21378
DIRAS2	hDN activated	FOXP2 hNP DAR	chr9	90702551	90703026	Intergenic	-59683

Table 4.2

Gene	DAR Type	Differential expression	Chr	Start	End	Annotation	BPs to TSS
DIXDC1	hDN repressed	CTRL hNP DAR	chr11	111983069	111983537	intron 7 of 19	5994
DNAH11	hDN activated	FOXP2 hNP DAR	chr7	21642415	21642805	intron 28 of 82	99395
DNAH11	hDN activated	FOXP2 hNP DAR	chr7	21656130	21656607	intron 29 of 82	113153
DNAH11	hDN activated	FOXP2 hNP DAR	chr7	21617962	21618304	promoter-TSS	74918
DNAH7	hDN activated	CTRL hNP DAR	chr2	196117216	196117815	Intergenic	-48703
DNAH7	hDN activated	CTRL hNP DAR	chr2	196113071	196114113	Intergenic	-44780
DOCK4	hNP repressed	CTRL hNP DAR	chr7	112161447	112163553	intron 1 of 22	43907
DOCK4	hNP repressed	CTRL hNP DAR	chr7	112112777	112113371	intron 1 of 22	93333
DOCK4	hNP repressed	CTRL hNP DAR	chr7	112050058	112050593	intron 1 of 22	156082
DRP2	hDN activated	FOXP2 hNP DAR	chrX	101207954	101208653	Intergenic	-11641
DSC3	hDN activated	CTRL hNP DAR	chr18	30763660	30764514	Intergenic	278728
DSC3	hDN activated	CTRL hNP DAR	chr18	30944888	30945440	Intergenic	97651
EHBP1	hNP activated	FOXP2 hNP DAR	chr2	62654992	62655308	intron 2 of 3	-18701
ELAVL2	hDN activated	CTRL hNP DAR	chr9	23829551	23830029	exon 1 of 5	-3725
EMP1	hDN repressed	CTRL hNP DAR	chr12	13195692	13197204	promoter-TSS	-220
EN1	hDN activated	FOXP2 hDN DAR	chr2	118784096	118785055	Intergenic	63608
EN1	hDN activated	FOXP2 hDN DAR	chr2	118847598	118848098	promoter-TSS	335
EPHX1	hDN repressed	FOXP2 hNP DAR	chr1	225799903	225800457	Intergenic	-9894
ERRFI1	hDN repressed	CTRL hNP DAR	chr1	8027979	8028456	intron 1 of 2	-1884
ETV5	hDN repressed	CTRL hNP DAR	chr3	186044816	186045481	Intergenic	63964
EVA1C	hDN repressed	FOXP2 hNP DAR	chr21	32406297	32406840	Intergenic	-5869
F2RL2	hDN repressed	FOXP2 hNP DAR	chr5	76623234	76623647	promoter-TSS	-6
FAM101A	hDN activated	FOXP2 hDN DAR	chr12	124144421	124145016	intron 2 of 4	-144446
FAM101A	hDN activated	FOXP2 hDN DAR	chr12	124175367	124176146	intron 3 of 4	-113408
FAM122A	hDN repressed	FOXP2 hNP DAR	chr9	68851557	68852174	intron 5 of 20	71817
FAM181B	hDN activated	FOXP2 hNP DAR	chr11	82737893	82738498	Intergenic	-4331
FAM184B	hNP activated	FOXP2 hNP DAR	chr4	17762705	17763875	intron 1 of 17	18222
FAM184B	hNP activated	FOXP2 hNP DAR	chr4	17709544	17710224	intron 1 of 17	71628
FAM189A2	hDN activated	FOXP2 hNP DAR	chr9	69443845	69444429	intron 10 of 12	114812
FAM189A2	hDN activated	FOXP2 hNP DAR	chr9	69445231	69445707	intron 10 of 12	116144
FAM189A2	hDN activated	FOXP2 hNP DAR	chr9	69460075	69460367	TTS	130896
FAM69A	hDN activated	CTRL hNP DAR	chr1	92879683	92880172	intron 1 of 4	-2777
FAM81B	hDN repressed	FOXP2 hNP DAR	chr5	95471509	95472413	intron 40 of 42	80617
FBN1	hDN repressed	CTRL hNP DAR	chr15	48530397	48531133	intron 8 of 65	115023
FGF13	hDN activated	FOXP2 hDN DAR	chrX	139026499	139027150	intron 1 of 2	-159269
FGFBP3	hDN repressed	CTRL hNP DAR	chr10	91886961	91888115	Intergenic	21963
FGL2	hDN repressed	FOXP2 hNP DAR	chr7	77238125	77238522	intron 3 of 18	-38490
FGL2	hDN repressed	FOXP2 hNP DAR	chr7	77247304	77247522	intron 3 of 3	-47580
FHOD3	hDN repressed	FOXP2 hNP DAR	chr18	36351071	36351895	intron 1 of 24	53787
FHOD3	hDN repressed	FOXP2 hNP DAR	chr18	36350184	36350742	intron 1 of 24	52767
FLNB	hDN repressed	FOXP2 hNP DAR	chr3	57969708	57970324	Intergenic	-38384

Table 4.2

Gene	DAR Type	Differential expression	Chr	Start	End	Annotation	BPs to TSS
FMN2	hDN activated	FOXP2 hNP DAR	chr1	240107041	240107485	intron 1 of 17	15378
FMN2	hDN activated	FOXP2 hNP DAR	chr1	240071612	240072012	intron 2 of 6	-20073
FMNL3	hNP activated	FOXP2 hNP DAR	chr12	49705454	49706093	intron 1 of 3	1641
FNDC1	hDN repressed	CTRL hNP DAR	chr6	159151960	159152523	Intergenic	-17156
FOLH1	hDN activated	FOXP2 hDN DAR	chr11	49283862	49284271	Intergenic	-75396
FRAS1	hDN activated	FOXP2 hDN DAR	chr4	78102162	78102569	intron 2 of 9	44795
FRAS1	hDN activated	FOXP2 hDN DAR	chr4	78075803	78076417	intron 2 of 9	18540
FRAS1	hDN activated	FOXP2 hDN DAR	chr4	78254994	78255527	promoter-TSS	197690
FREM1	hDN activated	FOXP2 hDN DAR	chr9	14780154	14781081	intron 1 of 1	-1084
FREM2	hNP activated	FOXP2 hNP DAR	chr13	38700137	38700444	intron 2 of 23	13254
GABBR1	hNP activated	FOXP2 hNP DAR	chr6	29611477	29612051	promoter-TSS	16464
GABBR1	hNP activated	FOXP2 hNP DAR	chr6	29622331	29622982	promoter-TSS	5572
GABRG3	hNP repressed	FOXP2 hNP DAR	chr15	27025432	27026197	intron 2 of 5	54532
GALNT5	hDN repressed	FOXP2 hDN DAR	chr2	157204442	157204928	Intergenic	-53143
GALNT5	hDN repressed	FOXP2 hDN DAR	chr2	156935642	156936012	Intergenic	-322001
GATM	hDN repressed	CTRL hNP DAR	chr15	45372030	45372902	intron 1 of 3	6316
GDF10	hDN activated	FOXP2 hDN DAR	chr10	47136826	47137213	Intergenic	-163205
GDF10	hDN activated	FOXP2 hDN DAR	chr10	47286739	47287955	Intergenic	-12877
GDPD5	hNP repressed	FOXP2 hDN DAR	chr11	75520081	75521333	intron 1 of 7	4847
GHR	hDN activated	FOXP2 hNP DAR	chr5	42570923	42571816	intron 1 of 7	5505
GJA1	hDN repressed	FOXP2 hNP DAR	chr6	121885841	121886224	Intergenic	450455
GJA1	hDN repressed	FOXP2 hNP DAR	chr6	121770865	121771246	Intergenic	335478
GJA1	hDN repressed	FOXP2 hNP DAR	chr6	121858916	121859425	promoter-TSS	423593
GLUD1	hDN activated	CTRL hNP DAR	chr10	87093669	87096007	promoter-TSS	181
GNAS	hDN activated	CTRL hNP DAR	chr20	58907660	58908362	promoter-TSS	15847
GNG12	hNP activated	FOXP2 hNP DAR	chr1	67889929	67890360	intron 1 of 9	-56672
GNG12	hNP activated	FOXP2 hNP DAR	chr1	67850552	67851238	intron 1 of 9	-17423
GPC4	hDN repressed	CTRL hNP DAR	chrX	133560950	133561653	intron 7 of 7	-146124
GPC4	hDN repressed	CTRL hNP DAR	chrX	133330855	133331414	intron 2 of 8	84043
GPR19	hDN activated	CTRL hNP DAR	chr12	12697916	12698395	Intergenic	-1968
GPR37	hDN activated	FOXP2 hNP DAR	chr7	124566474	124566971	Intergenic	199303
GPR78	hDN repressed	FOXP2 hNP DAR	chr4	8537002	8537533	Intergenic	-42970
GRAMD1B	hDN activated	FOXP2 hDN DAR	chr11	123461038	123461679	TTS	-64278
GRIK2	hDN activated	FOXP2 hDN DAR	chr6	102417509	102417968	Intergenic	1018753
GRIK2	hDN activated	FOXP2 hDN DAR	chr6	102741918	102742392	Intergenic	1343170
GRIK2	hDN activated	FOXP2 hDN DAR	chr6	101344531	101345015	Intergenic	-54212
GRIK2	hDN activated	FOXP2 hDN DAR	chr6	102866937	102867463	Intergenic	1468215
GRIK2	hDN activated	FOXP2 hDN DAR	chr6	103042302	103042856	Intergenic	1643594
GRIK2	hDN activated	FOXP2 hDN DAR	chr6	101650426	101651658	intron 3 of 16	252057
GRIK3	hDN repressed	CTRL hNP DAR	chr1	37082413	37084459	Intergenic	-49193
GRIK4	hNP repressed	CTRL hNP DAR	chr11	120641343	120642242	intron 2 of 3	77356

Table 4.2

Gene	DAR Type	Differential expression	Chr	Start	End	Annotation	BPs to TSS
GRIK4	hNP repressed	CTRL hNP DAR	chr11	120562876	120565548	promoter-TSS	-224
GRIP1	hDN activated	FOXP2 hDN DAR	chr12	66501332	66501867	intron 2 of 18	177546
GRIP1	hDN activated	FOXP2 hDN DAR	chr12	66515378	66516016	TTS	163448
GRM3	hDN activated	FOXP2 hDN DAR	chr7	86707328	86707858	intron 1 of 1	63679
GSX1	hNP repressed	CTRL hNP DAR	chr13	27746547	27746996	Intergenic	-45872
GSX1	hNP repressed	CTRL hNP DAR	chr13	27744287	27745717	Intergenic	-47641
GTF2F2	hDN repressed	CTRL hNP DAR	chr13	45121471	45122066	intron 1 of 7	1272
HIVEP2	hDN activated	CTRL hNP DAR	chr6	142857126	142857670	intron 1 of 9	87803
HIVEP3	hNP activated	FOXP2 hNP DAR	chr1	41842312	41842849	intron 1 of 8	76127
HK1	hDN repressed	CTRL hNP DAR	chr10	69278260	69279380	intron 2 of 5	8820
HLF	hDN activated	FOXP2 hNP DAR	chr17	55334283	55334929	Intergenic	69646
HLF	hDN activated	FOXP2 hNP DAR	chr17	55188365	55188809	Intergenic	-76373
HMP19	hDN activated	FOXP2 hNP DAR	chr5	174084884	174085260	intron 1 of 3	39468
HNMT	hNP repressed	FOXP2 hNP DAR	chr2	138183752	138184088	Intergenic	219682
HNMT	hNP repressed	FOXP2 hNP DAR	chr2	138107377	138107731	Intergenic	143316
HNMT	hNP repressed	FOXP2 hNP DAR	chr2	138201298	138201719	Intergenic	237270
HOPX	hDN repressed	FOXP2 hNP DAR	chr4	56685363	56685887	Intergenic	-3919
HPSE	hDN repressed	FOXP2 hNP DAR	chr4	83320359	83320876	intron 3 of 12	14196
HS3ST1	hNP repressed	FOXP2 hNP DAR	chr4	11514887	11515296	Intergenic	-86178
HS3ST1	hNP repressed	FOXP2 hNP DAR	chr4	11525604	11526196	Intergenic	-96987
HS3ST1	hNP repressed	FOXP2 hNP DAR	chr4	11408238	11408781	intron 1 of 1	20404
HS3ST1	hNP repressed	FOXP2 hNP DAR	chr4	11424006	11424372	intron 1 of 1	4724
HTR2A	hDN activated	FOXP2 hNP DAR	chr13	47215672	47216083	Intergenic	-318801
HTRA1	hDN repressed	FOXP2 hNP DAR	chr10	122469127	122469675	intron 1 of 8	7876
ID3	hDN repressed	CTRL hNP DAR	chr1	23561773	23562783	Intergenic	-2484
IDH2	hDN activated	CTRL hNP DAR	chr15	90054658	90055171	intron 1 of 1	45707
IFIT2	hDN repressed	CTRL hNP DAR	chr10	89314620	89315133	intron 1 of 3	12927
IFITM3	hDN repressed	FOXP2 hNP DAR	chr11	342202	342878	Intergenic	-21626
IGF2R	hDN repressed	FOXP2 hNP DAR	chr6	159978897	159980003	intron 1 of 47	10351
IGSF3	hDN activated	CTRL hNP DAR	chr1	116652795	116653211	intron 2 of 11	13953
INHBA	hDN activated	FOXP2 hNP DAR	chr7	41886096	41886698	Intergenic	-183289
INHBA	hDN activated	FOXP2 hNP DAR	chr7	41834910	41835503	Intergenic	-132098
IQGAP1	hDN repressed	CTRL hNP DAR	chr15	90400733	90401243	intron 2 of 37	12747
ITGA2	hDN repressed	CTRL hNP DAR	chr5	52997175	52997935	intron 1 of 28	8229
ITGA6	hDN activated	CTRL hNP DAR	chr2	172380516	172381360	Intergenic	-46416
ITGAV	hNP repressed	CTRL hNP DAR	chr2	186569806	186570189	Intergenic	-20066
ITGAV	hNP repressed	CTRL hNP DAR	chr2	186543819	186544899	Intergenic	-45704
ITGAV	hNP repressed	CTRL hNP DAR	chr2	186617211	186617548	intron 2 of 29	17174
ITGAV	hNP repressed	CTRL hNP DAR	chr2	186612901	186613500	intron 2 of 29	12995
IVNS1ABP	hDN activated	FOXP2 hNP DAR	chr1	185292605	185293243	exon 1 of 1	24405
KCNB1	hDN activated	FOXP2 hDN DAR	chr20	49479540	49480610	intron 2 of 2	2569

Table 4.2

Gene	DAR Type	Differential expression	Chr	Start	End	Annotation	BPs to TSS
KCND2	hDN activated	CTRL hNP DAR	chr7	120521931	120522664	intron 1 of 5	248629
KCNH1	hDN activated	FOXP2 hNP DAR	chr1	210781223	210781915	intron 9 of 10	352546
KCNIP4	hNP activated	FOXP2 hDN DAR	chr4	20954615	20954930	intron 1 of 8	-72062
KCNJ16	hNP activated	CTRL hNP DAR	chr17	70067061	70067590	exon 3 of 3	-7900
KCNJ2	hDN repressed	FOXP2 hDN DAR	chr17	70563016	70563771	Intergenic	393858
KCNJ6	hDN activated	CTRL hNP DAR	chr21	37817848	37818626	intron 2 of 3	98201
KCNMA1	hNP activated	FOXP2 hDN DAR	chr10	77682318	77682840	Intergenic	-44760
KCNMA1	hNP activated	FOXP2 hDN DAR	chr10	77631253	77631820	intron 1 of 27	6283
KCNQ3	hNP activated	FOXP2 hNP DAR	chr8	132486777	132487408	Intergenic	-6335
KCNQ3	hNP activated	FOXP2 hNP DAR	chr8	132316152	132316713	intron 1 of 14	130830
KDR	hNP activated	FOXP2 hNP DAR	chr4	55078871	55079311	3' UTR	46504
KIRREL	hDN repressed	FOXP2 hNP DAR	chr1	158045357	158046274	intron 1 of 12	52542
KIRREL3	hDN activated	FOXP2 hDN DAR	chr11	126995622	126997571	intron 2 of 3	4274
KLF5	hDN repressed	CTRL hNP DAR	chr13	73056007	73056691	intron 1 of 3	1373
KLHL13	hDN activated	FOXP2 hNP DAR	chrX	117982720	117983116	intron 1 of 6	2495
L3MBTL3	hDN activated	FOXP2 hNP DAR	chr6	129992765	129993319	Intergenic	-25541
LAMP1	hDN repressed	CTRL hNP DAR	chr13	113294401	113296103	Intergenic	-1902
LBH	hNP activated	FOXP2 hNP DAR	chr2	30287139	30287806	intron 2 of 2	55941
LDLRAD3	hDN repressed	CTRL hNP DAR	chr11	35918412	35920170	promoter-TSS	-24690
LGI2	hNP activated	FOXP2 hNP DAR	chr4	25005809	25006231	intron 7 of 7	24772
LHFPL3	hNP repressed	CTRL hNP DAR	chr7	104321916	104322277	Intergenic	-6560
LHFPL3	hNP repressed	CTRL hNP DAR	chr7	104317940	104318396	Intergenic	-10488
LHFPL3	hNP repressed	CTRL hNP DAR	chr7	104367797	104368324	intron 1 of 3	39404
LIMCH1	hDN activated	CTRL hNP DAR	chr4	41638873	41639263	intron 9 of 25	26296
LIMCH1	hDN activated	CTRL hNP DAR	chr4	41365468	41366246	intron 1 of 6	5072
LIMCH1	hDN activated	CTRL hNP DAR	chr4	41369615	41370190	intron 1 of 6	9117
LIPG	hDN repressed	FOXP2 hNP DAR	chr18	49608312	49608829	Intergenic	46539
LMO2	hDN repressed	CTRL hNP DAR	chr11	33890950	33892510	intron 1 of 5	559
LMO2	hDN repressed	CTRL hNP DAR	chr11	33889071	33889788	intron 1 of 5	2860
LMO4	hDN activated	CTRL hNP DAR	chr1	87279125	87279977	Intergenic	-48917
LONRF2	hDN repressed	FOXP2 hDN DAR	chr2	100350055	100351066	Intergenic	-27827
LSAMP	hDN activated	CTRL hNP DAR	chr3	116423247	116423893	intron 1 of 6	21968
LUZP2	hNP repressed	FOXP2 hDN DAR	chr11	24238827	24239777	intron 5 of 5	-257668
MACROD2	hDN activated	FOXP2 hNP DAR	chr20	15220864	15221674	intron 1 of 13	24411
MAN1C1	hDN repressed	CTRL hNP DAR	chr1	25707974	25708620	intron 2 of 11	90829
MAN1C1	hDN repressed	CTRL hNP DAR	chr1	25615314	25619728	promoter-TSS	53
MAP3K1	hDN activated	CTRL hNP DAR	chr5	56763448	56764293	Intergenic	-51203
MAPK4	hNP repressed	CTRL hNP DAR	chr18	50544624	50545079	Intergenic	-15263
MARCKS	hDN activated	FOXP2 hDN DAR	chr6	113829107	113830013	intron 1 of 1	-27775
MARVELD3	hDN repressed	CTRL hNP DAR	chr16	71637321	71638142	promoter-TSS	11578
MATN2	hDN repressed	FOXP2 hNP DAR	chr8	97929008	97929753	intron 2 of 18	60297

Table 4.2

Gene	DAR Type	Differential expression	Chr	Start	End	Annotation	BPs to TSS
MATN2	hDN repressed	FOXP2 hNP DAR	chr8	97890895	97891338	intron 2 of 18	22033
MDFIC	hDN activated	FOXP2 hNP DAR	chr7	114929973	114930393	intron 1 of 3	8029
MEGF9	hDN repressed	CTRL hNP DAR	chr9	120710222	120710670	intron 1 of 5	4041
MEGF9	hDN repressed	CTRL hNP DAR	chr9	120689830	120690927	intron 1 of 5	24109
METTL7A	hNP repressed	CTRL hNP DAR	chr12	50922886	50923189	promoter-TSS	-1714
METTL7A	hNP repressed	CTRL hNP DAR	chr12	50923957	50925505	promoter-TSS	-20
MID1	hDN repressed	FOXP2 hNP DAR	chrX	10634617	10635050	intron 1 of 10	-14199
MKI67	hDN repressed	CTRL hNP DAR	chr10	128167682	128168653	Intergenic	-41963
MMP2	hDN repressed	FOXP2 hNP DAR	chr16	55453821	55454514	intron 1 of 5	-24663
MOB1B	hDN repressed	CTRL hNP DAR	chr4	70894886	70896824	Intergenic	-6485
MOXD1	hNP repressed	FOXP2 hNP DAR	chr6	132456837	132457240	3' UTR	-55504
MOXD1	hNP repressed	FOXP2 hNP DAR	chr6	132297436	132297784	intron 11 of 11	103924
MOXD1	hNP repressed	FOXP2 hNP DAR	chr6	132334284	132334640	intron 4 of 11	67072
MOXD1	hNP repressed	FOXP2 hNP DAR	chr6	132445303	132445550	TTS	-43892
MTTP	hDN repressed	FOXP2 hNP DAR	chr4	99615358	99615799	intron 16 of 18	51500
MXI1	hDN activated	CTRL hNP DAR	chr10	110224225	110224765	intron 1 of 4	-1509
MXI1	hDN activated	CTRL hNP DAR	chr10	110224856	110227941	promoter-TSS	394
MYLK3	hDN activated	FOXP2 hNP DAR	chr16	46748256	46748685	promoter-TSS	-161
MYO1E	hDN repressed	CTRL hNP DAR	chr15	59401677	59402242	promoter-TSS	-29087
MYO3A	hNP activated	FOXP2 hDN DAR	chr10	25966837	25967227	intron 3 of 16	32959
MYO5C	hDN repressed	FOXP2 hNP DAR	chr15	52360793	52361231	intron 24 of 39	-65214
MYO7A	hDN activated	FOXP2 hDN DAR	chr11	77144407	77145125	intron 3 of 48	16496
MYZAP	hDN activated	FOXP2 hDN DAR	chr15	57588366	57589074	Intergenic	-3184
MYZAP	hDN activated	FOXP2 hDN DAR	chr15	57589686	57590088	Intergenic	-2017
NAT8L	hNP repressed	CTRL hNP DAR	chr4	2141286	2143103	intron 7 of 13	82682
NCAM1	hDN activated	FOXP2 hNP DAR	chr11	112811024	112811378	Intergenic	-150046
NCAM2	hNP repressed	FOXP2 hNP DAR	chr21	20973518	20973956	Intergenic	-24578
NDP	hDN activated	CTRL hNP DAR	chrX	44144375	44145055	Intergenic	-171040
NDP	hDN activated	CTRL hNP DAR	chrX	43968209	43970937	TTS	4102
NECAB1	hDN activated	FOXP2 hDN DAR	chr8	90783926	90784583	intron 1 of 5	-7439
NFIX	hDN activated	CTRL hNP DAR	chr19	13016485	13017424	intron 1 of 1	-7017
NGB	hDN activated	FOXP2 hDN DAR	chr14	77275103	77276099	exon 20 of 20	-4289
NHS	hDN repressed	CTRL hNP DAR	chrX	17292047	17292564	Intergenic	-83115
NHSL2	hDN repressed	FOXP2 hNP DAR	chrX	71941864	71942157	intron 1 of 7	30922
NID1	hDN repressed	CTRL hNP DAR	chr1	236027084	236027600	intron 7 of 19	37839
NKAIN2	hDN activated	FOXP2 hDN DAR	chr6	123908577	123909592	intron 1 of 6	105238
NKAIN2	hDN activated	FOXP2 hDN DAR	chr6	124429504	124429827	intron 3 of 6	146660
NKAIN2	hDN activated	FOXP2 hDN DAR	chr6	124610397	124610936	intron 4 of 7	327661
NKAIN2	hDN activated	FOXP2 hDN DAR	chr6	124055586	124056391	intron 1 of 6	-227017
NKAIN2	hDN activated	FOXP2 hDN DAR	chr6	124329928	124330442	intron 2 of 7	47180
NNMT	hDN activated	FOXP2 hNP DAR	chr11	114219777	114220439	intron 2 of 2	-75705

Table 4.2

Gene	DAR Type	Differential expression	Chr	Start	End	Annotation	BPs to TSS
NR3C1	hDN activated	CTRL hNP DAR	chr5	143445647	143446396	Intergenic	-10509
NR3C1	hDN activated	CTRL hNP DAR	chr5	143355689	143356100	intron 2 of 8	47795
NRCAM	hNP activated	FOXP2 hNP DAR	chr7	108413777	108414402	intron 1 of 5	42308
NRCAM	hNP activated	FOXP2 hNP DAR	chr7	108308793	108309453	intron 2 of 5	-68953
NT5E	hDN activated	FOXP2 hNP DAR	chr6	85388418	85389497	exon 2 of 2	-60627
NT5E	hDN activated	FOXP2 hNP DAR	chr6	85473755	85474098	intron 3 of 8	24342
NWD1	hDN repressed	CTRL hNP DAR	chr19	16737932	16738263	intron 3 of 18	18121
OAF	hDN activated	FOXP2 hNP DAR	chr11	120217638	120219040	TTS	7300
OGFRL1	hNP activated	FOXP2 hNP DAR	chr6	71157318	71157839	Intergenic	-131196
OGFRL1	hNP activated	FOXP2 hNP DAR	chr6	71324088	71325010	intron 1 of 4	35775
OGFRL1	hNP activated	FOXP2 hNP DAR	chr6	71254267	71254776	intron 3 of 3	-34253
OGFRL1	hNP activated	FOXP2 hNP DAR	chr6	71238339	71238856	promoter-TSS	-50177
OLFML1	hDN repressed	CTRL hNP DAR	chr11	7498874	7499749	intron 3 of 3	13942
OLFML1	hDN repressed	CTRL hNP DAR	chr11	7488080	7488737	TTS	3039
OLIG1	hDN activated	CTRL hNP DAR	chr21	33064169	33065317	exon 5 of 5	-5401
PAMR1	hDN repressed	FOXP2 hNP DAR	chr11	35548880	35549371	Intergenic	-18825
PAMR1	hDN repressed	FOXP2 hNP DAR	chr11	35530069	35530472	promoter-TSS	30
PAPPA	hDN activated	FOXP2 hNP DAR	chr9	116102556	116102869	Intergenic	-51080
PAPPA2	hDN activated	FOXP2 hDN DAR	chr1	176638380	176638704	intron 3 of 22	175371
PAQR3	hNP activated	FOXP2 hNP DAR	chr4	78937794	78938269	intron 1 of 7	1397
PARP8	hDN activated	FOXP2 hDN DAR	chr5	50745404	50746039	TTS	78783
PARVA	hDN repressed	FOXP2 hNP DAR	chr11	12411822	12412741	intron 1 of 7	34802
PCP4L1	hDN repressed	CTRL hNP DAR	chr1	161266080	161266629	intron 1 of 2	7627
PDE8B	hNP activated	FOXP2 hNP DAR	chr5	77299991	77300369	intron 2 of 5	89299
PDIA4	hDN repressed	CTRL hNP DAR	chr7	149054853	149055631	Intergenic	-26552
PDLIM3	hDN activated	CTRL hNP DAR	chr4	185567592	185568301	Intergenic	-32388
PDLIM4	hDN repressed	FOXP2 hNP DAR	chr5	132251139	132251854	intron 3 of 3	-6162
PDLIM5	hNP activated	CTRL hNP DAR	chr4	94457548	94458200	TTS	6017
PDP1	hNP activated	FOXP2 hNP DAR	chr8	94035940	94036458	Intergenic	119148
PDP1	hNP activated	FOXP2 hNP DAR	chr8	93959404	93959745	Intergenic	42523
PDP1	hNP activated	FOXP2 hNP DAR	chr8	93938493	93938927	TTS	21659
PELI2	hDN repressed	CTRL hNP DAR	chr14	56002202	56002950	Intergenic	-115799
PERP	hDN repressed	CTRL hNP DAR	chr6	138088180	138088734	TTS	19066
PGRMC2	hDN repressed	CTRL hNP DAR	chr4	128290967	128291657	Intergenic	-2483
PGRMC2	hDN repressed	CTRL hNP DAR	chr4	128289407	128290925	Intergenic	-1337
PHACTR2	hDN activated	CTRL hNP DAR	chr6	143743125	143744214	intron 2 of 11	65704
PI15	hDN repressed	CTRL hNP DAR	chr8	74786126	74786866	intron 6 of 6	-38041
PIGT	hDN repressed	CTRL hNP DAR	chr20	45412695	45413048	Intergenic	-3196
PIK3C2A	hDN repressed	CTRL hNP DAR	chr11	17150563	17150994	intron 1 of 12	19029
PKIA	hDN activated	FOXP2 hDN DAR	chr8	78278954	78279781	Intergenic	-236734
PKIA	hDN activated	FOXP2 hDN DAR	chr8	78511039	78511859	intron 2 of 4	-4652

Table 4.2

Gene	DAR Type	Differential expression	Chr	Start	End	Annotation	BPs to TSS
PLCB1	hDN activated	FOXP2 hNP DAR	chr20	8089648	8090156	Intergenic	-42363
PLCB1	hDN activated	FOXP2 hNP DAR	chr20	8156002	8156285	intron 2 of 6	23878
PLCB1	hDN activated	FOXP2 hNP DAR	chr20	8361046	8361439	intron 2 of 6	228977
PLEKHA1	hNP activated	FOXP2 hNP DAR	chr10	122362358	122363287	Intergenic	-11756
PLEKHA5	hDN activated	FOXP2 hNP DAR	chr12	19004175	19004677	Intergenic	-125266
PLEKHA5	hDN activated	FOXP2 hNP DAR	chr12	19227334	19227773	intron 1 of 25	22228
PLEKHA5	hDN activated	FOXP2 hNP DAR	chr12	19197012	19197377	intron 3 of 31	-8131
PLSCR4	hDN activated	FOXP2 hDN DAR	chr3	146280837	146281267	Intergenic	-29873
PLSCR4	hDN activated	FOXP2 hDN DAR	chr3	146300444	146301903	Intergenic	-49994
PLSCR4	hDN activated	FOXP2 hDN DAR	chr3	146279789	146280381	Intergenic	-28906
PLXDC1	hDN repressed	FOXP2 hDN DAR	chr17	39123352	39124207	intron 1 of 12	27870
PNMA2	hNP activated	CTRL hNP DAR	chr8	26457836	26458223	intron 5 of 5	55938
POLQ	hDN repressed	FOXP2 hNP DAR	chr3	121482740	121483173	intron 19 of 30	63050
PPIF	hDN repressed	FOXP2 hNP DAR	chr10	79266130	79267269	intron 1 of 3	-80765
PPP1R3C	hNP repressed	FOXP2 hNP DAR	chr10	91652351	91652874	Intergenic	-19511
PQLC3	hNP activated	FOXP2 hNP DAR	chr2	11175142	11175826	intron 6 of 6	20112
PRIMA1	hDN activated	FOXP2 hNP DAR	chr14	93693885	93694309	intron 46 of 48	94323
PRKAR2B	hDN activated	FOXP2 hNP DAR	chr7	106986600	106987068	Intergenic	-57899
PRLR	hDN activated	FOXP2 hDN DAR	chr5	35308284	35309017	Intergenic	-78061
PRMT6	hDN repressed	FOXP2 hNP DAR	chr1	106523591	106523965	Intergenic	-532867
PRMT6	hDN repressed	FOXP2 hNP DAR	chr1	106924341	106924908	Intergenic	-132021
PSAT1	hDN activated	CTRL hNP DAR	chr9	78390510	78391116	Intergenic	93738
PSAT1	hDN activated	CTRL hNP DAR	chr9	78309050	78309467	intron 6 of 8	12183
PTHLH	hDN activated	FOXP2 hDN DAR	chr12	28017120	28017604	Intergenic	-45379
PTHLH	hDN activated	FOXP2 hDN DAR	chr12	27922633	27923262	Intergenic	47014
PTHLH	hDN activated	FOXP2 hDN DAR	chr12	27914910	27915842	Intergenic	54585
PTHLH	hDN activated	FOXP2 hDN DAR	chr12	28054595	28055022	Intergenic	-82825
PTPN3	hNP activated	FOXP2 hNP DAR	chr9	109447793	109448678	intron 1 of 19	3149
PTPRQ	hDN activated	FOXP2 hNP DAR	chr12	80352463	80352872	intron 6 of 17	-91679
PTPRQ	hDN activated	FOXP2 hNP DAR	chr12	80551909	80552297	intron 25 of 44	107757
PTRF	hDN repressed	CTRL hNP DAR	chr17	42428310	42429032	Intergenic	-5351
RAB11FIP1	hDN repressed	FOXP2 hNP DAR	chr8	37891735	37892129	intron 1 of 4	7565
RAI14	hDN repressed	FOXP2 hNP DAR	chr5	34509978	34510367	Intergenic	-146156
RAI14	hDN repressed	FOXP2 hNP DAR	chr5	34608742	34609564	Intergenic	-47175
RAI14	hDN repressed	FOXP2 hNP DAR	chr5	34717574	34718122	intron 2 of 5	30289
RASGRF1	hDN activated	FOXP2 hNP DAR	chr15	78979599	78979981	promoter-TSS	25870
RBBP8	hDN repressed	FOXP2 hNP DAR	chr18	22999170	22999554	intron 14 of 17	65486
RBPMS	hDN repressed	FOXP2 hNP DAR	chr8	30279382	30280224	Intergenic	-104698
RCAN2	hDN activated	FOXP2 hNP DAR	chr6	46378528	46379497	intron 2 of 4	-53120
RCAN2	hDN activated	FOXP2 hNP DAR	chr6	46342236	46342917	intron 2 of 4	-16684
RDH10	hNP activated	FOXP2 hDN DAR	chr8	73302629	73303318	intron 1 of 2	8371

Table 4.2

Gene	DAR Type	Differential expression	Chr	Start	End	Annotation	BPs to TSS
RGMA	hDN activated	CTRL hNP DAR	chr15	93296700	93297267	Intergenic	-207769
RGS4	hDN repressed	FOXP2 hNP DAR	chr1	163035779	163036313	Intergenic	-32560
RGS8	hDN activated	FOXP2 hDN DAR	chr1	182668330	182668967	intron 2 of 5	4284
RHOU	hDN activated	FOXP2 hNP DAR	chr1	228841961	228842607	Intergenic	107207
RNF144A	hDN activated	CTRL hNP DAR	chr2	6915322	6915825	exon 2 of 2	-1819
RSPH4A	hDN activated	FOXP2 hNP DAR	chr6	116610898	116611396	Intergenic	-5332
RTP1	hDN activated	FOXP2 hNP DAR	chr3	187185861	187186186	Intergenic	-11463
S100A10	hNP activated	FOXP2 hNP DAR	chr1	151989355	151989827	intron 1 of 2	4647
SCD5	hDN activated	CTRL hNP DAR	chr4	82811816	82812739	Intergenic	-13420
SCG2	hNP repressed	FOXP2 hDN DAR	chr2	223528010	223528645	Intergenic	74172
SCN3B	hDN activated	FOXP2 hNP DAR	chr11	123616446	123617048	intron 16 of 19	37860
SDC2	hDN repressed	CTRL hNP DAR	chr8	96520349	96520962	intron 1 of 3	27001
SDC3	hDN activated	FOXP2 hNP DAR	chr1	30844594	30845120	TTS	63776
SDK2	hDN activated	FOXP2 hDN DAR	chr17	73625879	73626748	intron 1 of 44	17775
SELENBP1	hDN repressed	FOXP2 hNP DAR	chr1	151373748	151374342	Intergenic	-1311
SEPSECS	hDN repressed	FOXP2 hDN DAR	chr4	25099347	25100373	Intergenic	60722
SERPINA3	hDN repressed	FOXP2 hNP DAR	chr14	94598773	94599851	intron 3 of 7	-13065
SERPINB8	hNP activated	FOXP2 hNP DAR	chr18	63963660	63964071	intron 3 of 5	-6164
SERPINE1	hDN repressed	CTRL hNP DAR	chr7	101133797	101135111	intron 5 of 8	7365
SERPINE2	hNP repressed	CTRL hNP DAR	chr2	224041492	224042795	Intergenic	-2824
SESN3	hDN activated	FOXP2 hNP DAR	chr11	95335986	95336259	Intergenic	-103581
SESN3	hDN activated	FOXP2 hNP DAR	chr11	95248691	95249373	Intergenic	-16491
SESN3	hDN activated	FOXP2 hNP DAR	chr11	95442761	95443121	Intergenic	-210400
SEZ6	hDN activated	FOXP2 hNP DAR	chr17	29007960	29008470	intron 2 of 2	-1775
SH3GL1	hNP repressed	CTRL hNP DAR	chr19	4396745	4397852	intron 1 of 9	3120
SHISA9	hNP activated	FOXP2 hNP DAR	chr16	12976794	12977396	intron 2 of 4	75475
SLA	hDN activated	FOXP2 hDN DAR	chr8	133131905	133132362	intron 17 of 18	-29067
SLA	hDN activated	FOXP2 hDN DAR	chr8	133102176	133103388	promoter-TSS	284
SLC15A4	hDN repressed	FOXP2 hNP DAR	chr12	128799064	128799624	exon 2 of 3	24652
SLC1A1	hDN repressed	FOXP2 hNP DAR	chr9	4509193	4509806	intron 1 of 11	19072
SLC24A2	hNP repressed	FOXP2 hNP DAR	chr9	20015545	20015970	Intergenic	-228738
SLC24A2	hNP repressed	FOXP2 hNP DAR	chr9	19988162	19988745	Intergenic	-201434
SLC24A2	hNP repressed	FOXP2 hNP DAR	chr9	19875287	19875862	Intergenic	-88555
SLC24A3	hDN activated	CTRL hNP DAR	chr20	19176499	19177041	Intergenic	-35876
SLC35B4	hDN repressed	CTRL hNP DAR	chr7	134308575	134308947	intron 2 of 7	8314
SLC35F2	hNP activated	FOXP2 hNP DAR	chr11	107819377	107819743	intron 4 of 10	39628
SLC44A5	hDN activated	FOXP2 hNP DAR	chr1	75522409	75522873	TTS	88473
SLC47A2	hDN repressed	CTRL hNP DAR	chr17	19727223	19728754	Intergenic	-11258
SLC6A11	hDN activated	FOXP2 hDN DAR	chr3	10868141	10868884	intron 5 of 13	52280
SLC6A13	hDN activated	CTRL hNP DAR	chr12	304790	305176	intron 24 of 27	-42110
SLC7A14	hDN repressed	CTRL hNP DAR	chr3	170531610	170532312	intron 1 of 7	54113

Table 4.2

Gene	DAR Type	Differential expression	Chr	Start	End	Annotation	BPs to TSS
SLCO1A2	hNP repressed	CTRL hNP DAR	chr12	21324562	21325262	promoter-TSS	9986
SLCO5A1	hDN activated	FOXP2 hDN DAR	chr8	69871471	69872357	Intergenic	-36850
SLF2	hDN repressed	CTRL hNP DAR	chr10	100889377	100891695	Intergenic	-22033
SLIT3	hDN repressed	FOXP2 hNP DAR	chr5	169350728	169351194	Intergenic	-49832
SMAD3	hDN repressed	FOXP2 hNP DAR	chr15	67029866	67030266	intron 1 of 4	-35791
SMAD3	hDN repressed	FOXP2 hNP DAR	chr15	67044029	67044688	intron 1 of 4	-21499
SMIM18	hDN activated	FOXP2 hDN DAR	chr8	30629586	30629913	intron 3 of 5	-8851
SNAI2	hDN repressed	CTRL hNP DAR	chr8	48899223	48900254	Intergenic	21702
SNX29	hDN activated	FOXP2 hNP DAR	chr16	11994405	11995107	intron 1 of 5	18022
SNX5	hDN repressed	CTRL hNP DAR	chr20	17971253	17972070	intron 2 of 2	-2670
SOBP	hNP repressed	CTRL hNP DAR	chr6	107602892	107603439	intron 5 of 6	113052
SOBP	hNP repressed	CTRL hNP DAR	chr6	107602283	107602638	intron 5 of 6	112347
SOX9	hDN repressed	CTRL hNP DAR	chr17	72158774	72159942	intron 2 of 2	38338
SPARC	hDN repressed	FOXP2 hNP DAR	chr5	151698987	151699784	intron 2 of 2	-12331
SPON1	hDN activated	FOXP2 hDN DAR	chr11	13831693	13832031	intron 1 of 1	-130775
SPON1	hDN activated	FOXP2 hDN DAR	chr11	14042998	14043511	intron 3 of 15	80617
SREBF1	hDN repressed	FOXP2 hDN DAR	chr17	17885856	17887136	intron 3 of 13	-49485
SRRM4	hNP activated	FOXP2 hNP DAR	chr12	118750506	118751048	Intergenic	-230718
SST	hDN activated	FOXP2 hNP DAR	chr3	187519296	187520137	Intergenic	150697
ST3GAL6	hNP activated	FOXP2 hNP DAR	chr3	98779759	98780635	intron 4 of 4	47493
ST6GAL2	hNP repressed	CTRL hNP DAR	chr2	107107371	107107870	Intergenic	-220513
STK32A	hNP activated	FOXP2 hNP DAR	chr5	147310182	147310736	intron 4 of 12	75443
STK32A	hNP activated	FOXP2 hNP DAR	chr5	147303861	147304585	intron 4 of 12	69207
STMN2	hDN activated	CTRL hNP DAR	chr8	79629287	79629650	intron 1 of 4	18654
STXBP5L	hDN activated	FOXP2 hDN DAR	chr3	120846033	120846515	Intergenic	-61929
SUSD1	hDN activated	FOXP2 hNP DAR	chr9	112166409	112166920	intron 1 of 17	8633
SVIL	hDN activated	FOXP2 hNP DAR	chr10	29633205	29633658	intron 3 of 35	1541
TANC2	hDN activated	CTRL hNP DAR	chr17	63151760	63152483	exon 1 of 1	142584
TBC1D4	hDN activated	FOXP2 hNP DAR	chr13	75437598	75437947	intron 1 of 19	44396
TCF7L2	hNP activated	CTRL hNP DAR	chr10	112958196	112958844	intron 3 of 10	8270
TFCP2L1	hDN activated	CTRL hNP DAR	chr2	121376952	121378033	intron 34 of 39	-92290
TFPI2	hDN repressed	FOXP2 hNP DAR	chr7	93817583	93817996	intron 1 of 3	73202
TGM2	hDN activated	FOXP2 hDN DAR	chr20	38203220	38203804	Intergenic	-38214
TLE4	hDN activated	CTRL hNP DAR	chr9	79489069	79489727	Intergenic	-82375
TLE4	hDN activated	CTRL hNP DAR	chr9	79609709	79610785	intron 5 of 20	38474
TLE4	hDN activated	CTRL hNP DAR	chr9	79610933	79611494	intron 5 of 20	39440
TLE4	hDN activated	CTRL hNP DAR	chr9	79662377	79663195	promoter-TSS	91013
TMEM163	hDN repressed	CTRL hNP DAR	chr2	134572919	134573528	intron 2 of 7	145778
TMEM200A	hDN activated	FOXP2 hDN DAR	chr6	130394048	130395043	intron 2 of 2	-26551
TMEM233	hNP activated	FOXP2 hNP DAR	chr12	119595964	119596468	intron 1 of 3	2757
TMEM47	hDN repressed	FOXP2 hDN DAR	chrX	34558460	34559131	Intergenic	98493

Table 4.2

Gene	DAR Type	Differential expression	Chr	Start	End	Annotation	BPs to TSS
TNN	hNP activated	FOXP2 hNP DAR	chr1	175070996	175071497	intron 1 of 18	3388
TNN	hNP activated	FOXP2 hNP DAR	chr1	175089285	175089706	intron 5 of 16	21637
TNS1	hNP activated	FOXP2 hNP DAR	chr2	217947194	217947706	intron 3 of 18	-3377
TRPC6	hNP repressed	CTRL hNP DAR	chr11	101726955	101727413	intron 1 of 1	-143256
TRPM8	hNP repressed	CTRL hNP DAR	chr2	233924337	233925786	intron 1 of 23	7663
TRPM8	hNP repressed	CTRL hNP DAR	chr2	233930968	233931896	intron 2 of 4	14034
TSC22D3	hNP repressed	CTRL hNP DAR	chrX	107738384	107739507	intron 2 of 2	-21884
TSKU	hNP repressed	FOXP2 hDN DAR	chr11	76756154	76757150	Intergenic	-25661
TTYH1	hNP repressed	CTRL hNP DAR	chr19	54419521	54422760	intron 1 of 3	5709
UBE2E1	hDN activated	FOXP2 hNP DAR	chr3	23648632	23649405	Intergenic	-156875
UBE2E1	hDN activated	FOXP2 hNP DAR	chr3	23840452	23840918	intron 3 of 3	30242
UBE2E1	hDN activated	FOXP2 hNP DAR	chr3	23819919	23820466	intron 3 of 3	9749
UBE2E2	hDN activated	FOXP2 hDN DAR	chr3	23481079	23481942	promoter-TSS	278217
UBE2QL1	hDN activated	FOXP2 hDN DAR	chr5	6455376	6455995	intron 1 of 1	7062
UNC5B	hDN repressed	FOXP2 hDN DAR	chr10	71137972	71139123	Intergenic	-73988
UNC5B	hDN repressed	FOXP2 hDN DAR	chr10	71059412	71059908	Intergenic	-152875
VASH2	hNP activated	FOXP2 hNP DAR	chr1	212928472	212929503	Intergenic	-21533
VASH2	hNP activated	FOXP2 hNP DAR	chr1	212979914	212980766	intron 5 of 5	29820
VAV2	hDN repressed	CTRL hNP DAR	chr9	133934501	133936171	intron 1 of 3	56988
VCAM1	hDN activated	CTRL hNP DAR	chr1	100735046	100735861	exon 1 of 1	15813
VEPH1	hDN activated	FOXP2 hNP DAR	chr3	157501860	157502307	intron 1 of 3	1264
VLDLR	hDN repressed	FOXP2 hNP DAR	chr9	2414403	2414782	Intergenic	-207201
VSNL1	hNP activated	FOXP2 hNP DAR	chr2	17615711	17616274	intron 2 of 3	75452
VSNL1	hNP activated	FOXP2 hNP DAR	chr2	17643103	17643769	intron 2 of 3	102896
VSNL1	hNP activated	FOXP2 hNP DAR	chr2	17608285	17608599	intron 2 of 3	67902
VSTM4	hDN activated	FOXP2 hNP DAR	chr10	49072165	49072634	intron 4 of 7	43133
WARS	hDN repressed	CTRL hNP DAR	chr14	100362413	100362931	promoter-TSS	12918
WASF3	hDN activated	FOXP2 hNP DAR	chr13	26502861	26503210	Intergenic	-54668
WASF3	hDN activated	FOXP2 hNP DAR	chr13	26423551	26424078	Intergenic	-133889
WEE1	hDN repressed	CTRL hNP DAR	chr11	9565840	9566554	Intergenic	-7484
WEE1	hDN repressed	CTRL hNP DAR	chr11	9568793	9569662	Intergenic	-4454
WLS	hDN repressed	CTRL hNP DAR	chr1	68236890	68237484	Intergenic	-4586
WWP1	hDN activated	CTRL hNP DAR	chr8	86319886	86320728	intron 1 of 3	-22458
WWP1	hDN activated	CTRL hNP DAR	chr8	86305337	86306305	intron 1 of 3	-36944
ZBTB44	hDN activated	FOXP2 hNP DAR	chr11	130369099	130369639	intron 2 of 5	-54657
ZDHHC22	hDN activated	FOXP2 hDN DAR	chr14	77157837	77159347	intron 1 of 3	-16801
ZNF385D	hDN repressed	FOXP2 hNP DAR	chr3	21795150	21795452	intron 3 of 4	-43977
ZNF483	hNP activated	FOXP2 hNP DAR	chr9	111529693	111530433	intron 2 of 5	4904
ZNF488	hDN activated	FOXP2 hNP DAR	chr10	47402254	47403980	Intergenic	-18844
ZNF704	hNP activated	FOXP2 hNP DAR	chr8	80915480	80915899	Intergenic	-40908
ZNF704	hNP activated	FOXP2 hNP DAR	chr8	80720633	80721199	intron 1 of 5	153865

Table 4.2							
Gene	**DAR Type**	**Differential expression**	**Chr**	**Start**	**End**	**Annotation**	**BPs to TSS**
ZNF704	hNP activated	FOXP2 hNP DAR	chr8	80864657	80865273	intron 1 of 8	9816
ZNF804A	hDN activated	FOXP2 hDN DAR	chr2	184593912	184594208	Intergenic	-4306

Table 4.3 *Differentially expressed genes from two rounds of RNA-seq with hNPs and hDNs (Corresponds to figures 4.8-11 and 4.13-15)*

First round differentially expressed genes correspond to figures 4.8-9. Second round differentially expressed genes correspond to figure 4.11 and 4.13-15. The CMP filtered sets from both rounds are compared in figure 4.10.

Table 4.3	log2 fold change first round		log2 fold change second round			
Gene	**CPM filtered hNP**	**CPM filtered hDN**	**CPM filtered hNP**	**CPM filtered hDN**	**RPKM filtered hNP**	**RPKM filtered hDN**
MARCH1		0.73				
MARCH2	-0.49					
MARCH4	1.11	0.69	0.42	0.86	0.40	0.85
SEPT4	-0.65					
SEPT9	-0.60					
SEPT11	0.42					
A1BG						0.44
A2M	-0.72	-2.19		-0.44		-0.43
ABCA5	0.51	0.51				
ABCA8	-0.59	-0.95				
ABCB1		-0.84		-0.75		-0.74
ABCC3	1.08			-0.50		-0.49
ABCC4		0.82				
ABCC9		0.97		0.47		0.47
ABCG4				0.52		
ABHD17C			-0.34		-0.33	
ABI3BP				-0.51		
ABL2	0.44					
ABLIM1		-0.31				
ABTB2		0.75				
ACADL		0.79				
ACER3	-0.46					
ACKR1		0.74				
ACP6	0.49					
ACSL3		-0.53				

Table 4.3	log2 fold change first round		log2 fold change second round			
Gene	CPM filtered hNP	CPM filtered hDN	CPM filtered hNP	CPM filtered hDN	RPKM filtered hNP	RPKM filtered hDN
ACSL6	-0.84					
ACTA2				-0.40		-0.39
ACTG2				-0.58		
ACTL6B			0.53		0.51	
ACTN2	-0.73					
ACTN4		-0.54				
ACTR3B				0.40		0.40
ACVR1C		0.75				
ADAM19	0.53					
ADAM9		-0.45				
ADAMTS15	1.27	-0.80				
ADAMTS16		-1.85				
ADAMTS17				-0.61		-0.59
ADAMTS18	0.93	-2.33		-0.97		-0.95
ADAMTS3	0.36	-0.92				
ADAMTS4	0.78					
ADAMTS6	0.71	1.26				
ADAMTS8		1.10				
ADAMTS9	0.79			-0.73		-0.72
ADAMTSL1	0.81	1.66	0.54	0.37		0.37
ADARB2		1.21				
ADCY1		0.87		0.45		0.44
ADCY2	-0.43					
ADCY9		-0.80				
ADCYAP1R1		1.69		0.42		0.42
ADD2		0.49		0.36		0.36
ADGRA1		0.99				
ADGRA2	0.80					
ADGRB3		0.64				
ADGRD1				0.50		
ADGRG1		0.77				
ADGRG6	0.73					
ADGRL2	0.80					
ADGRL3		1.18				
ADGRL4	0.75					
ADM	-0.85	-1.94				
ADORA1		0.74				
ADORA2B	-0.93	-0.81				
ADRA2C		1.89		0.82		0.81
ADRBK2	0.68		0.38		0.37	

Table 4.3	log2 fold change first round		log2 fold change second round			
Gene	CPM filtered hNP	CPM filtered hDN	CPM filtered hNP	CPM filtered hDN	RPKM filtered hNP	RPKM filtered hDN
AFAP1L1	0.70					
AFP		-1.04				
AGAP2		0.49				
AGBL4		0.84				
AGL		0.45				
AGPAT4		-0.58		-0.36		-0.35
AHCYL2		-0.73				
AHI1		0.40				
AHNAK		-0.50		-0.32		-0.31
AHNAK2		-1.68				
AHSA1	-0.44					
AIM1		1.23				
AIM2		0.73				
AJAP1	-1.11	-1.63		-0.32		-0.32
AK7				0.45		0.44
AKAP14		-3.06				
AKAP6		0.64				
AKAP7		0.51				
AKNA					0.31	
AKR1C1		-0.80				
ALCAM		-0.60				
ALDH1A1		-1.41				
ALDH1B1	-0.59	-0.69		-0.53		-0.52
ALDH1L2	0.42					
ALDH3A2		-0.45				
ALDH3B1		-1.30				
ALDH9A1	0.49					
ALPK2	-0.79					
ALPK3		0.86		0.57		0.56
AMBN	1.13	0.57				
AMIGO2		-0.43	-0.35	-0.44	-0.34	-0.43
AMOTL1	0.30					
AMOTL2		-0.79		-0.41		-0.40
AMPH		0.53				
AMZ1		1.33				
ANG		-0.98				
ANGPT1		1.60				
ANK1	0.68					
ANK3				0.40		0.40
ANKFN1	-0.64					

Table 4.3	log2 fold change first round		log2 fold change second round			
Gene	CPM filtered hNP	CPM filtered hDN	CPM filtered hNP	CPM filtered hDN	RPKM filtered hNP	RPKM filtered hDN
ANKH			0.37		0.36	
ANKRD1		-0.89				
ANKRD13A		-0.41				
ANKRD29		0.91				
ANKRD40		-0.31				
ANKRD44	0.62	1.02				
ANKRD66		1.61		0.43		
ANKS1B		0.51				
ANKUB1		-0.84				
ANO4	-0.65					
ANO6		-0.36				
ANXA1	-0.39	-0.61	-0.36		-0.36	
ANXA2			-0.33		-0.33	
ANXA3		-1.20				
ANXA6		1.07				
AP1S3	0.85					
APBA1	-0.61	0.54				
APBA2		0.55				
APCDD1	-0.63					
APLN	0.81					
APLNR				0.56		0.53
APLP2		-0.39				
APOBEC3C		-0.74		-0.50		-0.48
APOD	-0.75					
APOE		0.79				
APOL4	0.80			0.36		0.36
AQP1		1.64				
ARAP2		-0.35				
ARAP3	0.70					
ARHGAP1		0.44				
ARHGAP10		0.81				
ARHGAP20		0.81		0.34		0.34
ARHGAP21	0.32					
ARHGAP22	-0.96	-0.85				
ARHGAP26	0.82					
ARHGAP29		-0.82		-0.43		-0.42
ARHGAP32	0.43					
ARHGAP36	1.03			1.77		1.72
ARHGAP42		-0.43				
ARHGAP44	-0.74					

Table 4.3	log2 fold change first round		log2 fold change second round			
Gene	CPM filtered hNP	CPM filtered hDN	CPM filtered hNP	CPM filtered hDN	RPKM filtered hNP	RPKM filtered hDN
ARHGEF3	0.57					
ARHGEF37	0.76					
ARL2		-0.72				
ARL4C	0.68					
ARL4D	-0.72	-0.76				
ARMC2	0.47					
ARPP21	0.62	1.25		1.02		1.00
ARSE		-0.89		-0.52		-0.50
ARSF		2.33				
ASCL1				0.56		0.55
ASIC4		0.91		0.50		0.49
ASPH		-0.44				
ASTN1		0.55				
ASTN2		-1.31		-0.36		-0.35
ATAD2		-0.57				
ATCAY			0.43		0.43	
ATOH8		-0.47				
ATP10B	1.05					
ATP13A5		1.58				
ATP1A2		-0.80		-0.39		-0.38
ATP1A3		0.45				
ATP2B1		0.62				
ATP2B2	-0.69					
ATP2B3		0.84		0.43		0.42
ATP6V0E2		0.56				
ATP8B1		-0.63				
B3GALNT1		0.50				
B3GALT1	0.47					
B3GALT5		-0.45				
B3GNT2	0.68					
B4GALT1	0.50					
B4GALT5		0.53				
BAALC	-0.48					
BACH2	0.58	0.50				
BAIAP3		0.62				
BAMBI		-1.47		-0.45		-0.44
BBC3	-0.84					
BBOX1	-0.82			0.42		0.41
BCAM		-0.72				
BCAR3				-0.34		-0.34

Table 4.3	log2 fold change first round		log2 fold change second round			
Gene	CPM filtered hNP	CPM filtered hDN	CPM filtered hNP	CPM filtered hDN	RPKM filtered hNP	RPKM filtered hDN
BCAT1	1.15					
BCAT2		-0.86				
BCHE		1.24				
BCKDHB		-0.49				
BCL11A	0.76			0.31		0.31
BCL11B			0.39		0.38	
BCL2	0.35					
BCL2L11	0.45					
BCL6	0.95					
BCO2		0.85				
BEAN1		0.59				
BEND5		0.60				
BEST3	-0.85					
BICC1	0.48					
BIN1		0.81				
BMF		-0.72				
BMP2		-1.17				
BMP4		0.90				
BMP6	-0.75	-2.28				
BMP7				-0.54		-0.53
BMP8B		-1.17				
BNC2		-0.47				
BRINP1		0.87				
BRINP2		1.57		0.98		0.97
BRINP3		0.85				
BRS3		2.07				
BSN			0.40		0.39	
BTG1	0.66					
BTG3	0.33					
BTNL9		0.88				
BVES				-0.31		-0.30
C10orf105		1.47				
C10orf54		-1.59		-0.52		-0.51
C11orf87		0.64				0.38
C11orf96	-1.02					
C12orf49	-0.34					
C15orf59	-0.71					
C1orf115		0.44				
C1orf21	0.33	0.74				
C1orf226		0.61				

Table 4.3	log2 fold change first round		log2 fold change second round			
Gene	CPM filtered hNP	CPM filtered hDN	CPM filtered hNP	CPM filtered hDN	RPKM filtered hNP	RPKM filtered hDN
C1orf95		1.03		0.43		0.43
C1QL4		2.37		0.89		0.84
C1QTNF4		1.54				
C1R		-0.65				
C21orf91		-0.35				
C22orf42				0.58		
C2CD2	0.54					
C2orf50	0.99					0.43
C2orf72		0.80				
C2orf80	-1.01					
C2orf88		0.93				
C3		1.32				
C3orf52		-2.18		-0.52		-0.51
C3orf58		-0.50				
C3orf70	-0.41					
C4orf19	-0.71			-0.45		-0.44
C5		0.49				
C5orf46				-0.51		-0.47
C5orf49				0.42		0.41
C6orf163			0.41			
C7			0.42	0.52	0.41	0.50
C7orf57		0.61		0.44		0.43
C8orf34	3.34	1.03		0.67		0.66
C8orf37	0.38	0.34				
C9orf3		-0.80				
CA10				0.65		
CA4		0.91				
CA8				-0.57		-0.55
CABLES1	-0.54	-0.99		-0.57		-0.55
CABYR	0.63					
CACNA1A	0.74	1.46	0.42	1.08		1.05
CACNA1D		1.09		0.48		0.47
CACNA1E				0.67		0.66
CACNA1G		1.22		0.47		0.46
CACNA2D2		0.94				
CACNA2D3		1.05		0.52		0.50
CACNB2	-0.41					
CACNG4		0.44				
CADM2		0.88				
CADM3		1.16				

Table 4.3	log2 fold change first round		log2 fold change second round			
Gene	CPM filtered hNP	CPM filtered hDN	CPM filtered hNP	CPM filtered hDN	RPKM filtered hNP	RPKM filtered hDN
CADPS	0.96	0.82		0.35		0.34
CALB1		0.90		0.74		0.72
CALB2		-0.75				
CALD1		-0.88		-0.48		-0.47
CALN1	0.50	1.31				
CALR				-0.31		-0.30
CALU		-0.54		-0.38		-0.37
CAMK1G		1.72				
CAMK2B	-0.50			0.37		0.36
CAMK2D		-0.53				
CAMK2N1	0.49					
CAMK4		0.50	0.35	0.50	0.35	0.50
CAMKV		1.95		0.84		0.83
CAMTA1		0.42				
CAPN2	0.34					
CAPSL				0.74		0.70
CARD10				-0.44		-0.43
CASP1		1.08				
CASP6		-0.65				
CASP7		0.76				
CASQ1		0.78				
CAT		0.52				
CAV2	0.64					
CBLN2		1.21				
CBLN4		1.41				
CBX4	-0.53					
CCBE1	-0.73	2.28		0.73		
CCDC108				0.49		
CCDC109B		-0.37				
CCDC13				0.58		0.56
CCDC136	0.59					
CCDC170				0.35		0.35
CCDC173		0.60				
CCDC175	-0.70					
CCDC178		1.22				
CCDC184		1.16				
CCDC39		0.85		0.62		
CCDC40				0.34		0.33
CCDC50	0.34					
CCDC69		1.01				

Table 4.3	log2 fold change first round		log2 fold change second round			
Gene	CPM filtered hNP	CPM filtered hDN	CPM filtered hNP	CPM filtered hDN	RPKM filtered hNP	RPKM filtered hDN
CCDC80	0.35			-0.46		-0.45
CCL2			-0.50	-0.49	-0.49	-0.48
CCNB3	0.74					
CCND1		-1.36		-0.64	-0.30	-0.63
CCND2		0.62				
CCNE2		-0.54				
CCS		-0.55				
CCSER1		1.31				
CCT6B	0.60					
CD164		-0.35				
CD34	1.09					
CD38		1.41		0.49		0.49
CD44	0.80		-0.34		-0.33	
CD47		-0.46				
CD59	-0.61	-0.75				
CD74			-0.42		-0.40	
CD83		0.74				
CD8A		2.63		0.51		0.49
CDC14A	0.56					
CDC42EP2		1.91		0.73		0.71
CDH1		-1.10		-0.55		
CDH10				0.48		0.47
CDH13	-0.79	-1.48		-0.43		-0.42
CDH18		1.49		0.72		
CDH20	-0.90					
CDH23		1.59		0.52		
CDH5		-1.07				
CDH6	0.54					
CDH8		-0.70				
CDK1		-0.51				
CDK14		0.33				
CDK5R1	-0.43		0.32		0.31	
CDK6		-0.69				
CDKL1	-0.52					
CDKN1A		-0.71	-0.42		-0.41	
CDKN1C		-0.61				
CDO1		-0.59				
CDON				0.33		0.33
CDR2		-0.57				
CELF3			0.64		0.63	

Table 4.3	log2 fold change first round		log2 fold change second round			
Gene	CPM filtered hNP	CPM filtered hDN	CPM filtered hNP	CPM filtered hDN	RPKM filtered hNP	RPKM filtered hDN
CELF4		0.94	0.66	0.52	0.64	0.52
CELF5			0.43		0.42	
CELSR1		-0.56				
CELSR3			0.39		0.38	
CEMIP				-0.66		-0.64
CENPE		-0.57				
CENPN		-0.50				
CENPU		-0.50				
CEP55		-0.66				
CERKL		1.36				
CERS2		-0.47				
CFAP100				0.48		
CFAP126				0.64		0.64
CFAP46				0.38		0.37
CFAP52		0.83		0.74		0.73
CFAP54				0.38		0.38
CFAP69		0.56				
CFAP74				0.66		
CFAP77				0.44		0.42
CFAP99				0.50		
CFI	-0.55	-0.62				
CGNL1	0.71			-0.43		-0.41
CHCHD10	-0.64					
CHD5				0.36		0.36
CHDH		0.63				
CHGA		0.71	0.43		0.41	
CHGB			0.41		0.40	
CHL1	0.95					
CHMP4B		0.35				
CHN1		-0.56		-0.45		-0.45
CHODL				-0.81		-0.80
CHPF		-0.50				
CHRDL1		-1.61		-0.63		-0.62
CHRFAM7A	0.77	1.29				
CHRM3		1.02				
CHRM5				0.51		
CHRNA7		1.04				
CHRNA9	0.75					
CHRNB2			0.42		0.41	
CHST1		0.96				

Table 4.3	log2 fold change first round		log2 fold change second round			
Gene	CPM filtered hNP	CPM filtered hDN	CPM filtered hNP	CPM filtered hDN	RPKM filtered hNP	RPKM filtered hDN
CHST2	0.77					
CHST7	-0.64			-0.59		-0.57
CHST9		-0.69				
CKB	-0.75					
CLDN1	1.10			-0.61		-0.59
CLDN11	-0.75	-1.10				
CLDN2		-1.00				
CLGN		0.52				
CLIC6		1.70				
CLINT1		0.38				
CLMP		1.38				
CLSPN		-0.49				
CLVS2			0.46		0.45	
CMKLR1				-0.54		
CMPK2		0.54				
CNGA3	0.45					
CNIH3		-0.81				
CNKSR2		0.45				
CNN1	0.93					
CNNM4		-0.60				
CNR1	1.28	1.84		0.73		0.73
CNRIP1		0.49				
CNTN2		0.71	0.42		0.41	
CNTN5				0.46		
CNTN6	1.01					
CNTNAP2	0.70	1.01		0.45		0.45
CNTNAP4				0.58		0.57
COBL				0.43		0.42
COBLL1	-0.49					
COL11A1	-0.51	-1.11		-0.61		-0.59
COL12A1		2.53		0.62		0.61
COL14A1		-1.29		-1.20		-1.17
COL16A1	-0.76					
COL1A1		-1.54				
COL1A2		-0.60		-0.50		-0.49
COL24A1		1.16				
COL28A1	-0.85					
COL2A1	-0.66	2.85		1.25		1.22
COL4A1		-0.88				
COL4A2		-0.76				

Table 4.3	log2 fold change first round		log2 fold change second round			
Gene	CPM filtered hNP	CPM filtered hDN	CPM filtered hNP	CPM filtered hDN	RPKM filtered hNP	RPKM filtered hDN
COL4A3		-1.07		-0.59		-0.58
COL4A4				-0.50		-0.49
COL4A5		-0.68				
COL4A6		-0.60		-0.32		-0.31
COL5A2				-0.61		-0.60
COL5A3		-0.74				
COL6A6		1.21				
COL8A1		-1.43	-0.43		-0.42	
COL8A2	-0.99	-1.37	-0.42	-0.46	-0.41	-0.45
COL9A3		-1.21				
COLCA2		1.28		0.49		0.46
COLGALT2	-0.47	-0.69				
COMMD5	-0.65					
COPRS	-0.51					
COTL1				-0.31		-0.30
CP		-2.16				
CPD		-0.44				
CPEB3		0.55		0.38		0.38
CPLX2			0.66		0.64	
CPM				-0.78		-0.75
CPNE4		-0.50				
CPNE5		1.07				
CPT1A				-0.34		-0.34
CPXM2	0.76	0.95		0.40		0.40
CPZ		-2.31				
CRABP1		1.62				
CREB3L2		-0.54		-0.36		-0.35
CREB5	0.46					
CRHBP		-1.87	-0.46	-0.73	-0.42	-0.71
CRHR2		1.01		0.85		0.81
CRIM1	1.21	-0.74		-0.80		-0.78
CRISPLD1		-0.94				
CRTAP		-0.50				
CRY1						0.31
CRYAB	0.65	-0.94		-0.48		-0.47
CSF1		-0.70				
CSGALNACT1		1.09				
CSMD1		1.64		0.51		
CSMD2	1.06			0.52		0.51
CSPG4	0.83					

Table 4.3	log2 fold change first round		log2 fold change second round			
Gene	CPM filtered hNP	CPM filtered hDN	CPM filtered hNP	CPM filtered hDN	RPKM filtered hNP	RPKM filtered hDN
CSPG5	-0.37	1.36				
CSRP2	-0.60	-0.87		-0.39		-0.38
CST3	-0.67					
CTDNEP1	-0.48					
CTGF	0.82	-0.85		-0.80		-0.79
CTH	-0.85					
CTNNA2		1.31		0.52		0.52
CTNNAL1	0.50					
CTSD		-0.48				
CTSV		-1.17		-0.49		-0.47
CUBN		-0.83				
CXCL16		-0.58				
CXCL2		1.44				
CXCL5		1.14				
CXCR4		-0.60				
CXXC4		0.90				
CYFIP2		0.33				
CYP1B1	0.81					
CYP27C1		0.81				
CYP2J2	-0.84					
CYR61	0.64			-0.75		-0.73
CYTL1		-0.92		-0.69		-0.64
DAB1		1.68		0.87		0.86
DAB2	-0.61	-0.74		-0.50		-0.49
DACT1		0.62	0.33	0.58	0.32	0.57
DAPK2				-0.43		-0.41
DAPL1	1.00					
DAW1		0.71		0.60		0.59
DCBLD2	0.43					
DCDC1				0.69		0.68
DCDC2		-0.80				
DCHS2		0.94		0.33		0.33
DCLK1	-0.33					
DCT				0.36		0.36
DDIT4	-0.71					
DDIT4L		0.98				
DDO		-0.99				
DENND2A	0.52					
DENND2C		-0.62				
DEPTOR	0.76					

Table 4.3	log2 fold change first round		log2 fold change second round			
Gene	CPM filtered hNP	CPM filtered hDN	CPM filtered hNP	CPM filtered hDN	RPKM filtered hNP	RPKM filtered hDN
DFNA5	0.51	0.51				
DGKE	0.64					
DGKG		1.53		0.53		
DGKH		0.55		0.40		0.40
DIAPH3		-0.62				
DIEXF		-0.37				
DIO2	2.35	1.79				
DIRAS2	0.82	1.32		0.35		0.35
DIRAS3		0.50				
DIXDC1		-0.41				
DKK3		-0.74				
DLC1	-0.37			-0.59		-0.58
DLG2	-0.79					
DLGAP2	0.73					
DLGAP5		-0.49				
DLK1	0.96					
DMD		-0.62		-0.32		-0.31
DMKN		-0.89				
DMRT2	-0.92					
DMTN				0.55		0.53
DNA2		-0.49				
DNAH11		1.06		0.69		0.68
DNAH12		0.71		0.75		
DNAH5		0.82				
DNAH7				0.39		0.39
DNAH9		0.97		0.56		0.55
DNAI1						0.43
DNAJC1		-0.44				
DNAJC10		-0.32				
DNER	0.49	0.77				
DNM1		0.48		0.46		0.45
DOC2B	0.81	1.49				
DOCK10		0.57		-0.33		-0.32
DOCK4	-0.56					
DOK6				0.32		0.32
DOPEY2		0.37				
DPP10		0.49				
DPP4	0.82	1.24				
DPP6		0.69				
DPYD		-0.77				

Table 4.3	log2 fold change first round		log2 fold change second round			
Gene	CPM filtered hNP	CPM filtered hDN	CPM filtered hNP	CPM filtered hDN	RPKM filtered hNP	RPKM filtered hDN
DPYSL3	0.72	0.48				
DRC3				0.45		0.44
DRD1		1.64				
DRP2		1.39		0.46		0.46
DSC3		0.89		0.49		
DSCAM		0.94		0.44		0.43
DSCAML1			0.44		0.43	
DSP				-0.60		
DSTN		-0.51				
DTX1		0.46				
DTX4		0.93				
DTYMK		-0.45				
DUSP10	0.72	0.74		0.47		0.46
DUSP18		0.50				
DUSP4	-0.45					
DUSP6				-0.64		-0.63
DYRK2				0.32		0.32
E2F8	0.56					
EBF3		0.88				
ECE1		-0.56		-0.37		-0.36
ECEL1		1.85				
ECM2		-1.48				
EDA		0.97				
EDN1		-1.38		-1.17		-1.14
EDN3		5.86		1.99		1.90
EDNRB		0.72				
EFCAB1				0.40		0.40
EFCAB12				0.61		0.59
EFCC1	-0.78					
EFEMP1		-1.33		-0.59		-0.57
EFHC2		0.43				
EFHD1		1.51		0.70		0.68
EFNB2		-0.46				
EGF		-0.83				
EGFLAM				0.75		0.72
EGLN2		-0.56				
EGLN3		-0.49				
EGR1				-0.43		-0.42
EHBP1	0.50					
EHD3		0.95				

Table 4.3	log2 fold change first round		log2 fold change second round			
Gene	CPM filtered hNP	CPM filtered hDN	CPM filtered hNP	CPM filtered hDN	RPKM filtered hNP	RPKM filtered hDN
EHD4		-1.04		-0.56		-0.55
EHF		0.96				
ELAVL2		0.42				0.35
ELAVL3			0.38		0.37	
ELAVL4		0.91	0.39		0.39	
ELF4	0.78					
ELFN2				0.46		0.44
ELMO1		0.65		0.46		0.45
ELMOD1		0.59		0.46		0.45
ELOVL1		-0.62		-0.36		-0.35
ELOVL6	0.43					
EMC6	-0.62					
EMID1				0.43		0.42
EMILIN3		0.73		0.49		0.48
EML4	0.49					
EMP1		-0.91	-0.39		-0.38	
EMP2		-0.67		-0.34		-0.33
EN1		1.34				
ENAH		-0.34				
ENC1		-0.54				
ENDOD1	0.47					
ENKUR				0.38		0.38
ENO1		-0.41				
ENOX1	0.65	0.65	0.41		0.40	
ENPP2	-1.12	-0.98		-0.42		-0.41
ENPP5		-0.66				
ENTPD1		0.45				
EOGT		-0.59				
EPAS1	2.23			-0.37		-0.36
EPB41			0.39		0.38	
EPB41L1		0.43				
EPB41L4B	1.68	1.11		0.38		0.38
EPDR1				-0.38		-0.37
EPHA3		1.01				
EPHA4		0.88				
EPHA5		1.00				
EPHB2		0.52	0.49		0.47	
EPHB3		-0.76		-0.51		-0.50
EPHX1		-0.59				
ERBB2		0.64				

Table 4.3	log2 fold change first round		log2 fold change second round			
Gene	CPM filtered hNP	CPM filtered hDN	CPM filtered hNP	CPM filtered hDN	RPKM filtered hNP	RPKM filtered hDN
ERC2				0.37		0.36
ERCC6L		-0.53				
ERICH2	-0.51					
ERMN		-0.85				
ERRFI1		-0.45				
ESCO2		-0.62				
ESR1		1.85		0.51		
ESYT2		-0.50				
ESYT3		1.26				
ETNPPL		2.37		0.66		0.62
ETV1		-0.52				
ETV5		-0.56	-0.32	-0.61	-0.31	-0.59
EVA1A						-0.44
EVC		0.59				
EXPH5	0.64					
F11R		-0.80				
F2R	-0.58					
F2RL2		-1.04		-0.52		-0.51
F3	0.60					
FABP5		0.69				
FAM101A		1.27		0.66		0.63
FAM107A	-0.93	-0.61				
FAM110C		0.67				
FAM111B		-0.59				
FAM114A1				-0.35		-0.35
FAM122A		-0.64				
FAM127A	-0.52					
FAM129A	0.68					
FAM133A		-0.71				
FAM135B	-0.63					
FAM13C	0.70					
FAM155B		1.36		0.53		0.52
FAM160A1			0.47			
FAM167A		1.20		0.56		0.56
FAM180B		2.38				
FAM181B		0.66				
FAM183A				0.64		0.61
FAM184B	0.83	0.68				
FAM189A2		1.89				
FAM196A	1.62	1.06				

Table 4.3	log2 fold change first round		log2 fold change second round			
Gene	CPM filtered hNP	CPM filtered hDN	CPM filtered hNP	CPM filtered hDN	RPKM filtered hNP	RPKM filtered hDN
FAM196B				-0.53		-0.50
FAM198B		0.53	-0.38		-0.37	
FAM19A5	-0.85	-1.03				
FAM216B		-1.89				
FAM221A		-0.48				
FAM43B		0.94				
FAM45A	-0.46					
FAM69A		0.79				
FAM69C	-0.62					
FAM72A		-0.81				
FAM81B		-1.30				
FAM83G		-1.22				
FAM84A	0.94	0.66		0.51		0.51
FAM84B	0.46					
FANK1				0.39		0.38
FAT1		-0.48		-0.42		-0.41
FAT2		1.30		0.99		0.98
FAT4	1.16					
FBLN1		1.03				
FBLN5	0.66	-0.70		-0.47		-0.47
FBN1		-0.78		-0.43		-0.42
FBN2		-0.86		-0.37		-0.37
FBXL7		0.34				
FBXO32	1.61	-0.70		-0.36		-0.35
FCHO2		0.34				
FCHSD2		0.44				
FERMT2						-0.30
FEZ1	-0.46					
FGF11	-0.61					
FGF13		0.46				
FGF14				1.17		1.15
FGF18		2.30				
FGF19						0.39
FGF5		-0.77				
FGF7	-0.81					
FGFR1		-1.09				
FGFR2		-0.83				
FGL2	-0.70	-1.19				
FHAD1				0.48		0.47
FHDC1	0.66			0.47		0.45

Table 4.3	log2 fold change first round		log2 fold change second round			
Gene	CPM filtered hNP	CPM filtered hDN	CPM filtered hNP	CPM filtered hDN	RPKM filtered hNP	RPKM filtered hDN
FHOD3	0.34	-0.52				
FIBIN	-0.94					
FIGN		0.69				
FILIP1		-0.92				
FKBP1A		-0.43				
FKBP5	0.48					
FLNB		-0.63		-0.30		
FLRT1		0.78				
FLRT2		1.89		0.33		0.33
FLRT3	0.97					
FLVCR1	0.42					
FMN2		0.48				
FMNL2	0.34					
FMNL3	0.85					
FMO1		1.30				
FMO4		0.62				
FNDC1		-3.80		-0.77		-0.75
FNDC3B		-0.70				
FNDC5		1.17				
FOLH1	0.58					
FOS		-0.71	-0.36		-0.35	
FOSL2	1.02					
FOXO1		-0.69		-0.48		-0.47
FOXP2	1.15	5.95	2.64	2.93	2.55	3.06
FRAS1		0.73				
FREM1		1.83				
FREM2	0.47					
FRMD3		-1.00				
FRMD4A	0.84	0.66				
FRMD4B		-0.45				
FRMD6		-0.63				
FRMD7		0.90		0.35		0.35
FRMPD1	-0.82			-0.54		-0.52
FRMPD4		-2.18			0.36	
FRRS1	0.97					
FRRS1L	0.65	0.89				
FRY			0.39		0.38	
FRZB		-0.86				
FSD1L		0.40				
FST	-0.53					

Table 4.3	log2 fold change first round		log2 fold change second round			
Gene	CPM filtered hNP	CPM filtered hDN	CPM filtered hNP	CPM filtered hDN	RPKM filtered hNP	RPKM filtered hDN
FSTL1		-1.10		-0.43		-0.42
FSTL4		1.45		0.55		
FUT8	0.44					
FUT9		0.84				
FZD2	-0.49					
FZD5		-0.79				
G0S2		0.99				
GAB3	1.27					
GABBR1	0.83					
GABBR2	-0.91			-0.34		-0.34
GABPB2		-0.38				
GABRA3		1.14		0.48		0.46
GABRA4	1.18					
GABRB2		-0.51				
GABRB3		0.52				
GABRG2		1.07				
GABRG3	-1.02					
GAD1	-0.65					
GAD2	0.75	0.84	0.64	0.59	0.63	0.58
GAL		1.02				
GALC		-0.40				
GALNT10		-0.44		-0.46		-0.45
GALNT13				-0.45		-0.43
GALNT18		-1.84				
GALNT5		-1.45		-0.58		-0.57
GAP43		0.72		0.41		0.41
GAR1		-0.58				
GAREML		0.57				
GAS1				0.35		0.35
GAS6		-0.62				
GATM		-0.69				
GBP3		0.61				
GBP4		1.26				
GBX2			0.56		0.54	
GCH1	0.79					
GCNT1		-1.04				
GCOM1		1.17				
GDA		0.88				
GDAP1L1			0.46		0.45	
GDF10		0.93		0.66		0.65

Table 4.3	log2 fold change first round		log2 fold change second round			
Gene	CPM filtered hNP	CPM filtered hDN	CPM filtered hNP	CPM filtered hDN	RPKM filtered hNP	RPKM filtered hDN
GDPD2				0.38		0.37
GFAP		-0.66				
GFRA1		1.30				
GHR		1.56				
GJA1		-0.62		-0.42		-0.42
GLCE	0.46					
GLI1				0.50		
GLI3		0.63				
GLIPR1				-0.36		-0.35
GLRA2			0.52		0.50	
GLRB		0.49				
GLT8D2	-0.71					
GLTSCR1L	0.54					
GLUD1		0.43				
GLUL	-0.54					
GMPR	-0.81		-0.46		-0.45	
GNAO1	-0.63					
GNAS		0.36				
GNB2	-0.62					
GNG11		-0.48		-0.36		-0.35
GNG12	0.60					
GNG3		1.03		0.59		0.58
GNG4				0.33		0.33
GNS		-0.56		-0.49		-0.48
GOLGA7B				0.48		0.47
GPAT3		-0.93				
GPATCH4		-0.49				
GPC3	0.92					
GPC4		-0.85		-0.49		-0.48
GPC6	-1.02					
GPD1L		0.53				
GPM6A		0.48				
GPNMB	-0.70	-1.19	-0.42		-0.41	
GPR12	-0.66	0.87		0.55		0.53
GPR158	0.58			0.56		0.55
GPR179			0.55	0.47		0.46
GPR19		0.85				
GPR37		1.14				
GPR37L1	-0.56					
GPR39		0.74				

Table 4.3	log2 fold change first round		log2 fold change second round			
Gene	CPM filtered hNP	CPM filtered hDN	CPM filtered hNP	CPM filtered hDN	RPKM filtered hNP	RPKM filtered hDN
GPR50	1.15					
GPR63		0.53		0.43		0.43
GPR78		-1.66				
GPR83		-1.89		-1.08	-0.37	-1.06
GPR88						0.37
GPRC5B	-0.51					
GPRIN3		0.94				
GPX3	-0.96	-0.53				
GRAMD1B		0.84				
GRAMD4		0.64				
GRHL3	0.76			-0.47		-0.46
GRIA1	-0.46	-0.91				
GRIA3	-0.46					
GRIA4	-0.64					
GRID2		1.84				
GRIK1	-0.67	1.48				
GRIK2		1.67		0.52		0.51
GRIK3		-0.73				
GRIK4	-1.07					
GRIN1				0.68		0.66
GRIN2B	-0.84					
GRIP1	-0.48	0.53			0.32	
GRIP2					0.35	
GRM3		2.22		0.51		0.49
GRM5	-0.90	0.74		0.48		0.48
GRM7	-1.58	0.72				
GSG1L		2.18		0.65		0.63
GSX1	-1.41					
GTF2F2		-0.68				
GUCY1A3	0.64			0.71		0.69
GUCY1B3		-0.86				
GYG2		0.49				
GYPC		-0.57				
HACD1					-0.37	
HAPLN3	0.66					
HAS3	1.04	1.14		0.53		0.52
HBEGF		-1.10		-0.45		-0.44
HCN1		-0.89		-0.42		-0.40
HEG1		-0.45		-0.40		-0.39
HEPH	0.78	1.40		0.40		0.40

Table 4.3	log2 fold change first round		log2 fold change second round			
Gene	CPM filtered hNP	CPM filtered hDN	CPM filtered hNP	CPM filtered hDN	RPKM filtered hNP	RPKM filtered hDN
HERPUD1		-0.50		-0.31		-0.30
HEXB		-0.51				
HEY1		1.05				
HEY2	0.53	0.71				
HIBADH	0.42	0.50				
HIF1A	0.35					
HIGD1A		-0.40				
HILPDA		0.76		0.32		0.32
HIP1	-0.40					
HIST1H3E	-0.69					
HIST3H2A		1.33				
HIST3H2BB		1.76				
HIVEP1				-0.34		-0.33
HIVEP2				0.31		0.31
HIVEP3	0.78					
HK1		-0.40				
HK2	0.53					
HKDC1	-0.77					
HLA-DMA			-0.46		-0.44	
HLA-DMB		-0.99				
HLA-DOA		-0.96			-0.37	
HLA-DPA1			-0.50		-0.49	
HLA-DPB1			-0.48		-0.46	
HLA-DRA	-0.71		-0.60		-0.58	
HLA-DRB1		-0.92	-0.64		-0.62	
HLF		2.04				
HMMR		-0.72				
HMP19			0.46	0.31	0.45	0.31
HN1L		-0.40				
HNMT	-0.62					
HOMER2	0.57					
HOPX		-1.38		-0.60		-0.59
HOXB5		0.91				
HPCAL1		0.56				
HPCAL4				0.41		0.41
HPSE		-1.46				
HRH1				-0.40		-0.39
HRK		0.73				
HS3ST1	-0.89					
HS3ST5	-0.78	-2.01		-0.56		-0.53

Table 4.3	log2 fold change first round		log2 fold change second round			
Gene	CPM filtered hNP	CPM filtered hDN	CPM filtered hNP	CPM filtered hDN	RPKM filtered hNP	RPKM filtered hDN
HS6ST2				0.40		0.39
HS6ST3		1.11		0.52		
HSD11B1		1.09		0.45		0.44
HSD17B14		-0.73				
HSD17B6				0.54		0.51
HSPB8	0.91	1.62		0.82		0.80
HSPG2		-0.89				
HTR1D	1.00					
HTR1F		1.13				
HTR2A		1.11				
HTRA1	0.44	-0.57		-0.31		-0.31
HVCN1		0.89				
HYDIN				0.48		0.48
ICA1		1.00				
ICA1L		0.40				
ICMT		-0.40				
ID1		-2.24				
ID3	0.66	-1.74				
IDH2		0.40				
IER3				-0.51		-0.50
IFI27		1.01				
IFIT3	-0.50					
IGDCC4		0.46				
IGF1R	0.38					
IGFBP2		-1.29				
IGFBP3	1.03	-2.12		-0.75		-0.74
IGFBP4		0.87				
IGFBP7		-0.77	-0.41	-0.54	-0.40	-0.53
IGSF1	0.54					
IGSF10		1.25				
IGSF3		0.39				
IL18	1.03					
IL1RAP			-0.41	-0.41	-0.41	-0.40
IL1RAPL1		0.87				
IL33				0.51		0.50
ILDR2		-0.47				
IMMP2L	0.58			-0.33		-0.33
INA			0.44		0.43	
INF2		-0.77				
INHBA		1.25		0.62		

Table 4.3	log2 fold change first round		log2 fold change second round			
Gene	CPM filtered hNP	CPM filtered hDN	CPM filtered hNP	CPM filtered hDN	RPKM filtered hNP	RPKM filtered hDN
INPP5D	0.76					
IQCD		0.62				
IQGAP1		-0.40				
IQGAP2		0.74				
IQSEC2		0.63				
IQSEC3			0.42	0.35	0.41	0.35
IRF2BP2	0.50	0.46				
IRS4		0.83				
IRX2		1.00				
IRX3	1.79					
ISL1			-0.44		-0.43	
ISLR				-1.00		-0.98
ISLR2		0.95	0.48			
ISM2				-0.57		
ITGA11				-1.00		
ITGA2		-1.34		-0.46		-0.46
ITGA3	0.73					
ITGA4				-0.53		
ITGA6		0.40				
ITGA7		-0.50				
ITGA9		1.85		0.74		0.73
ITGAV	-0.52			-0.43		-0.42
ITGB1		-0.51				
ITGB3		-0.94				
ITGB5	-0.90		-0.32	-0.46	-0.31	-0.46
ITGB6	-0.93					
ITIH5				0.45		0.45
ITPR1		-0.71		-0.39		-0.39
ITPR2	0.51					
ITPR3	-0.74					
ITPRIPL2		-0.54				
ITSN1		-0.58				
IVNS1ABP		0.36				
JADE1		-0.51				
JADE3	0.54					
JUN	0.44	-0.56				
JUP		-0.56				
KALRN			0.43		0.43	
KANK2		-0.70				
KCNA1		-1.69				

Table 4.3	log2 fold change first round		log2 fold change second round			
Gene	CPM filtered hNP	CPM filtered hDN	CPM filtered hNP	CPM filtered hDN	RPKM filtered hNP	RPKM filtered hDN
KCNA4		0.99				
KCNA5			0.44			0.41
KCNB1		1.22	0.51	0.52		0.51
KCNB2		1.73				
KCND2		0.83				
KCNG1	0.82	-1.26				
KCNH7	-0.66		0.40		0.39	
KCNH8			0.53		0.51	
KCNIP1	-0.56			-0.62		-0.61
KCNIP3		0.57				
KCNIP4				0.32		0.32
KCNJ13	-1.12	-1.92				
KCNJ16	1.11					
KCNJ2				-0.67		-0.65
KCNJ3				0.49		
KCNJ9				0.43		0.42
KCNK10		0.84				
KCNK2		0.57				
KCNK9				0.54		
KCNMA1	0.69					
KCNQ3	0.96					
KCNQ4		1.03				
KCNS2				0.56		
KCNS3		1.32				
KCTD21		-0.51				
KDELR3		-0.88		-0.76		-0.73
KDM6B			0.38		0.37	
KDM7A	0.50					
KDR	1.66					
KIAA0040		1.10				
KIAA0319	0.89	0.72		0.41		0.40
KIAA0355		-0.49				
KIAA1024			0.41		0.40	
KIAA1161	-0.66	-0.99		-0.49		-0.48
KIAA1211L	0.84					
KIAA1217		-1.06		-0.31		-0.30
KIAA1324L		0.65				
KIAA1549L	-0.55					
KIAA1614		-0.75				
KIAA1644		-1.25				

Table 4.3	log2 fold change first round		log2 fold change second round			
Gene	CPM filtered hNP	CPM filtered hDN	CPM filtered hNP	CPM filtered hDN	RPKM filtered hNP	RPKM filtered hDN
KIAA1671	0.41					
KIAA2012		0.99				
KIF21B			0.66		0.65	
KIF26B		1.49		0.52		0.52
KIF5A		0.41				
KIF5C		0.59				
KIF9				0.46		0.45
KIRREL		-0.60		-0.47		-0.46
KIRREL3		0.77	0.37		0.37	
KITLG		-0.56				
KLF17	0.81					
KLF5		-0.76				
KLHDC7A				-0.66		
KLHL13		0.45				
KLHL14		1.21				
KLHL32		1.91				
KLHL4		0.70				
KLHL42		0.43				
KY		1.03				
L1CAM		0.65	0.47		0.46	
L3MBTL3		0.48				
LAMA2	1.35	2.01				
LAMA3		0.93				
LAMB1		-0.98		-0.35		-0.34
LAMC1		-0.62				
LAMP1		-0.42				
LAMP5		-0.61				
LANCL3	1.44	0.96				
LATS2				-0.35		-0.34
LAYN		-1.46		-0.50		-0.48
LBH	1.18					
LCA5		-0.45				
LCTL				-0.52		-0.51
LDB2		1.07				
LDLRAD3		-0.40				
LDLRAD4	0.61					
LEF1	-0.58	-0.61				
LFNG		0.67				
LGALS12		1.11		0.53		0.52
LGALS3		-0.73	-0.39		-0.38	

Table 4.3	log2 fold change first round		log2 fold change second round			
Gene	CPM filtered hNP	CPM filtered hDN	CPM filtered hNP	CPM filtered hDN	RPKM filtered hNP	RPKM filtered hDN
LGALS3BP		-0.59				
LGALS8	-0.50					
LGI1	-0.81	-0.87				
LGI2	0.79	0.90				
LGMN		-0.66		-0.36		-0.35
LGR4				-0.48		-0.47
LHCGR		-0.72				
LHFPL3	-0.70					
LIMCH1		0.42				
LIMK2		1.14				
LIMS1	0.40					
LINGO1		0.92				
LIPG		-0.62				
LIX1		-0.62				
LMAN2L		-0.42				
LMCD1		-0.47		-0.59		-0.58
LMO2	-0.43	-0.75				
LMOD1		-1.13		-0.58		-0.56
LNPEP	0.47					
LNX1	1.06					
LNX2		-0.43		-0.35		-0.34
LOXL1	-0.56					
LOXL2						-0.43
LPCAT2		-1.21		-1.12	-0.38	-1.10
LPL	-1.25	-1.09	-0.40	-0.66	-0.39	-0.64
LPP	0.38					
LRAT		-0.63		-0.36		-0.35
LRFN1		0.89				
LRIT3		-1.27				
LRP1B		0.50				
LRP8			0.36		0.36	
LRRC10B		1.19		0.54		0.51
LRRC15	1.37					
LRRC16B					0.35	
LRRC2		-2.20				
LRRC3B	-1.24					
LRRC4C		0.92				
LRRC55		1.09				
LRRC7		0.85				0.37
LRRC8C		-0.47				

Table 4.3	log2 fold change first round		log2 fold change second round			
Gene	CPM filtered hNP	CPM filtered hDN	CPM filtered hNP	CPM filtered hDN	RPKM filtered hNP	RPKM filtered hDN
LRRN1		0.57				
LRRN2		0.43				
LRRTM1		1.29				
LRRTM2	-0.40	0.58		0.31		0.31
LSAMP		0.88				
LTBP2	0.62	-0.86		-0.46		-0.44
LTBP4		-1.14				
LUM	-0.98		-0.45		-0.44	
LURAP1L		0.77				
LUZP2	-1.08					
LY6H	-0.94					
LYN			-0.33		-0.32	
LYPD6B	0.88					
LYST	0.47					
LZTS1		-0.74				
MAATS1	0.68	0.47		0.48		0.47
MAB21L1		-0.76				
MACROD2		0.91				
MAFB	0.44					
MAGEE1		0.48				
MAGEE2		-0.94				
MAK				0.51		0.49
MAML3			0.36		0.35	
MAN1C1		-0.52				
MAN2B2		-0.50				
MAP1B	0.43					
MAP1LC3C		-1.52				
MAP3K1		0.86		0.34		0.34
MAP3K19				0.56		0.55
MAP3K3		0.54				
MAP4		-0.57				
MAPK15				0.53		
MAPT		0.67		0.32		0.31
MARVELD3		-1.20				
MASP1		1.00				
MAST4	-0.48					
MATN2		-0.95		-0.42		-0.42
MB21D2		0.69				
MCC				-0.38		-0.37
MCHR1	0.89	1.62				

Table 4.3	log2 fold change first round		log2 fold change second round			
Gene	CPM filtered hNP	CPM filtered hDN	CPM filtered hNP	CPM filtered hDN	RPKM filtered hNP	RPKM filtered hDN
MCTP1	-0.45					
MDGA2		1.05		0.42		0.41
MDM1		0.35				
MEF2C		0.49				
MEGF11		0.73				
MEGF9		-0.47				
MEIS1		0.59				
MERTK		-0.67				
MET	-0.72	-1.31	-0.41	-0.55	-0.39	-0.54
METRNL	-0.61	-0.89				
METTL21B		-0.56				
METTL7A	-0.82					
METTL7B		-1.27			-0.37	
MEX3B		0.67				
MFAP4		-1.65		-0.74		-0.73
MFAP5		1.12				
MFGE8		-0.38				-0.38
MFSD10	-0.76					
MFSD2A				-0.33		-0.32
MGAT3		0.90				
MGAT4A	0.49	0.56				
MGAT4C	-0.72	-0.95				
MGST1		-0.48				
MGST3	-0.51					
MLIP		-1.37				
MMP15		-0.84				
MMP16		-0.48				
MMP17		0.83				
MMP19		-1.22		-0.72		-0.69
MMP2				-0.67		-0.66
MMP24			0.43		0.42	
MNS1	0.68					
MOGS		-0.49				
MOK				0.41		0.41
MORN3		-0.60				
MOXD1	-0.71					
MPC1	-0.32					
MPP4				-0.46		
MPPED2		0.38				
MRAS		0.41				

Table 4.3	log2 fold change first round		log2 fold change second round			
Gene	CPM filtered hNP	CPM filtered hDN	CPM filtered hNP	CPM filtered hDN	RPKM filtered hNP	RPKM filtered hDN
MREG	1.20					
MRPS12		-0.67				
MRPS6		-0.99		-0.39		-0.38
MRVI1		1.36				
MSRB3				-0.42		-0.41
MSTN		0.79				
MSX1		1.22				
MT1F		0.92				
MT1X		0.75				
MT2A		1.43				
MT3		1.19				
MTSS1L	-0.52					
MTTP		-0.62				
MTURN		0.64				
MTUS2	1.77			0.45		
MXI1		0.67				
MXRA5		1.00				
MYCL		0.80				
MYH14		-0.90				
MYH7		0.65				
MYH9		-0.69		-0.50		-0.49
MYLK		-1.11	-0.39	-0.82	-0.38	-0.80
MYLK3		1.03				
MYO10	-0.42					
MYO16		2.17		0.35		0.35
MYO1B	0.73					
MYO1E		-1.08		-0.68		-0.67
MYO3A	1.41		0.49		0.47	
MYO5B	-0.43					
MYO5C		-0.61				
MYO6		0.30				
MYO7A		1.98		0.60		0.59
MYOC		-1.21				
MYOM1		-0.89				
MYOZ3		0.72				
MYT1			0.63		0.61	
MYT1L			0.48	0.37		0.37
MYZAP		1.62				
NAALAD2		0.81				
NAALADL2		-0.54				

Table 4.3	log2 fold change first round		log2 fold change second round			
Gene	CPM filtered hNP	CPM filtered hDN	CPM filtered hNP	CPM filtered hDN	RPKM filtered hNP	RPKM filtered hDN
NACC2	-0.36	-0.61		-0.38		-0.37
NALCN	-1.06	-0.85				
NAV2	1.16					
NCALD	0.65	0.75				
NCAM1		0.45				
NCAN	-0.48			-0.31		-0.31
NCAPG		-0.56				
NDC80		-0.50				
NDRG4		0.56				
NDUFA7	0.70					
NEB	-1.00					
NEBL	1.02					
NECAB1						0.38
NEDD9		-0.87		-0.67		-0.66
NEFL			-0.36		-0.35	
NEGR1		1.26		0.65		0.64
NEK5		1.26		0.76		0.74
NELL2	0.90	2.50		0.77		0.76
NES	0.36					
NET1		-0.53				
NETO1	0.35	0.74				
NETO2		0.47				
NFASC	0.76	1.29	0.47		0.46	
NFE2L1		-0.56				
NFIX		0.38				
NFKBIZ	0.90					
NGB		2.14		0.47		
NGEF				0.46		0.45
NHS		-0.64				
NHSL2		-0.98				
NID1		-0.48		-0.48		-0.47
NID2		-0.58				
NIPAL2	0.88	0.74				
NIPAL3		-0.51				
NKAIN1		0.53				
NKAIN2	0.75	2.36		0.85		0.83
NKAIN4		1.06				
NMB		1.91		0.63		0.62
NME9		0.75				
NMNAT2			0.41		0.41	

Table 4.3	log2 fold change first round		log2 fold change second round			
Gene	CPM filtered hNP	CPM filtered hDN	CPM filtered hNP	CPM filtered hDN	RPKM filtered hNP	RPKM filtered hDN
NMRK1	-0.44					
NNAT		-0.68				
NNMT		1.43				
NOL4			0.31		0.30	
NOMO1		-0.40				
NOMO2		-0.71		-0.35		-0.34
NOS1AP		0.67		0.36		0.36
NOVA1		0.68				
NPAS3		0.71				
NPC2	-0.54					
NPFFR1		1.13				
NPM3		-0.66				
NPR3		-1.13		-0.50		-0.49
NPTX1				0.55		0.53
NPTXR	1.21	0.64		0.39		0.39
NPY	0.80					
NQO1		-0.74		-0.48		-0.47
NR3C1		0.36				
NR4A2		-0.76				
NRCAM	0.49					
NRG1				-0.41		-0.41
NRG4		0.80				
NRIP1		0.60				
NRIP3				0.37		0.37
NRL	-0.82					
NRP1		0.51				
NRP2	0.85					
NRSN1		1.47		0.58		0.58
NRXN2		0.76				
NSG1			0.39	0.32	0.38	0.32
NT5DC3	0.98	1.84		0.59		0.58
NT5E				-0.48		-0.47
NTF3						-0.44
NTM		2.39		0.83		0.82
NTNG1	-0.87	-2.26		-0.73		-0.71
NTNG2						0.41
NTRK2		1.12		0.32		0.32
NUAK1		-0.60				
NUDT11		0.47				
NUF2		-0.50				

Table 4.3	log2 fold change first round		log2 fold change second round			
Gene	CPM filtered hNP	CPM filtered hDN	CPM filtered hNP	CPM filtered hDN	RPKM filtered hNP	RPKM filtered hDN
NUPR1	-1.22	-1.53				
NWD1		-0.62				
NXPH3		-0.85				
OAF		1.11				
OGN		-0.74				
OLFM3	-0.71					
OLFML2A		-0.93		-0.60		-0.59
OLFML2B	1.40	0.98				
OLFML3	0.81					
OLIG1		0.84				
OLIG2	-0.34					
OMG	-0.91					
ONECUT2			0.43		0.42	
OPCML		1.82		0.99		0.98
OPRK1		-0.86				
OSBPL10	0.41				-0.36	
OSBPL1A		0.36				
OSGIN2		-0.40				
OTOF				-0.50		
OTOL1		1.89		0.95		0.87
OTUD1		0.50				
OTX2	-0.33					
P2RX7	-0.58					
P2RY1		0.58				
P3H2	0.57					
P3H3		-1.17				
P4HA2		-0.76				
P4HB		-0.42		-0.34		-0.33
PADI2		3.16		0.78		0.77
PAK3			0.33		0.33	
PAK7			0.48		0.46	
PALD1		0.99				
PALM2	0.76	1.32				
PALMD		1.08				
PAM		0.32				
PAMR1		-0.72				
PANX1				-0.36		-0.35
PAPPA		4.59		1.27		
PAQR3	0.74					
PAQR8	-0.86	-0.86				

Table 4.3	log2 fold change first round		log2 fold change second round			
Gene	CPM filtered hNP	CPM filtered hDN	CPM filtered hNP	CPM filtered hDN	RPKM filtered hNP	RPKM filtered hDN
PARD3	0.32					
PARD3B		-0.30				
PARD6B	0.67					
PARD6G	-0.37					
PARVA				-0.32		-0.31
PAX6				0.41		0.40
PBK		-0.60				
PBX3		0.70				
PCBP3			0.56		0.55	
PCDH1		0.99				
PCDH18		1.01		0.67		0.67
PCDH7	0.88	0.66				
PCDH8		2.17		0.55		0.54
PCDHA1		0.81				
PCLO	0.70					
PCP4					-0.34	
PCP4L1	-0.80					
PCSK1		-0.78				
PCSK5		-0.64				
PCSK9		1.04		0.87		0.84
PDCD1LG2	0.96					
PDE1B		1.17		0.73		0.71
PDE1C		-0.92		-0.36		-0.35
PDE4B	-0.42					
PDE4DIP	-0.37					
PDE7B	0.69	1.56		0.44		0.43
PDE8A		0.79				
PDE8B	1.87					
PDGFB		-1.87		-0.74		-0.73
PDGFRB	-0.77	-0.47		-0.37		-0.36
PDIA3		-0.52				
PDIA4		-0.52				
PDIA6		-0.33				
PDK3		-0.60				
PDLIM4		-0.71				
PDLIM5	0.54					
PDP1	0.55					
PDYN				1.63		1.58
PDZRN4			0.47		0.46	
PEA15		0.41				

Table 4.3	log2 fold change first round		log2 fold change second round			
Gene	CPM filtered hNP	CPM filtered hDN	CPM filtered hNP	CPM filtered hDN	RPKM filtered hNP	RPKM filtered hDN
PEG10			0.31		0.30	
PELI2		-0.86		-0.36		-0.35
PERP				-0.36		-0.35
PGM1		0.58				
PGM5				-0.54		-0.52
PGRMC2		-0.36				
PHACTR3	0.88	0.72				
PHF12		0.37				
PHF21B			0.34		0.34	
PHKA1	-0.47					
PHLDA1	-0.56					
PHLDB2		0.65				
PI15		-2.73		-0.90		-0.89
PIEZO1		-0.96				
PIGH		-0.42				
PIGT		-0.46				
PIK3C2A		-0.38				
PIK3C2B	-0.67					
PIP5K1B		-1.24		-0.51		-0.50
PIRT	0.54					
PITPNC1	-0.53					
PITPNM3		0.95		0.37		0.36
PKIB		0.91				
PKP2		1.43				
PLA2G12A		-0.84				
PLA2R1	0.65					
PLAG1		-0.90				
PLAU		-0.68		-0.67		-0.65
PLBD2		-0.67				
PLCB1				0.59		0.58
PLCB4		0.32				
PLCL1			0.47			
PLD5		-1.99		-0.55		-0.54
PLEKHA1	0.75					
PLEKHA4		-0.45				
PLEKHA5		0.55				
PLEKHA6		1.11				
PLEKHA7		-0.69				
PLEKHG3		-0.58				
PLEKHG5	0.70	0.49				

Table 4.3	log2 fold change first round		log2 fold change second round			
Gene	CPM filtered hNP	CPM filtered hDN	CPM filtered hNP	CPM filtered hDN	RPKM filtered hNP	RPKM filtered hDN
PLEKHH2	-0.63	-0.95			0.34	
PLPP1		-0.39				
PLPP2						-0.43
PLPP4		1.07		0.68		0.66
PLPP5		-0.41				
PLPPR5		0.63				
PLS1	0.99					
PLXDC1			-0.48		-0.47	
PLXDC2	0.63	-0.65				
PLXNA2		0.80	0.39		0.38	
PLXNA4		0.60	0.39	0.32	0.38	0.32
PLXND1		-0.75		-0.50		-0.49
PMP22			-0.33		-0.32	
PNMA2	0.54					
PNOC		-1.20	-0.37	-0.38	-0.36	-0.37
POPDC3		-1.01				
POU3F4			0.42		0.41	
PPARG		1.04				
PPARGC1A		2.06		0.54		0.54
PPDPF		-0.48				
PPEF1			-0.40		-0.39	
PPFIA3		1.06				0.41
PPFIA4		0.76		0.48		
PPFIBP2	-0.55					
PPIF		-0.84				
PPM1L		0.55				
PPP1CC		1.19		0.37		0.37
PPP1R14C		-0.78	-0.36		-0.35	
PPP1R17				0.62		0.58
PPP1R1A		1.74				
PPP1R1B		1.08				
PPP1R1C	-0.40					
PPP1R3C	-0.77					
PPP1R9A	0.51	0.40				
PPP2R2C		1.92		0.68		0.67
PPP2R5A	-0.45					
PQLC3	0.77					
PRAF2		-0.55				
PRDM1	-0.54					
PRDX1	-0.51					

Table 4.3	log2 fold change first round		log2 fold change second round			
Gene	CPM filtered hNP	CPM filtered hDN	CPM filtered hNP	CPM filtered hDN	RPKM filtered hNP	RPKM filtered hDN
PRDX6		-0.48				
PRELID2	0.74	0.71				
PRELP	-1.16					
PRICKLE1	-0.63					
PRIMA1		1.42		0.68		0.67
PRKAA2		0.49				
PRKAB2		0.32				
PRKCB				0.50		
PRKCD	0.63	0.89				
PRKCE	0.48	0.73				
PRLR		1.38		0.84		
PRMT6		-0.71		-0.32		-0.31
PRNP	-0.33	-0.47				
PROB1		-0.95				
PROCR		-1.81				
PROKR1	1.18	0.78				
PROS1		-0.54				
PROX1	0.39					
PRR18		0.75				
PRR29		0.83		0.62		0.60
PRR32		1.37				
PRR5		1.55				
PRR5L	0.60					
PRRG3		0.80				
PRRT3	-0.49					
PRRT4		1.17				
PRSS12				-0.58		-0.57
PRSS23		-0.90				
PRSS35				-0.39		-0.38
PRUNE2		-0.33				
PRX		-0.83				
PSAP		-0.38				
PSAT1		0.94				
PSD3	-0.43	-0.43				
PTBP3	0.50					
PTCHD1		1.10		0.72		
PTCHD4	0.36	-0.61				
PTGDS	-0.87					
PTGFR		0.79				
PTGR1				-0.36		-0.35

Table 4.3	log2 fold change first round		log2 fold change second round			
Gene	CPM filtered hNP	CPM filtered hDN	CPM filtered hNP	CPM filtered hDN	RPKM filtered hNP	RPKM filtered hDN
PTHLH		1.05				
PTK2	0.43					
PTK2B	-0.66	-0.93				
PTN		1.30				
PTPN3	0.87					
PTPN5				0.54		0.54
PTPRD		0.87				
PTPRQ		1.14				
PTPRR				0.45		0.44
PTPRT	-0.63					
PTPRU		-0.79				
PTRF		-0.68				
PUM3		-0.35				
PUS7		-0.41				
PXDNL		-1.26				
PXYLP1	0.40	0.67				
PYGM		1.88		0.75		0.73
QPCT		1.15				
QTRTD1		-0.53				
RAB11FIP1		-1.34		-0.70		-0.69
RAB11FIP4				0.34		0.34
RAB27A		-0.46				
RAB29	-0.31					
RAB30		0.70				
RAB31				-0.33		-0.33
RAB3A			0.41		0.39	
RAB3B	0.94					
RAB3C			0.43		0.41	
RAB3GAP2		-0.41				
RAB6B	-0.53	0.47				
RAD9A		0.64				
RAI2	1.32					
RALGAPA2	-0.42					
RALGPS1		0.41				
RAMP1		-1.11				
RAP1GAP	-0.50					
RAPGEF5	0.93			0.59		0.59
RARB		1.54		0.72		0.71
RARRES3	-0.81					
RASA3		-0.44				

Table 4.3	log2 fold change first round		log2 fold change second round			
Gene	CPM filtered hNP	CPM filtered hDN	CPM filtered hNP	CPM filtered hDN	RPKM filtered hNP	RPKM filtered hDN
RASD1		0.83				
RASD2		0.84				0.38
RASGEF1B		0.54				
RASGRF1		3.14		1.06		1.04
RASGRF2		-0.81		-0.42		-0.41
RASGRP1	1.33	1.10				
RASGRP2		0.80				
RASGRP3		0.61				
RASL10B		0.48				
RASSF3				-0.61		-0.60
RASSF5		0.85				
RASSF8				-0.35		-0.34
RASSF9		-0.45				
RAVER2		-0.43				
RBBP8		-0.55		-0.36		-0.35
RBFOX1		0.96				
RBFOX2			0.32		0.32	
RBM20				-0.36		-0.35
RBMS2	-0.43					
RBMX2	-0.31					
RBPMS		-0.74				
RCAN2		0.92				
RCAN3		-0.72	-0.33		-0.32	
RDH10	0.94					
RELL1		-0.67				
RELN		0.90				
RERG		1.37				
RET	-0.74					
RFFL	1.05					
RFTN1		-0.82				
RFX3		0.32				
RGCC		1.44				
RGMA		0.82				
RGMB				0.36		0.36
RGPD8	0.83					
RGS11		-1.02				
RGS16	0.73					
RGS19		-0.85				
RGS20	-0.67					
RGS3		1.03				

Table 4.3	log2 fold change first round		log2 fold change second round			
Gene	CPM filtered hNP	CPM filtered hDN	CPM filtered hNP	CPM filtered hDN	RPKM filtered hNP	RPKM filtered hDN
RGS4		-1.06				
RGS5	0.76	-2.15		-0.86		-0.85
RGS7BP	-0.75					
RGS8	0.95	1.49	0.67	0.68	0.64	0.68
RGS9	-1.05					-0.40
RHBDF1		-0.80				
RHBDL3		0.64				
RHOU		1.08				
RHPN2		-0.78				
RIMBP2			0.52		0.51	
RIMKLA		0.40	0.35		0.35	
RIMS3		1.00				
RIPPLY1		1.10				
RIPPLY2		0.91				
RNASE1		-2.55		-0.52		-0.49
RNASE4		-1.09				
RND1		0.74				
RNF112					0.37	
RNF122		0.50				
RNF144A		0.47				
RNF150		0.47				
RNF152		0.61				
RNF165		0.62		0.38		0.38
RNF182		0.50				
RNF187		0.47				
RNF19A	0.33					
RNF207		-0.78				
RNF5	-0.54					
ROBO1		0.90				
ROBO2	-0.57		0.45		0.44	
ROMO1	-0.65					
ROPN1L				0.57		0.54
ROR2			0.38		0.37	
RP11-511P7.5		0.85				
RP11-849H4.2		-0.75				
RP6-24A23.6		1.14				
RPE65		-1.01	-0.39		-0.38	
RPH3A				-0.44		-0.43
RPL10A	-0.34					
RPL13	-0.45					

Table 4.3	log2 fold change first round		log2 fold change second round			
Gene	CPM filtered hNP	CPM filtered hDN	CPM filtered hNP	CPM filtered hDN	RPKM filtered hNP	RPKM filtered hDN
RPL27	-0.36					
RPLP2	-0.49					
RPN2		-0.43				
RPRM		-0.84		-0.45		-0.43
RPS28	-0.97					
RPS6KA1		-1.01				
RPS6KA2		-0.52				
RRAS				-0.43		-0.42
RRBP1		-0.71		-0.36		-0.35
RRM2		-0.70				
RSPH1		0.53		0.38		0.37
RSPH4A		0.54		0.40		0.40
RTN1	-0.96					
RTN2		0.59				
RTN3		0.35				
RTP1		0.96				
RUNX1T1		0.85	0.59		0.58	
RYR2		0.90		0.46		
RYR3	-0.59	0.76		0.45		0.45
S100A10	0.85					
S100A11			-0.42		-0.41	
S100A16		0.75				
S100B		-0.52				
S1PR1		0.50				
S1PR3		0.59				
SALL4	0.97					
SAMD11		-1.85				
SAMD5	1.00					
SAPCD2		-0.76				
SASH1		0.55				
SAT1	-0.77					
SATB1		0.44				
SATB2	0.36					
SBSPON	2.34	1.19				
SCARB1		-0.54				
SCD				-0.32		-0.31
SCD5		0.52				
SCG2				0.47		0.47
SCG3	-0.59					
SCGN			0.40		0.39	

Table 4.3	log2 fold change first round		log2 fold change second round			
Gene	CPM filtered hNP	CPM filtered hDN	CPM filtered hNP	CPM filtered hDN	RPKM filtered hNP	RPKM filtered hDN
SCN1A				0.30		0.30
SCN2A				0.42		0.41
SCN3B		0.75	0.42		0.41	
SCN7A		1.73		0.54		
SCN9A		0.81				
SCNN1B		1.16				
SCPEP1		-0.57				
SCRT2			0.70	0.45	0.67	0.44
SCUBE1	1.22	3.99	0.47			
SCUBE2				0.50		0.49
SCYL2	0.43					
SDC2		-1.51	-0.35	-0.65	-0.34	-0.64
SDC3		1.41				
SDC4	1.01					
SDK1		-1.00				
SEL1L3	0.77					
SELENBP1	-0.66	-0.82				
SEMA3A	0.47	-0.68		-0.65		-0.64
SEMA3B		-1.02				
SEMA3C		-1.26		-0.50		-0.49
SEMA3D		-1.85				
SEMA4B	-0.59					
SEMA5A		-0.71				
SEMA6D				-0.36		-0.35
SEPP1	-0.96	-1.68				
SEPSECS		-0.51				
SERPINA3		-1.27				
SERPINB8	0.61					
SERPINB9		-1.32				
SERPINE1				-0.52		-0.51
SERPINE2	-0.75			-0.34		-0.33
SERPINH1	-0.38			-0.53		-0.52
SERPINI2		-1.01				
SERTAD4	0.72	0.99		0.46		0.45
SESN3		0.35				
SESTD1	0.39					
SEZ6		1.57				
SEZ6L	0.61					
SFRP1		0.54				
SFRP2		0.96		0.74		0.73

Table 4.3	log2 fold change first round		log2 fold change second round			
Gene	CPM filtered hNP	CPM filtered hDN	CPM filtered hNP	CPM filtered hDN	RPKM filtered hNP	RPKM filtered hDN
SFT2D2	0.32					
SGCD	-1.30	-0.49				
SGK1	0.88	1.36				
SH3BGRL2		-0.43				
SH3BP4				-0.33		-0.32
SH3BP5	0.67	0.37				
SH3GL2	0.59					
SH3GL3				0.48		0.46
SH3PXD2A	0.53					
SH3RF1		0.54				
SH3RF3		-0.54				
SH3TC2				-0.48		
SHANK2				0.34		0.34
SHCBP1		-0.66				
SHH				0.49		
SHISA2				0.36		0.36
SHISA3		-1.00				
SHISA6		1.55		0.49		0.48
SHISA7	-0.87					
SHROOM3		-0.59				
SHTN1		0.32				
SIDT1		1.18				
SIPA1L2	0.33					
SIPA1L3	-0.51					
SIX3		1.42				
SKAP1		0.95				
SLA		0.94		0.58		
SLC10A4			-0.36		-0.35	
SLC12A1				0.54		
SLC12A5		0.78		0.62		0.61
SLC12A8	-0.64	-0.59				
SLC16A12		-1.59				
SLC16A2		-0.51				
SLC16A6	0.74					
SLC17A6		0.92				
SLC17A8	0.83	1.02				
SLC1A1	0.66					
SLC1A2		0.90				
SLC1A5		-1.26		-0.63		-0.60
SLC22A15		0.73				

Table 4.3	log2 fold change first round		log2 fold change second round			
Gene	CPM filtered hNP	CPM filtered hDN	CPM filtered hNP	CPM filtered hDN	RPKM filtered hNP	RPKM filtered hDN
SLC22A3		2.62				
SLC24A4	2.58			0.73		
SLC25A43		-0.46				
SLC26A4	-0.70					
SLC26A7	0.72			0.52		0.51
SLC29A1		-1.31				
SLC2A12				-0.35		-0.34
SLC2A5		0.96				
SLC34A2		1.01		0.85		
SLC35B4		-0.41				
SLC35F2	1.01					
SLC35F4		1.44		0.65		0.63
SLC39A12		0.75				
SLC44A1		-0.49				
SLC44A3		0.69				
SLC44A5		0.60				
SLC47A1		-0.97				
SLC47A2		-1.11				
SLC4A10	0.75	1.50		0.61		0.60
SLC5A1		-1.54		-0.49		-0.47
SLC5A3		-1.48		-0.61		-0.60
SLC6A12				0.48		0.48
SLC6A13				0.74		0.72
SLC6A17				0.92		0.90
SLC6A20	-1.95		-0.75	-0.70	-0.72	
SLC6A6			0.46			
SLC7A11	-0.58					
SLC7A7		0.89				
SLC8A1	0.77	0.70				
SLC9A9		0.76				
SLC9B2	0.43	0.47				
SLCO1A2	-1.64					
SLCO1C1	-0.67					
SLCO5A1		0.49		0.35		0.35
SLF2	-0.42	-0.71				
SLIT1			0.55		0.54	
SLIT2				-0.44		-0.43
SLIT3		-1.54				
SLITRK1			0.45			
SLITRK2		0.90				

Table 4.3	log2 fold change first round		log2 fold change second round			
Gene	CPM filtered hNP	CPM filtered hDN	CPM filtered hNP	CPM filtered hDN	RPKM filtered hNP	RPKM filtered hDN
SLITRK3				0.53		
SLITRK4	0.75			0.47		
SLITRK5		0.50				
SLITRK6			0.42			
SMAD6		-0.81				
SMAD9		-0.51				
SMC4		-0.35				
SMC5		-0.50				
SMIM18		0.70				
SMIM4		-0.82				
SMOC2		-1.09				
SMPD2	-0.69					
SMPD3			0.49		0.48	
SMTNL2		0.87				
SNAI2		-1.01				
SNCB				0.62		0.57
SNTG1		-0.36				
SNTG2	-0.87					
SNX29		0.52				
SNX5		-0.35				
SOBP	-0.74					
SORBS2	0.45					
SORCS1	0.39					
SORCS3	0.70	0.53				
SOWAHA				0.47		0.45
SOX21	-0.55	-0.43				
SPAG5		-0.49				
SPAG8				0.48		0.47
SPARC				-0.33		-0.33
SPARCL1	-1.06		-0.36		-0.36	
SPATA2L		-0.77				
SPC24		-0.51				
SPEF1						0.44
SPOCK1		0.74	0.48		0.47	
SPON1		0.79				
SPRY1				-0.43		-0.42
SPRY2				-0.37		-0.36
SPRY4				-0.42		-0.41
SPSB1	0.87					
SPSB4		0.58				

Table 4.3	log2 fold change first round		log2 fold change second round			
Gene	CPM filtered hNP	CPM filtered hDN	CPM filtered hNP	CPM filtered hDN	RPKM filtered hNP	RPKM filtered hDN
SPTB				0.49		0.48
SPTLC3		0.41				
SPTSSB	1.04					
SQRDL		0.78				
SRD5A1		-0.42				
SREBF1		-0.66				
SRRM4	0.74		0.77		0.75	
SSC5D		-0.76				
SSFA2	-0.37					
SSR1		-0.33				
SST		1.87				
SSTR2		0.81				
ST18			0.50		0.49	
ST3GAL6	0.61					
ST6GAL1	1.10	0.79				
ST6GAL2	-0.68					
ST6GALNAC3		0.45				
ST8SIA2		0.50				
ST8SIA6		1.78		0.75		0.72
STAC		-0.99				
STAC2		-1.42				
STARD13				-0.43		-0.42
STC1	0.50					
STC2	1.56					
STEAP2	0.42	0.68				
STEAP3				-0.41		-0.40
STIM1		-0.33				
STK17A	-0.74			-0.53		-0.52
STK26		0.94				
STK32A	0.79					
STK32B		1.19		0.45		0.45
STKLD1		1.04				
STMN4		0.57		0.35		0.35
STOM	0.50					
STOML3		-1.67				
STON1		-0.88		-0.44		-0.44
STRA6				-0.93		-0.90
STX11		-0.73				
STX3	0.75	-0.70				
STXBP5L	0.45					

Table 4.3	log2 fold change first round		log2 fold change second round			
Gene	CPM filtered hNP	CPM filtered hDN	CPM filtered hNP	CPM filtered hDN	RPKM filtered hNP	RPKM filtered hDN
SUCLG1	-0.42					
SULF1		0.86				
SULF2	0.57	1.27				
SUMF1		-0.73				
SUSD4				0.43		0.42
SUSD5		-0.56				
SV2B		1.59				
SVEP1		-1.78		-0.55		-0.54
SVOP			0.54		0.52	
SWAP70		-0.84		-0.35		-0.34
SYBU				-0.34		-0.34
SYN1			0.41		0.39	
SYN2		2.11		0.54		
SYNC			-0.46		-0.44	
SYNE2	0.59					
SYNJ2		0.43				
SYNM		-0.82				
SYNPO		0.81				
SYNPO2				-0.38		-0.37
SYNPR			0.44		0.44	
SYT1		0.76		0.35		0.35
SYT12	0.71					
SYT13				0.49		0.48
SYT16			0.41	0.46		0.46
SYT4			0.60	0.93		0.92
SYT5		0.91		0.44		0.43
SYT7		1.91		0.80		0.78
SYTL2				-0.35		-0.35
SYTL3				0.47		0.46
TAC3					0.37	
TACR1				0.57		
TADA1	0.33					
TAF4B	-0.62	-0.72				
TAGLN				-0.50		-0.49
TARBP1	0.53					
TBC1D8B				-0.43		-0.42
TBC1D9		-0.52				
TBX2		-1.18				
TCEAL7	0.52					
TCF7L2	0.54					

Table 4.3	log2 fold change first round		log2 fold change second round			
Gene	CPM filtered hNP	CPM filtered hDN	CPM filtered hNP	CPM filtered hDN	RPKM filtered hNP	RPKM filtered hDN
TCTEX1D1			-0.44		-0.42	
TEK		-1.15		-0.60		-0.59
TEKT1				0.56		0.55
TENM3		-0.57		-0.51		-0.50
TENM4	0.96			0.45		0.44
TF		1.24		0.33		0.33
TFAP2E				0.58		0.55
TFCP2L1		0.87				
TFPI2		-0.92		-0.40		-0.39
TGFA				-0.69		-0.67
TGFB2		-0.58				-0.32
TGFBI	0.84			-0.56		
TGFBR2				-0.61		-0.60
TGM2		3.92		0.56		
TGOLN2		-0.30				
THAP8	-0.75					
THBS1		-1.69		-0.78		-0.76
THBS2	-0.55	0.40				
THBS3		-0.56				
THBS4		-0.64				
THRB		1.18	0.38		0.37	
THSD1	-0.50	-0.57				
THSD4				-0.66		-0.64
THSD7B	-0.55	1.01				
TIAM1	0.33					
TIMP2		-0.49				
TIMP3	0.35					
TIMP4	-0.72					
TKTL1		2.04		0.86		0.84
TLE1		0.78				
TLE2	-0.71					
TLE4		0.82				
TLN2				-0.36		-0.36
TLR3		-0.79				
TLR5		1.12				
TM4SF1	-0.63					
TMCC3			0.34		0.33	
TMED10		-0.32				
TMEM106C		0.68				
TMEM132B	1.28	1.93	0.38	0.45	0.37	0.44

Table 4.3	log2 fold change first round		log2 fold change second round			
Gene	CPM filtered hNP	CPM filtered hDN	CPM filtered hNP	CPM filtered hDN	RPKM filtered hNP	RPKM filtered hDN
TMEM132C		1.45				
TMEM132E		0.47				
TMEM133	0.42					
TMEM150C		0.75				
TMEM151A				0.51		
TMEM151B			0.59		0.58	
TMEM158					-0.31	
TMEM163		-0.68		-0.35		-0.34
TMEM178B		0.51				
TMEM179	-0.78					
TMEM185B		-0.32				
TMEM196			0.43		0.40	
TMEM2	0.70					
TMEM200A		1.20		0.42		0.41
TMEM205	-0.67					
TMEM221		-0.84				
TMEM229B	0.90	0.62				
TMEM233	2.09					
TMEM257		1.33				
TMEM266		1.34				
TMEM47		-0.57				
TMEM51		1.07				
TMEM63C		1.38				
TMEM74				0.67		
TMOD1		-0.59				
TMPRSS5				0.38		0.37
TMPRSS7		-1.93		-0.48		-0.47
TMTC1	0.74					
TMTC2	-0.70					
TNFAIP2		1.30				
TNFAIP8				0.51		
TNFRSF11B	-0.64	-1.09		-0.52		-0.51
TNFRSF19		0.85		0.36		0.36
TNFRSF25						0.40
TNFSF10				-0.65		
TNN	1.48					
TNNC1				-0.49		-0.46
TNR	-0.78	1.05		0.37		0.37
TNS1	0.76					
TNS3	-0.61	-0.63				

Table 4.3	log2 fold change first round		log2 fold change second round			
Gene	CPM filtered hNP	CPM filtered hDN	CPM filtered hNP	CPM filtered hDN	RPKM filtered hNP	RPKM filtered hDN
TOP1MT		-0.58				
TOX3			0.36		0.35	
TPBG				-0.40		-0.39
TPD52L1		1.59				
TPM1		-1.22		-0.52		-0.51
TPP1		-0.60				
TPPP		-1.29				
TPPP3		0.86		0.58		0.57
TRAF3		0.48				
TRAF4	-0.57					
TRAF5		-0.79				
TRAM2	-0.63	-0.70		-0.48		-0.48
TRH				0.58		0.55
TRIB1	0.79					
TRIL		0.76				
TRIM14	0.60					
TRIM22		-0.44	-0.37		-0.36	
TRIM36	0.44					
TRIM47		1.05				0.44
TRIM5		-0.38				
TRIM56		-0.43				
TRIM66		-0.55				
TRIP6		-0.57				
TRPC3	1.03					
TRPC4				-0.56		-0.55
TRPC6	-1.60					
TRPM1		1.13				
TRPM8	-1.06		-0.55		-0.53	
TRPS1		0.74				
TSC22D3	-0.67					
TSHZ1		0.41		0.43		0.43
TSHZ2		0.72				
TSKU		-0.51				
TSPAN12		0.93				
TSPAN33		0.59				
TSPAN7	-0.92	0.61				
TTC29		0.83				
TTC39A	0.67					
TTC39C		-0.42				
TTLL4		0.65				

Table 4.3	log2 fold change first round		log2 fold change second round			
Gene	CPM filtered hNP	CPM filtered hDN	CPM filtered hNP	CPM filtered hDN	RPKM filtered hNP	RPKM filtered hDN
TTLL9				0.45		0.44
TTN				0.59		
TTYH2		-0.70		-0.36		-0.35
TUB		0.37				
UAP1L1		-0.66				
UBALD2	-0.48					
UBE2E2		0.69				
UBXN11				0.40		0.40
UHRF1		-0.54				
ULBP3		-1.13				
UNC13A			0.43		0.42	
UNC5B		-0.84				
UNC79			0.56		0.54	
UPB1				0.50		
USP2	-0.60					
USP51		0.73				
USP53	0.49					
UTRN	0.32					
UXS1		-0.42				
VAMP3		-0.36				
VASH2	3.14		0.36		0.35	
VASN		-0.75				
VAT1L	0.96	-1.03		-0.39		-0.38
VAV2		-0.52				
VAV3	0.48					
VCAM1	-0.46	0.78		0.38		0.38
VCL		-0.71		-0.40		-0.39
VDR		1.61				
VEGFA		-0.98		-0.45		-0.44
VEPH1		1.02				
VIM		-0.57				
VSNL1				0.48		0.47
VSTM2A			0.87		0.82	
VSTM2L		0.88				
VSTM4		0.70				
VWA3A				0.74		0.73
VWC2L		0.94				
WASF3		0.43				
WBP2		0.42				
WBP5	0.71					

Table 4.3	log2 fold change first round		log2 fold change second round			
Gene	CPM filtered hNP	CPM filtered hDN	CPM filtered hNP	CPM filtered hDN	RPKM filtered hNP	RPKM filtered hDN
WDR63		0.54				
WEE1		-0.60				
WFDC1		-1.04				-0.31
WIF1				-0.92		-0.90
WIPF3		1.07		0.57		0.56
WNT2B				0.61		0.60
WNT7B		1.77				
WSCD2				0.48		
WWC1	-0.52	-0.57		-0.30		
WWP1		0.62				
WWTR1	0.37					
XAF1	0.64					
XKR4		0.85		0.47		0.47
XKR7			0.64		0.62	
ZAR1		-0.90				
ZBTB44		0.37				
ZCCHC12		0.69		0.39		0.39
ZDHHC13	0.92					
ZDHHC22		1.09				
ZDHHC23		-0.44				
ZFHX3			0.42		0.41	
ZFPM2		0.84				
ZGRF1		-0.42				
ZMIZ1		0.45				
ZMYND10		0.73		0.62		0.60
ZNF106	-0.40					
ZNF185				-0.48		-0.46
ZNF385B	-1.07	-0.93				
ZNF385D		-0.49				
ZNF436	-0.46					
ZNF483	0.87					
ZNF488		1.24				
ZNF503	-0.73					
ZNF521		0.96				
ZNF550		0.52				
ZNF556		0.94				
ZNF695	0.65					
ZNF70		0.45				
ZNF704	0.51					
ZNF727		-0.66				

Table 4.3	log2 fold change first round		log2 fold change second round			
Gene	CPM filtered hNP	CPM filtered hDN	CPM filtered hNP	CPM filtered hDN	RPKM filtered hNP	RPKM filtered hDN
ZNF804A		0.88				
ZNRF2	0.48					
ZRANB3		-0.44				
ZSWIM5			0.33		0.33	

Table 4.4 *Differentially expressed genes near DNA binding dependent and independent DARS (Corresponds to Figures 4.11, 4.14-15)*

Table 4.4

Gene	Differetial expression	DAR type	Chr	Start	End	Distance.to.TSS	Annotation
ABCC9	FOXP2WT hDN activated	hDN DNA binding independent open	chr12	21881933	21882433	54511	intron 7 of 30
ACTR3B	FOXP2WT hDN activated	hDN dependent closed	chr7	152989890	152990390	230391	Intergenic
ACTR3B	FOXP2WT hDN activated	hDN dependent closed	chr7	152909727	152910227	150228	Intergenic
ACTR3B	FOXP2WT hDN activated	hDN dependent closed	chr7	153061854	153062354	302355	Intergenic
ADAMTS17	FOXP2WT hDN repressed	hDN dependent closed	chr15	100125597	100126097	216131	promoter-TSS
ADAMTS9	FOXP2WT hDN repressed	hDN independent open	chr3	64725397	64725897	-37958	intron 1 of 5
ADAMTSL1	FOXP2WT hDN activated	hDN dependent open	chr9	18477174	18477674	3343	intron 1 of 28
ADCYAP1R1	FOXP2WT hDN activated	hDN dependent closed	chr7	31027871	31028371	-24340	Intergenic
ADRA2C	FOXP2WT hDN activated	hNP dependent open	chr4	3851175	3851675	84856	Intergenic
AKNA	FOXP2WT hNP activated	hNP dependent open	chr9	114405486	114405986	-11331	intron 9 of 11
ANK3	FOXP2WT hDN activated	hDN independent open	chr10	60677696	60678196	55580	intron 1 of 43
ANK3	FOXP2WT hDN activated	hDN independent open	chr10	60350775	60351275	38851	intron 2 of 43
ANKH	FOXP2WT hNP activated	hDN independent open	chr5	14937288	14937788	-65760	Intergenic
ASIC4	FOXP2WT hDN activated	hNP dependent open	chr2	219520006	219520506	6086	intron 1 of 4
ATCAY	FOXP2WT hNP activated	hDN dependent closed	chr19	3876832	3877332	-3538	Intergenic

Table 4.4

Gene	Differetial expression	DAR type	Chr	Start	End	Distance.to.TSS	Annotation
BCAR3	FOXP2WT hDN repressed	hDN independent open	chr1	93757596	93758096	-76008	intron 1 of 1
C11orf87	FOXP2WT hDN activated	hDN dependent closed	chr11	109088033	109088533	-333837	Intergenic
C1QL4	FOXP2WT hDN activated	hDN independent open	chr12	49331566	49332066	5372	TTS
C8orf34	FOXP2WT hDN activated	hDN independent open	chr8	68229321	68229821	-101151	intron 39 of 39
CABLES1	FOXP2WT hDN repressed	hDN dependent open	chr18	23114379	23114879	-19935	Intergenic
CACNA1E	FOXP2WT hDN activated	hNP dependent open	chr1	181557385	181557885	74085	intron 3 of 45
CACNA1E	FOXP2WT hDN activated	hNP dependent open	chr1	181423480	181423980	-59820	intron 1 of 10
CADPS	FOXP2WT hDN activated	hDN dependent closed	chr3	62948705	62949205	-73566	Intergenic
CALU	FOXP2WT hDN repressed	hNP dependent closed	chr7	128739017	128739517	-25	promoter-TSS
CAMK2B	FOXP2WT hDN activated	hNP dependent closed	chr7	44325211	44325711	170	promoter-TSS
CCL2	FOXP2WT hNP repressed	hDN dependent closed	chr17	34248460	34248960	-6567	Intergenic
CCL2	FOXP2WT hDN repressed	hDN dependent closed	chr17	34248460	34248960	-6567	Intergenic
CDH13	FOXP2WT hDN repressed	hNP dependent closed	chr16	82400000	82400500	-226544	Intergenic
CHODL	FOXP2WT hDN repressed	hDN dependent closed	chr21	17930006	17930506	12916	intron 1 of 4
CNR1	FOXP2WT hDN activated	hDN dependent open	chr6	88211348	88211848	-45550	Intergenic
CNTN2	FOXP2WT hNP activated	hDN independent closed	chr1	205012374	205012874	-30588	intron 22 of 23
COL11A1	FOXP2WT hDN repressed	hDN dependent closed	chr1	102737421	102737921	370825	Intergenic
COL12A1	FOXP2WT hDN activated	hDN independent closed	chr6	74921677	74922177	283980	Intergenic
COL1A2	FOXP2WT hDN repressed	hDN dependent open	chr7	94212089	94212589	-182222	Intergenic
COL2A1	FOXP2WT hDN activated	hDN independent open	chr12	47991504	47992004	12748	intron 15 of 52
COL4A4	FOXP2WT hDN repressed	hDN dependent open	chr2	227006086	227006586	158223	3' UTR

Table 4.4

Gene	Differetial expression	DAR type	Chr	Start	End	Distance.to.TSS	Annotation
COL4A4	FOXP2WT hDN repressed	hDN dependent open	chr2	227035766	227036266	128543	intron 37 of 47
COL4A6	FOXP2WT hDN repressed	hDN dependent open	chrX	108312876	108313376	125304	intron 2 of 44
CPEB3	FOXP2WT hDN activated	hDN dependent open	chr10	92083445	92083945	159584	intron 8 of 9
CRHBP	FOXP2WT hDN repressed	hDN dependent closed	chr5	76958963	76959463	6358	TTS
CRHBP	FOXP2WT hNP repressed	hDN dependent closed	chr5	76958963	76959463	6358	TTS
CRIM1	FOXP2WT hDN repressed	hDN independent open	chr2	36408292	36408792	52315	intron 2 of 16
CTGF	FOXP2WT hDN repressed	hDN dependent closed	chr6	131976771	131977271	-25643	intron 1 of 1
CTNNA2	FOXP2WT hDN activated	hDN dependent open	chr2	80608346	80608846	295217	TTS
CYR61	FOXP2WT hDN repressed	hDN dependent closed	chr1	85584262	85584762	3751	TTS
DAB1	FOXP2WT hDN activated	hDN dependent closed	chr1	58059723	58060223	190566	promoter-TSS
DACT1	FOXP2WT hDN activated	hDN independent closed	chr14	58621424	58621924	-12394	Intergenic
DACT1	FOXP2WT hNP activated	hDN independent closed	chr14	58621424	58621924	-12394	Intergenic
DCHS2	FOXP2WT hDN activated	hDN independent closed	chr4	154471911	154472411	19564	intron 1 of 7
DCT	FOXP2WT hDN activated	hDN independent open	chr13	94479489	94479989	-57	promoter-TSS
DLC1	FOXP2WT hDN repressed	hDN dependent closed	chr8	13239575	13240075	36723	intron 1 of 1
DOCK10	FOXP2WT hDN repressed	hDN dependent closed	chr2	225100229	225100729	-57866	Intergenic
DUSP10	FOXP2WT hDN activated	hDN independent closed	chr1	221715456	221715956	21194	intron 1 of 2
EHD4	FOXP2WT hDN repressed	hDN independent closed	chr15	41950378	41950878	21929	intron 2 of 5
ELAVL4	FOXP2WT hNP activated	hDN dependent open	chr1	50160778	50161278	51412	intron 2 of 6
ENPP2	FOXP2WT hDN repressed	hDN dependent open	chr8	119564814	119565314	27944	intron 4 of 6
EPB41L4B	FOXP2WT hDN activated	hNP dependent open	chr9	109258570	109259070	62144	intron 6 of 15

Table 4.4

Gene	Differetial expression	DAR type	Chr	Start	End	Distance.to.TSS	Annotation
EPHB2	FOXP2WT hNP activated	hNP dependent closed	chr1	22710458	22710958	-130	promoter-TSS
FAM101A	FOXP2WT hDN activated	hDN independent closed	chr12	124278589	124279089	-10325	intron 3 of 4
FAM198B	FOXP2WT hNP repressed	hNP dependent open	chr4	158169945	158170445	2371	promoter-TSS
FERMT2	FOXP2WT hDN repressed	hNP dependent closed	chr14	52950948	52951448	-101	promoter-TSS
FGF14	FOXP2WT hDN activated	hDN dependent closed	chr13	101875994	101876494	40401	promoter-TSS
FNDC1	FOXP2WT hDN repressed	hDN dependent closed	chr6	159152032	159152532	-17115	Intergenic
FOS	FOXP2WT hNP repressed	hNP dependent closed	chr14	75278455	75278955	-73	promoter-TSS
FOXP2	FOXP2WT hDN activated	hDN dependent closed	chr7	114182771	114183271	96711	intron 1 of 17
FOXP2	FOXP2WT hNP activated	hDN dependent closed	chr7	114182771	114183271	96711	intron 1 of 17
FRMD7	FOXP2WT hDN activated	hDN dependent closed	chrX	132127615	132128115	155	promoter-TSS
FRMPD4	FOXP2WT hNP activated	hNP dependent open	chrX	12125930	12126430	-12286	Intergenic
GAD2	FOXP2WT hDN activated	hDN dependent open	chr10	26243348	26243848	27291	intron 7 of 16
GAD2	FOXP2WT hNP activated	hDN dependent open	chr10	26243348	26243848	27291	intron 7 of 16
GALNT13	FOXP2WT hDN repressed	hDN dependent closed	chr2	153986469	153986969	42325	intron 1 of 11
GAS1	FOXP2WT hDN activated	hNP dependent closed	chr9	86947655	86948155	-716	promoter-TSS
GLRA2	FOXP2WT hNP activated	hDN dependent open	chrX	14440061	14440561	-88987	Intergenic
GNG11	FOXP2WT hDN repressed	hDN dependent open	chr7	93921763	93922263	309	5' UTR
GOLGA7B	FOXP2WT hDN activated	hNP dependent closed	chr10	97849791	97850291	-197	promoter-TSS
GRIK2	FOXP2WT hDN activated	hDN dependent open	chr6	103009419	103009919	1610684	Intergenic
GRIK2	FOXP2WT hDN activated	hDN dependent open	chr6	101150161	101150661	-248574	Intergenic
GRIK2	FOXP2WT hDN activated	hDN dependent open	chr6	101776935	101777435	378200	intron 6 of 16

Table 4.4

Gene	Differetial expression	DAR type	Chr	Start	End	Distance.to.TSS	Annotation
GRIK2	FOXP2WT hDN activated	hDN dependent open	chr6	101650501	101651001	251766	intron 3 of 16
GRIK2	FOXP2WT hDN activated	hDN dependent open	chr6	101429273	101429773	30538	TTS
GRM5	FOXP2WT hDN activated	hDN independent open	chr11	88860501	88861001	187321	intron 1 of 8
GSG1L	FOXP2WT hDN activated	hDN independent open	chr16	27720762	27721262	167145	intron 13 of 27
HCN1	FOXP2WT hDN repressed	hNP dependent open	chr5	45741162	45741662	-45294	Intergenic
HEG1	FOXP2WT hDN repressed	hNP dependent closed	chr3	125055752	125056252	-44	promoter-TSS
HMP19	FOXP2WT hDN activated	hDN independent open	chr5	174083381	174083881	38027	intron 1 of 1
HMP19	FOXP2WT hNP activated	hDN independent open	chr5	174083381	174083881	38027	intron 1 of 1
HS6ST2	FOXP2WT hDN activated	hDN independent open	chrX	132816650	132817150	144495	intron 3 of 5
HTRA1	FOXP2WT hDN repressed	hNP dependent closed	chr10	122461668	122462168	393	exon 1 of 9
IER3	FOXP2WT hDN repressed	hNP dependent closed	chr6	30779345	30779845	-35045	intron 1 of 3
IL33	FOXP2WT hDN activated	hDN independent open	chr9	6188436	6188936	-26463	Intergenic
IMMP2L	FOXP2WT hDN repressed	hDN dependent open	chr7	111562282	111562782	-15	promoter-TSS
ISL1	FOXP2WT hNP repressed	hNP dependent open	chr5	51194569	51195069	-188305	Intergenic
ITGAV	FOXP2WT hDN repressed	hDN dependent open	chr2	186641631	186642131	41676	intron 2 of 2
ITIH5	FOXP2WT hDN activated	hDN independent open	chr10	7551814	7552314	67609	Intergenic
ITIH5	FOXP2WT hDN activated	hDN independent open	chr10	7610483	7610983	8940	intron 2 of 6
KCNB1	FOXP2WT hDN activated	hNP dependent open	chr20	49381478	49381978	100916	intron 2 of 2
KCNH8	FOXP2WT hNP activated	hNP dependent open	chr3	19065005	19065505	-83270	Intergenic
KCNJ2	FOXP2WT hDN repressed	hDN independent closed	chr17	70366279	70366779	196994	intron 1 of 2
KDM6B	FOXP2WT hNP activated	hNP dependent closed	chr17	7835356	7835856	-4311	Intergenic

Table 4.4

Gene	Differetial expression	DAR type	Chr	Start	End	Distance.to.TSS	Annotation
KIAA1217	FOXP2WT hDN repressed	hDN dependent closed	chr10	23630648	23631148	-63848	Intergenic
KIF21B	FOXP2WT hNP activated	hDN dependent open	chr1	200971929	200972429	51521	TTS
KIRREL	FOXP2WT hDN repressed	hDN dependent closed	chr1	158045631	158046131	52608	intron 1 of 12
KIRREL	FOXP2WT hDN repressed	hDN dependent closed	chr1	158019413	158019913	26390	intron 1 of 12
LATS2	FOXP2WT hDN repressed	hDN dependent open	chr13	21006467	21006967	54866	intron 1 of 1
LRRC7	FOXP2WT hDN activated	hDN dependent open	chr1	69780031	69780531	20106	intron 1 of 24
LUM	FOXP2WT hNP repressed	hNP dependent closed	chr12	91098840	91099340	12675	Intergenic
MAP3K1	FOXP2WT hDN activated	hDN dependent closed	chr5	56763626	56764126	-51197	Intergenic
MAPT	FOXP2WT hDN activated	hNP dependent closed	chr17	45894142	45894642	10	promoter-TSS
MCC	FOXP2WT hDN repressed	hDN dependent closed	chr5	113356410	113356910	-61745	intron 2 of 18
MFGE8	FOXP2WT hDN repressed	hDN independent open	chr15	88954792	88955292	-41573	Intergenic
MYLK	FOXP2WT hDN repressed	hNP dependent open	chr3	123632223	123632723	-11790	intron 3 of 3
MYLK	FOXP2WT hNP repressed	hNP dependent open	chr3	123632223	123632723	-11790	intron 3 of 3
MYO16	FOXP2WT hDN activated	hNP dependent open	chr13	108882667	108883167	253694	intron 11 of 23
MYT1L	FOXP2WT hDN activated	hDN dependent closed	chr2	2674712	2675212	-343649	Intergenic
NEDD9	FOXP2WT hDN repressed	hDN dependent closed	chr6	11353938	11354438	28160	intron 1 of 1
NEFL	FOXP2WT hNP repressed	hDN dependent open	chr8	25034244	25034744	-77625	Intergenic
NELL2	FOXP2WT hDN activated	hDN dependent closed	chr12	44509448	44509948	365963	intron 20 of 20
NKAIN2	FOXP2WT hDN activated	hDN independent open	chr6	124429368	124429868	146613	intron 3 of 6
NOL4	FOXP2WT hNP activated	hDN dependent open	chr18	34297281	34297781	-73980	Intergenic
NOL4	FOXP2WT hNP activated	hDN dependent open	chr18	34220031	34220531	2189	TTS

Table 4.4

Gene	Differetial expression	DAR type	Chr	Start	End	Distance.to.TSS	Annotation
NT5E	FOXP2WT hDN repressed	hDN dependent open	chr6	85388454	85388954	-60880	exon 2 of 2
NTF3	FOXP2WT hDN repressed	hDN independent closed	chr12	5566975	5567475	73093	intron 25 of 26
NTM	FOXP2WT hDN activated	hDN dependent closed	chr11	131910504	131911004	-64	promoter-TSS
NTNG1	FOXP2WT hDN repressed	hDN dependent closed	chr1	107181588	107182088	33769	intron 2 of 6
PANX1	FOXP2WT hDN repressed	hDN independent open	chr11	94175506	94176006	46828	intron 2 of 4
PARVA	FOXP2WT hDN repressed	hDN dependent closed	chr11	12456981	12457481	79752	intron 1 of 7
PCDH18	FOXP2WT hDN activated	hDN dependent open	chr4	137680744	137681244	-148496	Intergenic
PCDH18	FOXP2WT hDN activated	hDN dependent open	chr4	137543126	137543626	-10878	Intergenic
PCDH18	FOXP2WT hDN activated	hDN dependent open	chr4	137799799	137800299	-267551	Intergenic
PCDH8	FOXP2WT hDN activated	hDN dependent open	chr13	52931711	52932211	-83321	Intergenic
PDZRN4	FOXP2WT hNP activated	hDN independent open	chr12	41277009	41277509	88811	intron 3 of 9
PEG10	FOXP2WT hNP activated	hDN dependent open	chr7	94658010	94658510	1935	intron 1 of 1
PERP	FOXP2WT hDN repressed	hDN dependent closed	chr6	138001706	138002206	105567	Intergenic
PLXDC1	FOXP2WT hNP repressed	hDN independent open	chr17	39123580	39124080	27819	intron 1 of 12
PLXNA4	FOXP2WT hDN activated	hDN dependent closed	chr7	132463807	132464307	112507	intron 3 of 3
PLXNA4	FOXP2WT hNP activated	hDN dependent closed	chr7	132463807	132464307	112507	intron 3 of 3
PPP2R2C	FOXP2WT hDN activated	hNP dependent open	chr4	6367538	6368038	14082	intron 6 of 9
PRIMA1	FOXP2WT hDN activated	hDN independent open	chr14	93753091	93753591	35079	intron 2 of 4
PRMT6	FOXP2WT hDN repressed	hDN dependent open	chr1	106746694	106747194	-309701	Intergenic
PRSS35	FOXP2WT hDN repressed	hNP dependent open	chr6	83505278	83505778	-6947	Intergenic
PYGM	FOXP2WT hDN activated	hDN independent open	chr11	64759809	64760309	656	promoter-TSS

Table 4.4

Gene	Differetial expression	DAR type	Chr	Start	End	Distance.to.TSS	Annotation
RAPGEF5	FOXP2WT hDN activated	hDN independent open	chr7	22251261	22251761	105403	intron 2 of 6
RGS8	FOXP2WT hDN activated	hDN dependent closed	chr1	182674507	182675007	-1825	intron 1 of 4
RGS8	FOXP2WT hNP activated	hDN dependent closed	chr1	182674507	182675007	-1825	intron 1 of 4
RNF165	FOXP2WT hDN activated	hDN independent open	chr18	46412245	46412745	78271	intron 1 of 5
ROR2	FOXP2WT hNP activated	hDN independent closed	chr9	91857459	91857959	92453	intron 1 of 8
RPRM	FOXP2WT hDN repressed	hDN dependent closed	chr2	153388207	153388707	90351	Intergenic
S100A11	FOXP2WT hNP repressed	hDN dependent closed	chr1	152036761	152037261	24	promoter-TSS
SCG2	FOXP2WT hDN activated	hDN independent closed	chr2	223591570	223592070	10679	Intergenic
SEMA3A	FOXP2WT hDN repressed	hDN dependent open	chr7	84040306	84040806	154345	intron 7 of 17
SEMA3C	FOXP2WT hDN repressed	hDN dependent closed	chr7	80942136	80942636	-23035	Intergenic
SEMA6D	FOXP2WT hDN repressed	hDN independent open	chr15	47473803	47474303	-244436	intron 3 of 5
SH3BP4	FOXP2WT hDN repressed	hNP dependent closed	chr2	234980413	234980913	28679	promoter-TSS
SHISA6	FOXP2WT hDN activated	hDN independent closed	chr17	11406780	11407280	165607	intron 3 of 4
SLC26A7	FOXP2WT hDN activated	hDN independent open	chr8	91504040	91504540	255002	Intergenic
SLC6A20	FOXP2WT hNP repressed	hDN dependent closed	chr3	45793412	45793912	2881	intron 1 of 2
SLIT2	FOXP2WT hDN repressed	hDN dependent open	chr4	19716236	19716736	-535419	intron 2 of 3
SPARC	FOXP2WT hDN repressed	hDN independent open	chr5	151682995	151683495	3809	intron 3 of 4
SPRY1	FOXP2WT hDN repressed	hDN dependent open	chr4	123260287	123260787	-136258	promoter-TSS
SPRY2	FOXP2WT hDN repressed	hDN dependent open	chr13	80198670	80199170	142031	Intergenic
SPRY4	FOXP2WT hDN repressed	hNP dependent closed	chr5	142324855	142325355	-50	promoter-TSS
ST18	FOXP2WT hNP activated	hNP dependent closed	chr8	52174173	52174673	235456	intron 4 of 20

Table 4.4

Gene	Differetial expression	DAR type	Chr	Start	End	Distance.to.TSS	Annotation
STARD13	FOXP2WT hDN repressed	hDN dependent open	chr13	33542532	33543032	134053	intron 1 of 5
SYBU	FOXP2WT hDN repressed	hDN dependent closed	chr8	109737624	109738124	-46083	Intergenic
SYNPO2	FOXP2WT hDN repressed	hDN independent closed	chr4	118901407	118901907	12816	intron 1 of 4
SYT4	FOXP2WT hDN activated	hDN independent open	chr18	43863073	43863573	-585673	Intergenic
SYT7	FOXP2WT hDN activated	hDN independent open	chr11	61549703	61550203	30919	intron 3 of 9
SYTL2	FOXP2WT hDN repressed	hDN dependent closed	chr11	85827669	85828169	-16760	Intergenic
TAC3	FOXP2WT hNP activated	hDN dependent open	chr12	57025083	57025583	-8773	intron 1 of 6
TAGLN	FOXP2WT hDN repressed	hDN dependent closed	chr11	117198922	117199422	-152	promoter-TSS
TENM4	FOXP2WT hDN activated	hDN independent closed	chr11	79885553	79886053	-445152	Intergenic
THBS1	FOXP2WT hDN repressed	hDN dependent closed	chr15	39530759	39531259	-50070	Intergenic
TMEM158	FOXP2WT hNP repressed	hNP dependent closed	chr3	45225462	45225962	610	exon 1 of 1
TNFRSF11B	FOXP2WT hDN repressed	hDN dependent closed	chr8	118961798	118962298	-9904	Intergenic
TNR	FOXP2WT hDN activated	hDN independent closed	chr1	175673312	175673812	70054	intron 1 of 23
TPBG	FOXP2WT hDN repressed	hDN dependent open	chr6	82693055	82693555	329061	Intergenic
TRPC4	FOXP2WT hDN repressed	hDN independent open	chr13	37736000	37736500	133552	intron 2 of 9
ZFHX3	FOXP2WT hNP activated	hNP dependent closed	chr16	73058703	73059203	-318	TTS
ZSWIM5	FOXP2WT hNP activated	hNP dependent closed	chr1	45206235	45206735	93	promoter-TSS

CHAPTER FIVE: Conclusions and significance

In 1990, when Hurst *et al.* described a large, multi-generational family in which half of the members exhibited speech and language impairment, a door to understanding the molecular biology underlying human communication was unlocked (Hurst et al., 1990). Members of this family, which came to be known as the KE family, generously volunteered as study subjects, allowing the scientific community to better understand the brain regions and circuits involved in this complex human trait (Vargha-Khadem et al., 1995, Watkins et al., 2002a, Watkins et al., 2002b, Liegeois et al., 2003, Belton et al., 2003, Liegeois et al., 2011). More than ten years later, after a painstaking hunt, a mutation in the FOXP2 gene was identified as the cause of this family's disorder, and this transcription factor became the first gene implicated in a speech and language development (Lai et al., 2001).

Eventually, Foxp2 loss of function was modeled in genetically engineered mice (Shu et al., 2005, French et al., 2007) including mice harboring the specific KE family mutation (Groszer et al., 2008, Fujita et al., 2008). The consequences of developing without functional FOXP2 include a lack of neonatal isolation ultrasonic vocalizations (USVs), which underscores the conserved importance of FoxP2 in communication (Groszer et al., 2008, Shu et al., 2005, Fujita et al., 2008). Motor learning is also impaired in these animals (Groszer et al., 2008, French et al., 2012), and while mice do not appear to be vocal learners (Holy and Guo, 2005), this phenotype suggests that the motor pathways necessary for proper language acquisition could be aberrant in humans.

While FoxP2 seems to have some conserved role in mice and humans, evidence that FOXP2 in humans may be particularly important for the development of this human-specific trait arose when the genomic sequence of the FoxP2 gene was compared across species (Enard et al., 2002). Surprisingly, human FOXP2 was found to harbor three specific amino acid changes when compared to mouse Foxp2, and two of these substitutions are hominin specific, appearing in Neanderthals, Denisovans, and humans, but not in non-human primates (Enard et al., 2002, Coop et al., 2008, Reich et al., 2010). Moreover, these changes have been shown to be functional in human cells and in "humanized" FOXP2 mice (Enard et al., 2009, Reimers-Kipping et al., 2011, Konopka et al., 2009).

Evidence from humanized and Foxp2 null mice, along with imaging data from the KE family, suggests that changes in striatal plasticity caused by the molecular evolution of FOXP2 contribute to human language ability (Groszer et al., 2008, Reimers-Kipping et al., 2011, Vargha-Khadem et al., 2005); however, many questions about the conserved and human specific roles of FoxP2 and their contributions to speech and language development remain unanswered.

For example, conserved direct targets of FOXP2 have been identified (Vernes et al., 2007, Spiteri et al., 2007, Vernes et al., 2011), yet the contributions of all of these targets, even to rodent communication, have not been explored. Here, we attempted to uncover the role of the neuropeptide cholecystokinin, or Cck, on the production and structure of neonatal isolation USVs. While we initially observed altered call numbers and structure with Cck loss of function, we later showed that reducing food intake in wild type and knockout animals altered the number of calls regardless of genotype.

Controlling for food intake by reducing the size of each litter and recording each litter at the same time of day mitigated the effect of loss of Cck function on neonatal USVs.

Difficulties with verbal and non-verbal communication are among the diagnostic criteria for Autism spectrum disorders (ASD), and ultrasonic vocalizations are commonly analyzed in mouse models of ASD as a proxy for these communications deficits (Lepp et al., 2013). While it has long been known that ingestion of protein and/or fat reduces rodent neonatal USVs in wild type rodents via a Cck dependent mechanism (Blass and Shide, 1993), few studies assaying the effect of a particular gene on USVs control for food intake. One could imagine that developmental deficits caused by knockout of a potential ASD gene could subtly alter feeding or access to food in a large litter and alter USVs downstream of that. Thus, the gene may not have a direct effect on neonatal communication. Our study suggests that controlling for food intake is necessary to prove the direct effect of gene knockout on neonatal isolation calls. This should be kept in mind when characterizing ASD mouse models and when studying the effects of knockdown of other Foxp2 target genes.

Additionally, while the cortex has been a focal point of language research since the identification of Broca's area and Wernicke's area, and affected KE family members show structural and functional alterations in these and other cortical subregions (Vargha-Khadem et al., 1995, Watkins et al., 2002a, Watkins et al., 2002b, Liegeois et al., 2003, Belton et al., 2003, Liegeois et al., 2011), the role of FOXP2 in the cortex is unknown. No overt cortical phenotype is observed in the Foxp2 loss of function animals, suggesting, perhaps, that FOXP2 plays a human specific role in this evolved brain structure. Differences between the thin, lissencephalic mouse cortex and the large,

foliated human cortex are already present during early stages of brain development (Lui et al., 2011). For instance, the subplate layer is vastly expanded in human fetal cortex, but would be impossible to observe in adult KE family members because of its transient nature (Kostovic and Rakic, 1990). However, this region is critical for establishing proper circuitry between thalamic afferents and their layer IV targets (Kanold and Luhmann, 2010), which could be altered in adult affected family members. While it's role in thalamocortical circuitry maturation has been observed in rodent and carnivore (Kanold and Luhmann, 2010), suggesting conserved mechanims, the expanded human subplate may have evolved to support the increased numbers of upper layer neurons in the primate cortex (Marin-Padilla, 1992). However, the molecular mechanisms driving these species differences in subplate development remain mostly unknown.

Thus, we were intrigued when *FOXP2* expression was found to be correlated with the subplate layer in human fetal cortex during mid-gestation (Miller et al., 2014), and we hypothesized that FOXP2 may be a driver of human subplate gene expression. Using genetically tractable cultured human neurons and transcriptome-wide gene expression analysis, we found that subplate-correlated genes are significantly enriched for FOXP2 activated genes accounting for up to fourteen percent of all subplate correlated genes. We next wondered whether FOXP2 activated human-specific subplate genes. To this end, we used publically available data sets (Oeschger et al., 2012, Hoerder-Suabedissen et al., 2013, Miller et al., 2014, Bakken et al., 2016) to identify human-specific, primate-specific, and conserved subplate-enriched genes. To our knowledge, this is the first time that transcriptome of this evolutionarily important

developmental region has been directly compared across species, making this a truly valuable data set for those studying cortical evolutionary development.

Fascinatingly, we found that *FOXP2* is more highly expressed in subplate than in cortical plate in human, while in macaque there is no difference in *FoxP2* expression between these layers. In mouse, however, *Foxp2* is more highly expressed in cortical plate, suggesting that there may be more *FoxP2* expressing cells in human subplate compared with macaque and mouse and that subplate *FoxP2* expression correlates with subplate size. We next compared the subplate-enriched genes of all three species with activated FOXP2 targets and found a significant enrichment in all three sets of genes. However, comparing the FOXP2 activated subplate genes across species allowed us to identify human-specific, primate-specific, and conserved subplate-enriched FOXP2 activated genes, suggesting that FOXP2 plays conserved and species-specific roles in the subplate. Moreover, human-specific FOXP2 activated genes are enriched for genes involved in glutamate receptor signaling and neuron projection development. This, along with the potential for increased numbers of *FOXP2* expressing cells in the human subplate, suggests a role for FOXP2 supporting the maturation of complex, human thalamocortical circuitry, which may be perturbed in affected KE family members.

Foxp2 in the subplate may also facilitate the maturation of these circuits in mice, and the human-specific function may be a matter of degree with more upper-layer neurons and more thalamic inputs necessitating more FOXP2-positive subplate cells for circuit maturation. However, the physiological properties of these thalamocortical circuits have not been assessed in cortex-specific *Foxp2* knockout animals, as Foxp2 its

self is only expressed in layer VI, and Foxp2 positive neurons in the adult mouse cortex project specifically to the thalamus, not to other cortical regions. Therefore, our study may lead to a new avenue of exploration of the cell non-autonomous effect of FoxP2 on cortical circuitry outside of layer VI.

FoxP2 in the cortex may facilitate cortical circuitry maturation through its activation of downstream targets, but while FoxP2 has been shown to both activate and repress gene expression in multiple species (Vernes et al., 2007, Spiteri et al., 2007, Vernes et al., 2011, Konopka et al., 2009) a mechanism for activation by FoxP2 in any species has yet to be proposed. Here, in an attempt to uncover the means by which FOXP2 activates gene expression in human neurons we performed RNA-seq and ATAC-seq in human neural progenitor cells (hNPs) and human differentiated neurons (hDNs). These cells have no endogenous *FOXP2* expression, thus, on this null background, we compared cells expressing a control construct with those expressing *FOXP2*-WT or *FOXP2*-KE, which harbors the mutation found in affected KE family member that renders FOXP2 unable to bind to DNA.

ATAC-seq data allowed us to identify regions of chromatin made differentially accessible with expression of *FOXP2*-WT and/or –KE compared to control. Were called these areas differentially accessible regions or DARs. Importantly, we found that while FOXP2-KE was unable to regulate gene expression, it was capable of altering the chromatin landscape. FOXP2 activated genes were enriched for genes involved in neuronal maturation, and were near DARs that were open with expression of *FOXP2*-WT or –KE, and thus were open independently of the ability of FOXP2 to bind to DNA. Motif enrichment analysis of these DNA-binding independent DARs identified NFI

factors as potential FOXP2 cofactors. NFI factors have already been implicated in brain development, and they overlap with FOXP2 in the lower layers of the cortex (das Neves et al., 1999, Wong et al., 2007, Campbell et al., 2008, Betancourt et al., 2014). While we have yet to prove that FOXP2 and any NFI factors physically interact, we have shown, for the first time, that FOXP2 along with a cofactor can activate neuronal gene expression without FOXP2 binding directly to DNA. If we can eventually show that this putative cofactor is, indeed, an NFI family member, it will be the first time that a FOXP2 cofactor has been identified via genomic analysis.

Through this analysis, we also showed that FOXP2 directly binds DNA at a FOX motif in order to repress target gene expression. A gene expression module enriched for FOXP2 repressed genes is also enriched for genes correlated with cortical germinal layers and involved in maintaining a proliferative state. While several reports of FoxP2 target genes have highlighted a role for this transcription factor in neuron development and neurite outgrowth (Vernes et al., 2007, Spiteri et al., 2007, Vernes et al., 2011, Konopka et al., 2009), a specific role for FoxP2 in the repression germinal zone genes, perhaps to push a progenitor into a mature neuron or to help maintain a mature neuronal identity, has not previously been described.

Thus, in this study we distinguished two separate modes of gene regulation by FOXP2 in human neurons. Namely, FOXP2, along with a putative NFI cofactor, opens chromatin in a DNA binding independent manner to activate the expression of genes expressed in mature neurons. FOXP2 also represses genes expressed in germinal layers by directly binding canonical FOX motifs. Interestingly, our results suggest that FOXP2 exerts these effects by acting mainly at enhancer regions, far from gene

promoters. Because a genome wide analysis of FOXP2 occupancy in human neurons has never been performed, this in itself is a novel finding. By altering chromatin at enhancer regions, these separable mechanisms of FOXP2 action likely converge to promote and maintain the mature neuronal identity of *FOXP2* expressing cells.

Taken together the results of my work push the FOXP2 field forward in a few different ways. Firstly, USV recordings are commonly used to assess the effect of loss of gene function on rodent communication. Thus, they will be useful in uncovering the roles of individual Foxp2 target genes in promoting call formation, as Foxp2-null animals are completely unable to form ultrasonic calls. Our study of the effect of *Cck* knockout on neonatal calls highlighted the importance of controlling for food intake when making these recordings to help avoid false positive results. Secondly, our study of FOXP2 in the human subplate not only identified human specific targets in this expanded, transient region, but it may also inspire research of the conserved, non-cell-autonomous role of FoxP2 in the maturation of thalamocortical circuitry. This could solve the mystery of the function of FoxP2 in the cortex. Lastly, we have identified two separate molecular mechanisms by which FOXP2 regulates gene expression in human neurons, even finding a potential FOXP2 co-activator. The results of these studies underscore the power of genomic and transcriptomic analysis to uncover the functions of FoxP2 across species and at the molecular level.

CHAPTER SIX: Methods

Experimental Model and Subject Details

Cck Knockout mice

Cck$^{+/-}$ on a C57BL/6J background were obtained from Jackson Laboratories (strain #017710). In this strain the cholecystokinin gene is disrupted by the insertion of a β-geo fusion cassette. Mice were kept in the barrier facilities of the University of Texas Southwestern Medical Center under a 12 h light–dark cycle and given ad libitum access to water and food unless otherwise stated. All studies with mice were approved by the University of Texas Southwestern Institutional Animal Care and Use Committee.

HEK 293T cells and lentivirus production

HEK 293T cells were plated in DMEM with 1% Antibiotic-Antimycotic and 10% FBS, kept at 37°C in 5% CO_2, and passaged at least three times after thawing with the final passage 12-24 hours prior to transfection. For transfection of one 10 cm plate, viral packaging vectors VSVG and psPAX2 (2μg each) and the lentiviral construct of interest (4 μg) were added to DMEM up to 250 μl. 32 μl of Fugene were then added to an additional 228 μl of DMEM, and the tube was flicked gently to mix. The plasmid solution was then added to the Fugene solution, the tube was flicked gently to mix and incubated for 30 minutes at room temperature. The 500 μl transfection mix was subsequently added dropwise, in a spiral motion to one 10 cm plate of HEK 293T cells at approximately 70-90% confluence and mixed. 12-24 hours later, the 293T cell media was replaced with proliferation media (Neurobasal A media, 2% Antibiotic-Antimycotic, 10% BIT, 1% Glutamax). 12-24 hours after media replacement the viral supernatant

was collected and centrifuged for 5 minutes at 1000 rpm. The supernatant was then filtered through a 45 µm filter, and stored in small aliquots at -80 °C.

Human neural progenitor (hNP) culture

Female human neural progenitor cultures were obtained from Lonza. Cells were stored in liquid nitrogen in Neurobasal A media with 10% DMSO until thawed and plated. Tissue culture plates were first coated for at least two hours at 37°C with 50 µg/mL polyornithine in PBS. The polyornithine solution was removed from the plate and replaced with 5 µg/mL fibronectin in PBS for at least two hours at 37°C. Immediately before plating cells, the fibronectin solution was completely aspirated off of the plates and the remaining fibronectin film was allowed to dry for up to 5 minutes. Frozen cells were quickly thawed at 37°C and resuspended in 5 mL of proliferation media without growth factors (500 mL Neurobasal A media with 60 mL BIT serum substitute, 12 mL Antibiotic-Antimycotic and 7 mL Glutamax) to dilute the DMSO. The cells were pelleted by centrifugation for 5 minutes at 1000 rpm. The pellet was resuspended in 10 mL plating media comprised of 50% proliferation media and 50% conditioned media (proliferation media removed during half feedings and filtered through a 0.22 µm filter) with 5 ng/µL EGF and 5 ng/µL FGF added. The resuspended cells were then pipetted onto a coated 10 cm plate. Three times per week 50% of the media on the plate was removed, stored as conditioned media, and replaced with fresh proliferation media containing 10 ng/mL EGF and 10 ng/mL FGF. When the cells reached 80-100% confluency they were passaged to new, coated plates. Briefly, the media was removed from the plates and the cells were washed with 5 mL PBS. Next, 0.25% trypsin was added to cover the cells and immediately removed. After incubating the cells in the

residual trypsin for approximately 1 minute, the trypsin was neutralized and cells were triturated and resuspended in 10 mL DMEM with 10% BSA or 10 mL conditioned media and pelleted by centrifugation for 5 minutes at 1000 rpm. The pellet was resuspended in plating media. One confluent plate was typically split into two to three new plates and kept at 37°C in 5% CO_2. 24 hours later, lentivirus was added in a dropwise manner. Cells were harvested four days after transduction.

Human differentiating neuron (hDN) culture

Differentiation from hNPs into human differentiating neurons (hDNs) began four days after lentiviral transduction. Cells were kept at 37°C in 5% CO_2. Tissue culture plates were first coated for at least two hours at 37°C with 50 µg/mL polyornithine in PBS. The polyornithine solution was removed from the plate and replaced with 5 µg/mL laminin in PBS for at least two hours at 37°C. Immediately before plating cells, the laminin solution was completely aspirated off of the plates but not allowed to dry before plating. hNPs were densely plated (3-5 million cells per 10 cm plate, 1million cells per well in a 6-well plate) in plating media as previously described (see Proliferating human neural progenitor (hNP) culture). After 48 hours, half of the media was removed from the plates and replaced with differentiation media (500 mL Neurobasal A media, 10 mL B27 without vitamin A, 12 mL Antibiotic-Antimycotic, 7 mL Glutamax, 10 ng/mL BDNF, 10 ng/mL NT-3, 10 ng/mL retinoic acid, 10 µM forskolin, and 10 mM KCl). Two days later, the media was completely removed, the cells were washed with PBS, and fresh differentiation media was added. For the first two weeks after initiation of differentiation, three times a week, 50% of the media was changed to fresh differentiation media with concentrations of growth factors adjusted to the total volume. After this initial two-week

period, the cells were again washed with PBS and fresh differentiation media was added. For the following second two-week period, the cells were again fed three times per week with an adjusted 50% media change.

Method Details

Recording of neonatal ultra-sonic vocalizations

USVs were recorded from pups isolated from their dams at P4, P7, P10, and P14 as described in Araujo et al., 2015. Pups were placed into clean plastic containers inside soundproof styrofoam boxes and recorded for 3 min. Recordings were acquired using an UltraSoundGate condenser microphone (Avisoft Bioacoustics, CM16) positioned at a fixed height of 20 cm above the pups and were amplified and digitized (~20 dB gain, sampled at 16 bits, 250 kHz) using UltraSoundGate 416H hardware and Avisoft RECORDER software (Avisoft Bioacoustics). Sound spectrograms were prepared in MATLAB (50% overlapping, 512-point Hamming windows), resulting in 1.024-msec temporal resolution and 488.3-Hz spectral resolution. Spectrograms were band-pass filtered to 20–120 kHz and filtered for white noise. Positions of ultrasonic calls were determined automatically using a previously published method (Holy and Guo, 2005).

Vocalization behavior occurred in spurts of activity (“bouts”) separated by longer pauses. To quantify bouts of vocalization, spectrograms were segmented using a pause length of ≥0.25 sec, which was chosen based on the empirical distribution of pause times between calls. All intercall pauses <0.25 sec represent constituents of the same bout of vocalization. The means of the dominant frequency (“mean frequency”) as well as the duration time of individual calls were averaged over all calls by animal. The

presence of instantaneous pitch jumps in calls was determined by a previously published method (Holy and Guo, 2005), and the fraction of all calls containing such jumps was determined for each animal. The trend slope (in hertz per millisecond) of calls lacking instantaneous pitch jumps was determined by linear regression, and slopes were averaged over all calls by animal.

Neonate Fasting

P7 or P10 neonates were removed from the dam and placed in a clean, standard mouse cage warmed to 30°C. A moist Chix wipe was placed in the cage to increase humidity. Neonates were fasted for 2 hours, and then ultrasonic vocalizations were immediately recorded. Only litters containing six pups were fasted and recorded. If the litter contained greater than six pups, pups were randomly culled at P0 until the litter size equaled six.

Open field task

The open field assay was performed on adult *Cck*$^{+/-}$, *Cck*$^{-/-}$, and littermate control mice by individually placing each animal in a 16-in × 16-in Plexiglass box and allowing them to explore the arena for 5 min. Videos of each mouse were obtained and scored for average velocity of movement and total distance moved using the EthoVision XT software package (Noldus).

Three-chamber social approach task

The three-chamber social approach task was performed on adult *Cck*$^{+/-}$, *Cck*$^{-/-}$ and littermate control mice using a Plexiglass arena with center, right, and left chambers connected by closable doors as per (Yang et al., 2011). A poster board wrapper was placed around the chamber during the task in order to reduce side-bias. First, mice

were allowed to explore the center chamber only for ten minutes. Next the doorways were opened and the mouse was allowed to explore all three empty chambers for ten minutes. This is the habituation phase. Then the subject is again confined to the center chamber while a cage containing a sex-matched target mouse is placed on once side of the chamber while an identical empty cage is placed on the other side of the chamber. The locations of the target and empty cages are randomized for each mouse. The doors are then opened and the subject is allowed to explore all three chambers. This is the test phase. Videos of each mouse were obtained during the habituation and test phases and scored for the time spent in each chamber and total distance moved using the EthoVision XT software package (Noldus).

Tissue preparation and X-gal staining

Adult female and male mice were anesthetized with 80–100 mg/kg Euthasol (UT Southwestern Medical Center Animal Resources Center Veterinary Drug Services), perfused with PBS containing (Sigma-Aldrich) followed by fixative (4% PFA in PBS), and then immediately decapitated. Whole brains were removed and incubated in fixative for 24 h at 4°C and then incubated in 30% sucrose (made in PBS with 0.02% sodium azide) for 24–48 h at 4°C. Afterward, brains were sectioned at 35–40 μm on a cryostat. Sections were then stored in PBS containing 0.02% sodium azide until being used for X-gal staining.

Sections were then submerged in solution containing 1mg/ml X-gal, 2mM $MgCl_2$, 5mM each Kferri and Kferro cyanide, in 1X PBS in the wells of a six-well plate and incubated over night at 30°C covered with foil for light protection. The slices were then

counter stained with Nuclear Fast Red solution and mounted on coverslips, and imaged on a Zeiss Stereo Discovery Microscope V12.

Tissue collection and RNA extraction

After USV recordings, animals were cryoanesthetized and euthanized via decapitation and tissue was collected from the thalamus, cortex, and proximal intestine of each pup. Tail snips were also collected for genotyping. Tissue was placed in RNAlater and stored at -80°C until genotypes of the animals were determined. RNA was extracted from tissue collected from wildtype and knockout animals using the Qiagen miRNeasy Kit.

Plasmids

pLUGIP, a lentiviral expression vector with a Ubi-c promoter driven GFP-IRES-Puromycin was used in the first RNA-seq experiment as the control vector. The eGFP in the vector was replaced with FOXP2-WT-3X-FLAG (Konopka et al., 2009) and used to express exogenous FOXP2-WT via lentiviral transduction. For the second RNA-seq experiment and the parallel ATAC-seq experiment, site directed mutagenesis was used first to remove the 3X-FLAG tag from pLUGIP FOXP2-WT-3X-FLAG and then to add a V5 tag to the untagged vector to make pLUGIP FOXP2-WT-V5. For pLUGIP FOXP2-KE-V5 a point mutation was made in the untagged pLUGIP FOXP2-WT to change R at position 553 to H in the DNA-binding domain of FOXP2. Subsequently, site directed mutagenesis was used to add a V5 tag. A V5 tag was also added to the end of eGFP in pLUGIP to make pLUGIP-GFP-V5.

Site directed mutagenesis was performed as follows with the appropriate primer pair listed in the Key Resources table:

A forward and reverse primer pair, one of which contained the desired substitution/insertion/deletion, was designed using Agilent's Quikchange Primer Design tool for the mutagenizing primer and Primer3 (Untergasser et al., 2012) for the other primer. To generate a megaprimer from the template, 1 µL of template at 1 µg/µL was mixed with 12.5 µL Primestar Max, .75 µL of 1 µM of the appropriate forward and reverse primer pair mix and 10.75 µL H_2O. This mixture was cycled as follows:

(1) 98°C, 2 minutes

(2) 98°C, 10 seconds

(3) 55°C, 5 seconds

(4) 72°C, 10 seconds

(5) Repeat steps 2-4, 30x

(6) 72°C, 7 minutes

(7) 4°C hold

The product was run on a 1.5-2% agarose gel and the megaprimer near predicted size was excised and purified using the Thermo Scientific™ GeneJET™ Gel Extraction Kit as per the manufacturers instructions and eluted in 15 µL H_2O. 12 µL of this PCR product was then mixed with Primestar Max and .5 µL of the original template at 1 µg/µL. This mixture was cycled as follows:

For insertion mutagenesis:

(1) 95°C, 5 minutes

(2) 95°C, 1 minute

(3) 52°C, 1 minute

(4) 68°C, 1 minute/kb

(5) Repeat steps 2-4, 5x

(6) 95°C, 1 minute

(7) 55°C, 1 minute

(8) 68°C, 1 minute/kb

(9) Repeat steps 2-4, 15x

(10) 68°C, 15 minutes

(11) 10°C hold

For deletion mutagenesis:

(1) 98°C, 2 minutes

(2) 98°C, 10 seconds

(3) 55°C, 5 seconds

(4) 72°C, 1 minute/kb

(5) Repeat steps 2-4, 30x

(6) 72°C, 7 minute

(7) 10°C hold

After this PCR step 0.5 µL DpnI was added and the reaction was incubate 37°C for 1-3 hours. Next, the DpnI digested PCR product and 100ng template were run in separate lanes of a 1% agarose gel and the product near template band size was excised. The DNA was purified using the Thermo Scientific™ GeneJET™ Gel Extraction Kit as per the manufacturers instructions and eluted in 8 µL H_2O and placed on ice. 45 µL of XL10-Gold Ultracompetent Cells were transferred to a cold 2 mL tube for transformation. 2 µL XL10-Gold β-Mercaptoethanol (β-ME) mix was added to the cells. This mix was incubated on ice for 10 minutes and swirled every 2 minutes. 8 µL of the

purified final mutagenized plasmid was added to the cells and incubated for 30 minutes on ice. The cells plus plasmid were then heat-shocked in a 42°C water bath for 30 seconds and placed on ice for 2 minutes. 50 µL of SOC media was added and the mixture was incubated at 30°C for 1 hour with shaking. The cells were then spread on one LB with ampicillin petri dish and incubated overnight at 30°C. Subsequently, colonies were mini-prepped, and the constructs were Sanger sequenced to confirm that the desired mutations were made. After sequencing the constructs were maxi-prepped and used for lentiviral production.

Cell culture RNA-collection

Total RNA from three or four replicates of each described condition from approximately $1x10^6$ hNPs or hDNs per replicate was harvested using the Qiagen miRNeasy Mini Kit.

cDNA synthesis and qRT-PCR

Up to 1µg RNA was DNAseI treated using amplification grade DNAseI (Life Technologies) and then annealed to 1µL of 50ng/µL random hexamers before being reverse transcribed using the SSIII FIRST-STRAND SUPER MIX (Life Technologies).

qRT-PCR was performed in quadruplicate on the CFX384 Touch™ Real-Time PCR Detection System (Bio-Rad). The reaction mix contained iTaq SYBR Green Supermix (Bio-Rad) and 0.3 mM of each primer. Cycling conditions were 50°C for 2 min and 95°C for 3 min, followed by 45 cycles at 95°C for 15 s and 58°C for 45 s, and, finally, 95°C for 15 s, 60°C for 20 s, and 95°C for 15 s.

RNA-sequencing library prep

For the experiment described in Ch3, RNA-seq libraries were prepared as described in detail previously (Takahashi et al., 2015). Total RNA quality was assessed using an Agilent Bioanalyzer RNA 6000 Nano chip. mRNA poly-A selection was performed using NEXTflex Poly(A) Beads as per manufacturer's instructions beginning with 2 µg of total RNA per samples. 14 µL mRNA was fragmented by chemical fragmentation in 5 µL RNA-fragmentation buffer (250 mM Tris-HCL pH 8.3, 375 mM KCl, and 10 mM $MgCl_2$) at 95°C for 10 minutes. 1 µL random hexamer mix was added to fragmented RNA and the mixture was incubated at 65°C for 5 minutes and then immediately placed on ice. Fragmented RNA was reverse transcribed using Enzscript (M-MLV Reverse Transcriptase Rnase H-) in First strand synthesis buffer (2 µL 100 mM DTT; 1 µL 10 mM dNTPs; .5 µL 120 ng/µL Antinomycin D; .5 µL RNase Inhibitor per reaction). The mix was incubated at 25°C for 10 minutes, 42°C for 50 minutes, and then 70 °C for 15 minutes. Next, directional second strand synthesis was performed by adding 3 µL 10 x Blue buffer, 1 µL dNTP/dUTP mix (1:1:1:2), .5 µL RNase H, 1 µL DNA Polymerase to 24.5 µL of the first strand synthesis product. The mix was incubated at 16 °C for 1 hour. Clean up was performed with the EpiNext DNA Purification HT System as per the manufacturer's instructions. DNA was resuspended in 17 µL 10mM Tris-HCl, pH 8.0. Subsequently, Second strand synthesis DNA was mixed with 1 µL 10 mM dATP, 2 µL 10 x Blue buffer, and .5 µL klenow 3'-5' exo minus LC. The mix was incubated at 37°C for 30 minutes followed by 70°C for 5 minutes. 2 µL of a .6 µM NEXTflex™ Barcoded Adapter was added to 20.5 µL of the adenylated DNA along with 25 µL 2 x ligase buffer, 2 µL ligase storage buffer (10 mM Tris–HCl, pH 7.4, .1 mM EDTA, pH 8.0, 1 mM DTT, 50 mM KCl, 50% glycerol), 1 µL T4 DNA ligase. Samples

were incubated at 22°C for 15 minutes. We performed two clean ups back to back with the EpiNext DNA Purification HT System as per the manufacturer's instructions. Adapter ligated DNA was resuspended in 35 µL 10mM Tris-HCl, pH 8.0. PCR amplification was performed by adding 1 µL Uracil DNA Glycosylase, 12 µL Kapa HiFi DNA Polymerase PCR master mix made as per the KAPA HiFi PCR Kit, and 2 µL 12.5 µM NEXTflex™ Primer Mix. Cycling was carried out as follows:

(1) 37°C, 30 minutes

(2) 98°C, 2 minutes

(3) 98°C, 30 seconds

(4) 65°C, 30 seconds

(5) 72°C, 60 seconds

(6) Repeat steps 3-5, 12x

(7) 72°C, 4 minutes

After amplification we performed two clean ups back to back with the EpiNext DNA Purification HT System as per the manufacturer's instructions.

For the experiments described in Ch.4, libraries were prepared using the TruSeq Stranded mRNA Library Prep as per the manufacturer's instructions by UTSW McDermott Next Generation Sequencing Core.

The quality and concentration of the libraries from both experiments was checked on an Agilent Bioanalyzer High Sensitivity DNA chip. The samples described in Ch.3 and in the experiments including the KE control in Ch.4 were pooled and sequenced by the UTSW McDermott Next Generation Sequencing Core using Illumina's NextSeq500. Reads are strand specific, single end, and 75bp long. The initial hNP RNA-seq

experiments described in Ch.4 were stranded, single-end 50-base-pair (bp) reads and sequencing was performed by the McDermott Sequencing Core at the University of Texas Southwestern Medical Center on an Illumina HiSeq 2000 sequencer (Illumina)

Chromatin immunoprecipitation (ChIP)

Approximately twenty-million OF4155 hNPs were used per experimental condition. Cells were fixed in 1% methanol-free formaldehyde for 10 min at room temperature and then quenched with glycine (125 mM final). Cells were washed twice in 1× cold PBS, resuspended in 10 mL of lysis buffer (50 mM HEPES-KOH at pH 7.5, 140 mM NaCl, 1 mM EDTA, 10% glycerol, 0.5% IGEPAL-CA630, 0.25% TritonX-100, 10 µL/mL protease inhibitor [PI] cocktail [Sigma], 7 µL/mL PMSF), and incubated for 10 min on ice. Pelleted cell nuclei were then resuspended in 1 mL of nucleus lysis buffer (200 mM NaCl, 1 mM EDTA, 0.5 mM EGTA, 10 mM Tris-HCl at pH 8.0, 10 µL/mL PI, 7 µL/mL PMSF) and incubated for 10 min at room temp. They were then dounce homogenized for 10 strokes and spun down for 10 mins at 4°C at 4000 RPM. Samples were sonicated in 250 µL of shearing buffer (1 mM EDTA, 0.5 mM EGTA, 10 mM Tris-HCl at pH 8.0, 0.1% SDS, 10 µL/mL PI, 7 µL/mL PMSF) using a Bioruptor (Diagenode) at 3-min intervals for a total of 1 hour. Ten percent of volume from each sample was collected for input controls. One hundred micrograms of precleared sheared chromatin and 1 µg of mouse anti-FLAG antibody were incubated overnight at 4°C while rotating. Magnetic IgG Dynabeads (Invitrogen) were washed three times with 5 mg/mL BSA solution in PBS and then incubated with sheared chromatin/antibody solution for 2 h at 4°C. Magnets were applied to samples at 4°C, and beads were washed with 500 µL of each of the following solutions supplemented with PI and rotated for 5 min at 4°C

followed by magnetic separation: (1) low-salt wash buffer (0.1% SDS, 1% TritonX-100, 2 mM EDTA, 20 mM Tris-HCl at pH 8.0, 150 mM NaCl), (2) high-salt wash buffer (0.1% SDS, 1% TritonX-100, 2 mM EDTA, 20 mM Tris-HCl at pH 8.0, 500 mM NaCl), (3) LiCl wash buffer (0.25 M LiCl, 1% IGEPAL-CA630, 1% deoxycholic acid, 1 mM EDTA, 10 mM Tris-HCl at pH 8.0), and (4) TE buffer. After washes, beads were resuspended in elution buffer (50 mM Tris-HCl, 10 mM EDTA, 1% SDS) and incubated for 15 min at 65°C with vortexing every 2 min. Beads were magnetically separated, supernatant was collected, and cross-linking of all samples and inputs was reversed overnight at 65°C. DNA was purified using Qiagen MinElute columns and quantified using a Qubit Fluorometer. Sequencing was performed by the University of Texas Southwestern Medical Center McDermott Sequencing Core.

hNP and hDN immunocytochemistry

Coverslips were fixed in PBS with 4% PFA for 15 mins, washed three times with TBS, permeablized with TBS containing .05% Triton X-100, washed three times with TBS, and blocked with TBS containing .02% Triton X-100 and 5-10% donkey serum. Coverslips were incubated with antibodies and dilutions specific to each experiment in TBS containing .02% Triton X-100 and 5% donkey serum overnight at 4°C. This was followed by incubation with 1:10,000 of the appropriate Alexa Fluor® IgG secondary antibodies in TBS containing .02% Triton X-100 and 5% donkey serum. Coverslips were mounted with ProLong® Diamond Antifade Reagent with DAPI (Life Technologies) and imaged as described below.

H3K27ac immunocytochemistry

hNPs from the OF4155 line were seeded onto coverslips coated with poly-ornithine and fibronectin as per hNP culturing methods described above. The cells were then transduced with FOXP2-FLAG lentivirus, and four days later immunocytochemistry was performed as described above. Immunostaining was performed with 1:500 rabbit anti-H3K27ac antibody (Abcam ab472) and 1:10,000 mouse anti-FLAG antibody (Sigma F1804) in TBS containing .02% Triton X-100 and 5% donkey serum. This was followed by incubation with 1:10,000 Alexa Fluor® 488 Donkey Anti-Mouse IgG and 1:10,000 Alexa Fluor® 555 Donkey Anti-Rabbit IgG secondary antibodies in TBS containing .02% Triton X-100 and 5% donkey serum. Coverslips were mounted with ProLong® Diamond Antifade Reagent with DAPI (Life Technologies) and imaged using a Zeiss Observer.Z1 inverted microscope and ZEN 2011 software.

Neurosphere migration assay

Proliferating hNPs (Lonza line OF4106) were plated on poly-ornithine and laminin and transduced with either a V5-tagged FOXP2-WT, V5-tagged FOXP2-KE, or V5-tagged CTRL-GFP lentivirus. 48 hours later the cells were dissociated with .025% trypsin. Cells were mixed in 1:1 ratios of FOXP2-WT expressing and CTRL-GFP expressing hNPs, or FOXP2-KE expressing and GFP-ctrl expressing hNPs. The cell mixtures were used to form neurospheres. Briefly, $3x10^4$ cells in proliferation media were seeded into Corning Costar 96-well round bottom Ultra-Low Attachment Multiwell Plates. After 48 hours the neurospheres that formed were transferred to 24-well plates containing acid washed 12 mm glass coverslips coated with poly-ornithine and laminin using wide-bore Axygen® 200µL Universal Fit Filter Tips. Each coverslip contained one neurosphere, and the wells were filled with differentiation media.

After 48 hours, when hNPs had begun to migrate radially from the sphere, immunocytochemistry was performed as described above. Immunostaining was performed with 1:500 goat anti-FOXP2 antibody (Santa Cruz 21069) which detects both FOXP2-WT and –KE and 1.5 µg/mL rabbit anti-doublecortin (DCX) antibody in TBS containing .02% Triton X-100 and 5% donkey serum. This was followed by incubation with 1:10,000 Alexa Fluor® 555 Donkey Anti-Goat IgG and 1:10,000 Alexa Fluor® 647 Donkey Anti-Rabbit IgG secondary antibodies in TBS containing .02% Triton X-100 and 5% donkey serum. Coverslips were mounted with ProLong® Diamond Antifade Reagent with DAPI (Life Technologies) and imaged using the tile scan feature of a Zeiss 710 confocal microscope.

FOXP2-NFI co-immunoprecipitations

Five 10 cm plates of hDNs transduced with FOXP2-WT were used for co-immunoprecipitations. The chromatin was first cross-linked by addition of ethylene glycol bis(succinimidyl succinate) (EGS) directly to the media of each plate at a final concentration of 2mM as per Takahashi *et al.,* 2015 (Takahashi et al., 2015). The plates were incubated with EGS for 20 minutes at room temperature. Next, 16% methanol-free formaldehyde was added to each plate to a final concentration of 1%, and the plates were incubated for an additional 8 minutes at room temperature. The reaction was quenched with a final concentration of 50 mM glycine, and each plate was washed twice with ice-cold PBS before the cells were harvested from the plate by scraping.

The cells were then pelleted by centrifugation at 4 °C and re-suspended in 200 µL ChIP lysis buffer:

Lysis Buffer (make fresh)	**for 5mL**
ultrapure H2O	4.66 mL

1M Tris-HCl, pH 8.0	50 µL
5M NaCl	100 µL
0.5M EDTA, pH 8.0	10 µL
0.5M EGTA, pH 8.0	5 µL
10% Na-Deoxycholate	50 µL
20% N-laurylsarcosine	125 µL

*Add 10 µL /mL protease inhibitor cocktail fresh

Next, the cells were sonicated using the Diagenode Biorupter on medium power,10 seconds on and 20 seconds off, for two round of 5 minutes. The sonicated material was then centrifuged at 12,000 rpm for 5 minutes at 4 °C and the supernatant was collected. A minimum of 1.8 mL of IP buffer (.02M Tris-HCl pH 8.0; 1mM EDTA pH 8.0, 1% Triton-X, .15M NaCl) was then added to the supernatant in order to dilute the ChIP lysis buffer for immunoprecipitation. Per condition, 50 µL of Dynabeads Protein G previously washed three times with 1 mL IP buffer was added to the diluted sonicated material for 30 minutes of pre-clearing at 4 °C. After pre-clearing, a Bradford assay was conducted. Subsequently, three immunoprecipitations were performed using 260 µg of protein each, and ~45 µg of protein was kept as input. 5 µg of the following antibodies were used to precipitate NFIA (Rb anti-NFIA, Sigma HPA008884), NFIB (Rb anti-NFIB, HPA003956), and normal rabbit IgG (Cell Signaling 2729). Protein, antibody, and 50 µL of IP buffer washed Dynabeads Protein G were incubated together for 2 hours at 4 °C. Following incubation, the supernatant was discarded and the Dynabeads were washed for 5 minutes, 3 times with IP buffer at 4 °C. Next, the Dynabeads were re-suspended in 30 µL sample buffer (Western dye + DTT diluted 5X in IP buffer) and incubated at 95 °C for 5 minutes. The supernatant was collected and analyzed along with input via SDS-PAGE followed and transferred to an Immun-Blot PVDF membrane (Bio-Rad

Laboratories, 162-0177), blocked with blocking buffer (1% skim milk in TBS with 0.1% Tween-20) for 30 min at room temperature. The input was run on two lanes and was blotted with 1:1000 anti-V5 antibody (Life Technologies R960-25) and either anti-NFIA or anti-NFIB at .4 µg/mL. The IP lanes were blotted with 1:1000 anti-V5 antibody to detect the co-immunoprecipitation of V5 tagged FOXP2 and NFIA or NFIB overnight at 4 °C. Licor IRDye secondary antibodies of the appropriate species were used to visualize the proteins and images were collected using the Odyssey infrared imaging system (LI-COR Biosciences).

QUANTIFICATION AND STATISTICAL ANALYSIS

RNA-seq sample randomization

Prior to library preparation or submission to the McDermott Sequencing Core at the University of Texas Southwestern Medical Center, RNA samples were randomized by ordering the samples based on a random list of numbers generated by the RAND() function in Excel. The samples were then relabeled in a way that de-identified them, and libraries were prepped based on the random order and not by sample type in order to reduce batch effect.

RNA-seq mapping, QC and expression quantification

For the RNA-seq experiments described in Ch3 and the experiments including the KE control in Ch4, adapter removal and quality trimming was performed using Trimmomatic (Bolger et al., 2014). Reads were aligned to the human hg38 (GRCh38) reference genome using STAR 2.5.2b (Dobin et al., 2013). Gencode v24 annotation was used as reference to build STAR indexes and alignment annotation. For each sample, a BAM file including mapped and unmapped reads with spanning splice

junctions was produced. Secondary alignment and multi-mapped reads were further removed using in-house scripts. Only uniquely mapped reads were retained for further analyses. Quality control metrics were performed using RseqQC using the hg38 gene model provided (Wang et al., 2012). These steps include: number of reads after multiple-step filtering, ribosomal RNA reads depletion, and defining reads mapped to exons, UTRs, and intronic regions. Picard tool was implemented to refine the QC metrics (http://broadinstitute.github.io/picard/). The median number of reads per sample for experiment 1 is ~26 million and two is ~22 million. Gene level expression was calculated using HTseq version 0.9.1 using intersection-strict mode by exon (Anders et al., 2015). Counts were calculated based on protein-coding genes annotation from the Gencode v24 annotation file.

For the experiment including hNPs from two lines from Ch4 the data was analyzed as per Araujo et al. 2015 (Araujo et al., 2015). Briefly, reads were aligned to hg19 TopHat (Trapnell et al., 2009) and Bowtie (Langmead et al., 2009). To obtain the gene counts, we used the HTSeq package (Anders et al., 2015) and the reads were normalized using the RPKM (reads per kilobase per million mapped reads) method (Mortazavi et al., 2008) implemented in the RSeQC package (Wang et al., 2012). We performed a RPKM filtering considering genes with RPKM values of 0.5 in treatments or controls.

RNA-seq differential expression analysis

The four replicates originally collected for the RNA- experiment described in Ch3 were collected on different days. After sequencing, PCA analysis of these samples

revealed that samples from the fourth replicate of each condition were outliers, and thus they were removed from the analysis.

For the data in Ch3 Counts Per Million mapped reads (CPM) rather than Reads Per Kilobase of transcript, per Million mapped reads (RPKM) were used because the libraries exhibited 3' end read distribution bias. DESeq (Anders and Huber, 2010) was used for differential expression (DE) analysis between genes expressed in hNPs expressing FOXP2 or CTRL-GFP, and also between hDNs expressing FOXP2 or CTRL-GFP. Genes were considered for DE analysis if CMP was ≥ 0.5 in all replicates of at least one condition in the comparison.

RPKM values from the experiment containing the KE control in Ch4 we used`. DESeq2 (Love et al., 2014) was used for DE analysis between genes expressed hNPs expressing FOXP2-WT or CTRL-GFP, hNPs expressing FOXP2-KE or CTRL-GFP, hDNs expressing FOXP2-WT or CTRL-GFP, hDNs expressing FOXP2-KE or CTRL-GFP. Genes were considered for DE analysis if RPKM was ≥ 0.5 in all replicates of at least one condition in the comparison.

For the experiment including hNPs from two lines, we performed a RPKM filtering considering genes with RPKM values of 0.5 in treatments or controls. We identified DE genes using the intersection between genes identified using EdgeR (Robinson et al., 2010) and DESeq (Anders and Huber, 2010).

In all cases, genes were considered differentially expressed if the $\log_2$ FOXP2/GFP fold change was greater than or equal to ± 0.3 and FDR was less than or equal to 0.05.

ChIP-seq data analysis

Reads were mapped to the human genome (hg19) using TopHat (Trapnell et al. 2009) and Bowtie (Langmead et al. 2009). The aligned reads were subsequently downsampled according to the lowest number of reads detected, whereas the potential duplicated reads were removed using the Picard package (http://broadinstitute.github.io/picard). SicerDF (Xu et al., 2014) was used to call peak enriched in the *FOXP2* expressing samples over the GFP control samples. Peaks were annotated using GREAT (McLean et al., 2010). Any gene that annotated to a peak was included even if one peak mapped to more than one gene.

PCA analysis of in vivo and in vitro expression data

Microarray expression data from the Allen Institute's Atlas of the Developing Human Brain processed as in Miller et al. 2014 was obtained directly from Jeremy Miller (Miller et al., 2014). Microarray expression data from the highest expressing probe from 20268 genes across 526 samples from tissue laser micro-dissected from the frontal, temporal, parietal, and occipital lobes of four human fetal cortexes (15 pcw, 16 pcw, and two 21 pcw subjects) was plotted along with CMP expression data from RNA-seq experiment 1. Prior to plotting, the two data sets were quantile normalized using the normalize.quantiles function in the preprocessCore Bioconductor R package (https://github.com/bmbolstad/preprocessCore). Next the batch effect was removed using the removeBatchEffect function from the limma package (Ritchie et al., 2015). Finally, principle components were calculated using the prcomp function in the stats package with the default settings. The data was plotted with the ggfortify autoplot function, and modified in Adobe Illustrator for clarity.

Identification of layer correlated genes

The list of layer-correlated genes for every fetal brain analyzed can be found in Miller et al. 2014 supplementary table 3. The layer to which each gene was correlated was identified by finding “the layer with maximum expression” and “the template correlation (setting the layer in the previous column to 1, and all other layers to 0), and Bayes ANOVA p-value (across all layers) for each gene in each of the four prenatal human brains” (Miller and Ding et al. 2014, supplementary table 3 key). Only genes with a reported p-value of less than 0.01 were used in this study’s analysis

Subplate gene evolution analysis

For comparisons of human and macaque layer correlated genes data from microarray expression data from the Allen Institute’s Atlas of the Developing Human Brain processed as in Miller et al. 2014 and microarray expression data from NIH Blueprint Non-Human Primate (NHP) Atlas (Bakken et al., 2016) were used. The macaque data was transformed to remove $\log_2$ normalization to match the processing of the human data (*i.e*. 2^normalized expression value). Only samples from regions represented in data sets from both species were analyzed. Namely, samples from primary visual and somatosensory cortexes from frontal, temporal, parietal, and occipital lobes were considered. To increase the number of samples per developmental stage, human 15 and 16 pcw samples were combined into one stage relabeled “16pcw” and both 21pcw time points were combined into stage relabeled “21pcw” instead of being considered separately. Because the macaque samples did not distinguish between inner and outer cortical plate (CPi and CPo) all human CPi and CPo samples were combine under the general label “CP”. For each human and macaque developmental stage considered, layer correlated genes were identified as in (Miller et al., 2014).

Briefly, an “on/off” matrix was created for each layer of each developmental stage where each column of the matrix represented a sample and each row a layer. A “1” was placed in the row if the sample that the column represented came from the layer the row represented. Zeros were placed in non-matching columns and rows. For example, all subplate sample columns would have a “1” in the subplate row and “0” in all other rows. The expression pattern of each gene was then correlated to every row of the “on/off” matrix, such that a gene only expressed in the subplate would correlate perfectly with the subplate row of the on/off matrix. The row (layer) with the highest correlation was recorded for each gene. An ANOVA test was then run to test if the correlations of a gene to each layer were significantly different from one another, and genes with correlation p-value of <0.05 were considered for the human/macaque comparisons. Hypergeometric p-values were calculated for the overlaps between FOXP2 DE genes and layer correlated genes using 15585 as background (see section: Hypergeometric overlap tests). The Fisher Exact test was used to test for a difference in the proportion of conserved and species-specific genes between VZ genes generally and FOXP2 repressed VZ targets and between SP genes and FOXP2 activated SP targets.

For comparisons between mouse, macaque, and human raw microarray data from E15 and E18 mouse, primary somatosensory subplate and lower cortical layers were generously provided by Anna Hoerder-Suabedissen and Zoltán Molnár (Hoerder-Suabedissen et al., 2013). Data was analyzed using R. Expression values were calculated using robust multi-array average (RMA) implemented in Affy library (Gautier et al., 2004). Four biological replicates from each layer at each time point were analyzed. Gene names ending in “Rik” were removed from analysis. Macaque and

human samples were $\log_2$ normalized, and only samples from SP and CPi/CPo from primary somatosensory cortex were used in the analysis. We did not distinguish between CPi and CPo, calling all of these samples “cortical plate”. Developmental stages from all species were combined into one data set per species with batch effect developmental age removed within each species. Mouse gene symbols were converted to human gene symbols using the biomaRt package (Durinck et al., 2009), and only genes expressed across all species were analyzed. Next, a custom linear model was used to find differentially expressed genes between the subplate and cortical plate at either time point and genes from either species were considered differentially expressed if the BH adjusted p-value was < 0.05. Genes with a positive fold change were more highly expressed in the subplate and negative in the cortical plate. The sign of the fold change was reversed in figure 3.3C for aesthetic reasons.

ATAC-seq mapping and QC

The raw reads were mapped to hg38 using bowtie1 (Langmead et al., 2009) with the parameters -p 12 -y -v 2 --best --strata -m 3 -k 1 -X 2000 as per the Hardison ATAC-seq pipeline from ENCODE (https://www.encodeproject.org/pipelines/ENCPL035XIO/). Samtools (Li et al., 2009) was used to filter for MAPq score greater than 10. Reads mapping to the mitochondria and unmapped contigs were removed. Reads mapping to a subset of high-signal regions generally unique to ATAC-seq, which were defined by the Greenleaf lab and are thought to represent mitochondrial homologues were also removed (Buenrostro et al., 2015a, Buenrostro et al., 2015b). Duplicates were removed from each replicate using Picard MarkDuplicates (http://broadinstitute.github.io/picard/) with REMOVE_DUPLICATES=TRUE.

DAR identification

After the final bam files were generated, MACS2 callpeak was used to identify peaks with the following parameters: -f BAMPE --nomodel --nolambda --keep-dup all (Zhang et al., 2008). Peaks were filtered using the consensus excludable ENCODE blacklist (http://hgdownload.cse.ucsc.edu/goldenPath/hg19/encodeDCC/wgEncodeMapability/). Any peaks with a MACS2 fold change less than 6 were filtered out for the experiment including the KE control and four for the experiment with WT and CTRL only, resulting in a list of high confidence peaks for further analysis

For the experiments without the KE control, a consensus peak set was made containing peaks that occur more than once in any sample (i.e. present in at least 2 of 12) using the bioconductor package DiffBind (Ross-Innes et al., 2012). Reads for each sample were normalized to their full library size, and EdgeR (Robinson et al., 2010) was used to determine differential accessibility. Reads within the consensus peaks were compared between each condition and the average of reads in all of the other conditions (i.e. hDN FOXP2-WT vs !hDN FOXP2-WT). Regions with an FDR < 0.05 that contained at least two fold more reads than the comparison were considered significantly differentially accessible regions (DARs).

For the experiments with the KE control Homer mergePeaks (Heinz et al., 2010) was used to identify MACS2 peaks overlapping in at least three of four replicates of each condition. Then the area 250 bp up and downstream of the summits of these overlapping peaks was analyzed for differential accessibility using the bioconductor package DiffBind using the option summits=250 in DBA count (Ross-Innes et al., 2012).

FOXP2-KE and FOXP2-WT peaks were compared separately in a pairwise manner to CTRL-GFP peaks in the hNPs and hDNs (hNP FOXP2-WT vs. hNP CTRL-GFP; hNP FOXP2-KE vs. hNP CTRL-GFP; hDN FOXP2-WT vs. hDN CTRL-GFP; hDN FOXP2-KE vs. hDN CTRL-GFP). Reads for each sample were normalized to their full library size, and EdgeR (Robinson et al., 2010) was used to determine differential accessibility. Regions with an FDR < 0.05 were considered significantly differentially accessible regions (DARs).

DARs with fewer reads in the FOXP2-WT or -KE condition compared to CTRL are considered closed DARs, while those with more reads in the FOXP2-WT or -KE condition compared to CTRL are considered open DARs. DNA-binding independent DARs are regions that are significantly differentially accessible in the same direction (open or closed) with expression of both FOXP2-WT and FOXP2-KE compared to control in hNPs only or hDNs only. DNA-binding dependent DARs are only present with expression of FOXP2-WT and not FOXP2-KE in hNPs only or hDNs only.

DARs vs ENCODE ChIP data

Each DAR in each condition was annotated to a genomic feature (3' UTR, 5' URT, exon, intergenic regions, promoter-transcription start site, transcription termination site) using the Homer suite's annotatePeaks.pl package (Heinz et al., 2010). For each group of condition specific DARs, 1000 background sets of genomic regions containing the same number of regions as the condition specific group were created. The background regions were randomly selected from the open chromatin regions across all conditions. Each background set contained the same fraction of regions annotated to specific genomic features as the condition specific DAR group it was being used as a

background for. A bed file containing the locations of the genomic regions bound by transcription factors assayed in the ENCODE project was downloaded using the UCSC table browser. Regions bound by transcription factors of interest were overlapped with condition specific DARs and with the 1000 background region sets corresponding with each condition specific DAR group. The mean number of overlaps of each transcription factor's bound regions with the 1000 background set regions was calculated and compared to the overlap of the actual condition specific DAR group. The enrichment score for condition specific DARs vs transcription factor bound sites is the z-score of the actual number of overlaps compared to the distribution of the number of overlaps in the 1000 background sets. A higher z-score denotes more overlap of condition specific DARs with the transcription factor bound sites than background.

DARs vs imputed chromatin states

A bed file (E081_25_imputed12marks_mnemonics.bed.gz) listing regions with imputed chromatin states defined by 12 regulatory marks from human fetal brain tissue was downloaded from the Roadmap Epigenomics Project web portal (http://egg2.wustl.edu/roadmap/data/byFileType/chromhmmSegmentations/ChmmModels/imputed12marks/jointModel/final/) (Ernst and Kellis, 2015). These regions were lifted over from hg19 to hg38 with UCSC's LiftOver tool (http://genome.ucsc.edu/cgi-bin/hgLiftOver). Region abbreviations are as described in table 6.4. ZNF genes & repeats and Quiescent/Low regions were not included in the analysis. Bedtools fisher function (Quinlan and Hall, 2010) was used to calculated the p-value of the overlap between DAR types and chromatin states and p-values were BH corrected for multiple comparisons within DAR type. Left- and right-tail tests were included in the final

heatmap. The sign on the $-\log_{10}$(FDR) was inverted in the final heat map if the left-tail test was significant to denote under enrichment.

DAR genes vs DE genes enrichment analysis

DNA-binding dependent and independent DARs were annotated to the gene with the nearest transcription start site using annoatePeaks.pl from Homer (Heinz et al., 2010) with a custom Homer formatted annotation file made from the Gencode v24 annotation file used for RNA-seq alignment. After identifying the genes nearest to DARs, genes near more than one type of DAR (hDN DNA-binding independent closed, hNP DNA-binding dependent open etc.) were excluded to make mutually exclusive DAR gene lists. These mutually exclusive lists were then overlapped with DE genes from RNA-seq experiment 2. The significance of the enrichment for DAR genes that are also DE genes was evaluated with a hypergeometric test, Benjamini-Hochberg adjusted for all comparisons. Overlaps deemed significant had an adjusted p-value < 0.05.

DAR motif enrichment analysis

Homer findMotifsGenome.pl program (Heinz et al., 2010) was used to identify *de novo* enriched motifs in hDN DNA-binding dependent closed and hDN DNA-binding independent open DARs using the DiffBind consensus peak set as background. Homer's known motif enrichment algorithm (also part of findMotifsGenome.pl) was used to find the enrichment of *de novo* identified FOX (hDN DNA-binding dependent closed homer motif3 p= 1e-16) and NF1-halfsite motifs (hDN DNA-binding independent open homer motif1, p= 1e-16) in the other hDN DAR groups compared to the consensus background peak set.

WGCNA

Weighted gene coexpression network analysis was performed using RPKM data from the two lines analyzed in the hNP experiment with the WGCNA R package (Langfelder and Horvath, 2008). The options used for the blockwiseModules function were: blockwiseModules (datExpr,corType="bicor", maxBlockSize = 15000, networkType="signed", power=14, minModuleSize=30, mergeCutHeight=0.25, numericLabels=TRUE, saveTOMs=FALSE, pamRespectsDendro=FALSE).

Weighted gene coexpression network analysis was performed with RPKM data from the experiment including KE data using the WGCNA R package (Langfelder and Horvath, 2008). Before analysis, the batch effect between hNP and hDN data was removed using the removeBatchEffect function from the limma package (Ritchie et al., 2015) in order to identify modules correlated with *FOXP2* expression and not only differentiation. The options used for the blockwiseModules function were: corType="pearson", maxBlockSize = 14000, networkType="signed", power=10, minModuleSize=50, TOMType = "signed", TOMDenom = "mean", deepSplit=2, verbose=5, mergeCutHeight=0.1, detectCutHeight = 0.999, reassignThreshold = 1e-6.

Cytoscape (Shannon et al., 2003) was used for visualization of the top 500 connections by weight.

Module gene ontology

Toppfun from the Toppgene suit (Chen et al., 2009) was used for gene ontology analysis. All significant (FDR BH < 0.05) GO:Biological Process enrichments were then summarized using Revigo (Supek et al., 2011) with a medium allowed similarity before plotting.

H3K27ac fluorescence intensity quantification

In ImageJ H3K27ac positive nuclei were individual selected using the freeform drawing tool. Area, integrated density and mean fluorescence value were measured for each nucleus and three small regions surrounding each nucleus to be used as background. The corrected nuclear fluorescence for each nucleus was calculated by multiplying the area of each nucleus by the average mean fluorescence of the background regions and subtracting the product from the integrated density of the nucleus. The average corrected H3K27ac nuclear fluorescence of FOXP2 positive and negative cells was compared using the Mann-Whitney test.

Neurosphere assay quantification

In order to make unbiased measurements, the distance between the center of the neurosphere and cells of interest that migrated outside of the neurosphere core was measured using a custom ImageJ program. Specifically, the brightness/contrast of all images was adjusted to a maximum of 100 in the FOXP2, GFP, and DCX channels and a maximum of 75 in the DAPI channel. The background was removed from all channels using the “subtract background” feature with default settings, and the “Despeckle” with default settings was also employed across all channels. Subsequently, a circle was drawn around the core of the neurosphere outside of which individual cells were recognizable. Next, outliers in each channel with a brightness threshold below 50 and a radius of less than 6 pixels were removed (6 pixels allowed for cell bodies and nuclei but excluded most processes). The program measured the distance from the center of the sphere of areas that were DAPI positive, FOXP2 positive, and DCX positive; DAPI positive, FOXP2 positive, and DCX negative; DAPI positive, GFP positive, and DCX positive; or DAPI positive, GFP positive, and DCX negative. The average distance

migrated by CTRL-GFP nuclei and FOXP2-WT or –KE nuclei was compared within each sphere, and a paired student's t-test was performed to test for significant differences between groups. The percent DCX positive nuclei was calculated for CTRL-GFP nuclei and FOXP2-WT or –KE nuclei within each sphere, and a paired student's t-test was performed to test for significant differences between groups. N= 8 FOXP2-WT spheres and N= 7 FOXP2-KE spheres analyzed. Measurements were conducted manually on a separate group of spheres with the experimenter blinded to genotype. Results were similar to those reported by the custom program.

Hypergeometric overlap tests

The hypergeometric overlap test function is as follows:

```
library(gmp)
enrich_pvalue <- function(N, A, B, k)
{
m <- A + k
n <- B + k
i <- k:min(m,n)
as.numeric( sum(chooseZ(m,i)*chooseZ(N-m,n-i))/chooseZ(N,n) )
}
enrich_pvalue(N,A,B,k)
```

15585 was used for the background gene number for all hypergeometric overlap tests. This number represents genes with RPKM of 1 in 80% of the samples from at least one cortical region at one time in the Allen Human Brain Atlas (Hawrylycz et al., 2012), and has been previously used for this purpose (Parikshak et al., 2013).

Gene expression heat maps

Expression heat maps were made using the pheatmap package in R (https://CRAN.R-project.org/package=pheatmap). Expression was centered and scaled by column mean or by row mean as indicated in the figure legend. For heat maps showing the expression of human fetal cortical genes ((Miller et al., 2014) the average expression of the gene of interest in samples corresponding to each layer was used.

Bar plots

All bar plots with error bars represent mean ± SD. The exact value of n and the appropriate statistical tests for each analysis are listed in the figure or figure legend. Significance was defined as p-value or BH adjusted p-value (when appropriate) of <0.05.

Tables

Table 6.1 *Cell lines used in each experiment*

Table 6.1

Experiment	Cell line	Sex	Figures
First round hNP and hDN RNA-seq	Lonza OF4016	Female	3.1-.4, 4.8B-C, 4.9-10
Neurosphere assay	Lonza OF4016	Female	3.6-7
Line1 hNP RNA-seq	Wexler 102208	Male	4.2-3
Line2 hNP RNA-seq	Lonza OF4155	Female	4.2-3
hNP ChIP-seq	Lonza OF4155	Female	4.2-3
Line3 hNP qRT-PCR confirmations	Geschwind lab Line1C	Male	4.3C
H3K27ac immunostaining	Lonza OF4155	Female	4.4B
hNP and hDN immunostaining	Geschwind lab Line1C	Male	4.5A
WT FOXP2 and CTRL ATAC-seq	Lonza OF4016	Female	4.5B-D, 4.6-9
Second round hNP and hDN RNA-seq with KE control	Lonza OF4016	Female	4.10, 4.11C, 4.15

Table 6.2 *Primers designed for this study*

Table 6.2

Target	Experiment	Forward primer	Reverse primer
Cck	genotyping common	TGGTTAGAAGAGAGATGAGCTACAAA	
Cck	WT reverse		CATCACCACGCACAGACATA
Cck	Mutant reverse		GCATCGTAACCGTGCATCT
Cck	qRT-PCR	CTGGCAAGATACATCCAGCA	ACTCATACTCCTCGGCACTG
RYBP	qRT-PCR	CGTCTGCACCTTCAGAAACA	TCTCCTTTTTAGGGGGTGGT
BTG2	qRT-PCR	AGCGAGCAGAGGCTTAAGGT	CGGTAGGACACCTCATAGGG
TUBE1	qRT-PCR	TGGACCTTAATGAAATCAGCA	AGACTGTGTTTGGGGTCTGC
GADD45A	qRT-PCR	TGCGAGAACGACATCAACAT	TTCCCGGCAAAAACAAATAA
CHD2	qRT-PCR	GGACAGTTCGCTACACAGCA	TTCGCTCTCAGATTCCGACT
CBX4	qRT-PCR	ACCGGAGGAGAACATCCTG	CTGCACCACTAGCGGTTTG

Table 6.3 *Primary antibodies used in this study*

Table 6.3

Primary antibody	Dilution	Source	Catalog number
goat anti-FOXP2 (N-terminal)	ICC 1:500	Santa Cruz	21069
rabbit anti-doublecortin (DCX)	ICC 1.5 µg/mL	Abcam	ab18723
rabbit anti-MAP2	ICC 1:1000	Millipore	AB5622
mouse anti-FLAG	ICC 1:10,000; ChIP 1 µg	Sigma	F1804
rabbit anti-H3K27ac	ICC 1:500	Abcam	ab4729
rabbit anti-NFIA	ChIP 5 µg; western .4 µg/mL	Sigma	HPA008884
rabbit anti-NFIB	ChIP 5 µg; western .4 µg/mL	Sigma	HPA003956
mouse anti-V5	western 1:1000	Life Technologies	R960-25
rabbit IgG	ChIP 5 µg	Cell Signaling	2729

Table 6.4 *Abbreviations used for imputed chromatin regions*

Table 6.4

Abbreviations	DESCRIPTION
TssA	Active TSS
PromU	Promoter Upstream TSS
PromD1	Promoter Downstream TSS 1
PromD2	Promoter Downstream TSS 2
Tx5	Transcribed - 5' preferential
Tx	Strong transcription
Tx3	Transcribed - 3' preferential
TxWk	Weak transcription
TxReg	Transcribed & regulatory (Prom/Enh)
TxEnh5	Transcribed 5' preferential and Enh
TxEnh3	Transcribed 3' preferential and Enh
TxEnhW	Transcribed and Weak Enhancer
EnhA1	Active Enhancer 1
EnhA2	Active Enhancer 2
EnhAF	Active Enhancer Flank
EnhW1	Weak Enhancer 1
EnhW2	Weak Enhancer 2
EnhAc	Primary H3K27ac possible Enhancer
DNase	Primary DNase
ZNF/Rpts	ZNF genes & repeats
Het	Heterochromatin
PromP	Poised Promoter
PromBiv	Bivalent Promoter
ReprPC	Repressed Polycomb
Quies	Quiescent/Low

Table 6.5 *Other reagents and resources*

Table 6.5

REAGENT or RESOURCE	SOURCE	IDENTIFIER
Bacterial and Virus Strains		
XL10-Gold Ultracompetent Cells	Agilent	Cat#200315

Chemicals, Peptides, and Recombinant Proteins		
10 mM dNTPs	Enzymatics	Cat#N2050-10-L
10 x Blue buffer	Enzymatics	Cat#B0110
100 mM DTT	Enzymatics	Supplied with EnzScriptTM
1M Tris–HCl, pH 7.4	Fisher	Cat#BP152-5
2X Rapid Ligation buffer	Enzymatics	Cat#B1010L
500 mM EDTA, pH 8.0	Sigma-Aldrich Corporation	Cat#E5134-500G
Actinomycin D	Sigma Aldrich	Cat#A1410
Agencourt AMpure XP beads	Beckman Coulture	Cat# A63881
Antibiotic-Antimycotic (100X), liquid	Life Technologies	Cat#15240-062
B27 without vitamin A	Life Technologies	Cat#12587010
BDNF	Peprotech	Cat#450-02
BIT	STEMCELL Technologies	Cat#9500
dATP	Promega	Cat#U1205
dCTP	Promega	Cat#U1225
dGTP	Promega	Cat#U1215
Dimethyl sulfoxide (DMSO); filtered (for TC)	Sigma	Cat#D2438-50ML
DMEM	Fisher	Cat#SH3024301
DNA Polymerase I	Enzymatics	Cat#P7050L
donkey serum	Millipore	Cat#S30-100ML
dUTP	Promega	Cat#U1191
EnzscriptTM (M-MLV Reverse Transcriptase Rnase H-)	Promega	Cat#M3681
EpiNext DNA Purification HT System	EpiGentek	Cat#P-1063-X4
FBS	Thermo Fisher Scientific	Cat#10437028
FGF	STEMCELL Technologies	Cat#2634
fibronectin	Sigma	Cat# F1141-5MG
Forskolin, Coleus forskohlii | CAS 66575-29-9 | Calbiochem | 50MG	EMD Millipore	Cat#344270-50MG
Fugene	Fisher	Cat#PR-E2691
Glutamax	Life Technologies	Cat#35050-061
IGEPAL CA-630	Sigma	Cat#13021
klenow 3'-5' exo minus LC	Enzymatics	Cat#7010-LC-L
Laminin, Mouse	Corning	Cat#354232
Methanol-free Formaldehyde Ampules	Fisher Scientific	Cat#PI28906
Neurobasal A	Thermo Fisher Scientific	Cat#10888-022
Neurotrophin-3 (NT-3)	Peprotech	Cat#450-03
NEXTflex Poly(A) Beads	Bioo Scientific	Cat#512981
Poly-L-ornithine hydrobromide	Sigma	Cat#P3655
ProLong® Diamond Antifade Reagent with DAPI	Life Technologies	Cat#P36971
random hexamers	Integrated DNA Technologies	Cat#51-01-18-26
Recombinant Human EGF	STEMCELL Technologies	Cat#2633
Retinoic acid, =98% (HPLC)	Sigma Aldrich	Cat#R2625-50mg

Rnase H	Enzymatics	Cat#Y9220L
RNase Inhibitor	Enzymatics	Cat#Y9240L
T4 DNA ligase rapid	Enzymatics	Cat#L6030-HC-L
Triton X-100	Fisher	Cat#BP151-100
Trizma Hydrochloride Solution, pH 8.0, 1 M	Sigma-Aldrich Corporation	Cat#T2694-100ML
Trypsin-EDTA (0.25%), phenol red	Thermo Fisher Scientific	Cat#25200114
100x SYBR Green I	Invitrogen	Cat#S-7563
NEBNext High-Fidelity 2x PCR Master Mix	New England Labs	Cat#M0541
Dpn1	New England Labs	Cat#R0176S
XL10-Gold® β-Mercaptoethanol (β-ME) mix	Agilent	Cat#200315
Critical Commercial Assays		
KAPA HiFi PCR Kit	Kapa Biosystems	Cat#KK2101
NEXTflex™ Barcoded Adapters	biooscientific	Cat#NOVA-514106
Nextera DNA Library Preparation Kit	Illumina	Cat#FC-121-1030
Qiagen MinElute Kit	Qiagen	Cat#28004
KAPA Library Quantification Kit	Roche	Cat#07960140001
Bioanalyzer RNA 6000 Nano chip	Agilent	Cat#5067-1511
High Sensitivity DNA Kit	Agilent	Cat#5067-4626
GeneJET™ Gel Extraction Kit	Thermo Scientific	Cat#FERK0692
XL10-Gold b-mercaptoethanol mix	Agilent	Cat#200315
Deposited Data		
Expression Atlas of the Developing Human Brain	Miller et al. 2014	http://brainspan.org/ RRID:SCR_008083
Layer Correlated Genes table	Miller et al. 2014 Supplemental table 3	
Mouse E15 and E18 subplate and cortical plate raw microarray expression data	Hoerder-Suabedissen et al., 2013	generously provided by Anna Hoerder-Suabedissen and Zoltán Molnár
consensus excludable ENCODE blacklist (lifted over to hg38)	ENCODE	http://hgdownload.cse.ucsc.edu/goldenPath/hg19/encodeDCC/wgEncodeMapability/).
ATAC-seq mitochondrial blacklists hg19 (lifted over to hg38)	Buenrostro et al., 2015	https://sites.google.com/site/atacseqpublic/atac-seq-analysis-methods/mitochondrialblacklists-1
Gencode v24 (GRCh38.p5)	Gencode	https://www.gencodegenes.org/releases/24.html
NIH Blueprint Non-Human Primate (NHP) Atlas Microdissection Microarray	Bakken et al., 2016	http://www.blueprintnhpatlas.org/static/download
Roadmap Epigenomics 25-state model	Kundaje et al., 2015	http://egg2.wustl.edu/roadmap/data/byFileType/chromhmmSegmentations/ChmmModels/imputed12marks/jointModel/final/ RRID:SCR_008924
the DECIPHER project	Firth, H.V. et al (2009)	This study makes use of data generated by the DECIPHER community. A full list of centres who contributed to the generation of the data is available from http://decipher.sanger.ac.uk and via email from decipher@sanger.ac.uk.

		Funding for the project was provided by the Welcome Trust
Oligonucleotides for vector construction		
Add V5 to pLUGIP Forward primer: ACGTAAACGGCCACAAGTTC	This paper	N/A
Add V5 to pLUGIP Reverse primer: GTCGCGGCCGCTTTACGTAGAATCGAGACCGAGGAGAGGGTTAGGGATAGGCTTACCACCAGAACCACCCTTGTACAGCTCGTC	This paper	N/A
Remove 3xFLAG from pLUGIP FOXP2-WT-3xFLAG forward primer: ATGTTAAAGGAGCAGTATGG	This paper	N/A
Remove 3xFLAG from pLUGIP FOXP2-WT-3xFLAG reverse primer: TACCGGGCCCTATTCCAGATCTTCAGATAAAGGC	This paper	N/A
Make KE mutant in pLUGIP-FOXP2-WT-notag forward primer: ACTTGGAAGAATGCAGTACATCATAATCTTAGCCTGCAC	This paper	N/A
Make KE mutant in pLUGIP-FOXP2-WT-notag reverse primer: AGGCTCTTCTTCAATCTCTCTGTCG	This paper	N/A
Add V5 to pLUGIP FOXP2-WT or -KE-notag forward primer: ATGTTAAAGGAGCAGTATGG	This paper	N/A
Add V5 to pLUGIP FOXP2-WT or -KE-notag reverse primer: TACCGGGCCCTACGTAGAATCGAGACCGAGGAGAGGGTTAGGGATAGGCTTACCACCAGAACCACCTTCCAGATCTTCAGATAAAGGC	This paper	N/A
Recombinant DNA		
pLUGIP FOXP2-WT-3X-FLAG	Konopka et al., 2009	N/A
pLUGIP FOXP2-WT-V5	This paper	N/A
pLUGIP-GFP-V5	This paper	N/A
pLUGIP FOXP2-KE-V5	This paper	N/A
pLP/VSVG	Invitrogen	https://www.addgene.org/vector-database/6099/
psPAX2	Addgene	Cat#12260
Software and Algorithms		
Primer3	Untergasser et al. 2012	https://primer3plus.com/cgi-bin/dev/primer3plus.cgi
limma 3.26.9	Ritchie et al., 2015	http://bioconductor.org/packages/limma/
Adobe Illustrator 18.0.0		
Picard 1.77	The Broad Institute	http://broadinstitute.github.io/picard/
bowtie 0.12.7	Langmead et al., 2009	
STAR 2.5.2b	Dobin et al., 2013	https://github.com/alexdobin/STAR
homer v4.6	Heinz et al., 2010	http://homer.ucsd.edu/homer/
WGCNA 1.51	Langfelder and Horvath, 2008	http://www.genetics.ucla.edu/labs/horvath/CoexpressionNetwork/Rpackages/WGCNA/
R 3.2.5	R Core Team, 2016	URL https://www.R-project.org/

Toppgene	Chen et al., 2009	https://toppgene.cchmc.org
Cytoscape 3.3.0	Shannon et al., 2003	http://www.cytoscape.org
Htseq version 0.9.1	Anders et al., 2015	https://htseq.readthedocs.io/en/release_0.9.1/
Trimmomatic 0.36	Bolger et al., 2014	http://www.usadellab.org/cms/?page=trimmomatic
DESeq .22.1	Anders and Huber, 2010	http://bioconductor.org/packages/DESeq/
DESeq2 1.10.1	Love et al., 2014	http://bioconductor.org/packages/DESeq2/
MACS2 2.1.1.20160226	Zhang et al., 2008	http://liulab.dfci.harvard.edu/MACS/
DiffBind 1.16.3	Ross-Innes et al., 2012	http://bioconductor.org/packages/DiffBind/
pheatmap 1.0.8		https://CRAN.R-project.org/package=pheatmap
EdgeR 3.12.1	Robinson et al., 2010	http://bioconductor.org/packages/edgeR/
biomaRt 2.26.1	Durinck et al., 2009	http://bioconductor.org/packages/biomaRt/
Bedtools v2.25.0	Quinlan et al., 2010	http://bedtools.readthedocs.io/en/latest/
Other		
Corning Costar 96-well round bottom Ultra-Low Attachment Multiwell Plate	Sigma	Cat#CSL7007
wide-bore Axygen® 200µL Universal Fit Filter Tips	Corning	Cat#TF-205-WB-R-S

Bibliography

ADAM, I., MENDOZA, E., KOBALZ, U., WOHLGEMUTH, S. & SCHARFF, C. 2017. CNTNAP2 is a direct FoxP2 target in vitro and in vivo in zebra finches: complex regulation by age and activity. *Genes Brain Behav,* 16**,** 635-642.

ANDERS, S. & HUBER, W. 2010. Differential expression analysis for sequence count data. *Genome Biol,* 11**,** R106.

ANDERS, S., PYL, P. T. & HUBER, W. 2015. HTSeq--a Python framework to work with high-throughput sequencing data. *Bioinformatics,* 31**,** 166-9.

ANGEVINE, J. B., JR. & SIDMAN, R. L. 1961. Autoradiographic study of cell migration during histogenesis of cerebral cortex in the mouse. *Nature,* 192**,** 766-8.

ARAUJO, D. J., ANDERSON, A. G., BERTO, S., RUNNELS, W., HARPER, M., AMMANUEL, S., RIEGER, M. A., HUANG, H. C., RAJKOVICH, K., LOERWALD, K. W., DEKKER, J. D., TUCKER, H. O., DOUGHERTY, J. D., GIBSON, J. R. & KONOPKA, G. 2015. FoxP1 orchestration of ASD-relevant signaling pathways in the striatum. *Genes Dev,* 29**,** 2081-96.

AREY, R. N., ENWRIGHT, J. F., 3RD, SPENCER, S. M., FALCON, E., OZBURN, A. R., GHOSE, S., TAMMINGA, C. & MCCLUNG, C. A. 2014. An important role for cholecystokinin, a CLOCK target gene, in the development and treatment of manic-like behaviors. *Mol Psychiatry,* 19**,** 342-50.

ARRANZ, A. M., PERKINS, K. L., IRIE, F., LEWIS, D. P., HRABE, J., XIAO, F., ITANO, N., KIMATA, K., HRABETOVA, S. & YAMAGUCHI, Y. 2014. Hyaluronan deficiency due to Has3 knock-out causes altered neuronal activity and seizures via reduction in brain extracellular space. *J Neurosci,* 34**,** 6164-76.

ARRIAGA, G. & JARVIS, E. D. 2013. Mouse vocal communication system: are ultrasounds learned or innate? *Brain Lang,* 124**,** 96-116.

ARRIAGA, G., ZHOU, E. P. & JARVIS, E. D. 2012. Of mice, birds, and men: the mouse ultrasonic song system has some features similar to humans and song-learning birds. *PLoS One,* 7**,** e46610.

ATASOY, D., APONTE, Y., SU, H. H. & STERNSON, S. M. 2008. A FLEX switch targets Channelrhodopsin-2 to multiple cell types for imaging and long-range circuit mapping. *J Neurosci,* 28**,** 7025-30.

BAGLEY, J. A., REUMANN, D., BIAN, S., LEVI-STRAUSS, J. & KNOBLICH, J. A. 2017. Fused cerebral organoids model interactions between brain regions. *Nat Methods,* 14**,** 743-751.

BAKKEN, T. E., MILLER, J. A., DING, S. L., SUNKIN, S. M., SMITH, K. A., NG, L., SZAFER, A., DALLEY, R. A., ROYALL, J. J., LEMON, T., SHAPOURI, S., AIONA, K., ARNOLD, J., BENNETT, J. L., BERTAGNOLLI, D., BICKLEY, K., BOE, A., BROUNER, K., BUTLER, S., BYRNES, E., CALDEJON, S., CAREY, A., CATE, S., CHAPIN, M., CHEN, J., DEE, N., DESTA, T., DOLBEARE, T. A., DOTSON, N., EBBERT, A., FULFS, E., GEE, G., GILBERT, T. L., GOLDY, J., GOURLEY, L., GREGOR, B., GU, G., HALL, J., HARADON, Z., HAYNOR, D. R., HEJAZINIA, N., HOERDER-SUABEDISSEN, A., HOWARD, R., JOCHIM, J., KINNUNEN, M., KRIEDBERG, A., KUAN, C. L., LAU, C., LEE, C. K., LEE, F., LUONG, L., MASTAN, N., MAY, R., MELCHOR, J., MOSQUEDA, N., MOTT, E., NGO, K., NYHUS, J., OLDRE, A., OLSON, E., PARENTE, J., PARKER, P. D.,

PARRY, S., PENDERGRAFT, J., POTEKHINA, L., REDING, M., RILEY, Z. L., ROBERTS, T., ROGERS, B., ROLL, K., ROSEN, D., SANDMAN, D., SARREAL, M., SHAPOVALOVA, N., SHI, S., SJOQUIST, N., SODT, A. J., TOWNSEND, R., VELASQUEZ, L., WAGLEY, U., WAKEMAN, W. B., WHITE, C., BENNETT, C., WU, J., YOUNG, R., YOUNGSTROM, B. L., WOHNOUTKA, P., GIBBS, R. A., ROGERS, J., HOHMANN, J. G., HAWRYLYCZ, M. J., HEVNER, R. F., MOLNAR, Z., PHILLIPS, J. W., DANG, C., JONES, A. R., AMARAL, D. G., BERNARD, A. & LEIN, E. S. 2016. A comprehensive transcriptional map of primate brain development. *Nature,* 535**,** 367-75.

BARBAS, H., GARCIA-CABEZAS, M. A. & ZIKOPOULOS, B. 2013. Frontal-thalamic circuits associated with language. *Brain Lang,* 126**,** 49-61.

BAYATTI, N., MOSS, J. A., SUN, L., AMBROSE, P., WARD, J. F., LINDSAY, S. & CLOWRY, G. J. 2008. A molecular neuroanatomical study of the developing human neocortex from 8 to 17 postconceptional weeks revealing the early differentiation of the subplate and subventricular zone. *Cereb Cortex,* 18**,** 1536-48.

BELTON, E., SALMOND, C. H., WATKINS, K. E., VARGHA-KHADEM, F. & GADIAN, D. G. 2003. Bilateral brain abnormalities associated with dominantly inherited verbal and orofacial dyspraxia. *Hum Brain Mapp,* 18**,** 194-200.

BETANCOURT, J., KATZMAN, S. & CHEN, B. 2014. Nuclear factor one B regulates neural stem cell differentiation and axonal projection of corticofugal neurons. *J Comp Neurol,* 522**,** 6-35.

BICKNESE, A. R., SHEPPARD, A. M., O'LEARY, D. D. & PEARLMAN, A. L. 1994. Thalamocortical axons extend along a chondroitin sulfate proteoglycan-enriched pathway coincident with the neocortical subplate and distinct from the efferent path. *J Neurosci,* 14**,** 3500-10.

BISHOP, D. V., NORTH, T. & DONLAN, C. 1995. Genetic basis of specific language impairment: evidence from a twin study. *Dev Med Child Neurol,* 37**,** 56-71.

BLASS, E. M. & SHIDE, D. J. 1993. Endogenous cholecystokinin reduces vocalization in isolated 10-day-old rats. *Behav Neurosci,* 107**,** 488-92.

BOLGER, A. M., LOHSE, M. & USADEL, B. 2014. Trimmomatic: a flexible trimmer for Illumina sequence data. *Bioinformatics,* 30**,** 2114-20.

BRADWEJN, J., KOSZYCKI, D., PAYEUR, R., BOURIN, M. & BORTHWICK, H. 1992. Replication of action of cholecystokinin tetrapeptide in panic disorder: clinical and behavioral findings. *Am J Psychiatry,* 149**,** 962-4.

BRADWEJN, J., KOSZYCKI, D. & SHRIQUI, C. 1991. Enhanced sensitivity to cholecystokinin tetrapeptide in panic disorder. Clinical and behavioral findings. *Arch Gen Psychiatry,* 48**,** 603-10.

BUENROSTRO, J. D., WU, B., CHANG, H. Y. & GREENLEAF, W. J. 2015a. ATAC-seq: A Method for Assaying Chromatin Accessibility Genome-Wide. *Curr Protoc Mol Biol,* 109**,** 21 29 1-9.

BUENROSTRO, J. D., WU, B., LITZENBURGER, U. M., RUFF, D., GONZALES, M. L., SNYDER, M. P., CHANG, H. Y. & GREENLEAF, W. J. 2015b. Single-cell chromatin accessibility reveals principles of regulatory variation. *Nature,* 523**,** 486-90.

BURTON, P. R., TOBIN, M. D. & HOPPER, J. L. 2005. Key concepts in genetic epidemiology. *Lancet,* 366**,** 941-51.

BYSTRON, I., MOLNÁR, Z. & OF …, O.-V. 2005. Tangential networks of precocious neurons and early axonal outgrowth in the embryonic human forebrain. *Journal of …*.

CALVIGIONI, D., MÁTÉ, Z., FUZIK, J., GIRACH, F., ZHANG, M.-D., VARRO, A., BEIERSDORF, J., SCHWINDLING, C., YANAGAWA, Y., DOCKRAY, G. J., MCBAIN, C. J., HÖKFELT, T., SZABÓ, G., KEIMPEMA, E. & HARKANY, T. 2017. Functional Differentiation of Cholecystokinin-Containing Interneurons Destined for the Cerebral Cortex. *Cerebral Cortex,* 27**,** 2453-2468.

CAMP, J. G., BADSHA, F., FLORIO, M., KANTON, S., GERBER, T., WILSCH-BRAUNINGER, M., LEWITUS, E., SYKES, A., HEVERS, W., LANCASTER, M., KNOBLICH, J. A., LACHMANN, R., PAABO, S., HUTTNER, W. B. & TREUTLEIN, B. 2015. Human cerebral organoids recapitulate gene expression programs of fetal neocortex development. *Proc Natl Acad Sci U S A,* 112**,** 15672-7.

CAMPBELL, C. E., PIPER, M., PLACHEZ, C., YEH, Y. T., BAIZER, J. S., OSINSKI, J. M., LITWACK, E. D., RICHARDS, L. J. & GRONOSTAJSKI, R. M. 2008. The transcription factor Nfix is essential for normal brain development. *BMC Dev Biol,* 8**,** 52.

CASTELLUCCI, G. A., MCGINLEY, M. J. & MCCORMICK, D. A. 2016. Knockout of Foxp2 disrupts vocal development in mice. *Sci Rep,* 6**,** 23305.

CHABOUT, J., SARKAR, A., PATEL, S. R., RADDEN, T., DUNSON, D. B., FISHER, S. E. & JARVIS, E. D. 2016. A Foxp2 Mutation Implicated in Human Speech Deficits Alters Sequencing of Ultrasonic Vocalizations in Adult Male Mice. *Front Behav Neurosci,* 10**,** 197.

CHANG, E. F., RAYGOR, K. P. & BERGER, M. S. 2015. Contemporary model of language organization: an overview for neurosurgeons. *J Neurosurg,* 122**,** 250-61.

CHEN, J., BARDES, E. E., ARONOW, B. J. & JEGGA, A. G. 2009. ToppGene Suite for gene list enrichment analysis and candidate gene prioritization. *Nucleic Acids Res,* 37**,** W305-11.

CHEN, K. S., HARRIS, L., LIM, J. W. C., HARVEY, T. J., PIPER, M., GRONOSTAJSKI, R. M., RICHARDS, L. J. & BUNT, J. 2017. Differential neuronal and glial expression of nuclear factor I proteins in the cerebral cortex of adult mice. *J Comp Neurol,* 525**,** 2465-2483.

CHOKAS, A. L., TRIVEDI, C. M., LU, M. M., TUCKER, P. W., LI, S., EPSTEIN, J. A. & MORRISEY, E. E. 2010. Foxp1/2/4-NuRD interactions regulate gene expression and epithelial injury response in the lung via regulation of interleukin-6. *J Biol Chem,* 285**,** 13304-13.

CHUN, J. J. & SHATZ, C. J. 1989. Interstitial cells of the adult neocortical white matter are the remnant of the early generated subplate neuron population. *J Comp Neurol,* 282**,** 555-69.

CIRILLO, L. A., LIN, F. R., CUESTA, I., FRIEDMAN, D., JARNIK, M. & ZARET, K. S. 2002. Opening of compacted chromatin by early developmental transcription factors HNF3 (FoxA) and GATA-4. *Mol Cell,* 9**,** 279-89.

CIRILLO, L. A., MCPHERSON, C. E., BOSSARD, P., STEVENS, K., CHERIAN, S., SHIM, E. Y., CLARK, K. L., BURLEY, S. K. & ZARET, K. S. 1998. Binding of the winged-helix transcription factor HNF3 to a linker histone site on the nucleosome. *EMBO J,* 17**,** 244-54.

CLARK, K. L., HALAY, E. D., LAI, E. & BURLEY, S. K. 1993. Co-crystal structure of the HNF-3/fork head DNA-recognition motif resembles histone H5. *Nature,* 364**,** 412-20.

CONSORTIUM, E. P. 2012. An integrated encyclopedia of DNA elements in the human genome. *Nature,* 489**,** 57-74.

COOP, G., BULLAUGHEY, K., LUCA, F. & PRZEWORSKI, M. 2008. The timing of selection at the human FOXP2 gene. *Mol Biol Evol,* 25**,** 1257-9.

CRAWLEY, J. N. 1985. Comparative distribution of cholecystokinin and other neuropeptides. Why is this peptide different from all other peptides? *Ann N Y Acad Sci,* 448**,** 1-8.

CRAWLEY, J. N. & CORWIN, R. L. 1994. Biological actions of cholecystokinin. *Peptides,* 15**,** 731-55.

CUSTO GREIG, L. F., WOODWORTH, M. B., GALAZO, M. J., PADMANABHAN, H. & MACKLIS, J. D. 2013. Molecular logic of neocortical projection neuron specification, development and diversity. *Nat Rev Neurosci,* 14**,** 755-69.

DAS NEVES, L., DUCHALA, C. S., TOLENTINO-SILVA, F., HAXHIU, M. A., COLMENARES, C., MACKLIN, W. B., CAMPBELL, C. E., BUTZ, K. G. & GRONOSTAJSKI, R. M. 1999. Disruption of the murine nuclear factor I-A gene (Nfia) results in perinatal lethality, hydrocephalus, and agenesis of the corpus callosum. *Proc Natl Acad Sci U S A,* 96**,** 11946-51.

DAUGE, V., BESLOT, F., MATSUI, T. & ROQUES, B. P. 2001. Mutant mice lacking the cholecystokinin2 receptor show a dopamine-dependent hyperactivity and a behavioral sensitization to morphine. *Neurosci Lett,* 306**,** 41-4.

DE LA TORRE-UBIETA, L., STEIN, J. L., WON, H., OPLAND, C. K., LIANG, D., LU, D. & GESCHWIND, D. H. 2018. The Dynamic Landscape of Open Chromatin during Human Cortical Neurogenesis. *Cell,* 172**,** 289-304 e18.

DERER, P. & NAKANISHI, S. 1983. Extracellular matrix distribution during neocortical wall ontogenesis in "normal" and "Reeler" mice. *J Hirnforsch,* 24**,** 209-24.

DERIZIOTIS, P., O'ROAK, B. J., GRAHAM, S. A., ESTRUCH, S. B., DIMITROPOULOU, D., BERNIER, R. A., GERDTS, J., SHENDURE, J., EICHLER, E. E. & FISHER, S. E. 2014. De novo TBR1 mutations in sporadic autism disrupt protein functions. *Nat Commun,* 5**,** 4954.

DOBIN, A., DAVIS, C. A., SCHLESINGER, F., DRENKOW, J., ZALESKI, C., JHA, S., BATUT, P., CHAISSON, M. & GINGERAS, T. R. 2013. STAR: ultrafast universal RNA-seq aligner. *Bioinformatics,* 29**,** 15-21.

DOCKRAY, G. J. 1976. Immunochemical evidence of cholecystokinin-like peptides in brain. *Nature,* 264**,** 568-70.

DOCKRAY, G. J. 2014. Gastrointestinal hormones and the dialogue between gut and brain. *J Physiol,* 592**,** 2927-41.

DUQUE, A., KRSNIK, Z., KOSTOVIC, I. & RAKIC, P. 2016. Secondary expansion of the transient subplate zone in the developing cerebrum of human and nonhuman primates. *Proc Natl Acad Sci U S A,* 113**,** 9892-7.

DURINCK, S., SPELLMAN, P. T., BIRNEY, E. & HUBER, W. 2009. Mapping identifiers for the integration of genomic datasets with the R/Bioconductor package biomaRt. *Nat Protoc,* 4**,** 1184-91.

EASTWOOD, S. L. & HARRISON, P. J. 2003. Interstitial white matter neurons express less reelin and are abnormally distributed in schizophrenia: towards an integration of molecular and morphologic aspects of the neurodevelopmental hypothesis. *Mol Psychiatry,* 8**,** 769, 821-31.

EBISU, H., IWAI-TAKEKOSHI, L., FUJITA-JIMBO, E., MOMOI, T. & KAWASAKI, H. 2016. Foxp2 Regulates Identities and Projection Patterns of Thalamic Nuclei During Development. *Cereb Cortex*.

EHRET, G. 2005. Infant rodent ultrasounds -- a gate to the understanding of sound communication. *Behav Genet,* 35**,** 19-29.

ENARD, W. 2011. FOXP2 and the role of cortico-basal ganglia circuits in speech and language evolution. *Curr Opin Neurobiol,* 21**,** 415-24.

ENARD, W., GEHRE, S., HAMMERSCHMIDT, K., HOLTER, S. M., BLASS, T., SOMEL, M., BRUCKNER, M. K., SCHREIWEIS, C., WINTER, C., SOHR, R., BECKER, L., WIEBE, V., NICKEL, B., GIGER, T., MULLER, U., GROSZER, M., ADLER, T., AGUILAR, A., BOLLE, I., CALZADA-WACK, J., DALKE, C., EHRHARDT, N., FAVOR, J., FUCHS, H., GAILUS-DURNER, V., HANS, W., HOLZLWIMMER, G., JAVAHERI, A., KALAYDJIEV, S., KALLNIK, M., KLING, E., KUNDER, S., MOSSBRUGGER, I., NATON, B., RACZ, I., RATHKOLB, B., ROZMAN, J., SCHREWE, A., BUSCH, D. H., GRAW, J., IVANDIC, B., KLINGENSPOR, M., KLOPSTOCK, T., OLLERT, M., QUINTANILLA-MARTINEZ, L., SCHULZ, H., WOLF, E., WURST, W., ZIMMER, A., FISHER, S. E., MORGENSTERN, R., ARENDT, T., DE ANGELIS, M. H., FISCHER, J., SCHWARZ, J. & PAABO, S. 2009. A humanized version of Foxp2 affects cortico-basal ganglia circuits in mice. *Cell,* 137**,** 961-71.

ENARD, W., PRZEWORSKI, M., FISHER, S. E., LAI, C. S., WIEBE, V., KITANO, T., MONACO, A. P. & PAABO, S. 2002. Molecular evolution of FOXP2, a gene involved in speech and language. *Nature,* 418**,** 869-72.

ERDMANN, G., SCHUTZ, G. & BERGER, S. 2007. Inducible gene inactivation in neurons of the adult mouse forebrain. *BMC Neurosci,* 8**,** 63.

ERNST, J. & KELLIS, M. 2015. Large-scale imputation of epigenomic datasets for systematic annotation of diverse human tissues. *Nat Biotechnol,* 33**,** 364-76.

ESTRUCH, S. B., GRAHAM, S. A., CHINNAPPA, S. M., DERIZIOTIS, P. & FISHER, S. E. 2016. Functional characterization of rare FOXP2 variants in neurodevelopmental disorder. *J Neurodev Disord,* 8**,** 44.

ESTRUCH, S. B., GRAHAM, S. A., QUEVEDO, M., VINO, A., DEKKERS, D. H. W., DERIZIOTIS, P., SOLLIS, E., DEMMERS, J., POOT, R. A. & FISHER, S. E. 2018. Proteomic analysis of FOXP proteins reveals interactions between cortical transcription factors associated with neurodevelopmental disorders. *Hum Mol Genet,* 27**,** 1212-1227.

FERLAND, R. J., CHERRY, T. J., PREWARE, P. O., MORRISEY, E. E. & WALSH, C. A. 2003. Characterization of Foxp2 and Foxp1 mRNA and protein in the developing and mature brain. *J Comp Neurol,* 460**,** 266-79.

FIRTH, H. V., RICHARDS, S. M., BEVAN, A. P., CLAYTON, S., CORPAS, M., RAJAN, D., VAN VOOREN, S., MOREAU, Y., PETTETT, R. M. & CARTER, N. P. 2009. DECIPHER: Database of Chromosomal Imbalance and Phenotype in Humans Using Ensembl Resources. *Am J Hum Genet,* 84**,** 524-33.

FISHER, S. E. & SCHARFF, C. 2009. FOXP2 as a molecular window into speech and language. *Trends Genet,* 25**,** 166-77.

FISHER, S. E., VARGHA-KHADEM, F., WATKINS, K. E., MONACO, A. P. & PEMBREY, M. E. 1998. Localisation of a gene implicated in a severe speech and language disorder. *Nat Genet,* 18**,** 168-70.

FONTENOT, M. R., BERTO, S., LIU, Y., WERTHMANN, G., DOUGLAS, C., USUI, N., GLEASON, K., TAMMINGA, C. A., TAKAHASHI, J. S. & KONOPKA, G. 2017. Novel transcriptional networks regulated by CLOCK in human neurons. *Genes Dev,* 31**,** 2121-2135.

FRANCO, S. J. & MULLER, U. 2011. Extracellular matrix functions during neuronal migration and lamination in the mammalian central nervous system. *Dev Neurobiol,* 71**,** 889-900.

FRASER, J. R., LAURENT, T. C. & LAURENT, U. B. 1997. Hyaluronan: its nature, distribution, functions and turnover. *J Intern Med,* 242**,** 27-33.

FRENCH, C. A. & FISHER, S. E. 2014. What can mice tell us about Foxp2 function? *Curr Opin Neurobiol,* 28**,** 72-9.

FRENCH, C. A., GROSZER, M., PREECE, C., COUPE, A. M., RAJEWSKY, K. & FISHER, S. E. 2007. Generation of mice with a conditional Foxp2 null allele. *Genesis,* 45**,** 440-6.

FRENCH, C. A., JIN, X., CAMPBELL, T. G., GERFEN, E., GROSZER, M., FISHER, S. E. & COSTA, R. M. 2012. An aetiological Foxp2 mutation causes aberrant striatal activity and alters plasticity during skill learning. *Mol Psychiatry,* 17**,** 1077-85.

FRIEDLANDER, M. J. & TORRES-REVERON, J. 2009. The changing roles of neurons in the cortical subplate. *Front Neuroanat,* 3**,** 15.

FUJITA, E., TANABE, Y., SHIOTA, A., UEDA, M., SUWA, K., MOMOI, M. Y. & MOMOI, T. 2008. Ultrasonic vocalization impairment of Foxp2 (R552H) knockin mice related to speech-language disorder and abnormality of Purkinje cells. *Proc Natl Acad Sci U S A,* 105**,** 3117-22.

FUJITA-JIMBO, E. & MOMOI, T. 2014. Specific expression of FOXP2 in cerebellum improves ultrasonic vocalization in heterozygous but not in homozygous Foxp2 (R552H) knock-in pups. *Neurosci Lett,* 566**,** 162-6.

GAUB, S., FISHER, S. E. & EHRET, G. 2016. Ultrasonic vocalizations of adult male Foxp2-mutant mice: behavioral contexts of arousal and emotion. *Genes Brain Behav,* 15**,** 243-59.

GAUB, S., GROSZER, M., FISHER, S. E. & EHRET, G. 2010. The structure of innate vocalizations in Foxp2-deficient mouse pups. *Genes Brain Behav,* 9**,** 390-401.

GAUTIER, L., COPE, L., BOLSTAD, B. M. & IRIZARRY, R. A. 2004. affy--analysis of Affymetrix GeneChip data at the probe level. *Bioinformatics,* 20**,** 307-15.

GHOSH, A., ANTONINI, A., MCCONNELL, S. K. & SHATZ, C. J. 1990. Requirement for subplate neurons in the formation of thalamocortical connections. *Nature,* 347**,** 179-81.

GILBERT, A. N. 1986. Mammary number and litter size in Rodentia: The "one-half rule". *Proc Natl Acad Sci U S A,* 83**,** 4828-30.

GOPNIK, M. & CRAGO, M. B. 1991. Familial aggregation of a developmental language disorder. *Cognition,* 39**,** 1-50.

GRABOWSKA, M. M., ELLIOTT, A. D., DEGRAFF, D. J., ANDERSON, P. D., ANUMANTHAN, G., YAMASHITA, H., SUN, Q., FRIEDMAN, D. B., HACHEY, D. L., YU, X., SHEEHAN, J. H., AHN, J. M., RAJ, G. V., PISTON, D. W., GRONOSTAJSKI, R. M. & MATUSIK, R. J. 2014. NFI transcription factors interact with FOXA1 to regulate prostate-specific gene expression. *Mol Endocrinol,* 28**,** 949-64.

GRAY, L. T., YAO, Z., NGUYEN, T. N., KIM, T. K., ZENG, H. & TASIC, B. 2017. Layer-specific chromatin accessibility landscapes reveal regulatory networks in adult mouse visual cortex. *Elife,* 6.

GROSZER, M., KEAYS, D. A., DEACON, R. M., DE BONO, J. P., PRASAD-MULCARE, S., GAUB, S., BAUM, M. G., FRENCH, C. A., NICOD, J., COVENTRY, J. A., ENARD, W., FRAY, M., BROWN, S. D., NOLAN, P. M., PAABO, S., CHANNON, K. M., COSTA, R. M., EILERS, J., EHRET, G., RAWLINS, J. N. & FISHER, S. E. 2008. Impaired synaptic plasticity and motor learning in mice with a point mutation implicated in human speech deficits. *Curr Biol,* 18**,** 354-62.

HAESLER, S., ROCHEFORT, C., GEORGI, B., LICZNERSKI, P., OSTEN, P. & SCHARFF, C. 2007. Incomplete and inaccurate vocal imitation after knockdown of FoxP2 in songbird basal ganglia nucleus Area X. *PLoS Biol,* 5**,** e321.

HAESLER, S., WADA, K., NSHDEJAN, A., MORRISEY, E. E., LINTS, T., JARVIS, E. D. & SCHARFF, C. 2004. FoxP2 expression in avian vocal learners and non-learners. *J Neurosci,* 24**,** 3164-75.

HAHN, M. E., KARKOWSKI, L., WEINREB, L., HENRY, A., SCHANZ, N. & HAHN, E. M. 1998. Genetic and developmental influences on infant mouse ultrasonic calling. II. Developmental patterns in the calls of mice 2-12 days of age. *Behav Genet,* 28**,** 315-25.

HAHN, M. E. & LAVOOY, M. J. 2005. A review of the methods of studies on infant ultrasound production and maternal retrieval in small rodents. *Behav Genet,* 35**,** 31-52.

HAMMERSCHMIDT, K., RADYUSHKIN, K., EHRENREICH, H. & FISCHER, J. 2009. Female mice respond to male ultrasonic 'songs' with approach behaviour. *Biol Lett,* 5**,** 589-92.

HAMMERSCHMIDT, K., SCHREIWEIS, C., MINGE, C., PAABO, S., FISCHER, J. & ENARD, W. 2015. A humanized version of Foxp2 does not affect ultrasonic vocalization in adult mice. *Genes Brain Behav,* 14**,** 583-90.

HARRO, J., VASAR, E. & BRADWEJN, J. 1993. CCK in animal and human research on anxiety. *Trends in Pharmacological Sciences,* 14**,** 244-249.

HAWRYLYCZ, M. J., LEIN, E. S., GUILLOZET-BONGAARTS, A. L., SHEN, E. H., NG, L., MILLER, J. A., VAN DE LAGEMAAT, L. N., SMITH, K. A., EBBERT, A., RILEY, Z. L., ABAJIAN, C., BECKMANN, C. F., BERNARD, A., BERTAGNOLLI, D., BOE, A. F., CARTAGENA, P. M., CHAKRAVARTY, M. M., CHAPIN, M., CHONG, J., DALLEY, R. A., DAVID DALY, B., DANG, C., DATTA, S., DEE, N., DOLBEARE, T. A., FABER, V., FENG, D., FOWLER, D. R., GOLDY, J.,

GREGOR, B. W., HARADON, Z., HAYNOR, D. R., HOHMANN, J. G., HORVATH, S., HOWARD, R. E., JEROMIN, A., JOCHIM, J. M., KINNUNEN, M., LAU, C., LAZARZ, E. T., LEE, C., LEMON, T. A., LI, L., LI, Y., MORRIS, J. A., OVERLY, C. C., PARKER, P. D., PARRY, S. E., REDING, M., ROYALL, J. J., SCHULKIN, J., SEQUEIRA, P. A., SLAUGHTERBECK, C. R., SMITH, S. C., SODT, A. J., SUNKIN, S. M., SWANSON, B. E., VAWTER, M. P., WILLIAMS, D., WOHNOUTKA, P., ZIELKE, H. R., GESCHWIND, D. H., HOF, P. R., SMITH, S. M., KOCH, C., GRANT, S. G. N. & JONES, A. R. 2012. An anatomically comprehensive atlas of the adult human brain transcriptome. *Nature,* 489**,** 391-399.

HEINZ, S., BENNER, C., SPANN, N., BERTOLINO, E., LIN, Y. C., LASLO, P., CHENG, J. X., MURRE, C., SINGH, H. & GLASS, C. K. 2010. Simple combinations of lineage-determining transcription factors prime cis-regulatory elements required for macrophage and B cell identities. *Mol Cell,* 38**,** 576-89.

HENG, Y. H., BARRY, G., RICHARDS, L. J. & PIPER, M. 2012. Nuclear factor I genes regulate neuronal migration. *Neurosignals,* 20**,** 159-67.

HESS, J., ANGEL, P. & SCHORPP-KISTNER, M. 2004. AP-1 subunits: quarrel and harmony among siblings. *J Cell Sci,* 117**,** 5965-73.

HICKOK, G., HOUDE, J. & RONG, F. 2011. Sensorimotor integration in speech processing: computational basis and neural organization. *Neuron,* 69**,** 407-22.

HISAOKA, T., NAKAMURA, Y., SENBA, E. & MORIKAWA, Y. 2010. The forkhead transcription factors, Foxp1 and Foxp2, identify different subpopulations of projection neurons in the mouse cerebral cortex. *Neuroscience,* 166**,** 551-63.

HOERDER-SUABEDISSEN, A. & MOLNAR, Z. 2013. Molecular diversity of early-born subplate neurons. *Cereb Cortex,* 23**,** 1473-83.

HOERDER-SUABEDISSEN, A. & MOLNAR, Z. 2015. Development, evolution and pathology of neocortical subplate neurons. *Nat Rev Neurosci,* 16**,** 133-46.

HOERDER-SUABEDISSEN, A., OESCHGER, F. M., KRISHNAN, M. L., BELGARD, T. G., WANG, W. Z., LEE, S., WEBBER, C., PETRETTO, E., EDWARDS, A. D. & MOLNAR, Z. 2013. Expression profiling of mouse subplate reveals a dynamic gene network and disease association with autism and schizophrenia. *Proc Natl Acad Sci U S A,* 110**,** 3555-60.

HOERDER-SUABEDISSEN, A., WANG, W. Z., LEE, S., DAVIES, K. E., GOFFINET, A. M., RAKIC, S., PARNAVELAS, J., REIM, K., NICOLIC, M., PAULSEN, O. & MOLNAR, Z. 2009. Novel markers reveal subpopulations of subplate neurons in the murine cerebral cortex. *Cereb Cortex,* 19**,** 1738-50.

HOLY, T. E. & GUO, Z. 2005. Ultrasonic songs of male mice. *PLoS Biol,* 3**,** e386.

HONDA, T., WADA, E., BATTEY, J. F. & WANK, S. A. 1993. Differential Gene Expression of CCKA and CCKB Receptors in the Rat Brain. *Molecular and Cellular Neuroscience,* 4**,** 143-154.

HONIG, L. S., HERRMANN, K. & SHATZ, C. J. 1996. Developmental changes revealed by immunohistochemical markers in human cerebral cortex. *Cereb Cortex,* 6**,** 794-806.

HURST, J. A., BARAITSER, M., AUGER, E., GRAHAM, F. & NORELL, S. 1990. An extended family with a dominantly inherited speech disorder. *Dev Med Child Neurol,* 32**,** 352-5.

HUTSLER, J. J., LOVE, T. & ZHANG, H. 2007. Histological and magnetic resonance imaging assessment of cortical layering and thickness in autism spectrum disorders. *Biol Psychiatry,* 61**,** 449-57.

INNIS, R. B. & SNYDER, S. H. 1980. Distinct cholecystokinin receptors in brain and pancreas. *Proc Natl Acad Sci U S A,* 77**,** 6917-21.

IVY, A. C. 1929. A hormone mechanism for gall-bladder contraction & evacuation. *The American Journal of Surgery,* 7**,** 455-459.

JOHNSON, M. B., SUN, X., KODANI, A., BORGES-MONROY, R., GIRSKIS, K. M., RYU, S. C., WANG, P. P., PATEL, K., GONZALEZ, D. M., WOO, Y. M., YAN, Z., LIANG, B., SMITH, R. S., CHATTERJEE, M., COMAN, D., PAPADEMETRIS, X., STAIB, L. H., HYDER, F., MANDEVILLE, J. B., GRANT, P. E., IM, K., KWAK, H., ENGELHARDT, J. F., WALSH, C. A. & BAE, B. I. 2018. Aspm knockout ferret reveals an evolutionary mechanism governing cerebral cortical size. *Nature,* 556**,** 370-375.

KANG, H. J., KAWASAWA, Y. I., CHENG, F., ZHU, Y., XU, X., LI, M., SOUSA, A. M., PLETIKOS, M., MEYER, K. A., SEDMAK, G., GUENNEL, T., SHIN, Y., JOHNSON, M. B., KRSNIK, Z., MAYER, S., FERTUZINHOS, S., UMLAUF, S., LISGO, S. N., VORTMEYER, A., WEINBERGER, D. R., MANE, S., HYDE, T. M., HUTTNER, A., REIMERS, M., KLEINMAN, J. E. & SESTAN, N. 2011. Spatio-temporal transcriptome of the human brain. *Nature,* 478**,** 483-9.

KANOLD, P. O., KARA, P., REID, R. C. & SHATZ, C. J. 2003. Role of subplate neurons in functional maturation of visual cortical columns. *Science,* 301**,** 521-5.

KANOLD, P. O. & LUHMANN, H. J. 2010. The subplate and early cortical circuits. *Annu Rev Neurosci,* 33**,** 23-48.

KANOLD, P. O. & SHATZ, C. J. 2006. Subplate neurons regulate maturation of cortical inhibition and outcome of ocular dominance plasticity. *Neuron,* 51**,** 627-38.

KENNEDY, J. L., BRADWEJN, J., KOSZYCKI, D., KING, N., CROWE, R., VINCENT, J. & FOURIE, O. 1999. Investigation of cholecystokinin system genes in panic disorder. *Molecular Psychiatry,* 4**,** 284.

KOKS, S., ABRAMOV, U., VERAKSITS, A., BOURIN, M., MATSUI, T. & VASAR, E. 2003. CCK2 receptor-deficient mice have increased sensitivity of dopamine D2 receptors. *Neuropeptides,* 37**,** 25-9.

KONOPKA, G., BOMAR, J. M., WINDEN, K., COPPOLA, G., JONSSON, Z. O., GAO, F., PENG, S., PREUSS, T. M., WOHLSCHLEGEL, J. A. & GESCHWIND, D. H. 2009. Human-specific transcriptional regulation of CNS development genes by FOXP2. *Nature,* 462**,** 213-7.

KONOPKA, G., FRIEDRICH, T., DAVIS-TURAK, J., WINDEN, K., OLDHAM, M. C., GAO, F., CHEN, L., WANG, G. Z., LUO, R., PREUSS, T. M. & GESCHWIND, D. H. 2012a. Human-specific transcriptional networks in the brain. *Neuron,* 75**,** 601-17.

KONOPKA, G. & ROBERTS, T. F. 2016. Insights into the Neural and Genetic Basis of Vocal Communication. *Cell,* 164**,** 1269-1276.

KONOPKA, G., WEXLER, E., ROSEN, E., MUKAMEL, Z., OSBORN, G. E., CHEN, L., LU, D., GAO, F., GAO, K., LOWE, J. K. & GESCHWIND, D. H. 2012b. Modeling the functional genomics of autism using human neurons. *Mol Psychiatry,* 17**,** 202-14.

KOPIN, A. S., MATHES, W. F., MCBRIDE, E. W., NGUYEN, M., AL-HAIDER, W., SCHMITZ, F., BONNER-WEIR, S., KANAREK, R. & BEINBORN, M. 1999. The cholecystokinin-A receptor mediates inhibition of food intake yet is not essential for the maintenance of body weight. *J Clin Invest,* 103**,** 383-91.

KOSTOVIC, I. & GOLDMAN-RAKIC, P. S. 1983. Transient cholinesterase staining in the mediodorsal nucleus of the thalamus and its connections in the developing human and monkey brain. *J Comp Neurol,* 219**,** 431-47.

KOSTOVIC, I. & JUDAS, M. 2002. Correlation between the sequential ingrowth of afferents and transient patterns of cortical lamination in preterm infants. *Anat Rec,* 267**,** 1-6.

KOSTOVIC, I., JUDAS, M., RADOS, M. & HRABAC, P. 2002. Laminar organization of the human fetal cerebrum revealed by histochemical markers and magnetic resonance imaging. *Cereb Cortex,* 12**,** 536-44.

KOSTOVIC, I. & RAKIC, P. 1980. Cytology and time of origin of interstitial neurons in the white matter in infant and adult human and monkey telencephalon. *J Neurocytol,* 9**,** 219-42.

KOSTOVIC, I. & RAKIC, P. 1990. Developmental history of the transient subplate zone in the visual and somatosensory cortex of the macaque monkey and human brain. *J Comp Neurol,* 297**,** 441-70.

KRAUSE, J., LALUEZA-FOX, C., ORLANDO, L., ENARD, W., GREEN, R. E., BURBANO, H. A., HUBLIN, J. J., HANNI, C., FORTEA, J., DE LA RASILLA, M., BERTRANPETIT, J., ROSAS, A. & PAABO, S. 2007. The derived FOXP2 variant of modern humans was shared with Neandertals. *Curr Biol,* 17**,** 1908-12.

KUHLWILM, M., GRONAU, I., HUBISZ, M. J., DE FILIPPO, C., PRADO-MARTINEZ, J., KIRCHER, M., FU, Q., BURBANO, H. A., LALUEZA-FOX, C., DE LA RASILLA, M., ROSAS, A., RUDAN, P., BRAJKOVIC, D., KUCAN, Z., GUSIC, I., MARQUES-BONET, T., ANDRES, A. M., VIOLA, B., PAABO, S., MEYER, M., SIEPEL, A. & CASTELLANO, S. 2016. Ancient gene flow from early modern humans into Eastern Neanderthals. *Nature,* 530**,** 429-33.

KURT, S., FISHER, S. E. & EHRET, G. 2012. Foxp2 mutations impair auditory-motor association learning. *PLoS One,* 7**,** e33130.

KURT, S., GROSZER, M., FISHER, S. E. & EHRET, G. 2009. Modified sound-evoked brainstem potentials in Foxp2 mutant mice. *Brain Res,* 1289**,** 30-6.

LACOURSE, K. A., SWANBERG, L. J., GILLESPIE, P. J., REHFELD, J. F., SAUNDERS, T. L. & SAMUELSON, L. C. 1999. Pancreatic function in CCK-deficient mice: adaptation to dietary protein does not require CCK. *Am J Physiol,* 276**,** G1302-9.

LAI, C. S., FISHER, S. E., HURST, J. A., LEVY, E. R., HODGSON, S., FOX, M., JEREMIAH, S., POVEY, S., JAMISON, D. C., GREEN, E. D., VARGHA-KHADEM, F. & MONACO, A. P. 2000. The SPCH1 region on human 7q31: genomic characterization of the critical interval and localization of translocations associated with speech and language disorder. *Am J Hum Genet,* 67**,** 357-68.

LAI, C. S., FISHER, S. E., HURST, J. A., VARGHA-KHADEM, F. & MONACO, A. P. 2001. A forkhead-domain gene is mutated in a severe speech and language disorder. *Nature,* 413**,** 519-23.

LAI, C. S., GERRELLI, D., MONACO, A. P., FISHER, S. E. & COPP, A. J. 2003. FOXP2 expression during brain development coincides with adult sites of pathology in a severe speech and language disorder. *Brain,* 126**,** 2455-62.

LANCASTER, M. A., CORSINI, N. S., WOLFINGER, S., GUSTAFSON, E. H., PHILLIPS, A. W., BURKARD, T. R., OTANI, T., LIVESEY, F. J. & KNOBLICH, J. A. 2017. Guided self-organization and cortical plate formation in human brain organoids. *Nat Biotechnol,* 35**,** 659-666.

LANCASTER, M. A., RENNER, M., MARTIN, C. A., WENZEL, D., BICKNELL, L. S., HURLES, M. E., HOMFRAY, T., PENNINGER, J. M., JACKSON, A. P. & KNOBLICH, J. A. 2013. Cerebral organoids model human brain development and microcephaly. *Nature,* 501**,** 373-9.

LANGFELDER, P. & HORVATH, S. 2008. WGCNA: an R package for weighted correlation network analysis. *BMC Bioinformatics,* 9**,** 559.

LANGMEAD, B., TRAPNELL, C., POP, M. & SALZBERG, S. L. 2009. Ultrafast and memory-efficient alignment of short DNA sequences to the human genome. *Genome Biol,* 10**,** R25.

LENNON, P. A., COOPER, M. L., PEIFFER, D. A., GUNDERSON, K. L., PATEL, A., PETERS, S., CHEUNG, S. W. & BACINO, C. A. 2007. Deletion of 7q31.1 supports involvement of FOXP2 in language impairment: clinical report and review. *Am J Med Genet A,* 143A**,** 791-8.

LEPP, S., ANDERSON, A. & KONOPKA, G. 2013. Connecting signaling pathways underlying communication to ASD vulnerability. *Int Rev Neurobiol,* 113**,** 97-133.

LI, H., HANDSAKER, B., WYSOKER, A., FENNELL, T., RUAN, J., HOMER, N., MARTH, G., ABECASIS, G., DURBIN, R. & GENOME PROJECT DATA PROCESSING, S. 2009. The Sequence Alignment/Map format and SAMtools. *Bioinformatics,* 25**,** 2078-9.

LI, S., WEIDENFELD, J. & MORRISEY, E. E. 2004. Transcriptional and DNA binding activity of the Foxp1/2/4 family is modulated by heterotypic and homotypic protein interactions. *Mol Cell Biol,* 24**,** 809-22.

LIEGEOIS, F., BALDEWEG, T., CONNELLY, A., GADIAN, D. G., MISHKIN, M. & VARGHA-KHADEM, F. 2003. Language fMRI abnormalities associated with FOXP2 gene mutation. *Nat Neurosci,* 6**,** 1230-7.

LIEGEOIS, F., MORGAN, A. T., CONNELLY, A. & VARGHA-KHADEM, F. 2011. Endophenotypes of FOXP2: dysfunction within the human articulatory network. *Eur J Paediatr Neurol,* 15**,** 283-8.

LIU, Z., LI, X., ZHANG, J.-T., CAI, Y.-J., CHENG, T.-L., CHENG, C., WANG, Y., ZHANG, C.-C., NIE, Y.-H., CHEN, Z.-F., BIAN, W.-J., ZHANG, L., XIAO, J., LU, B., ZHANG, Y.-F., ZHANG, X.-D., SANG, X., WU, J.-J., XU, X., XIONG, Z.-Q., ZHANG, F., YU, X., GONG, N., ZHOU, W.-H., SUN, Q. & QIU, Z. 2016. Autism-like behaviours and germline transmission in transgenic monkeys overexpressing MeCP2. *Nature,* 530**,** 98.

LO, C. M., SAMUELSON, L. C., CHAMBERS, J. B., KING, A., HEIMAN, J., JANDACEK, R. J., SAKAI, R. R., BENOIT, S. C., RAYBOULD, H. E., WOODS, S. C. & TSO, P. 2008. Characterization of mice lacking the gene for cholecystokinin. *Am J Physiol Regul Integr Comp Physiol,* 294**,** R803-10.

LOVE, M. I., HUBER, W. & ANDERS, S. 2014. Moderated estimation of fold change and dispersion for RNA-seq data with DESeq2. *Genome Biol,* 15**,** 550.

LUI, J. H., HANSEN, D. V. & KRIEGSTEIN, A. R. 2011. Development and evolution of the human neocortex. *Cell,* 146**,** 18-36.

MACDERMOT, K. D., BONORA, E., SYKES, N., COUPE, A. M., LAI, C. S., VERNES, S. C., VARGHA-KHADEM, F., MCKENZIE, F., SMITH, R. L., MONACO, A. P. & FISHER, S. E. 2005. Identification of FOXP2 truncation as a novel cause of developmental speech and language deficits. *Am J Hum Genet,* 76**,** 1074-80.

MANTO, M., BOWER, J. M., CONFORTO, A. B., DELGADO-GARCIA, J. M., DA GUARDA, S. N., GERWIG, M., HABAS, C., HAGURA, N., IVRY, R. B., MARIEN, P., MOLINARI, M., NAITO, E., NOWAK, D. A., OULAD BEN TAIB, N., PELISSON, D., TESCHE, C. D., TILIKETE, C. & TIMMANN, D. 2012. Consensus paper: roles of the cerebellum in motor control--the diversity of ideas on cerebellar involvement in movement. *Cerebellum,* 11**,** 457-87.

MARICIC, T., GUNTHER, V., GEORGIEV, O., GEHRE, S., CURLIN, M., SCHREIWEIS, C., NAUMANN, R., BURBANO, H. A., MEYER, M., LALUEZA-FOX, C., DE LA RASILLA, M., ROSAS, A., GAJOVIC, S., KELSO, J., ENARD, W., SCHAFFNER, W. & PAABO, S. 2013. A recent evolutionary change affects a regulatory element in the human FOXP2 gene. *Mol Biol Evol,* 30**,** 844-52.

MARIN-PADILLA, M. 1978. Dual origin of the mammalian neocortex and evolution of the cortical plate. *Anat Embryol (Berl),* 152**,** 109-26.

MARIN-PADILLA, M. 1992. Ontogenesis of the pyramidal cell of the mammalian neocortex and developmental cytoarchitectonics: a unifying theory. *J Comp Neurol,* 321**,** 223-40.

MARSHALL, F. H., BARNES, S., HUGHES, J., WOODRUFF, G. N. & HUNTER, J. C. 1991. Cholecystokinin Modulates the Release of Dopamine from the Anterior and Posterior Nucleus Accumbens by Two Different Mechanisms. *Journal of Neurochemistry,* 56**,** 917-922.

MARTYNOGA, B., MATEO, J. L., ZHOU, B., ANDERSEN, J., ACHIMASTOU, A., URBAN, N., VAN DEN BERG, D., GEORGOPOULOU, D., HADJUR, S., WITTBRODT, J., ETTWILLER, L., PIPER, M., GRONOSTAJSKI, R. M. & GUILLEMOT, F. 2013. Epigenomic enhancer annotation reveals a key role for NFIX in neural stem cell quiescence. *Genes Dev,* 27**,** 1769-86.

MARX, M. & FELDMEYER, D. 2013. Morphology and physiology of excitatory neurons in layer 6b of the somatosensory rat barrel cortex. *Cereb Cortex,* 23**,** 2803-17.

MCLEAN, C. Y., BRISTOR, D., HILLER, M., CLARKE, S. L., SCHAAR, B. T., LOWE, C. B., WENGER, A. M. & BEJERANO, G. 2010. GREAT improves functional interpretation of cis-regulatory regions. *Nat Biotechnol,* 28**,** 495-501.

MEYER, G., SCHAAPS, J. P. & OF …, M.-L. 2000. Embryonic and early fetal development of the human neocortex. *Journal of ….*

MILLER, J. A., DING, S. L., SUNKIN, S. M., SMITH, K. A., NG, L., SZAFER, A., EBBERT, A., RILEY, Z. L., ROYALL, J. J., AIONA, K., ARNOLD, J. M., BENNET, C., BERTAGNOLLI, D., BROUNER, K., BUTLER, S., CALDEJON, S., CAREY, A., CUHACIYAN, C., DALLEY, R. A., DEE, N., DOLBEARE, T. A., FACER, B. A., FENG, D., FLISS, T. P., GEE, G., GOLDY, J., GOURLEY, L., GREGOR, B. W., GU, G., HOWARD, R. E., JOCHIM, J. M., KUAN, C. L., LAU, C., LEE, C. K.,

LEE, F., LEMON, T. A., LESNAR, P., MCMURRAY, B., MASTAN, N., MOSQUEDA, N., NALUAI-CECCHINI, T., NGO, N. K., NYHUS, J., OLDRE, A., OLSON, E., PARENTE, J., PARKER, P. D., PARRY, S. E., STEVENS, A., PLETIKOS, M., REDING, M., ROLL, K., SANDMAN, D., SARREAL, M., SHAPOURI, S., SHAPOVALOVA, N. V., SHEN, E. H., SJOQUIST, N., SLAUGHTERBECK, C. R., SMITH, M., SODT, A. J., WILLIAMS, D., ZOLLEI, L., FISCHL, B., GERSTEIN, M. B., GESCHWIND, D. H., GLASS, I. A., HAWRYLYCZ, M. J., HEVNER, R. F., HUANG, H., JONES, A. R., KNOWLES, J. A., LEVITT, P., PHILLIPS, J. W., SESTAN, N., WOHNOUTKA, P., DANG, C., BERNARD, A., HOHMANN, J. G. & LEIN, E. S. 2014. Transcriptional landscape of the prenatal human brain. *Nature,* 508**,** 199-206.

MOLNAR, Z. & BLAKEMORE, C. 1995a. Guidance of thalamocortical innervation. *Ciba Found Symp,* 193**,** 127-49; discussion 192-9.

MOLNAR, Z. & BLAKEMORE, C. 1995b. How do thalamic axons find their way to the cortex? *Trends Neurosci,* 18**,** 389-97.

MOLNAR, Z., METIN, C., STOYKOVA, A., TARABYKIN, V., PRICE, D. J., FRANCIS, F., MEYER, G., DEHAY, C. & KENNEDY, H. 2006. Comparative aspects of cerebral cortical development. *Eur J Neurosci,* 23**,** 921-34.

MONTIEL, J. F., WANG, W. Z., OESCHGER, F. M., HOERDER-SUABEDISSEN, A., TUNG, W. L., GARCIA-MORENO, F., HOLM, I. E., VILLALON, A. & MOLNAR, Z. 2011. Hypothesis on the dual origin of the Mammalian subplate. *Front Neuroanat,* 5**,** 25.

MORINO, P., HERRERA‐MARSCHITZ, M., CASTEL, M. N., UNGERSTEDT, U., VARRO, A., DOCKRAY, G. & HÖKFELT, T. 1994. Cholecystokinin in Cortico‐striatal Neurons in the Rat: Immunohistochemical Studies at the Light and Electron Microscopical Level. *European Journal of Neuroscience,* 6**,** 681-692.

MORTAZAVI, A., WILLIAMS, B. A., MCCUE, K., SCHAEFFER, L. & WOLD, B. 2008. Mapping and quantifying mammalian transcriptomes by RNA-Seq. *Nat Methods,* 5**,** 621-8.

MURDOCH, B. E. 2010. The cerebellum and language: historical perspective and review. *Cortex,* 46**,** 858-68.

MURUGAN, M., HARWARD, S., SCHARFF, C. & MOONEY, R. 2013. Diminished FoxP2 levels affect dopaminergic modulation of corticostriatal signaling important to song variability. *Neuron,* 80**,** 1464-76.

NEPH, S., VIERSTRA, J., STERGACHIS, A. B., REYNOLDS, A. P., HAUGEN, E., VERNOT, B., THURMAN, R. E., JOHN, S., SANDSTROM, R., JOHNSON, A. K., MAURANO, M. T., HUMBERT, R., RYNES, E., WANG, H., VONG, S., LEE, K., BATES, D., DIEGEL, M., ROACH, V., DUNN, D., NERI, J., SCHAFER, A., HANSEN, R. S., KUTYAVIN, T., GISTE, E., WEAVER, M., CANFIELD, T., SABO, P., ZHANG, M., BALASUNDARAM, G., BYRON, R., MACCOSS, M. J., AKEY, J. M., BENDER, M. A., GROUDINE, M., KAUL, R. & STAMATOYANNOPOULOS, J. A. 2012. An expansive human regulatory lexicon encoded in transcription factor footprints. *Nature,* 489**,** 83-90.

NIU, Y., SHEN, B., CUI, Y., CHEN, Y., WANG, J., WANG, L., KANG, Y., ZHAO, X., SI, W., LI, W., XIANG, ANDY P., ZHOU, J., GUO, X., BI, Y., SI, C., HU, B., DONG, G., WANG, H., ZHOU, Z., LI, T., TAN, T., PU, X., WANG, F., JI, S., ZHOU, Q.,

HUANG, X., JI, W. & SHA, J. 2014. Generation of Gene-Modified Cynomolgus Monkey via Cas9/RNA-Mediated Gene Targeting in One-Cell Embryos. *Cell,* 156**,** 836-843.

NOBLE, F. & ROQUES, B. P. 2006. Cholecystokinin Peptides in Brain Function. *In:* LAJTHA, A. & LIM, R. (eds.) *Handbook of Neurochemistry and Molecular Neurobiology: Neuroactive Proteins and Peptides.* Boston, MA: Springer US.

NOBLE, F., WANK, S. A., CRAWLEY, J. N., BRADWEJN, J., SEROOGY, K. B., HAMON, M. & ROQUES, B. P. 1999. International Union of Pharmacology. XXI. Structure, Distribution, and Functions of Cholecystokinin Receptors. *Pharmacological Reviews,* 51**,** 745.

NOWAKOWSKI, T. J., BHADURI, A., POLLEN, A. A., ALVARADO, B., MOSTAJO-RADJI, M. A., DI LULLO, E., HAEUSSLER, M., SANDOVAL-ESPINOSA, C., LIU, S. J., VELMESHEV, D., OUNADJELA, J. R., SHUGA, J., WANG, X., LIM, D. A., WEST, J. A., LEYRAT, A. A., KENT, W. J. & KRIEGSTEIN, A. R. 2017. Spatiotemporal gene expression trajectories reveal developmental hierarchies of the human cortex. *Science,* 358**,** 1318-1323.

OESCHGER, F. M., WANG, W. Z., LEE, S., GARCIA-MORENO, F., GOFFINET, A. M., ARBONES, M. L., RAKIC, S. & MOLNAR, Z. 2012. Gene expression analysis of the embryonic subplate. *Cereb Cortex,* 22**,** 1343-59.

OHTAKA-MARUYAMA, C., OKAMOTO, M., ENDO, K., OSHIMA, M., KANEKO, N., YURA, K., OKADO, H., MIYATA, T. & MAEDA, N. 2018. Synaptic transmission from subplate neurons controls radial migration of neocortical neurons. *Science,* 360**,** 313-317.

PALMER, T. D., SCHWARTZ, P. H., TAUPIN, P., KASPAR, B., STEIN, S. A. & GAGE, F. H. 2001. Cell culture. Progenitor cells from human brain after death. *Nature,* 411**,** 42-3.

PARIKSHAK, N. N., LUO, R., ZHANG, A., WON, H., LOWE, J. K., CHANDRAN, V., HORVATH, S. & GESCHWIND, D. H. 2013. Integrative functional genomic analyses implicate specific molecular pathways and circuits in autism. *Cell,* 155**,** 1008-21.

PIÑON, M., JETHWA, A., JACOBS, E., CAMPAGNONI, A. & MOLNÁR, Z. 2009. Dynamic integration of subplate neurons into the cortical barrel field circuitry during postnatal development in the Golli‐tau‐eGFP (GTE) mouse. *The Journal of Physiology,* 587**,** 1903-1915.

POMERANTZ, S. M., NUNEZ, A. A. & BEAN, N. J. 1983. Female behavior is affected by male ultrasonic vocalizations in house mice. *Physiol Behav,* 31**,** 91-6.

PRICE, D. J., ASLAM, S., TASKER, L. & GILLIES, K. 1997. Fates of the earliest generated cells in the developing murine neocortex. *J Comp Neurol,* 377**,** 414-22.

PTAK, S. E., ENARD, W., WIEBE, V., HELLMANN, I., KRAUSE, J., LACHMANN, M. & PAABO, S. 2009. Linkage disequilibrium extends across putative selected sites in FOXP2. *Mol Biol Evol,* 26**,** 2181-4.

QUADRATO, G., NGUYEN, T., MACOSKO, E. Z., SHERWOOD, J. L., MIN YANG, S., BERGER, D. R., MARIA, N., SCHOLVIN, J., GOLDMAN, M., KINNEY, J. P., BOYDEN, E. S., LICHTMAN, J. W., WILLIAMS, Z. M., MCCARROLL, S. A. &

ARLOTTA, P. 2017. Cell diversity and network dynamics in photosensitive human brain organoids. *Nature,* 545**,** 48-53.

QUINLAN, A. R. & HALL, I. M. 2010. BEDTools: a flexible suite of utilities for comparing genomic features. *Bioinformatics,* 26**,** 841-2.

RAKIC, P. 1974. Neurons in rhesus monkey visual cortex: systematic relation between time of origin and eventual disposition. *Science,* 183**,** 425-7.

REHFELD, J. F. & NIELSEN, F. C. 1995. Molecular Forms and Regional Distribution of Cholecystokinin in the Central Nervous System. *In:* BRADWEJN, J. & VASAR, E. (eds.) *Cholecystokinin and Anxiety: From Neuron to Behavior.* Berlin, Heidelberg: Springer Berlin Heidelberg.

REICH, D., GREEN, R. E., KIRCHER, M., KRAUSE, J., PATTERSON, N., DURAND, E. Y., VIOLA, B., BRIGGS, A. W., STENZEL, U., JOHNSON, P. L., MARICIC, T., GOOD, J. M., MARQUES-BONET, T., ALKAN, C., FU, Q., MALLICK, S., LI, H., MEYER, M., EICHLER, E. E., STONEKING, M., RICHARDS, M., TALAMO, S., SHUNKOV, M. V., DEREVIANKO, A. P., HUBLIN, J. J., KELSO, J., SLATKIN, M. & PAABO, S. 2010. Genetic history of an archaic hominin group from Denisova Cave in Siberia. *Nature,* 468**,** 1053-60.

REIMERS-KIPPING, S., HEVERS, W., PAABO, S. & ENARD, W. 2011. Humanized Foxp2 specifically affects cortico-basal ganglia circuits. *Neuroscience,* 175**,** 75-84.

RITCHIE, M. E., PHIPSON, B., WU, D., HU, Y., LAW, C. W., SHI, W. & SMYTH, G. K. 2015. limma powers differential expression analyses for RNA-sequencing and microarray studies. *Nucleic Acids Res,* 43**,** e47.

ROADMAP EPIGENOMICS, C., KUNDAJE, A., MEULEMAN, W., ERNST, J., BILENKY, M., YEN, A., HERAVI-MOUSSAVI, A., KHERADPOUR, P., ZHANG, Z., WANG, J., ZILLER, M. J., AMIN, V., WHITAKER, J. W., SCHULTZ, M. D., WARD, L. D., SARKAR, A., QUON, G., SANDSTROM, R. S., EATON, M. L., WU, Y. C., PFENNING, A. R., WANG, X., CLAUSSNITZER, M., LIU, Y., COARFA, C., HARRIS, R. A., SHORESH, N., EPSTEIN, C. B., GJONESKA, E., LEUNG, D., XIE, W., HAWKINS, R. D., LISTER, R., HONG, C., GASCARD, P., MUNGALL, A. J., MOORE, R., CHUAH, E., TAM, A., CANFIELD, T. K., HANSEN, R. S., KAUL, R., SABO, P. J., BANSAL, M. S., CARLES, A., DIXON, J. R., FARH, K. H., FEIZI, S., KARLIC, R., KIM, A. R., KULKARNI, A., LI, D., LOWDON, R., ELLIOTT, G., MERCER, T. R., NEPH, S. J., ONUCHIC, V., POLAK, P., RAJAGOPAL, N., RAY, P., SALLARI, R. C., SIEBENTHALL, K. T., SINNOTT-ARMSTRONG, N. A., STEVENS, M., THURMAN, R. E., WU, J., ZHANG, B., ZHOU, X., BEAUDET, A. E., BOYER, L. A., DE JAGER, P. L., FARNHAM, P. J., FISHER, S. J., HAUSSLER, D., JONES, S. J., LI, W., MARRA, M. A., MCMANUS, M. T., SUNYAEV, S., THOMSON, J. A., TLSTY, T. D., TSAI, L. H., WANG, W., WATERLAND, R. A., ZHANG, M. Q., CHADWICK, L. H., BERNSTEIN, B. E., COSTELLO, J. F., ECKER, J. R., HIRST, M., MEISSNER, A., MILOSAVLJEVIC, A., REN, B., STAMATOYANNOPOULOS, J. A., WANG, T. & KELLIS, M. 2015. Integrative analysis of 111 reference human epigenomes. *Nature,* 518**,** 317-30.

ROBINSON, M. D., MCCARTHY, D. J. & SMYTH, G. K. 2010. edgeR: a Bioconductor package for differential expression analysis of digital gene expression data. *Bioinformatics,* 26**,** 139-40.

RODENAS-CUADRADO, P., HO, J. & VERNES, S. C. 2014. Shining a light on CNTNAP2: complex functions to complex disorders. *Eur J Hum Genet,* 22**,** 171-8.

ROSEN, E. Y., WEXLER, E. M., VERSANO, R., COPPOLA, G., GAO, F., WINDEN, K. D., OLDHAM, M. C., MARTENS, L. H., ZHOU, P., FARESE, R. V., JR. & GESCHWIND, D. H. 2011. Functional genomic analyses identify pathways dysregulated by progranulin deficiency, implicating Wnt signaling. *Neuron,* 71**,** 1030-42.

ROSS-INNES, C. S., STARK, R., TESCHENDORFF, A. E., HOLMES, K. A., ALI, H. R., DUNNING, M. J., BROWN, G. D., GOJIS, O., ELLIS, I. O., GREEN, A. R., ALI, S., CHIN, S. F., PALMIERI, C., CALDAS, C. & CARROLL, J. S. 2012. Differential oestrogen receptor binding is associated with clinical outcome in breast cancer. *Nature,* 481**,** 389-93.

ROUSSO, D. L., QIAO, M., KAGAN, R. D., YAMAGATA, M., PALMITER, R. D. & SANES, J. R. 2016. Two Pairs of ON and OFF Retinal Ganglion Cells Are Defined by Intersectional Patterns of Transcription Factor Expression. *Cell Rep,* 15**,** 1930-44.

SAKAI, Y., SHAW, C. A., DAWSON, B. C., DUGAS, D. V., AL-MOHTASEB, Z., HILL, D. E. & ZOGHBI, H. Y. 2011. Protein interactome reveals converging molecular pathways among autism disorders. *Sci Transl Med,* 3**,** 86ra49.

SANJUAN, J., TOIRAC, I., GONZALEZ, J. C., LEAL, C., MOLTO, M. D., NAJERA, C. & DE FRUTOS, R. 2004. A possible association between the CCK-AR gene and persistent auditory hallucinations in schizophrenia. *Eur Psychiatry,* 19**,** 349-53.

SANKARAN, H., GOLDFINE, I. D., DEVENEY, C. W., WONG, K. Y. & WILLIAMS, J. A. 1980. Binding of cholecystokinin to high affinity receptors on isolated rat pancreatic acini. *J Biol Chem,* 255**,** 1849-53.

SCHAEFER, M. H., WANKER, E. E. & ANDRADE-NAVARRO, M. A. 2012. Evolution and function of CAG/polyglutamine repeats in protein-protein interaction networks. *Nucleic Acids Res,* 40**,** 4273-87.

SCHREIWEIS, C., BORNSCHEIN, U., BURGUIERE, E., KERIMOGLU, C., SCHREITER, S., DANNEMANN, M., GOYAL, S., REA, E., FRENCH, C. A., PULIYADI, R., GROSZER, M., FISHER, S. E., MUNDRY, R., WINTER, C., HEVERS, W., PAABO, S., ENARD, W. & GRAYBIEL, A. M. 2014. Humanized Foxp2 accelerates learning by enhancing transitions from declarative to procedural performance. *Proc Natl Acad Sci U S A,* 111**,** 14253-8.

SCHULZ, S. B., HAESLER, S., SCHARFF, C. & ROCHEFORT, C. 2010. Knockdown of FoxP2 alters spine density in Area X of the zebra finch. *Genes Brain Behav,* 9**,** 732-40.

SHANNON, P., MARKIEL, A., OZIER, O., BALIGA, N. S., WANG, J. T., RAMAGE, D., AMIN, N., SCHWIKOWSKI, B. & IDEKER, T. 2003. Cytoscape: a software environment for integrated models of biomolecular interaction networks. *Genome Res,* 13**,** 2498-504.

SHU, W., CHO, J. Y., JIANG, Y., ZHANG, M., WEISZ, D., ELDER, G. A., SCHMEIDLER, J., DE GASPERI, R., SOSA, M. A., RABIDOU, D., SANTUCCI, A. C., PERL, D., MORRISEY, E. & BUXBAUM, J. D. 2005. Altered ultrasonic vocalization in mice with a disruption in the Foxp2 gene. *Proc Natl Acad Sci U S A,* 102**,** 9643-8.

SHU, W., YANG, H., ZHANG, L., LU, M. M. & MORRISEY, E. E. 2001. Characterization of a new subfamily of winged-helix/forkhead (Fox) genes that are expressed in the lung and act as transcriptional repressors. *J Biol Chem,* 276**,** 27488-97.

SMART, I. H., DEHAY, C., GIROUD, P., BERLAND, M. & KENNEDY, H. 2002. Unique morphological features of the proliferative zones and postmitotic compartments of the neural epithelium giving rise to striate and extrastriate cortex in the monkey. *Cereb Cortex,* 12**,** 37-53.

SODERBERG, O., GULLBERG, M., JARVIUS, M., RIDDERSTRALE, K., LEUCHOWIUS, K. J., JARVIUS, J., WESTER, K., HYDBRING, P., BAHRAM, F., LARSSON, L. G. & LANDEGREN, U. 2006. Direct observation of individual endogenous protein complexes in situ by proximity ligation. *Nat Methods,* 3**,** 995-1000.

SPITERI, E., KONOPKA, G., COPPOLA, G., BOMAR, J., OLDHAM, M., OU, J., VERNES, S. C., FISHER, S. E., REN, B. & GESCHWIND, D. H. 2007. Identification of the transcriptional targets of FOXP2, a gene linked to speech and language, in developing human brain. *Am J Hum Genet,* 81**,** 1144-57.

STEIN, J. L., DE LA TORRE-UBIETA, L., TIAN, Y., PARIKSHAK, N. N., HERNANDEZ, I. A., MARCHETTO, M. C., BAKER, D. K., LU, D., HINMAN, C. R., LOWE, J. K., WEXLER, E. M., MUOTRI, A. R., GAGE, F. H., KOSIK, K. S. & GESCHWIND, D. H. 2014. A quantitative framework to evaluate modeling of cortical development by neural stem cells. *Neuron,* 83**,** 69-86.

STRAUSS, K. A., PUFFENBERGER, E. G., HUENTELMAN, M. J., GOTTLIEB, S., DOBRIN, S. E., PAROD, J. M., STEPHAN, D. A. & MORTON, D. H. 2006. Recessive symptomatic focal epilepsy and mutant contactin-associated protein-like 2. *N Engl J Med,* 354**,** 1370-7.

STROUD, J. C., WU, Y., BATES, D. L., HAN, A., NOWICK, K., PAABO, S., TONG, H. & CHEN, L. 2006. Structure of the forkhead domain of FOXP2 bound to DNA. *Structure,* 14**,** 159-66.

SUDHOF, T. C. 2012. Calcium control of neurotransmitter release. *Cold Spring Harb Perspect Biol,* 4**,** a011353.

SUPEK, F., BOSNJAK, M., SKUNCA, N. & SMUC, T. 2011. REVIGO summarizes and visualizes long lists of gene ontology terms. *PLoS One,* 6**,** e21800.

SVENDSEN, C. N., TER BORG, M. G., ARMSTRONG, R. J., ROSSER, A. E., CHANDRAN, S., OSTENFELD, T. & CALDWELL, M. A. 1998. A new method for the rapid and long term growth of human neural precursor cells. *J Neurosci Methods,* 85**,** 141-52.

TAKAHASHI, J. S., KUMAR, V., NAKASHE, P., KOIKE, N., HUANG, H. C., GREEN, C. B. & KIM, T. K. 2015. ChIP-seq and RNA-seq methods to study circadian control of transcription in mammals. *Methods Enzymol,* 551**,** 285-321.

TAKAHASHI, K., LIU, F. C., HIROKAWA, K. & TAKAHASHI, H. 2003. Expression of Foxp2, a gene involved in speech and language, in the developing and adult striatum. *J Neurosci Res,* 73**,** 61-72.

TAKAHASHI, K., LIU, F. C., HIROKAWA, K. & TAKAHASHI, H. 2008. Expression of Foxp4 in the developing and adult rat forebrain. *J Neurosci Res,* 86**,** 3106-16.

TERAMITSU, I., KUDO, L. C., LONDON, S. E., GESCHWIND, D. H. & WHITE, S. A. 2004. Parallel FoxP1 and FoxP2 expression in songbird and human brain predicts functional interaction. *J Neurosci,* 24**,** 3152-63.

THURMAN, R. E., RYNES, E., HUMBERT, R., VIERSTRA, J., MAURANO, M. T., HAUGEN, E., SHEFFIELD, N. C., STERGACHIS, A. B., WANG, H., VERNOT, B., GARG, K., JOHN, S., SANDSTROM, R., BATES, D., BOATMAN, L., CANFIELD, T. K., DIEGEL, M., DUNN, D., EBERSOL, A. K., FRUM, T., GISTE, E., JOHNSON, A. K., JOHNSON, E. M., KUTYAVIN, T., LAJOIE, B., LEE, B. K., LEE, K., LONDON, D., LOTAKIS, D., NEPH, S., NERI, F., NGUYEN, E. D., QU, H., REYNOLDS, A. P., ROACH, V., SAFI, A., SANCHEZ, M. E., SANYAL, A., SHAFER, A., SIMON, J. M., SONG, L., VONG, S., WEAVER, M., YAN, Y., ZHANG, Z., ZHANG, Z., LENHARD, B., TEWARI, M., DORSCHNER, M. O., HANSEN, R. S., NAVAS, P. A., STAMATOYANNOPOULOS, G., IYER, V. R., LIEB, J. D., SUNYAEV, S. R., AKEY, J. M., SABO, P. J., KAUL, R., FUREY, T. S., DEKKER, J., CRAWFORD, G. E. & STAMATOYANNOPOULOS, J. A. 2012. The accessible chromatin landscape of the human genome. *Nature,* 489**,** 75-82.

TOLNER, E. A., SHEIKH, A., YUKIN, A. Y. & OF …, K.-K. 2012. Subplate neurons promote spindle bursts and thalamocortical patterning in the neonatal rat somatosensory cortex. *Journal of ….*

TRAPNELL, C., PACHTER, L. & SALZBERG, S. L. 2009. TopHat: discovering splice junctions with RNA-Seq. *Bioinformatics,* 25**,** 1105-11.

TSAI, J. W., CHEN, Y., KRIEGSTEIN, A. R. & VALLEE, R. B. 2005. LIS1 RNA interference blocks neural stem cell division, morphogenesis, and motility at multiple stages. *J Cell Biol,* 170**,** 935-45.

TSUI, D., VESSEY, J. P., TOMITA, H., KAPLAN, D. R. & MILLER, F. D. 2013. FoxP2 regulates neurogenesis during embryonic cortical development. *J Neurosci,* 33**,** 244-58.

UNTERGASSER, A., CUTCUTACHE, I., KORESSAAR, T., YE, J., FAIRCLOTH, B. C., REMM, M. & ROZEN, S. G. 2012. Primer3--new capabilities and interfaces. *Nucleic Acids Res,* 40**,** e115.

USUI, N., CO, M., HARPER, M., RIEGER, M. A., DOUGHERTY, J. D. & KONOPKA, G. 2017. Sumoylation of FOXP2 Regulates Motor Function and Vocal Communication Through Purkinje Cell Development. *Biol Psychiatry,* 81**,** 220-230.

USUI, N., CO, M. & KONOPKA, G. 2014. Decoding the molecular evolution of human cognition using comparative genomics. *Brain Behav Evol,* 84**,** 103-16.

VAN DER LOOS, H. 1976. Barreloids in mouse somatosensory thalamus. *Neurosci Lett,* 2**,** 1-6.

VANDERHAEGHEN, J. J., SIGNEAU, J. C. & GEPTS, W. 1975. New peptide in the vertebrate CNS reacting with antigastrin antibodies. *Nature,* 257**,** 604-5.

VARGHA-KHADEM, F., GADIAN, D. G., COPP, A. & MISHKIN, M. 2005. FOXP2 and the neuroanatomy of speech and language. *Nat Rev Neurosci,* 6**,** 131-8.

VARGHA-KHADEM, F., O'GORMAN, A. M. & WATTERS, G. V. 1985. Aphasia and handedness in relation to hemispheric side, age at injury and severity of cerebral lesion during childhood. *Brain,* 108 (Pt 3)**,** 677-96.

VARGHA-KHADEM, F., WATKINS, K., ALCOCK, K., FLETCHER, P. & PASSINGHAM, R. 1995. Praxic and nonverbal cognitive deficits in a large family with a genetically transmitted speech and language disorder. *Proc Natl Acad Sci U S A,* 92**,** 930-3.

VARGHA-KHADEM, F., WATKINS, K. E., PRICE, C. J., ASHBURNER, J., ALCOCK, K. J., CONNELLY, A., FRACKOWIAK, R. S., FRISTON, K. J., PEMBREY, M. E., MISHKIN, M., GADIAN, D. G. & PASSINGHAM, R. E. 1998. Neural basis of an inherited speech and language disorder. *Proc Natl Acad Sci U S A,* 95**,** 12695-700.

VERNES, S. C., NEWBURY, D. F., ABRAHAMS, B. S., WINCHESTER, L., NICOD, J., GROSZER, M., ALARCON, M., OLIVER, P. L., DAVIES, K. E., GESCHWIND, D. H., MONACO, A. P. & FISHER, S. E. 2008. A functional genetic link between distinct developmental language disorders. *N Engl J Med,* 359**,** 2337-45.

VERNES, S. C., NICOD, J., ELAHI, F. M., COVENTRY, J. A., KENNY, N., COUPE, A. M., BIRD, L. E., DAVIES, K. E. & FISHER, S. E. 2006. Functional genetic analysis of mutations implicated in a human speech and language disorder. *Hum Mol Genet,* 15**,** 3154-67.

VERNES, S. C., OLIVER, P. L., SPITERI, E., LOCKSTONE, H. E., PULIYADI, R., TAYLOR, J. M., HO, J., MOMBEREAU, C., BREWER, A., LOWY, E., NICOD, J., GROSZER, M., BABAN, D., SAHGAL, N., CAZIER, J. B., RAGOUSSIS, J., DAVIES, K. E., GESCHWIND, D. H. & FISHER, S. E. 2011. Foxp2 regulates gene networks implicated in neurite outgrowth in the developing brain. *PLoS Genet,* 7**,** e1002145.

VERNES, S. C., SPITERI, E., NICOD, J., GROSZER, M., TAYLOR, J. M., DAVIES, K. E., GESCHWIND, D. H. & FISHER, S. E. 2007. High-throughput analysis of promoter occupancy reveals direct neural targets of FOXP2, a gene mutated in speech and language disorders. *Am J Hum Genet,* 81**,** 1232-50.

VIGGIANO, D., RUOCCO, L. A. & SADILE, A. G. 2003. Dopamine phenotype and behaviour in animal models: in relation to attention deficit hyperactivity disorder. *Neurosci Biobehav Rev,* 27**,** 623-37.

VILLAR, D., BERTHELOT, C., ALDRIDGE, S., RAYNER, T. F., LUKK, M., PIGNATELLI, M., PARK, T. J., DEAVILLE, R., ERICHSEN, J. T., JASINSKA, A. J., TURNER, J. M., BERTELSEN, M. F., MURCHISON, E. P., FLICEK, P. & ODOM, D. T. 2015. Enhancer evolution across 20 mammalian species. *Cell,* 160**,** 554-66.

WANG, L., WANG, S. & LI, W. 2012. RSeQC: quality control of RNA-seq experiments. *Bioinformatics,* 28**,** 2184-5.

WANG, W. Z., HOERDER-SUABEDISSEN, A., OESCHGER, F. M., BAYATTI, N., IP, B. K., LINDSAY, S., SUPRAMANIAM, V., SRINIVASAN, L., RUTHERFORD, M., MOLLGARD, K., CLOWRY, G. J. & MOLNAR, Z. 2010. Subplate in the developing cortex of mouse and human. *J Anat,* 217**,** 368-80.

WANG, W. Z., OESCHGER, F. M., LEE, S. & MOLNAR, Z. 2009. High quality RNA from multiple brain regions simultaneously acquired by laser capture microdissection. *BMC Mol Biol,* 10**,** 69.

WATKINS, K. E., DRONKERS, N. F. & VARGHA-KHADEM, F. 2002a. Behavioural analysis of an inherited speech and language disorder: comparison with acquired aphasia. *Brain,* 125**,** 452-64.

WATKINS, K. E., VARGHA-KHADEM, F., ASHBURNER, J., PASSINGHAM, R. E., CONNELLY, A., FRISTON, K. J., FRACKOWIAK, R. S., MISHKIN, M. & GADIAN, D. G. 2002b. MRI analysis of an inherited speech and language disorder: structural brain abnormalities. *Brain,* 125**,** 465-78.

WEBER, J. L. 1990. Human DNA polymorphisms and methods of analysis. *Curr Opin Biotechnol,* 1**,** 166-71.

WEI, J. & HEMMINGS, G. P. 1999. The CCK-A receptor gene possibly associated with auditory hallucinations in schizophrenia. *Eur Psychiatry,* 14**,** 67-70.

WEXLER, E. M., ROSEN, E., LU, D., OSBORN, G. E., MARTIN, E., RAYBOULD, H. & GESCHWIND, D. H. 2011. Genome-wide analysis of a Wnt1-regulated transcriptional network implicates neurodegenerative pathways. *Sci Signal,* 4**,** ra65.

WIJCHERS, P. J., BURBACH, J. P. & SMIDT, M. P. 2006a. In control of biology: of mice, men and Foxes. *Biochem J,* 397**,** 233-46.

WIJCHERS, P. J., HOEKMAN, M. F., BURBACH, J. P. & SMIDT, M. P. 2006b. Identification of forkhead transcription factors in cortical and dopaminergic areas of the adult murine brain. *Brain Res,* 1068**,** 23-33.

WONG, Y. W., SCHULZE, C., STREICHERT, T., GRONOSTAJSKI, R. M., SCHACHNER, M. & TILLING, T. 2007. Gene expression analysis of nuclear factor I-A deficient mice indicates delayed brain maturation. *Genome Biol,* 8**,** R72.

WU, Y., BORDE, M., HEISSMEYER, V., FEUERER, M., LAPAN, A. D., STROUD, J. C., BATES, D. L., GUO, L., HAN, A., ZIEGLER, S. F., MATHIS, D., BENOIST, C., CHEN, L. & RAO, A. 2006. FOXP3 controls regulatory T cell function through cooperation with NFAT. *Cell,* 126**,** 375-87.

XIANG, Y., TANAKA, Y., PATTERSON, B., KANG, Y. J., GOVINDAIAH, G., ROSELAAR, N., CAKIR, B., KIM, K. Y., LOMBROSO, A. P., HWANG, S. M., ZHONG, M., STANLEY, E. G., ELEFANTY, A. G., NAEGELE, J. R., LEE, S. H., WEISSMAN, S. M. & PARK, I. H. 2017. Fusion of Regionally Specified hPSC-Derived Organoids Models Human Brain Development and Interneuron Migration. *Cell Stem Cell,* 21**,** 383-398 e7.

XU, S., GRULLON, S., GE, K. & PENG, W. 2014. Spatial clustering for identification of ChIP-enriched regions (SICER) to map regions of histone methylation patterns in embryonic stem cells. *Methods Mol Biol,* 1150**,** 97-111.

YANG, M., SILVERMAN, J. L. & CRAWLEY, J. N. 2011. Automated three-chambered social approach task for mice. *Curr Protoc Neurosci,* Chapter 8**,** Unit 8 26.

YIN, H. H. & KNOWLTON, B. J. 2006. The role of the basal ganglia in habit formation. *Nat Rev Neurosci,* 7**,** 464-76.

YU, F., KEINAN, A., CHEN, H., FERLAND, R. J., HILL, R. S., MIGNAULT, A. A., WALSH, C. A. & REICH, D. 2009. Detecting natural selection by empirical comparison to random regions of the genome. *Hum Mol Genet,* 18**,** 4853-67.

ZARET, K. S. & CARROLL, J. S. 2011. Pioneer transcription factors: establishing competence for gene expression. *Genes Dev,* 25**,** 2227-41.

ZHANG, J., WEBB, D. M. & PODLAHA, O. 2002. Accelerated protein evolution and origins of human-specific features: Foxp2 as an example. *Genetics,* 162**,** 1825-35.

ZHANG, Y., LIU, T., MEYER, C. A., EECKHOUTE, J., JOHNSON, D. S., BERNSTEIN, B. E., NUSBAUM, C., MYERS, R. M., BROWN, M., LI, W. & LIU, X. S. 2008. Model-based analysis of ChIP-Seq (MACS). *Genome Biol,* 9**,** R137.

ZHOU, B., ZHONG, Q., MINOO, P., LI, C., ANN, D. K., FRENKEL, B., MORRISEY, E. E., CRANDALL, E. D. & BOROK, Z. 2008. Foxp2 inhibits Nkx2.1-mediated transcription of SP-C via interactions with the Nkx2.1 homeodomain. *Am J Respir Cell Mol Biol,* 38**,** 750-8.